

Université de Montréal

***Regulation of bone-derived hormones by post-translational
modifications***

Par

Omar Al Rifai

Programme de biologie moléculaire

Faculté de médecine

Thèse présenté(e) a la faculté de médecine
en vue de l'obtention du grade de Philosophiæ Doctor (Ph.D)
en biologie moléculaire, option médecine cellulaire et moléculaire

Janvier 2020

© Omar Al Rifai, 2020

Université de Montréal
Programme de biologie moléculaire/ Faculté de médecine
Institut de recherche clinique de Montréal

Cette thèse intitulé(e)

***Regulation of bone-derived hormones by post-translational
modifications***

Présenté par
Omar Al Rifai

A été évalué(e) par un jury composé des personnes suivantes

Dr. David Hipfner
Président-rapporteur

Dr. Mathieu Ferron
Directeur de recherche

Dr. Mike (Przemyslaw) Sapieha
Membre du jury

Dr. René St-Arnaud
Examineur externe

Dr. Frédérick Antoine Mallette
Représentant du doyen du FESP

Résumé

Les fonctions endocriniennes des os sont médiées par au moins deux hormones, l'ostéocalcine et le facteur de croissance fibroblastique 23 « *Fibroblast growth factor 23* » (FGF23), ces derniers sont sécrétés par les cellules osseuses, les ostéoblastes et les ostéocytes. L'ostéocalcine est produite par les ostéoblastes et régule le métabolisme du glucose et énergétique. Elle améliore ainsi la tolérance au glucose et la sensibilité à l'insuline. Également, elle favorise la sécrétion d'insuline et la prolifération des cellules β , elle augmente la dépense énergétique et réduit l'accumulation de graisse. L'ostéocalcine est gamma-carboxylée au niveau de trois résidus d'acide glutamique (Glu), un processus qui inhibe sa fonction endocrinienne chez la souris et l'humain. Le pH acide de la lacune de résorption décarboxyle l'ostéocalcine et libère sa forme non carboxylée (ucOCN), la forme active de cette hormone. Nos connaissances sur la régulation des fonctions endocriniennes d'ostéocalcine sont encore limitées à sa gamma-carboxylation. Puisque cette hormone est sécrétée par les ostéoblastes et les ostéocytes, des cellules endocriniennes non classique, nous avons émis l'hypothèse que l'ostéocalcine pourrait être soumise à d'autres modifications post-traductionnelles (PTMs) au niveau de la voie de sécrétion contrôlant ses fonctions endocriniennes. Dans la première partie de cette thèse, nous avons montré que le propeptide de l'ostéocalcine pouvait être clivé dans son extrémité C-terminale au niveau du motif de base « RLRR » par la pro-protéine convertase furine, un processus qui se produit indépendamment de la gamma-carboxylation de l'ostéocalcine. L'inactivation du gène codant pour la furine, spécifiquement dans les ostéoblastes et les ostéocytes chez la souris, abolit totalement le clivage de la pro-ostéocalcine et altère son activation et sa libération lors de la résorption osseuse. Par conséquent, ces souris sont caractérisées par un niveau bas d'ucOCN dans le sérum, ce qui entraîne une altération de la tolérance au glucose, une diminution de la sécrétion d'insuline et de la dépense énergétique ainsi qu'une augmentation de l'accumulation de graisses. De plus, ces souris ont une perte d'appétit indépendamment de l'ostéocalcine. La restriction de la nourriture pour les souris contrôles ou « *pair feeding* » rend le phénotype des souris déficientes en furine plus apparent. Il apparaît à un plus jeune âge avec une résistance à l'insuline. Dans la deuxième partie de cette thèse, nous avons découvert que l'ostéocalcine de souris est O-glycosylée au niveau de la sérine 8, un processus qui se produit indépendamment de

sa gamma-carboxylation et de son clivage. Cette modification, qui n'est pas présente chez l'ostéocalcine humaine, augmente la demi-vie de l'ostéocalcine de souris dans le plasma ex vivo et in vivo. Il est intéressant de noter que la tyrosine 12 dans l'ostéocalcine humaine correspond à la sérine 8 dans la séquence de la souris, tandis que la mutation Tyr12Ser est suffisante pour générer une ostéocalcine humaine *O*-glycosylée et lui conférer une demi-vie plus longue dans le plasma de la souris comparativement à la forme native.

FGF23 est une hormone sécrétée par les ostéoblastes et les ostéocytes. Elle régule la réabsorption de phosphate et la production de vitamine D dans le tubule proximal du rein. Sa fonction endocrine est inhibée par un clivage endoprotéolytique qui libère ses fragments N- et C-terminaux. La mutation du motif « RHTR », un site de clivage consensus pour les proprotéines convertases PC(s), a été identifiée chez les patients atteints du rachitisme hypophosphatémique génétiquement déterminés ou « *Autosomal dominant hypophosphatemic rickets* » (ADHR). Ces patients se caractérisent par une augmentation du taux de FGF23 intact, une hypophosphatémie et une ostéomalacie. Malgré l'importance de FGF23 dans plusieurs maladies, l'identité de l'enzyme responsable du clivage de FGF23 n'est pas encore connue, même si la furine et la proprotéine convertase subtilisine/kexine type 5 (PC5) peuvent cliver FGF23 in vitro. Dans la troisième partie de cette thèse, nous tentons de répondre à cette question en utilisant des souris déficientes en furine et/ou PC5 spécifiquement dans les ostéoblastes et les ostéocytes. Sous des conditions physiologiques, l'inactivation du gène de furine dans les ostéoblastes et les ostéocytes augmente le niveau du FGF23 intact par 25%. Malgré cette augmentation ces souris maintiennent une phosphatémie normale et elles ne montrent pas de signe d'ostéomalacie. On a aussi montré qu'une déficience en fer, une condition qui augmente la production de FGF23 au niveau de l'ARN messager et protéique, le FGF23 est totalement en forme intact dans les souris déficientes en furine, montrant que le clivage de FGF23 est totalement inhibé dans cette condition. En revanche, l'injection d'érythropoïétine ou d'interleukine 1- β , des conditions qui augmentent la production de FGF23, induit une augmentation significative du taux de FGF23 total dans le sérum des souris déficientes en furine et/ou PC5 dans les ostéoblastes et les ostéocytes, tandis que le niveau du FGF23 intact n'a pas augmenté de la même façon, suggérant que la FGF23 est correctement clivée

chez ces souris. D'une façon intéressante et malgré les défauts développementaux et le retard dans la minéralisation osseuse observée dans les souris complètement déficientes en PC5, la suppression conditionnelle de PC5 dans les ostéoblastes et les ostéocytes chez la souris n'a entraîné aucun défaut osseux. Cependant, l'inactivation du gène codant pour la furine dans les ostéoblastes et les ostéocytes chez la souris a augmenté les paramètres osseux trabéculaires et a diminué l'épaisseur de l'os cortical. De plus, ces souris ont eu une diminution de la densité minérale et la rigidité des os reflétant une mauvaise qualité osseuse.

En résumé, nous avons décrit pour la première fois que la furine est un régulateur multifonctionnel de la fonction des ostéoblastes et des ostéocytes *in vivo*. Elle régule le métabolisme du glucose en assurant le clivage de la pro-ostéocalcine, qui est nécessaire à la maturation et à la bio-activité de l'ostéocalcine, et en régulant l'appétit indépendamment de l'ostéocalcine. Ces résultats suggèrent la présence d'ostéokines supplémentaires régulant l'appétit et contrôlées par la furine. De plus, dans les ostéoblastes, la furine régule partiellement le clivage de FGF23 en assurant une phosphatémie normale, suggérant que la régulation de l'accumulation de masse osseuse par la furine est indépendante du FGF23. En outre, nous avons découvert que l'ostéocalcine de souris est soumise à l'*O*-glycosylation, une modification qui n'est pas conservée chez l'humain, ni chez d'autres espèces, et qui augmente la demi-vie de l'ostéocalcine de souris. La glycosylation artificielle confère à l'ostéocalcine humaine une demi-vie plus longue, offrant ainsi une approche permettant d'augmenter potentiellement la bio-activité de l'ostéocalcine humaine dans les futures applications thérapeutiques de l'ostéocalcine dans les maladies humaines.

Mots-clés: Ostéocalcine, FGF23, Furine, PC5, *O*-glycosylation, fonction endocrinienne, os.

Abstract

Bone endocrine functions are mediated by at least two hormones, osteocalcin and fibroblast growth factor 23 (FGF23) which are secreted by the bone cells, osteoblasts and osteocytes. Osteocalcin is an osteoblast-derived hormone regulating glucose and energy metabolism. It improves glucose tolerance and insulin sensitivity, promotes insulin secretion and β -cell proliferation, increases energy expenditure and reduces fat accumulation. Osteocalcin is gamma-carboxylated on three of its glutamic acid residues (Glu), a process that inhibits its endocrine function in mice and humans. It is the acidic pH in the resorption lacuna which decarboxylates osteocalcin releasing the uncarboxylated osteocalcin (ucOCN), the active form of this hormone. Our knowledge on osteocalcin regulation by post-translational modifications is limited to its gamma-carboxylation. Since osteocalcin is secreted by differentiated osteoblasts, a non-classical endocrine cell, we hypothesized that osteocalcin may be subjected to additional post translational modifications (PTMs) in the secretory pathway that regulates its endocrine functions. In the first part of the thesis we showed that osteocalcin's putative pro-peptide is cleaved in its C-terminus at the basic motif «RLRR», by the proprotein convertase furin. This process occurs independently of osteocalcin gamma-carboxylation. Furin inactivation specifically in osteoblasts in mice totally abolishes osteocalcin processing and impairs its activation and release during bone resorption. Consequently, these mice have decreased serum level of ucOCN resulting in impaired glucose tolerance, reduced insulin secretion and energy expenditure, and increased fat accumulation. Moreover, these mice have a decrease in the appetite independently of osteocalcin. Pair feeding of control mice resulted in more apparent phenotype in furin deficient mice, as it appears at younger age alongside with insulin resistance. In the second part of this thesis, we discovered that mouse osteocalcin is *O*-glycosylated on serine 8, a process that occurs independently of its gamma-carboxylation and processing. This modification is not conserved in human or any other species and it increases mouse osteocalcin half-life in plasma ex vivo and in vivo. Interestingly, tyrosine 12 in human osteocalcin corresponds to the serine 8 in the mouse sequence. Tyr12Ser mutation was sufficient to *O*-glycosylate human osteocalcin and to confer this hormone a longer half-life in mouse plasma compared to the native form.

FGF23 is a hormone secreted by osteoblasts and osteocytes which regulates phosphate reabsorption and vitamin D production in the kidney proximal tubule. Its endocrine function is inhibited by endoproteolytic cleavage which releases its N-terminal and C-terminal fragments. Mutations in the «RHTR» motif, a consensus cleavage site for proprotein convertases (PCs), were found in patients with autosomal dominant hypophosphatemic rickets (ADHR). These patients are characterized by an increased intact FGF23 levels, hypophosphatemia and osteomalacia. Despite the importance of FGF23 in the pathology of multiple diseases, the identity of the enzyme(s) involved in FGF23 cleavage is yet unclear, even though furin and the proprotein convertase subtilisin/kexin type 5 (PC5) were shown to cleave FGF23 in vitro. In the third part of the thesis, we addressed this question using mice model deficient in furin and/or PC5 in osteoblasts and osteocytes in mice. Under physiological conditions, furin inactivation resulted in a 25% increase in intact FGF23; however, these mice maintained normal phosphate level and did not shown any sign of osteomalacia. We also showed that under iron restriction, a condition that induce FGF23 expression at the mRNA and protein level, FGF23 processing is totally impaired in furin deficient mice. However, the injection of erythropoietin or interleukin 1- β , two conditions that increase FGF23 production, induce FGF23 serum level while it is still properly processed in mice deficient in furin and/or PC5 in osteoblasts and osteocytes. Interestingly, despite the patterning defects observed in global inactivation of PC5, conditional inactivation of PC5 in osteoblasts and osteocytes in mice did not result in any bone defect. However, furin inactivation in osteoblasts and osteocytes in mice increases trabecular bone parameters and decreases cortical thickness. Moreover, these mice have decreased bone mineral density and bone strength reflecting a poor bone quality.

In summary, we described for the first time that furin is a pleotropic regulator of osteoblast and osteocyte function in vivo. It regulates glucose and energy metabolism by mediating pro-osteocalcin processing which is required for osteocalcin maturation and bioactivity, and by regulating appetite independently of osteocalcin. These findings suggest the presence of additional osteokines controlling appetite and which are regulated by furin. Moreover, furin partially regulates FGF23 processing while maintaining normal phosphate

homeostasis, suggesting that the regulation of bone mass accrual by furin occurs independently of FGF23. Additionally, we discovered that mouse osteocalcin is subjected to *O*-glycosylation, a species-specific modification that is not conserved in humans or any other species and increases mouse osteocalcin half-life. Artificial *O*-glycosylation confer human osteocalcin a longer half-life, thus providing an approach to increase human osteocalcin bioactivity in future therapeutic applications of osteocalcin in human diseases.

Keywords: Osteocalcin, FGF23, Furin, PC5, *O*-glycosylation, endocrine function, bone.

Table of contents

Résumé	iii
Abstract.....	vi
Table of contents	ix
List of tables	xiii
List of figures	xiv
List of abbreviations	xvii
Acknowledgments	xxi
1. CHAPTER I: INTRODUCTION	23
1.1. PROTEIN POST-TRANSLATIONAL MODIFICATIONS	24
1.1.1. Protein phosphorylation.....	24
1.1.2. Proteolytic cleavage	25
<i>1.1.2.1. Proprotein convertases</i>	<i>26</i>
<i>1.1.2.2. Furin</i>	<i>28</i>
<i>1.1.2.3. The proprotein convertase subtilisin/kexin type 5.....</i>	<i>30</i>
1.1.3. Glycosylation.....	32
<i>1.1.3.1. N-glycosylation.....</i>	<i>32</i>
<i>1.1.3.2. O-glycosylation.....</i>	<i>33</i>
1.2. BONE BIOLOGY	36
1.2.1. Bone physiology and components	37
1.2.2. Regulation of osteoblasts differentiation	38
<i>1.2.2.1. Transcriptional regulation of osteoblasts differentiation</i>	<i>38</i>
<i>1.2.2.2. Regulation of osteoblast differentiation by autocrine and paracrine signals ..</i>	<i>40</i>
<i>1.2.2.3. Neuroendocrine signals regulating osteoblasts differentiation</i>	<i>41</i>

1.2.3.	Osteocytes	41
1.2.4.	Paracrine and endocrine functions of osteoblasts and osteocytes	42
1.3.	OSTEOCALCIN	44
1.3.1.	Osteocalcin structure	44
1.3.2.	Role of osteocalcin in bone development	47
1.3.3.	Osteocalcin post-translational modification	47
1.3.3.1.	<i>Osteocalcin gamma-carboxylation</i>	48
1.3.4.	Endocrine functions of osteocalcin	49
1.3.4.1.	<i>Osteocalcin regulates glucose and energy metabolism</i>	50
1.3.4.2.	<i>Osteocalcin regulates fertility</i>	52
1.3.4.3.	<i>Osteocalcin effect on brain development and function</i>	53
1.3.4.4.	<i>Osteocalcin regulates muscle mass and exercise capacity</i>	55
1.3.4.5.	<i>Osteocalcin regulates the response to acute stress</i>	56
1.3.5.	Hormonal regulation of osteocalcin in osteoblasts	57
1.3.5.1.	<i>Regulation of osteocalcin by Leptin</i>	58
1.3.5.2.	<i>Regulation of osteocalcin by insulin</i>	58
1.3.5.3.	<i>Regulation of osteocalcin by interleukin 6 (IL-6)</i>	59
1.3.5.4.	<i>Osteocalcin regulation by other signals</i>	59
1.3.6.	Endocrine function of human osteocalcin	59
1.4.	FIBROBLAST GROWTH FACTOR 23 (FGF23)	61
1.4.1.	Phosphorus is an essential element for the body	62
1.4.2.	FGF23 protein structure and function	62
1.4.3.	FGF23 receptor and signaling	64
1.4.4.	Transcriptional regulation of FGF23	65

1.4.4.1.	<i>FGF23 regulation by vitamin D</i>	66
1.4.4.2.	<i>FGF23 regulation by Aspartate-rich Matrix extracellular phosphoglycoprotein associated motif</i>	66
1.4.4.3.	<i>FGF23 regulation by hypoxia induced factor 1 alpha</i>	66
1.4.4.4.	<i>FGF23 regulation by Erythropoietin</i>	67
1.4.5.	Regulation of FGF23 by post-translational modifications	67
1.4.5.1.	<i>Proteolytic cleavage</i>	68
1.4.5.2.	<i>O-glycosylation</i>	68
1.4.5.3.	<i>Phosphorylation</i>	69
1.4.6.	FGF23 in human disease	70
1.4.7.	FGF23 in chronic kidney disease	70
2.	CHAPTER II: GENERAL HYPOTHESIS	72
3.	CHAPTER III: IDENTIFICATION OF PRO-OSTEOCALCIN CONVERTING ENZYME AND A NOVEL BONE ENDOCRINE FUNCTION	74
3.1.	HYPOTHESIS AND RELEVANCE	75
3.2.	FIRST PAPER	76
4.	CHAPTER IV: OSTEOCALCIN O-GLYCOSYLATION: A MOUSE SPECIFIC POST-TRANSLATIONAL MODIFICATION REGULATING ITS HALF-LIFE	119
4.1.	HYPOTHESIS AND RELEVANCE	120
4.2.	SECOND PAPER	121
5.	CHAPTER V: FURIN IN OSTEOBLASTS REGULATES FGF23 AND BONE MASS ACCRUAL	156
5.1.	HYPOTHESIS AND RELEVANCE	157
5.2.	THIRD PAPER	158
6.	CHAPTER VI: DISCUSSION	179

6.1. OSTEOCALCIN PROTEOLYTIC CLEAVAGE AND O-GLYCOSYLATION REGULATES ITS ENDOCRINE FUNCTIONS.....	180
6.1.1. Post-translational modifications in human osteocalcin	182
6.1.2. Significance of human osteocalcin modifications in clinical studies	183
6.2. FURIN IN OSTEOLASTS REGULATES BONE ENDOCRINE FUNCTION INDEPENDENTLY OF OSTEOCALCIN.	185
6.3. FURIN IN OSTEOLASTS AND OSTEOCYTES PARTIALLY MEDIATES FGF23 ENDOPROTEOLYTIC CLEAVAGE.....	188
6.3.1. Other possible sources of FGF23	189
6.3.2. Metabolic phenotype and the increase in FGF23 in <i>Furin^{osb}</i> <i>-/-</i> mice	191
6.3.3. The possible identity of the convertase(s) involved in FGF23 processing.....	192
6.4. FURIN BUT NOT PC5 REGULATES BONE MASS ACCRUAL	193
6.5. IMPACT ON FUTURE THEURAPEUTIC APPLICATIONS.....	194
6.6. FUTURE PERSPECTIVES.....	196
7. REFERENCES.....	200
8. ANNEXES.....	220
9. CURRICULUM VITAE	228

List of tables

Table 1-1. Different glycosidic bonds occurring in mammalian cells	34
Table 1-2. Human diseases associated with FGF23, its receptor and regulators	70
Table 3-1. LC-MS/MS analyses of cell supernatant of differentiated mouse osteoblasts treated or not with 50 μ M Dec-RVKR-CMK (RVKR) or 50 μ M warfarin	93
Table 6-1. SNPs in human osteocalcin cleavage site (R ₄₈ PRR ₅₁)	184
Supplemental Table 3-1. List of oligonucleotides used in this study.....	118
Supplemental Table 4-1. OCN serum levels in mice and human at different age	149
Supplemental Table 4-2. The monoisotopic mass and relative abundance of the different OCN forms detected in the supernatant of differentiated osteoblasts.....	150
Supplemental Table 4-3. The monoisotopic mass and relative abundance of the different OCN forms detected in the supernatant of differentiated osteoblasts.....	151
Supplemental Table 4-4. Human OCN SNPs.....	152
Supplemental Table 4-5. Primer List	154
Supplemental Table 5-1. Primer list.....	178

List of figures

Figure 1-1. Primary structure of proprotein convertases	27
Figure 1-2. Furin autoactivation by autoproteolytic cleavage	29
Figure 1-3. PC5A and PC5B: product of alternative splicing of the PCSK5 gene.....	31
Figure 1-4. Different mucin-type O-glycosylation cores	35
Figure 1-5. Anatomy of long bone modified from	36
Figure 1-6. Schematic representation of endochondral bone formation.....	38
Figure 1-7. Regulation of osteoblasts differentiation by transcription factors	40
Figure 1-8. Differentiation markers during transition from osteoblasts to osteocytes	42
Figure 1-9. Mature osteocalcin amino acid alignment	45
Figure 1-10. Secondary structure of porcine osteocalcin	46
Figure 1-11. Uncarboxylated (Glu) and carboxylated (Gla) osteocalcin crystal structure.....	46
Figure 1-12. Gamma carboxylation and vitamin K cycle.....	48
Figure 1-13. Effect of osteocalcin on fertility and testosterone production	53
Figure 1-14. Effect of osteocalcin on the brain	54
Figure 1-15. Osteocalcin signaling in myofiber and IL-6 feed forward effect.....	56
Figure 1-16. Osteocalcin regulation in acute stress response	57
Figure 1-17. Regulation of phosphate reabsorption by FGF23.....	63
Figure 1-18. Topology of FGF23, FGFR1c and α -klotho interaction.....	65
Figure 1-19. Transcriptional and post-translational modifications of FGF23	69
Figure 3-1. PC cleaves pro-OCN at the RXRR motif in osteoblasts	85
Figure 3-2. Furin cleaves pro-OCN in vitro	87
Figure 3-3. Furin but not PC5 is necessary for pro-OCN processing in osteoblasts.....	89
Figure 3-4. Furin and pro-OCN colocalize in osteoblasts.....	90
Figure 3-5. Pro-OCN processing and γ -carboxylation occur independently of each other in osteoblasts.....	92
Figure 3-6. Impaired pro-OCN processing in Furin ^{osb^{-/-}} mice	95
Figure 3-7. Pro-OCN is not efficiently decarboxylated by osteoclasts.....	96
Figure 3-8. Reduced glucose tolerance in Furin ^{osb^{-/-}} mice	98

Figure 3-9. Reduced energy expenditure and food intake in <i>Furin^{osb-/-}</i> mice.....	100
Figure 3-10. Pair feeding reveals a more severe metabolic phenotype in <i>Furin^{osb-/-}</i> mice.	102
Supplemental Figure 3-1. Biochemical characterization of the <i>Furin_{osb}^{-/-}</i> mice.....	113
Supplemental Figure 3-2. Metabolic phenotype of <i>Furin^{flox/flox}</i> and <i>Furin_{osb}^{-/-}</i> mice at 3, 6 and 9 months	115
Supplemental Figure 3-3. Reduced energy expenditure and food intake in <i>Furin_{osb}^{-/-}</i> mice at 3 months of age.....	116
Supplemental Figure 3-4. LCN2 is not processed by FURIN in osteoblasts.....	117
Figure 4-1. OCN is O-glycosylated in vitro and in vivo on Serine 57	132
Figure 4-2. Multiple <i>N-acetylgalactosaminyltransferase</i> (GalNAc-Ts) O-glycosylate OCN and this process is independent of its processing and γ -carboxylation	134
Figure 4-3. OCN O-glycosylation increases its half-life ex vivo and in vivo.....	137
Figure 4-4. Human OCN O-glycosylation increases its half-life ex vivo	139
Supplemental Figure 4-1. Mouse OCN O-glycosylation occurs independently of its carboxylation and processing in HEK293	147
Supplemental Figure 4-2. Different protease inhibitor failed to rescue non-glycosylated mouse and human ucOCN degradation.....	148
Figure 5-1. Increased FGF23 level and reduced phosphate excretion in <i>Furin^{osb-/-}</i> mice.....	163
Figure 5-2. Impaired FGF23 processing and hyperphosphatemia in <i>Furin^{osb-/-}</i> mice following iron restriction	166
Figure 5-3. FGF23 is normally processed following rhEPO and IL-1 β injection	168
Figure 5-4. PC5 inactivation did not impair FGF23 processing	170
Figure 6-1. Mouse osteocalcin post-translational modifications	182
Figure 6-2. Furin in osteoblasts regulates whole body energy metabolism.....	187
Annex Figure 8-1. Increase neoglucogenesis in <i>Furin^{osb-/-}</i> mice on normal and high fat high sucrose diet (HFHSD).....	220
Annex Figure 8-2. FGF23 target in control and <i>Furin^{osb-/-}</i> mice on normal or low iron diet.....	221
Annex Figure 8-3. <i>Furin^{osb-/-}</i> mice maintained normal serum iron.....	222

Annex Figure 8-4. *Furin^{osb}/-* mice maintained normal serum phosphate following two weeks of Erythropoietin (EPO) injection.**223**

Annex Figure 8-5. Normal bone quality in *Pcsk5^{osb}/-*.....**224**

Annex Figure 8-6. Poor bone quality in *Furin^{osb}/-*.**225**

Annex Figure 8-7. Increase bone volume, osteoblasts and osteoclasts in the trabecular bone of *Furin^{osb}/-* mice.**226**

Annex Figure 8-8. Decrease bone mineralization capacity of bone marrow osteoblasts derived from *Furin^{osb}/-* mice..**227**

List of abbreviations

7B2	Protein 7B2
ADAMTS	Disintegrin and metalloproteinase with thrombospondin motifs
ADHR	Autosomal dominant hypophosphatemic rickets
AKT	Protein kinase B (PKB)
ASARM	Aspartate-rich Matrix extracellular phosphoglycoprotein (MEPE) associated motif
ATF4	Activating transcription factor 4
BMP4	Bone morphogenic protein 4
Cbfa1	Core-binding factor subunit alpha-1
Cd36	Cluster of differentiation 36
CDK	Cyclin-dependent kinases
CGRP	Calcitonin gene-related protein
CHO	Chinese hamster ovary cells
CPT1B	Carnitine palmitoyltransferase 1B
CRD	Cysteine rich domain
CREB	cAMP response element-binding protein
DMP1	Dentin matrix protein 1
DNA	Deoxyribonucleic acid
E	Embryonic day
ECM	Extracellular matrix
EDTA	Ethylenediaminetetraacetic acid
EPO	Erythropoietin
ERK	Extracellular signal-regulated kinases
Esp	Receptor-like protein tyrosine phosphatase
FAM20C	Family with sequence similarity member C
Fatp1	Fatty acid transport protein 1
FGF23	Fibroblast growth factor 23
FGFR	Fibroblast growth receptor
FIAT	Factor inhibiting ATF4-mediated transcription
Foxo1	Forkhead box protein O1
Gal	Galactose
GalNAc	N-acetylgalactosamine
GalNAc-T	N-acetylgalactosaminyltransferase
Gdf11	Growth/differentiation factor 11
GGCX	Gamma-glutamyl carboxylase
Gla	Carboxy glutamic acid
GLAST	Glutamate Aspartate Transporter 1
GLP1	Glucagon-like-peptide-1
Glu	Glutamic acid
Gly uchOCN	O-glycosylated uncarboxylated human osteocalcin

Gly ucOCN	O-glycosylated uncarboxylated osteocalcin
Gpr158	G protein coupled receptor 158
GPRC6A	G-protein coupled receptor family C group 6 member A
HbA1c	Hemoglobin A1c
HEK293	Human embryonic kidney cells
HFTC	Hyperphosphatemic familial tumoral calcinosis
HIF-1α	Hypoxia induced factor 1 alpha
HIF-PH	Hif1 α prolyl hydroxylase
HSPG	Heparan sulfate proteoglycan
IL-1β	Interleukin 1 beta
IL6	Interleukin 6
Ins1	Insulin gene
IRS	Insulin receptor substrate
Kex2	Kexin 2
MAPK	Mitogen-activated protein kinase
M-CSF	Macrophage colony stimulating factor
MEPE	Matrix extracellular phosphoglycoprotein
MMP2	Matrix metalloproteinase 2
MS	Mass spectrometry
mTOR	Mammalian target of rapamycin
NFATc1	Nuclear factor of activated T cells 1
ng	Nanogram
OCN	Osteocalcin
OPG	Osteoprotegerin
PACE4	Paired Basic Amino Acid-cleaving Enzyme 4
PAGE	Polyacrylamide gel electrophoresis
PBS	Phosphate buffer saline
PCs	Proprotein convertases
Pgc1α	Peroxisome proliferator-activated receptor-gamma coactivator
PHEX	phosphate-regulating endopeptidase homology X-linked
Pitx2	Paired-like homeodomain transcription factor 2
Pro-OCN	Proosteocalcin
PTH	Parathyroid hormone
PTMs	Post-translational modifications
RAF	Rapidly Accelerated Fibrosarcoma
RANKL	Receptor activator of nuclear factor kappa-B ligand
RAS	Ras GTPase
RNA	Ribonucleic acid (RNA)
Runx2	Runt-related transcription factor 2
SDS	Sodium dodecyl sulfate
SNP	Single nucleotide polymorphism

SOST	Sclerostin
TAM	Tyrosine Axl MertK
TGF beta	Transforming growth factor beta
TGN	Trans Golgi network
TNF	Tumor necrosis factor
Twist 1	Twist-related protein 1
Twist 2	Twist-related protein 2
uchOCN	Uncarboxylated human osteocalcin
ucOCN	Uncarboxylated osteocalcin
Ucp1	Uncoupling proteins
ug	Microgram
VKORC1	Vitamin K oxido reductase
VWF	Von Willebrand factor
Wnt	Wingless
WT	Wild type
XLH	X-linked hypophosphatemia
ZFN	Zing finger nuclease

*To the wonderful people in my life
Who helped me to be the best version of myself*

Acknowledgments

The past five years were full of challenges and accomplishments. I am grateful to arrive at the end of this journey which could not have been possible without the support of many great persons at the academic and professional levels.

First, I would like to thank my mentor Dr. Mathieu Ferron for accepting me in his laboratory, for his supervision and continuous support. He helped me to improve my scientific knowledge and critical thinking. It was a great opportunity to work with a dedicated, motivated and enthusiastic researcher like him. He influenced my perspective in life, taught me how to achieve excellence in research, and introduced me to many influential people in my research field. He is a great mentor and a best friend. Yet, this work could not be achieved without the great supports of my colleagues in the lab and collaborators, which became family and friends. Thank you all for your contribution to this work and to my success in achieving my PhD. I am very thankful to Dr. Julie Lacombe for her supervision and critical advices, to Dr. Nabil Seidah and the members of his laboratory for their generosity and collaboration, to Mrs. Catherine Julien and Mrs. Jacqueline Chow, to Dr. Denis Faubert, to Mrs. Delia Susan-Resiga, to Dr. Rachid Essalmani, to Dr. Henrik Clausen and Dr. Yoshiki Narimatsu.

I am very appreciative to the members of my thesis jury for their commitment and precious time reading, evaluating, and correcting my thesis. Thank you, Dr. David Hipfner, Dr. Mike Sapieha, Dr. Frédérick Antoine Mallette and Dr. René St-Arnaud. I am also appreciative to my academic mentor Dr. Jean-Francois Cote for his support and advices, to Dr. Annik Prat, Dr. Murshed Monzur and Dr. Michel Tremblay for their advice and follow up during my past committee meetings. I would like also to thank Mrs. Virginie Leduc for her help in organizing my committee meeting and seminar, Dr. Richard Bertrand and Mrs. Liu Yan for their help during my journey at University of Montreal.

I would like to thank the Montreal clinical research institute (IRCM) staff and directors for their warm welcoming, their generosity, and their continuous effort to make the institute a good

place for all of us. Thanks to the animal facility and the IRCM core facility staff for their help and dedication. This work could not be achieved without the financial support of the university of Montreal, IRCM foundation, Fonds de recherche santé Quebec (FRQS), Montreal diabetes research center (MDRC) and the Canadian institute of health and research (CIHR).

I would also like to thank my welcoming family in Canada, Mathieu, Julie, Amélie, Catherine, Ashok, Jessica, Kevin and Céline for being there all the time. You made my journey easy and full of love. Thank you for the fruitful scientific and non-scientific discussions and the good times we spent together. Thanks to my lovely friends here in Montreal and back home for their supports and motivations. Ramzi, Hassan, Rami, Mohamed, Cedric, Julie, Stephanie, Vatsal, Nabil, Sabah, Nour, Hadla, Jalal, Farah, Islam, Rasheed, Saloua, Salwa, Nehme, Salma, Ahmed, Edwidge, Anne, Anna, Dhara, Wissam, May, Taghreed, Julian, Mr. Ayoub, Mr. Shalak, Dr. Usta and Dr. Nemer.

To the beautiful morning in all my morning, my great support in life, my protective soul, my mother and my wife. To my backbone and my awesome brother Alouch. I love you all. Thank you for everything you did to make my dream come true, hope the coming years bring all the best for all of us. To my dad, my great uncle and my beautiful cousin, you are always missed, your soul is always present to share with me the happy moments in life.

1. CHAPTER I

INTRODUCTION

1.1. PROTEIN POST-TRANSLATIONAL MODIFICATIONS

Multiple factors are involved in the diversity of living organisms. Protein synthesis from DNA involves two important processes: the transcription of DNA to messenger RNA (mRNA) and the translation of mRNA to proteins. Spatial-temporal gene expression, alternative splicing and epigenetics are some mRNA post-transcriptional modifications which diversify the translated proteins outcome. Furthermore, these proteins are subjected to post-translational modifications (PTMs) which help to determine their physical properties and biological functions. It is therefore estimated that although the human genome contains between 20,000-25,000 coding genes, more than one million different proteins can be generated from them.

There are more than 200 PTMs that have been reported and are involved in different cellular functions, such as protein folding, intracellular cell signaling, translocation, secretion, proteins interaction and gene expression. PTMs can be reversible, meaning that modified proteins can restore their native state, while irreversible modifications cannot be restored. These protein modifications include, but are not limited to, protein phosphorylation, methylation, acetylation, ubiquitination, gamma carboxylation and hydroxylation. In the next section, I will discuss the PTMs that are relevant to the work presented in this thesis.

1.1.1. Protein phosphorylation

Phosphorylated protein represents 30-50% of the proteome. It involves the addition of a phosphate group to the hydroxyl group of serine, threonine, or tyrosine residues. The addition of this covalent bond is catalyzed by protein kinases which require adenosine triphosphates (ATP) and magnesium ion (Mg^{2+}) as cofactors. In humans, there are around 518 identified kinases that are divided to 8 different families: AGC (protein kinases A, G, C family), CaMK (calmodulin dependent protein kinases), CK1 (casein kinases 1 or cell kinases 1), STE (sterile kinases), TK (tyrosine kinases), TKL (tyrosine kinases-like), RGC (receptor guanylate cyclase) and the CMGC family (including cyclin-dependent kinases (CDKs), mitogen-activated protein kinases (MAP kinases), glycogen synthase kinases (GSK) and CDK-like kinases) [1]. These kinases are involved in

the phosphorylation of myriad substrates and the regulation of different processes, such as regulation of enzymatic activity (e.g., HMG-CoA reductase, glycogen synthase, etc.), signaling pathway (e.g., AKT, IRS1, IRS2), transcription (e.g., NFATc1, Foxo1), cells proliferation and differentiation (e.g., MAPK, ERK, RAS, RAF, CDK), and receptor activation (e.g., Insulin receptor, TAM receptor). Phosphorylation is a reversible post-translational modification. Protein phosphatases restore the native state of phosphorylated proteins, allowing a molecular switch and dynamic regulation of the substrates. Protein phosphatases are divided into three different families, PPP (phosphoprotein phosphatases), PPM (metallo-dependent protein phosphatases) and PTP (protein tyrosine phosphatases) [2, 3].

1.1.2. Proteolytic cleavage

Proteolytic cleavage is an irreversible modification that involves the hydrolysis of peptide bonds. This modification implicates around 588 peptidases divided in two different families, exopeptidases and endopeptidases. Exopeptidases include the aminopeptidases and the carboxypeptidases which cleave the N-terminal and C-terminal of proteins respectively. Endopeptidases cleave the peptide bond inside the protein sequence and they are classified based on their catalytic sites to 5 different categories, metalloproteases, aspartic proteases, cysteine proteases, threonine proteases and serine proteases [4, 5].

Proteolytic cleavage is critical for many biological processes, such as protein maturation, enzyme activation and intracellular signaling, in which proteolytic cleavage occurs in a precise and specific manner. However, proteolysis can also be a damaging process that occurs during extracellular matrix degradation and the elimination of misfolded proteins. An example of metalloproteases is the MMP1 and ADAMTS13. MMP1 is a collagenase involved in the degradation of collagen in the extra cellular matrix (ECM), ADAMTS13 was found to cleave the blood clotting protein VWF [6, 7]. Cathepsins D and γ -secretase are two examples of aspartic proteases. Cathepsin D is a lysosomal protease that is also secreted by cells. It is involved in different functions, such as activation of other cathepsin precursors (Cathepsin B and L) and degradation of Apolipoprotein B [8, 9]. γ -secretase is involved in the maturation of the amyloid beta protein

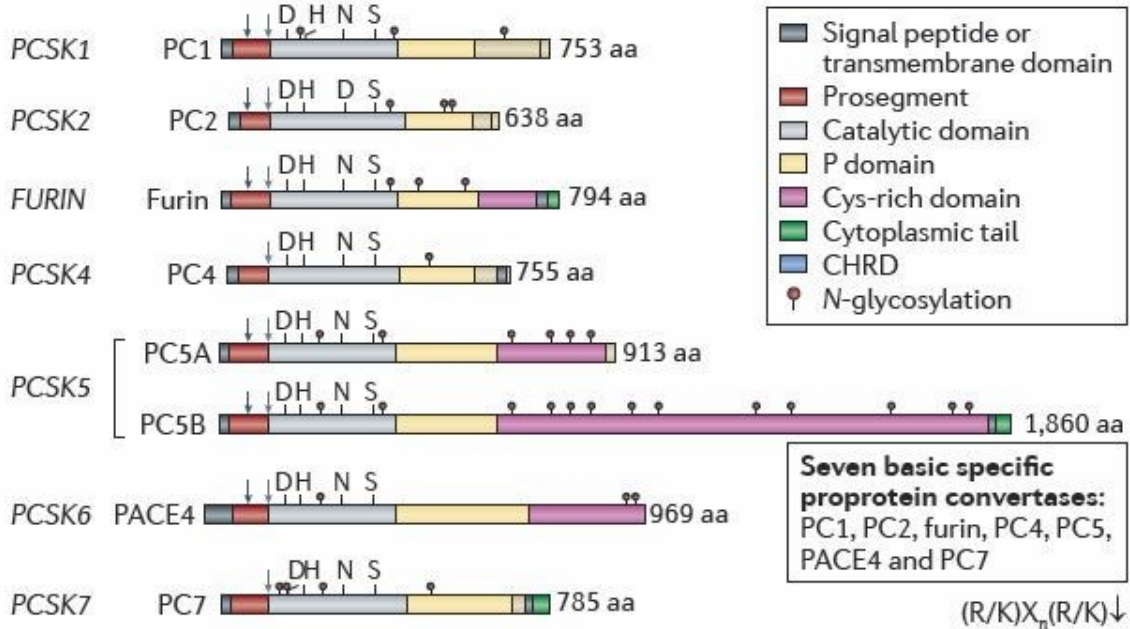
(A β), which is involved in the pathology of Alzheimer's disease [10]. Caspases are an example of cysteine proteases. They are synthesized in the inactive procaspases form and are involved in apoptosis, pyroptosis, inflammation and cellular differentiation. Following extrinsic or intrinsic apoptotic signals initiator, procaspases 8 or 9 are activated by autoproteolytic cleavage. Through their proteolytic domain, they activate executioner caspases 3 and 7 which mediate apoptosis and cell death signals [11]. Threonine proteases contain a threonine residue in its catalytic site and are found in the proteasome [12]. Serine proteases possess a serine residue in their catalytic site and are widely distributed in the nature and represent one third of the proteases [13, 14]. Examples of serine proteases are the coagulation factors. Following the activation of the coagulation cascade, the prothrombinases (factor Xa and Va) activate the prothrombin precursor and release the active enzyme [15]. Thrombin is a serine protease that catalyses the cleavage of factor XIII to XIIIa and fibrinogen to fibrin. Fibrin polymerization form a clot and stop the bleeding [16].

1.1.2.1. Proprotein convertases

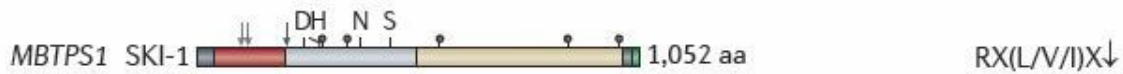
Proprotein convertases (PCs) are serine proteases. Based on MEROPS database (the database of proteolytic enzymes, their substrates and inhibitors) they are classified in the clan SB/subtilase family S8. The second largest family of serine peptidases is the S8 family and is divided into two subfamilies, S8A and kexin [13]. Proprotein convertase were first discovered because of their homology with yeast *kex2*, a calcium dependent serine protease which cleaves the pro- α -factor [17, 18]. They are a family of nine members classified into 3 categories, the Kexin-like, the pyrolysin-like, and the proteinase K-like (Figure 1-1) [19]. Kexin-like proprotein convertases cleave at the (R/K)X_n(R/K) \downarrow motif where (n) is equal to 0, 2, 4 or 6 amino acids. They contain seven members: PC1/3 (encoded by *PCSK1*), PC2 (encoded by *PCSK2*), furin (encoded by *PCSK3*), PC4 (encoded by *PCSK4*), PC5A and PC5B (encoded by *PCSK5*), PACE4 (encoded by *PCSK6*) and PC7 (encoded by *PCSK7*). SKI-1 (encoded by *MBTPS1*) belongs to the family of the pyrolysin-like subtilisin/kexin isoenzyme 1. It cleaves after the RX(L/V/I)X \downarrow , where X is not a cysteine or a proline residue. The proteinase K-like proprotein convertase subtilisin/kexin 9 does not cleaves substrates, it only cleaves itself after the (V/I/L)FAQ \downarrow .

Kexin-like

Gene



Pyrolysine-like



Proteinase K-like



Nature Reviews | Drug Discovery

Figure 1-1. Primary structure of proprotein convertases [19]

Structure of kexin-like, pyrolysine-like and proteinase K-like proprotein convertases. a.a: amino acid. D: Aspartic acid. H: Histidine. S: Serine. N: Asparagine. R: Arginine. K: Lysine. L: Leucine. V: Valine. I: Isoleucine. F: Phenylalanine. A: Alanine. Q: Glutamine. Single and double light gray and the dark gray arrow positions the primary and the secondary autocatalytic cleavage sites. P domain: a β -barrel domain that stabilize the catalytic domain. CHRD: Cys-His-rich domain which binds to heparan sulphate proteoglycans (HSPG).

Proprotein convertases are implicated in the proteolytic cleavage of proteins in the secretory pathways and extracellularly, leading to their activation or inactivation. PC1 and PC2 are localized in the secretory granules of classical endocrine cells and require acidic pH for optimal activity [20]. Furin acts in the cell surface and the *trans*-Golgi network. Endosomes facilitate its transport between these two compartments [21]. PC5B and PC7 have the same subcellular localization as furin. PC5A and PCAE4 bind the heparan sulfate proteoglycan (HSPG) and tissue inhibitor of metalloproteases [22]. SKI-1 does not localize to the cell surface. It is found in endosomes, lysosomes, *cis* and the mid Golgi network [23]. PCSK9 is a secreted protein with no enzymatic activity.

1.1.2.2. Furin

Furin is composed of 794 amino acids and encoded by the *FURIN* gene. It was discovered in 1986 because of its homology with *kex2*, a yeast endoprotease. Like other PCs, furin contains a signal peptide, a prosegment, a catalytic domain, a P domain, a cysteine rich domain (CRD), a transmembrane domain and a cytoplasmic tail (Figure 1-1). The signal peptide, which allows the trafficking of furin precursor (pro-furin) to the endoplasmic reticulum, is removed by signal peptidases. Furin prosegment contains in its C-terminus a dibasic motif, the autoproteolytic cleavage site of furin, which is important for furin folding and activation. The P domain is conserved among PCs and regulates their stability and their calcium and pH dependence. The furin C-terminus contains the cytosolic tail which controls its translocation between the *trans*-Golgi network (TGN), cell surface and endosomes.

The consensus site required for furin substrate cleavage is Arg-X-Lys/Arg-Arg↓ (where n=0, 2 or 4 amino acids). The maximum proteolytic activity occurs at pH between 5-8 and 1 mM of calcium concentration. Furin mediates its own activation (autoactivation) through autoproteolytic cleavage. In brief, the prodomain of furin is a chaperone responsible for the proper folding and activation of furin. Furin undergoes two sequential autoproteolytic cleavages in the endoplasmic reticulum and the TGN at the Arg107 and Arg75 respectively (Figure 1-2) [24]. Mature furin contains different motifs that mediates its intracellular trafficking to cell surface,

TGN, endosome and secretory granules. This distribution increases its access to a variety of substrate. Furin is implicated in the cleavage of a variety of substrates, such as transforming growth factor beta (TGFβ), parathyroid hormone, proalbumin, matrix extracellular phosphoglycoprotein (MEPE) and bone morphogenic protein 4 (BMP4) [25-27].

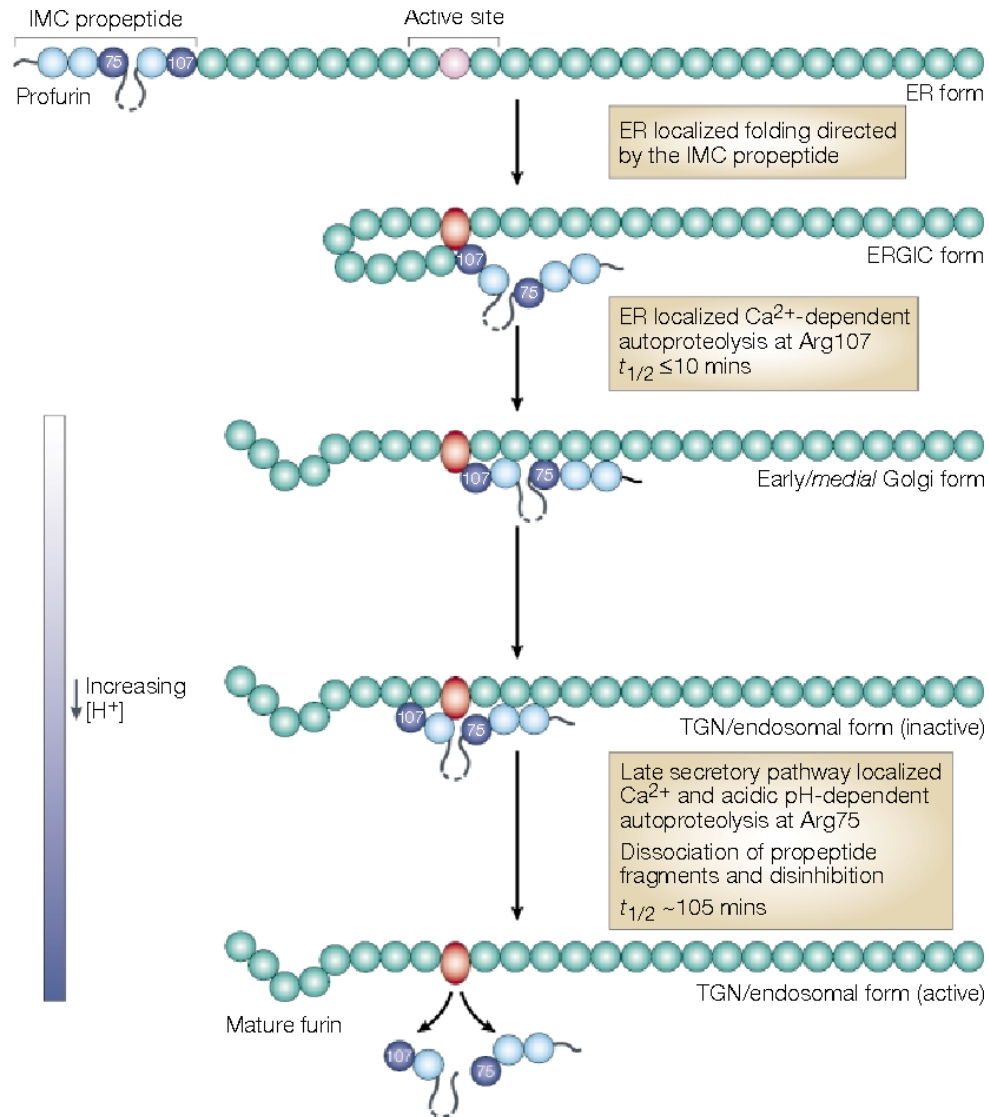


Figure 1-2. Furin autoactivation by autoproteolytic cleavage [21]

The catalytic site of profurin is in the inactive states (pink circle). The intramolecular chaperon (IMC propeptide) folding in the endoplasmic reticulum (ER) activates catalytic site (red circle) which cleaves its own propeptide at Arg107. The cleaved propeptide remains attached and inhibits furin activity. In late *trans*-Golgi network (TGN)/endosomes, the acidic pH allows the second propeptide autocleavage at Arg75 and the dissociation of the cleaved propeptide and the release of the active enzyme.

The global inactivation of the *Furin* gene in mice is embryonic lethal at embryonic day 10.5 (E10.5), due to a defect in heart ventral closure and axial rotation of the embryo [28]. This defect is associated with an abnormal expression pattern of *Pitx2* and *Lefty 1* and *Lefty 2* in the furin-deficient mice compared to control [29]. In situ hybridization at E7.5 revealed the expression of furin in the primitive endoderm, mesoderm, pericardial mesoderm and ectodermal cells of the epiblasts [28]. Despite the mouse lethality after *Furin* inactivation, which reflects its requirement for in vivo functions, and the widespread pattern of expression, few studies have addressed furin functions in vivo using conditional inactivation in specific tissues.

Mice deficient in furin in endothelial cells die 60 hours after birth as a result of cardiac malformation. Ex vivo culture of endothelial cells derived from these mice showed an impaired processing of endothelin-1, TGF β , BMP4 and adrenomedullin protein [27]. Loss-of-function mutations in BMP4 in mice exhibits similar cardiac abnormalities observed following the inactivation of furin in endothelial cells [30]. The deletion of *Furin* in macrophages and granulocytes does not have any consequences. However, furin deficiency in T cells enhance skin cancer progression and impair the function of effector and regulatory T cells [31, 32]. In liver furin was shown to inactivate PCSK9 processing, where furin inactivation in hepatocytes resulted in increase in PCSK9 and a decrease in LDL receptor [33]. In pancreatic β -cells *Furin* deletion alters the pH in the secretory granules by impairing the processing of the proton pump AC45, resulting in impaired pro-PC2 processing and reduced insulin secretion [34].

1.1.2.3. The proprotein convertase subtilisin/kexin type 5

The gene encoding PC5A and PC5B, *PCSK5*, was discovered in 1993 by Lusson *et al.* PC5A and PC5B are products of alternative splicing of the same gene: *PCSK5*. They share the first 20 exons. The main difference is exon 21 of PC5A which is replaced by 18 additional exons in PC5B (Figure 1-3) [35]. The first 20 exons encode the signal peptide, the prodomain, the catalytic domain, the P domain and the cysteine rich domain (CRD) in exon 21. The additional 18 exons in PC5B encodes for a longer CRD, a transmembrane domain, and a cytosolic tail, which confer PC5B

the ability of intracellular trafficking [35]. PC5A is secreted and interacts with the HSPG through its CRD domain [22].

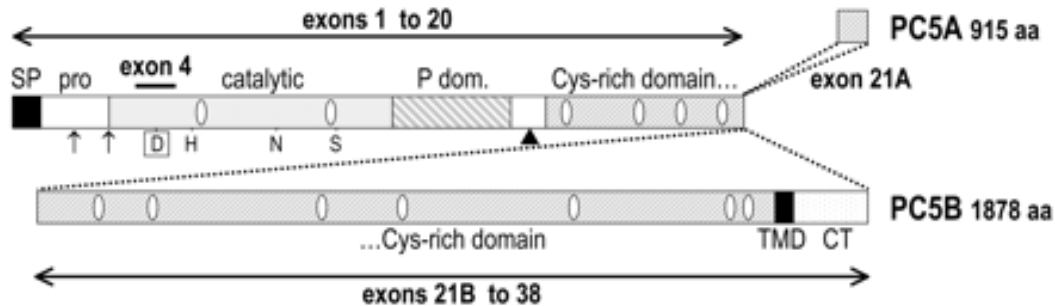


Figure 1-3. PC5A and PC5B: product of alternative splicing of the PCSK5 gene [35]

The first 20 exons of *Pcsk5* gene encodes the signal peptide (SP), prosegment (pro), the catalytic, P domain and the N-terminal part of the Cys-rich domain which are common for PC5A and PC5B. Exon 21A is specific to PC5A, while PC5B has 18 additional exons (exons 21B to 38). Additional exons in PC5B encodes for a longer Cys-rich domain (CRD), a transmembrane domain (TMD) and a long cytosolic tail (CT). The catalytic triad contains aspartic acid (D), Histidine (H), Serine (S) and the oxyanion asparagine (N). Autocatalytic cleavage sites are indicated with arrows while the intracellular cleavage site is pointed with arrows head. N-glycosylation sites are labeled with white ellipse.

In situ hybridization showed that *Pcsk5a* is dominantly expressed in the adrenal glands, ovary, lung, uterus, brain cortex, muscle, heart, aorta, stomach, spleen, testis, pituitary and cerebellum. PC5B is dominantly expressed in the kidney, jejunum and ileum [35]. Mice deficient in PC5A/B die at E18.5 [36, 37]. They have an altered anteroposterior patterning, extra vertebrae and lack tails. This phenotype is dependent on growth/differentiation factor 11 (Gdf11), which is not properly processed in the knockout mice [36]. These mice also exhibit a Gdf11 independent phenotype characterised by a smaller size, abnormal ossification, severe retardation, abnormal sternum and symphysis of pubic bones [36]. PC5 was also shown to be required for early heart development [38]. *Pcsk5* inactivation in the enterocytes of *ApcMin/+* mice, which have adenocarcinoma in the intestinal tract, increase the tumor number, suggesting that PC5/6 plays a protective role against tumorigenesis in the intestine [39].

1.1.3. Glycosylation

Protein glycosylation involves the addition of glycan groups to specific amino acids and occurs in eukaryotes and some prokaryotes [40]. The diversity of glycan structure, composition, length and the type of the glycosidic linkage increase the diversity of the proteome. Different types of glycosylation occur in mammalian cells. These include *N*-glycosylation, *O*-glycosylation, C-mannosylation, phosphoglycosylation and glypiation. The glycosylation process occurs mainly in the endoplasmic reticulum and the Golgi apparatus. Protein glycosylation plays crucial roles in different cellular processes, such as protein folding and secretion, protein anchoring to the membrane, antigen specificity, tumor cell invasion, cells signaling and many others.

1.1.3.1. *N*-glycosylation

N-glycosylation was first found in ovalbumin [41] and involves the addition of carbohydrates to the nitrogen of an asparagine (Asn) residue located in the *N*-glycosylation consensus motif (*Asn-X-Ser/Thr*). This modification is initiated in the endoplasmic reticulum and continued in Golgi apparatus. It involves different steps, glycan assembly, attachment, trimming and maturation. During the glycan assembly catalysed by glycosyltransferase, the *N*-acetylglucosamine (GlcNAc), glucose (Glc) and mannose (Man) are linked to the dolichol pyrophosphate (Dol-PP), a lipid anchored in the ER surface [42]. The next step involves the transfer and the attachment of the glycan bulk composed of Glc₃Man₉GlcNAc₂-PP-Dol to a specific Asn residue in the nascent polypeptide, a process that occurs in the ER lumen and that is mediated by the oligosaccharide transferase (OST) [43]. Glycan trimming occurs in the ER to ensure proper protein folding and it is continued in the cis-Golgi. In the ER, trimming is mediated by the α -glucosidase I and II and the ER- α -mannosidase. It involves the removal of three glucose molecules and one mannose residue (reviewed in [44]). After the removal of two glucose molecules, monoglucosylated peptides are recognized by the lectin chaperone calnexin and calreticulin which ensure the proper protein folding before the removal of the third glucose molecule. Following the release of the third glucose molecule, the glycoprotein is transferred from the ER to the cis-Golgi. Misfolded glycoproteins are recognized by the UDP-glucose:glycoprotein glucosyltransferase enzyme which glucosylates the protein to re-enter the lectin cycle and ensure

proper folding (reviewed in [45]). *N*-glycosylated protein maturation occurs in the Golgi through a process of trimming and addition of other glycan, such as the addition of *N*-acetylglucosamine and the removal of mannose. The maturation process is ended by capping which involves the addition of fucose, *N*-acetyl neuraminic acid, galactose and *N*-acetylgalactosamine [46].

1.1.3.2. *O*-glycosylation

Protein *O*-glycosylation is the addition of carbohydrates to the hydroxyl group of serine and threonine residues. Other amino acids such as tyrosine, hydroxyproline and hydroxylysine can also be *O*-glycosylated. Attached carbohydrates include the *N*-acetylgalactosamine (GalNAc), *N*-acetylglucosamine (GlcNAc), glucose (Glc), fucose (Fuc), mannose (Man) and galactose (Gal). The type of *O*-glycosylation is determined by the type of glycosidic bond and the attached carbohydrate (Table 1-1).

Mucin type *O*-glycosylation is named after mucin, a protein located on the surface of epithelial tissues, which was found to be *O*-glycosylated. Mucin type *O*-glycosylation occurs for a variety of proteins in the Golgi compartment and involves different steps catalysed by a number of glycosyltransferases. These steps are initiation, extension and capping (Figure 1-4) [47]. Unlike *N*-glycosylation, the *O*-glycosylation initiation step requires the addition of *N*-acetylgalactosamine to the hydroxyl group of a serine or threonine. This process is catalyzed by the polypeptide-*N*-acetyl-galactosaminyltransferases (ppGalNAcTs, or GalNAc-Ts) (Figure 1-4), a family of twenty different enzymes in human, and requires UDP-GalNAc as a substrate for the reaction (reviewed in [48]). The consensus *O*-glycosylation site of these enzymes is poorly understood. In vitro glycosylation assays using synthetic peptides showed that GalNAc-T1 and GalNAc-T2 have preference for proline residue at the position -1, +1 and +3 of the Ser/Thr glycosylation sites [49]. GalNAc-T7 and GalNAc-T10 prefer previously *O*-glycosylated peptide as substrates [50].

Table 1-1. Different glycosidic bonds occurring in mammalian cells

Glycosidic bond	O-glycosylation type	Example	Ref.
<i>GalNAc-α-Ser/Thr</i>	Mucin type	FGF23	[51]
<i>GlcNAc-β-Ser/Thr</i>	GlcNAc type	Epidermal Growth Factor, (EGF)	[52]
<i>Man-α-Ser/Thr</i>	Man type	Dystroglycans, brain glycoprotein	[53]
<i>Fuc-α-Ser/Thr</i>	Fuc type	Epidermal Growth Factor, (EGF)	[52]
<i>Glc-β-Ser</i>	Glc type	Epidermal Growth Factor, (EGF)	[52]
<i>Xyl-β-Ser</i>	Xyl type	Heparan sulfate glycosaminoglycan	[54]
<i>Gal-β-Hyl</i>	Gal type	Collagen	[55]
<i>Glc-α-Tyr</i>	Glc type	Glycogenin	[56]

Glycan elongation is a multistep process catalyzed by different enzymes (Figure 1-4). Core 1 β 1-3 galactosyltransferase C1GalT-1 or T synthase which adds a galactose residue and form core 1 adduct. Core 1 is further elongated by the addition of *N*-acetylglucosamine, a reaction catalysed by core 2 β 1-6 *N*-acetylglucosaminyltransferase C2GnT-1 and C2GnT-3. Core 3 and core 2/4 involves the addition *N*-acetylglucosamine to the Tn antigen catalysed by the β 1-3 *N*-acetylglucosaminyltransferase β 3GnT-6 and β 1-6 *N*-acetylglucosaminyltransferase C2GnT-2. *O*-glycosylation termination involves the addition of fucose or *N*-acetyl neuraminic acid (sialic acid). A process that is catalysed by the core 1 α 2-3 sialyltransferase ST3Gal I and ST3Gal IV, α 2-6 sialyltransferase ST6GalNAc (I, II, III, IV), Core 1 3-O-sulfotransferase Gal3ST4, secretor gene α 1-2 fucosyltransferase [48].

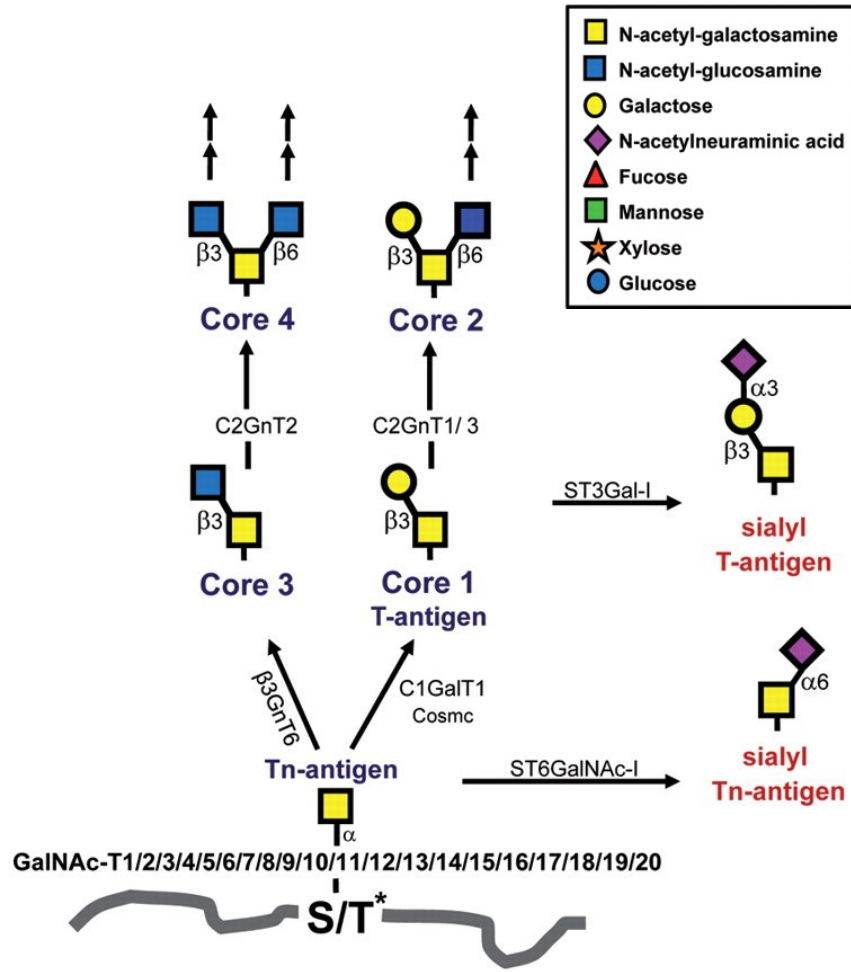


Figure 1-4. Different mucin-type O-glycosylation cores [48]

O-glycosylation core 1-4 formation is initiated by the addition of GalNAc catalysed by the GalNAc-Ts, a family of 20 members in human. Tn-antigen is elongated by the core 1 synthase (C1GalT1) and core 3 synthase (β 3GnT-6). Core 1 synthase requires the chaperon protein Cosmc. Core 1 and 3 are further elongated by C2GnT2 and C2Gnt1/3 respectively. The different cores branching can be terminated by the addition of fucose and sialic acids. Premature sialylation structure (labeled in red) are found in different type of cancer.

1.2. BONE BIOLOGY

For many years, bone has been considered as a tissue providing skeletal support and protecting organs, such as heart, lungs and brain. More than 200 bones with different shape and length fulfill those functions and draw the human shape [57]. However, bone is a living organ that undergoes physiological changes during development and aging, integrates with other tissue (i.e., muscles and fat), houses the bone marrow, and stores minerals. These functions of bone emphasize its dynamic aspect and the necessity of crosstalk with the surrounding environment.

The human skeleton is composed of two major types of bone: appendicular and axial bone. Each type of bone is composed of spongy bone (trabecular bone) surrounded by the compact bone (cortical bone) of the periosteum. Trabecular bones have a honeycomb like structure and harbor the bone marrow. The percentage of cortical versus trabecular bone can vary depending on the type of bone. For instance, long bone is composed of different percentages of cortical and trabecular bone (Figure 1-5). The upper and lower epiphysis are composed of 50:50 % of cortical/ trabecular bone. The diaphysis is composed of 95:5 % of cortical/ trabecular bone and houses the bone marrow. The diaphysis is separated from the epiphysis by the metaphysis which contain the growth plate.

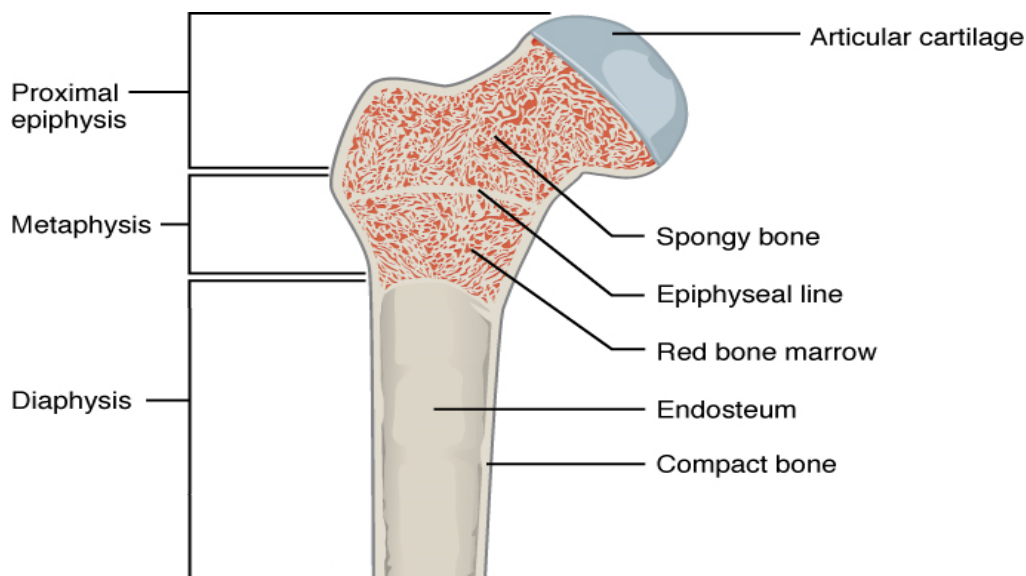


Figure 1-5. Anatomy of long bone modified from [57]

1.2.1. Bone physiology and components

Bone formation and remodelling involves three different cell types: chondrocytes, osteoblasts and osteoclasts. Chondrocytes and osteoblasts are derived from mesenchymal stem cells. They are involved in bone formation through endochondral and intramembranous ossification. Osteoclasts are derived from the hematopoietic stem cells; they differentiate from monocytes and mediate bone resorption, an important step in bone remodeling.

Bone tissues are formed through two different ossification processes: endochondral ossification and intramembranous ossification. Endochondral ossification occurs in most of the skeletal elements. It is initiated by the skeletal patterning through the condensation of mesenchymal cells (Figure 1-6). Mesenchymal cells in the periphery give rise to perichondrium, which secretes type I collagen. The central cells differentiate into pre-hypertrophic chondrocytes secreting type II collagen. These pre-hypertrophic cells then exit the cell cycle and secrete collagen type X, forming hypertrophic chondrocytes, the cartilage cells of the diaphysis [58, 59]. In parallel to that process, perichondrium cells differentiate to osteoblasts following *Runx2* expression [60], which give rise to the collar bone and become the periosteum. The extracellular matrix surrounding the hypertrophic chondrocytes, which undergoes apoptosis, is mineralized and vascularized, allowing the invasion of osteoblasts progenitors and hematopoietic progenitors from the periosteum and the formation of bone marrow. This process continues longitudinally in the secondary ossification center. The adjacent chondrocytes continue to mineralize and undergoes apoptosis. Myeloid derived osteoclasts allow the resorption and more vascularisation [61]. This process allows longitudinal bone growth and the formation of the growth plate. Intramembranous ossification occurs in the periosteum and in flat bones and does not require cartilage formation like endochondral ossification. It involves the direct differentiation of mesenchymal cells to pre-osteoblasts and osteoblasts which then mineralize. However, intramembranous ossification forms woven bone composed of irregular collagen fiber which is replaced by lamellar fiber through bone remodeling.

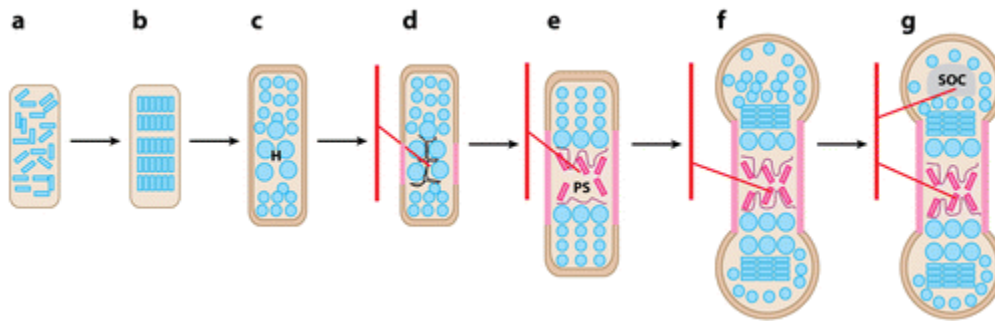


Figure 1-6. Schematic representation of endochondral bone formation [62]

Condensation of mesenchymal cells labeled in blue (a), differentiation to chondrocytes and proliferation (b), differentiation of hypertrophic chondrocytes (H) (c), differentiation of perichondrial cells to osteoblasts and formation of bone collar labeled in pink and apoptosis of hypertrophic chondrocytes (d), vascular invasion and formation of primary ossification center, primary spongiosa (PS) (e), longitudinal growth (f), formation of secondary ossification center (SOC) (g) [62].

1.2.2. Regulation of osteoblasts differentiation

Osteoblasts and chondrocytes share the same mesenchymal cell progenitors. However, specific transcriptional programs and precise signals triggers the formation of osteoblasts. After differentiation, osteoblasts secrete the extracellular matrix (ECM) proteins, such as collagen, osteopontin, bone sialoprotein, alkaline phosphatase and osteocalcin. Mineralisation involved the deposition of minerals to ECM proteins. In addition, differentiated osteoblasts support the differentiation of osteoclasts through the secretion of macrophage colony stimulating factor (M-CSF) and receptor activator of nuclear factor kappa-B ligand (RANKL).

1.2.2.1. Transcriptional regulation of osteoblasts differentiation

Runt-related transcription factor 2 (Runx2), also known as core-binding factor subunit alpha-1 (Cbfa1), is the master regulator of osteoblasts differentiation [60]. It activates the transcription of osteoblastic genes involved in ECM formation. Mice lacking both alleles of *Runx2* have osteogenesis defects caused by the absence of osteoblasts, resulting in a cartilaginous skeleton [63]. Heterozygous mice exhibit mineralization defects, ossification in the parietal, interparietal and supraoccipital bones. They also have hypoplastic calvicles and nasal bones [63]. Mutations in *Twist-1* and *Twist-2*, two nuclear protein with helix-loop-helix structure, were found

in patients with Saethre-Chotzen syndrome, a bone disease characterized by craniosynostosis, facial dysmorphism and soft tissue syndactyly [64, 65]. Mechanistic studies showed that these proteins inhibit osteoblast differentiation and *Runx2* expression (Figure 1-7) [66]. At the protein level, Runx2 is subjected to proteasomal degradation through ubiquitination. The zinc finger adapter protein Schnurri-3 (Shn3) favors the interaction of Runx2 with WW domain containing protein 1 (WWP1), which targets Runx2 to ubiquitination (Figure 1-7) [67].

Osterix (*Osx*) is another transcription factor regulating osteoblasts differentiation. It belongs to the family of zinc-finger protein and acts downstream of Runx2 (Figure 1-7). *Osx* interacts with the nuclear factor of activated T cells 1 (NFATc1) and activates the transcription of genes, such as collagen type 1 alpha 1 (*Col1a1*) (Figure 1-7) [68, 69].

The activating transcription factor 4 (ATF4) is a transcription factor and an important regulator of osteoblasts differentiation. It belongs to the family of cAMP response element-binding protein (CREB). This transcription factor is enriched in osteoblasts [70, 71] and promotes osteoblast differentiation. The deletion of its coding gene in mice resulted in bone formation defects and bone loss [72]. Recent studies showed that ATF4 is involved in ER-stress response and protects against neuronal death in Parkinson disease [73-75]. ATF4 is a substrate for the growth factor-regulated kinase RSK2 (Figure 1-7) [72]. Its transcriptional activity is also regulated by the interaction with other proteins. For instance, the interaction with the special AT-rich binding protein 2 (SATB2) enhances the interaction of ATF4 with its DNA binding site [76]. ATF4 dimerization with the inducible cAMP early receptor (ICER) and with the factor inhibiting ATF4-mediated transcription (FIAT) was shown to inhibit ATF4 transcription activity [77-80]. This inhibitory effect is further enhanced through the interaction of the nascent polypeptide-associated complex and coactivator alpha (α NAC) with the FIAT-ATF4 complex [81].

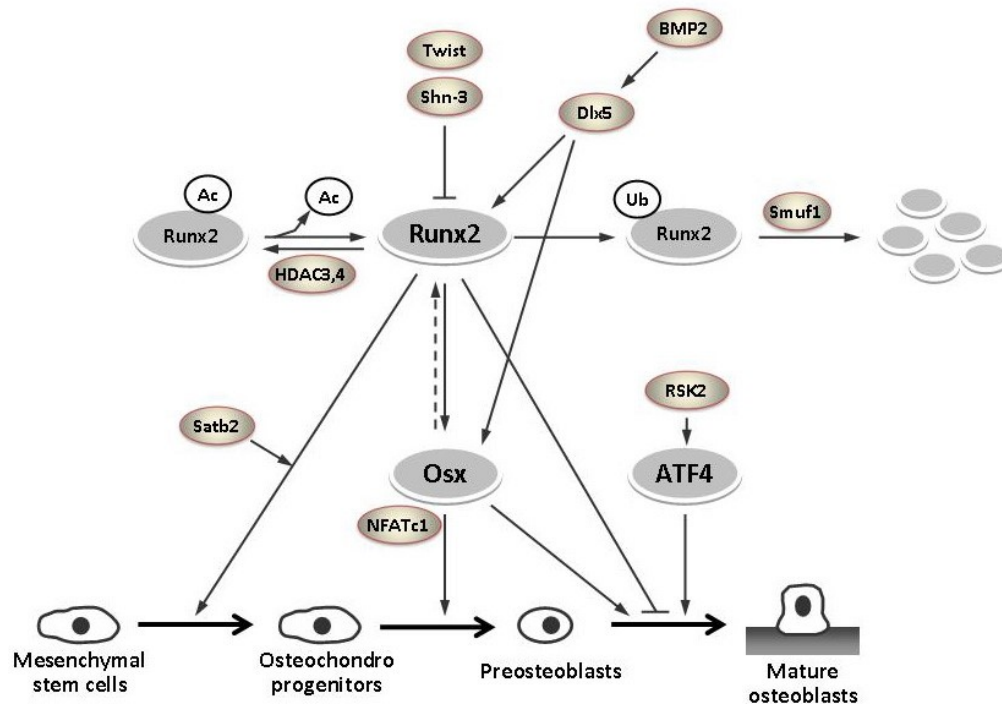


Figure 1-7. Regulation of osteoblasts differentiation by transcription factors [82]

Runx2 is a master regulator of osteoblasts differentiation. Twist inhibit *Runx2* gene expression while Shn3 target Runx2 to ubiquitination. The homeobox protein Dlx5 is induced by the bone morphogenic protein BMP2 and it promotes *Runx2* gene expression. *Osx* acts downstream Runx2 where it interacts with NFATc1. *Satb2* enhance Runx2 and ATF4 DNA binding. ATF4 is also regulated by RSK2.

1.2.2.2. Regulation of osteoblast differentiation by autocrine and paracrine signals

Multiple signals are implicated during osteoblasts commitment and differentiation. These signals include Indian Hedgehog (Ihh), fibroblast growth factor 18 (FGF18), bone morphogenic protein (BMPs) and wingless (Wnt) signaling. Ihh signaling through its receptor Patched 1 is required for chondrocytes formation and osteoblast differentiation. Mice deficient in *Ihh* are deprived of osteoblasts formation and Runx2 expressing cells [83]. FGF18 signaling through the FGFR2 receptor is crucial for osteoblasts differentiation [84]. Bone morphogenic protein plays an important role in early skeletogenesis. It mediates the skeletal patterning through the condensation of mesenchymal stem cells [85]. Wnt signaling through the frizzled receptor and the LDL receptor-related protein receptor 5 (*Lrp5*) activates beta catenin, a signaling pathway that is required for osteoblast differentiation and bone formation. Consistently, *Lrp5* gene inactivation

in osteocytes resulted in increased bone loss [86-89]. Lrp5 was also suggested to regulate bone mass through its expression in the intestine, where it regulates the production of serotonin [90]. Furthermore, osteoblasts secrete signaling molecules that regulates osteoclasts differentiation, such as MCSF and RANKL, which stimulates and osteoprotegerin (OPG), which blocks, differentiation (Reviewed in Xu *et al.* [91]).

1.2.2.3. Neuroendocrine signals regulating osteoblasts differentiation

The receptors of many neuropeptides, such as glutamate receptor (NMDA), calcitonin gene-related protein (CGRP), vasoactive intestinal peptide (VIP) and substance P receptor are expressed in bone, suggesting a potential role of these neuropeptides in the regulation of osteoblast differentiation [92-95]. Glutamate or NMDA treatment was shown to stimulate intracellular calcium release and depolarisation of osteoblasts [96], while partial inhibition of the glutamate receptor iGluRs in osteoblasts was shown to inhibits their differentiation [97, 98]. However, glutamate transporter (Glast) deficient mice did not show bone defects [99]. Moreover, CGRP was shown to induce cAMP formation and potassium efflux in osteoblastic cells line UMR-106-01 [100, 101]. Additional studies in vivo showed that CGRP transgenic mice had an increase in bone density, while mice deficient in alpha CGRP developed osteopenia [102, 103]. The adipocytes derived hormone leptin, which increases with obesity, was shown to inhibit bone formation through a hypothalamic signal acting on beta adrenergic receptor in osteoblasts [104, 105]. Additional studies suggested that leptin acts directly on osteoblasts to promote bone formation [106-108].

1.2.3. Osteocytes

Osteocytes compose 95% of residing bone cells and have an average life span of 25 years in human. They are derived from terminally differentiated osteoblasts embedded in the matrix lacuna [109]. The mechanism by which osteoblasts transition to osteocytes is yet unknown. E11 protein, also called podoplanin, was shown to be highly expressed in early embedded osteocytes. Osteocyte maturation requires the downregulation of osteoblast markers, such as bone sialoprotein, collagen and alkaline phosphatase [109, 110]. On the other hand, another set of

genes are upregulated, such as dentin matrix protein 1 (*DMP1*), phosphate-regulating endopeptidase homology X-linked (*PHEX*), matrix extracellular phosphoglycoprotein (*MEPE*) and sclerostin (*SOST*) which compose a gene signature of mature osteocytes (figure 1-8) [109, 111].

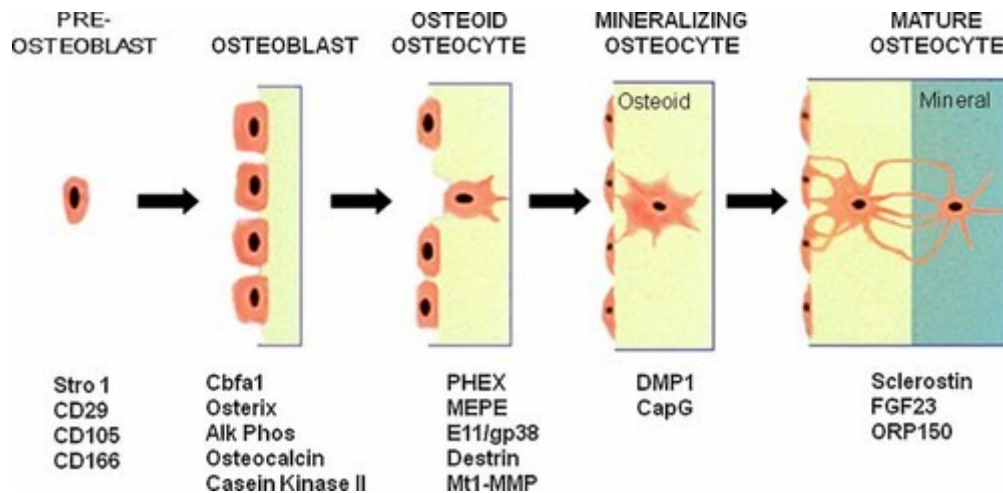


Figure 1-8. Differentiation markers during transition from osteoblasts to osteocytes [112]

An interesting feature of osteocytes is its potential of synchronized communication through their canaliculi, a process mediated through Gap junctions. These canaliculi serve as a canal to supply nutrients and oxygen for osteocytes. The interstitial fluid present in the canaliculi provides mechanosensory properties to osteocytes. Mechanical stimuli activates Wnt/beta catenin signaling in osteocytes, mediating osteocytes survival [113-115], whereas the decrease in mechanical loading leads to their apoptosis [116]. Osteocytes in the apoptotic state act as a signal for the recruitment of osteoclasts and bone resorption. Osteocytes derived RANKL and osteoprotegerin (OPG) control osteoclasts differentiation and activation of bone resorption in adult mice [117, 118].

1.2.4. Paracrine and endocrine functions of osteoblasts and osteocytes

The paracrine and endocrine function of osteoblasts and osteocytes is an important aspect of their biology that was not covered in the previous sections. Osteoblasts and osteocytes secrete many peptides which can act locally, in a paracrine fashion, and regulate the function of neighbouring cells. For instance, osteoblasts and osteocytes secrete RANKL, M-CSF and OPG,

three important modulators of osteoclastogenesis [117, 119-123]. RANKL and M-CSF stimulate osteoclast differentiation. The decoy receptor OPG blocks this process by blocking RANKL binding to its receptor RANK. Sclerostin is secreted by the mature osteocytes and blocks Wnt/ beta catenin signaling resulting in the inhibition of osteoblast differentiation [124]. It also stimulates osteoclast formation in a RANKL dependent pathway [120]. Wingless proteins WNT5A and WNT16 are two osteoblasts derived signals regulating osteoclastogenesis [113, 125, 126]. WNT5A was shown to promote osteoclastogenesis by stimulating the expression of RANK, the receptor of RANKL in osteoclasts. However, WNT16 modulates RANK signaling. It increases the expression of the decoy receptor OPG in osteoblasts, resulting in the inhibition of osteoclastogenesis indirectly. Vascular endothelial growth factor (VEGF) is secreted by osteoblasts. It regulates angiogenesis in bone and controls osteoblasts differentiation and osteogenesis [127-129].

Osteoblasts and osteocytes also secrete peptides into blood circulation that act in an endocrine fashion. These bone-derived hormones or “osteokines” (a term coined by the group of Dr. Ferron) include so far osteocalcin, lipocalin 2, sclerostin and fibroblast growth factor 23 (FGF23). Beside the discovery of osteocalcin endocrine function that will be discussed in the next sections, the ablation of osteoblasts and osteocytes further emphasizes the role of bone in the regulation of body metabolism and suggests the presence of additional osteokines. Osteoblasts ablation in vivo using diphtheria toxin results in metabolic defects, such as decrease in insulin level, increased blood glucose and food intake [130]. Additional studies showed that a body weight homeostat regulates fat mass through the regulation of appetite independently of leptin. This effect was abolished following osteocytes ablation [131].

Osteocalcin is secreted by osteoblasts. It regulates glucose and energy metabolism, male fertility, cognition, memory, muscle gain and exercise capacity. Lipocalin 2 is an osteoblast derived hormone regulating glucose and energy metabolism. It improves glucose tolerance, insulin secretion and sensitivity. Lipocalin 2 crosses the blood brain barrier and suppresses food intake through the melanocortin 4 receptor anorexigenic dependant pathway [132]. Fibroblast growth factor 23 (FGF23) is secreted by differentiated osteoblasts and osteocytes. It is a phosphaturic

peptide “phosphatonin” regulating phosphate reabsorption and vitamin D production in the kidney proximal tubule. Osteocalcin and FGF23 structure, endocrine function and regulation will be discussed in more detail in the next sections, since these two hormones are a major focus of the current thesis.

1.3. OSTEOCALCIN

Vitamin K-dependent carboxylation was first identified in the coagulation factors, including prothrombin, factor VII, factor IX, and factor X [133]. In 1975 Price *et al.* characterized a carboxylated (Gla) proteins in bone, this protein possesses carboxylglutamate residues and bind to the hydroxyapatite in mineralized tissue [134, 135]. Later in 1982 Haushka and Carr predicts the first osteocalcin structural model composed of two α -helical structure linked by a β -turn and stabilized by a disulfide bridge [136]. Osteocalcin is the most abundant non-collagenous protein in the bone ECM. Years after its discovery, the endocrine function of osteocalcin was elucidated. It was shown to regulates the function of multiple tissues including pancreas, liver, muscle, brain and fat. In the next section, osteocalcin structure and functions will be discussed in more details.

1.3.1. Osteocalcin structure

Osteocalcin is a small protein composed of 46 amino acids in mouse. Using mouse osteocalcin cDNA as a probe, hybridization with mouse genome revealed that mouse osteocalcin is encoded by two genes [137]. These genes are located next to each other on chromosome 3 and share 96% sequence identity. Osteocalcin gene 1 (*Bglap*) and osteocalcin gene 2 (*Bglap2*) share sequence similarity in their promoter which is not conserved in the third gene called osteocalcin related gene (*Bglap3*) [137]. The difference in the promoter sequence suggests that *Bglap* and *Bglap2* are expressed in the same tissue, but not *Bglap3* [137]. *Bglap* and *Bglap2* are expressed specifically in bone. *Bglap3* is expressed in kidney and represents 1% of *Bglap* and *Bglap2* expression level in bone. Osteocalcin specific element 1 (OSE1) and osteocalcin specific element 2 (OSE2) are two *cis*-acting elements controlling the expression of osteocalcin genes, OG1 and OG2 [138]. RUNX2 is a transcription factor that bind to OSE2 element, whereas ATF4 binds to OSE1 element [60, 139].

Human osteocalcin is composed of 49 amino acids and is encoded by a single gene, *BGLAP* located on chromosome 1. It shares sequence homology with osteocalcin in mice and other vertebrates (Figure 1-9). Osteocalcin is synthesized as a pre-pro-protein which undergoes sequential cleavage to remove the endoplasmic signal peptide and the pro-peptide [140]. In the ER osteocalcin also gets gamma-carboxylated on three of its glutamic acid residues, which are highly conserved between bony vertebrates [141]. These residues are labeled with yellow in figure 1-9.

<i>Homo sapiens</i>	YLYQWLGAPVPYDPDPLEPRRE VCE LNPDCDELADHIGFQEAYRRFYGPV--
<i>Mus musculus</i>	YL----GASVPSPDPLEPTRE QCE LNPACDELSQYGLKTAYKRIYGITII-
<i>Rattus norvegicus</i>	YLNGLGAPAPYDPDPLEPHRE VCE LNPNCDELADHIGFQDAYKRIYGTTV-
<i>Bos taurus</i>	YLDHWLGAPAPYDPDLEPKRE VCE LNPDCDELADHIGFQEAYRRFYGPV--
<i>Gallus gallus</i>	HYAQDSGVAGAPPNPLEAQRE VCE LSPDCDELADQIGFQEAYRRFYGPV--
<i>Xenopus tropicalis</i>	SYRYNVARGAAVTSPL ESQRE VCE VCE LNPDCDELADHIGFQEAYRRFYGPV--
<i>Sus scrofa</i>	YLDHGLGAPAPYDPDLEPRRE VCE LNPDCDELADHIGFQEAYRRFYGIA--
<i>Rana catesbeiana</i>	SNLRNAVFGTPVRDPLESKRE VCE LNPSCDELADHIGFQEAYRRFYGPI--
<i>Chelonia mydas</i>	NYVYKRFY---IIDPLE GKRE ICE VCE LNPDCDELADHIGFHKAYRRYYGAV--
<i>Felis catus</i>	YLAPGLGAPAPYDPDLEPKRE ICE LNPDCDELADHIGFQDAYRRFYGTV--
<i>Danio rerio</i>	AG---TAPGDLTPFQLE SLRE VCE VCE TNVACEHMMDTSGIITAYKTYGPIPF
	** ** * . *:: * *: **: **

Figure 1-9. Mature osteocalcin amino acid alignment

An asterisk indicates a fully conserved residue; a column indicates a strongly conserved residue; a dot indicates moderate or weak conservation.

Crystal structure analysis of porcine osteocalcin, which has 65% homology with the human and bovine osteocalcin, shows that mature osteocalcin is composed of three alpha helical structure surrounding a hydrophobic core (labeled with triangle in figure 1-10) and a disulfide bridge between cysteine 23 and cysteine 29 located in helix alpha 1 and helix alpha 2 respectively. Gamma-carboxylated glutamic acid residues (Gla 17, 21 and 24, labeled with γ in figure 1-10) and an aspartic acid residue (Asp30), located in the helix alpha 1 and helix alpha 2 respectively, forms a calcium binding pocket which binds five calcium ions (labeled with circle in figure 1-10) [142].



Figure 1-10. Secondary structure of porcine osteocalcin [142]

Alpha helical structures are labeled in red. Hydrophobic cores are labeled with triangle. The cysteine 23 and cysteine 29 involved in the disulfide bridge are labeled in yellow. Gamma-carboxylated glutamic acid residue (Glu 17, 21 and 24) are labeled with γ . Calcium binding pocket which binds five calcium ions are labeled with circles.

Calcium binding was shown to induce conformational changes in osteocalcin. These changes were predicted to be different from osteocalcin bound to hydroxyapatite [143]. Uncarboxylated osteocalcin (Glu) from bovine, which is not bound to calcium, showed that the alpha helical structure of osteocalcin is independent of calcium binding (Figure 1-11) [144].

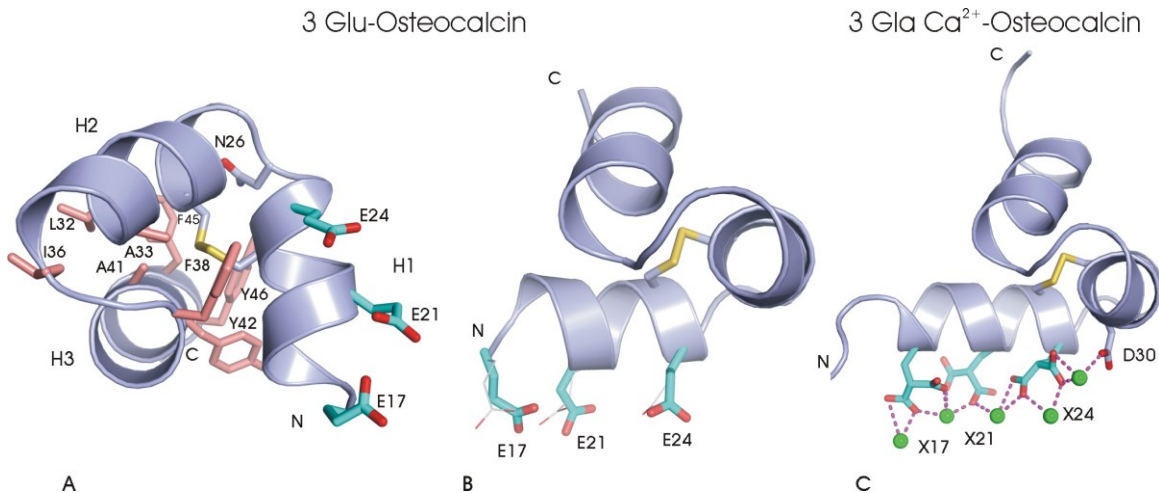


Figure 1-11. Uncarboxylated (Glu) and carboxylated (Gla) osteocalcin crystal structure [144]

(A and B) Structure of Bovine Glu-OCN structure. H1–H3 are the main helices, C23–C29 in yellow are the disulfide bond, salmon color represents the hydrophobic interaction (A). Glu residues are represented in cyan color (B). (C) Porcine Gla osteocalcin bound to calcium which are shown in green.

1.3.2. Role of osteocalcin in bone development

Osteocalcin is secreted by fully differentiated osteoblasts and odontoblasts [138]. It was originally isolated from as a bone carboxylated protein [134, 135]. Gamma-carboxylated osteocalcin binds with high affinity to hydroxyapatite, which is composed of calcium-phosphate crystals [137], and was shown to inhibit the formation of hydroxyapatite *in vitro* [145]. In another experimental model, rats were treated with warfarin to produce uncarboxylated osteocalcin. The bone of these rats was depleted of osteocalcin, as the uncarboxylated osteocalcin does not bind to the bone ECM. Bone particles depleted of osteocalcin showed resistance to bone resorption when implanted subcutaneously in normal rats, not treated with warfarin [146]. The outcome of this experiment was that the resistance to bone resorption is not mainly caused by the depletion of carboxylated osteocalcin. It also suggests the presence of additional carboxylated proteins in bone that are involved in the recruitment of osteoclasts and are depleted in warfarin treated rats. The first *in vivo* evidence of osteocalcin's role in bone formation was described following the generation of osteocalcin-deficient mice by Ducy *et al.* [147]. These mice were generated by the deletion of osteocalcin genes *Bglap* and *Bglap2*. No expression of *Bglap3* was detected in these mice, as no osteocalcin was detected in their serum and bone. At the age of six and nine months, these mice showed an increase in cancellous bone, cortical bone density and cortical thickness. Consequently, these mice had an increase in bone stiffness [147]. In terms of bone remodelling, osteocalcin deficient mice had an increase in osteoclast number. Ovariectomizing these mice, a condition which mimic postmenopausal osteoporosis, increased the bone resorption showing that osteoclast function was originally impaired in osteocalcin deficient mice. Despite the increase in bone formation rate (BFR), von Kossa staining did not show mineralization defect in these mice, suggesting that osteocalcin controls bone formation without affecting bone mineralization. Likewise, a mouse model overexpressing osteocalcin in osteoblasts did not show any mineralization defect [148].

1.3.3. Osteocalcin post-translational modification

Carboxylation was the first identified osteocalcin post-translational modification, as it was found as a carboxylated protein laying in the bone ECM and bound to the hydroxyapatite [135,

141]. Glutamic acid carboxylation was previously described in clotting factor II (prothrombin), VII, IX, X and the coagulation cascade proteins C, S and Z. It was also found in matrix Gla protein (MGP) [149, 150]. Clotting factor carboxylation is required for their calcium binding and enzyme activation [133, 150]. Moreover, osteocalcin was predicted to be synthesized as a precursor protein, pre-pro-osteocalcin [140, 141]. Like other secreted proteins, the signal peptide (pre) is removed by signal peptidases. However, the mechanism and the identity of the protease(s) involved in the removal of osteocalcin propeptide (pro) is yet unknown (a question that will be addressed in chapter 3 of this thesis).

1.3.3.1. Osteocalcin gamma-carboxylation

Gamma-carboxylation is a post-translational modification that occurs in the endoplasmic reticulum (ER). It involves the addition of a carboxyl group to a glutamic acid (Glu) residue to generate a gamma-carboxyglutamic acid (Gla) residue. This reaction is catalyzed by the gamma-glutamyl carboxylase (GGCX) and requires reduced vitamin K (VKH₂) as a cofactor [151]. Carboxylation of glutamic acid residues generates vitamin K epoxide (VKO), which is reduced back to VKH₂ by the vitamin K oxido reductase VKORC1 (Figure 1-12).

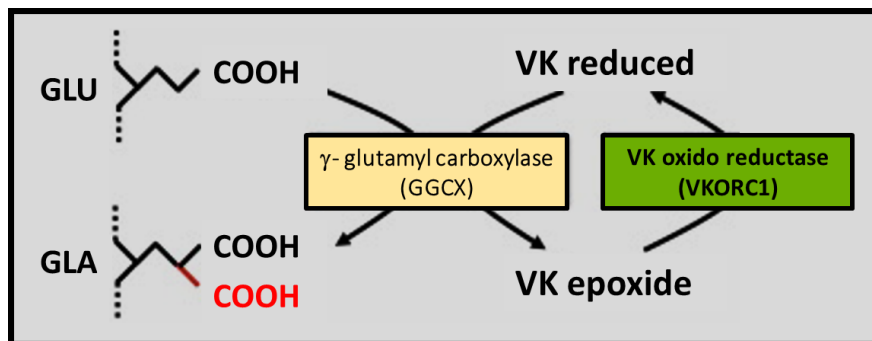


Figure 1-12. Gamma carboxylation and vitamin K cycle

Glutamic acid residue (GLU); Carboxyglutamic acid residue (GLA).

Warfarin, a widely used anticoagulant, inhibits VKORC1 and VKO recycling, resulting in the inhibition of protein carboxylation, including coagulation factors. Recent studies by our group has shown that VKORC1-like 1 (VKORC1L1) a paralogue of VKORC1 can reduce vitamin K in the

absence of VKORC1 in pre- and perinatal stages in vivo, thereby supporting carboxylation and normal haemostasis [152]. This partially redundant function of VKORC1L1 was shown to occur in liver and bone [153].

Osteocalcin is gamma-carboxylated on three of its glutamic acid residues. These residues are Glu13, Glu17 and Glu20 in mice which correspond to Glu17, Glu21 and Glu24 in human osteocalcin. Gamma-carboxylation inhibits osteocalcin endocrine functions in mice and negatively correlates with insulin resistance in human [154, 155]. In mice, the deletion of GGCX in osteoblasts impairs osteocalcin carboxylation. In this model, uncarboxylated osteocalcin was not found in bone ECM and was completely released to the circulation [155].

Osteocalcin carboxylation is a reversible modification which is removed by acidic pH [156]. Multiple evidences supported that osteocalcin is decarboxylated by the acidic pH in the resorption lacuna. In vitro assays mimicking the pH in the resorption lacuna (i.e., pH 4.5) showed that carboxylated osteocalcin is decarboxylated in this condition. Osteoclast ablation in mice, or alendronate treatment, which inhibits bone resorption, results in decreased circulating uncarboxylated osteocalcin [157, 158]. In addition, mice deficient in osteoprotegerin showed an increase in bone resorption and an increase in uncarboxylated osteocalcin [157].

1.3.4. Endocrine functions of osteocalcin

Multiple biological abnormalities were shown to affect bone mass accrual. Malnutrition was shown to reduce bone development in children and adults, while gonadal failure and menopause were shown to increase bone loss [159-162]. These clinical observations suggest an association between food intake, gonadal function and bone development. Furthermore, bone development requires bone remodelling, bone resorption by osteoclasts and bone formation by osteoblasts, a process that is energy consuming. This observation raised a question whether there is a crosstalk between bone remodelling process and energy metabolism. Consistent with this observation, the adipocyte derived hormone leptin, which reduces appetite, was shown to inhibit bone formation [104, 105]. This regulatory mechanism implies that bone exerts a feed-back

mechanism to maintain bone homeostasis and whole-body metabolism. Interestingly, the deletion of the genes encoding osteocalcin, the most abundant non collagenous protein in the bone extracellular matrix, did not affect bone mineralization. However, these mice showed an accumulation of fat, an observation that led to the discovery of osteocalcin's role in energy metabolism [163]. Further characterization of osteocalcin endocrine function showed that it does not only regulates energy metabolism but is also implicated in the regulation of muscle gain, exercise capacity, memory, cognition and response to stress and danger.

1.3.4.1. Osteocalcin regulates glucose and energy metabolism

The osteotesticular protein tyrosine phosphatase (OST-PTP), also known as embryonic stem cells phosphatase is a receptor-like protein tyrosine phosphatase which is involved during osteoblasts differentiation [164, 165]. The first evidence of an endocrine function of osteocalcin was described following the generation of OST-PTP conditional knockout in osteoblasts in mice (*Esp*^{-/-}) [163]. These mice showed an increase in insulin secretion, beta cell proliferation, insulin sensitivity and glucose tolerance. This phenotype suggests the presence of a cross-talk between bone, beta cells and insulin sensitive tissues. Further investigation showed that the *Esp*^{-/-} mice metabolic phenotype is normalized by the deletion of one allele of osteocalcin (*Esp*^{-/-}; *Ocn*^{+/-}) [163]. An additional study showed that insulin receptor is a substrate for OST-PTP [158]. The inactivation of OST-PTP (*Esp*^{-/-} mice) increases insulin signaling in osteoblasts and bone resorption. This process releases the uncarboxylated osteocalcin, the active form of this hormone [158]. Analysis of osteocalcin knockout mice (*Ocn*^{-/-}) showed a mirror image phenotype compared to *Esp*^{-/-} mice characterised by a decrease in glucose tolerance and insulin sensitivity, a reduction in beta cell proliferation and insulin secretion, and an increase in fat accumulation.

Multiple pieces of evidence supported that osteocalcin endocrine functions are mediated through its uncarboxylated form. Cell based assays showed that different doses of uncarboxylated osteocalcin differentially regulate insulin gene expression (*Ins1* and *Ins2*) and genes involved in beta cell proliferation (*CyclinD2*, and *Cdk4*) [166]. It also regulates adiponectin expression in white adipose tissue and *Pgc1 α* and *Ucp1* in brown adipocytes [166]. In mice, the deletion of GGCX in

osteoblasts increases the circulating level of uncarboxylated osteocalcin, resulting in improved glucose tolerance, insulin sensitivity and energy expenditure [155]. In addition, continuous infusion of uncarboxylated osteocalcin at a dose ranging from 0.3 ng/h to 30 ng/h improves insulin secretion and beta cell proliferation. It also prevents insulin resistance following diet- or hyperphagia-induced obesity [166]. Daily injection of uncarboxylated osteocalcin at 10 ng/g and 30 ng/g was shown to improve glucose handling and increase in beta cell mass and insulin secretion [167]. When challenged on high fat diet, which induces insulin resistance, mice injected with osteocalcin had improved glucose tolerance, insulin sensitivity and energy expenditure, and they accumulated less fat [167]. Moreover, Zhang *et al.* showed an improvement in insulin sensitivity and reduction of hyperglycemia following uncarboxylated osteocalcin injection in KKAY mice model which are obese and diabetic [168]. Additional studies showed the beneficial effect of active osteocalcin to improve glucose and energy metabolism, to promote insulin secretion and to decrease gonadal fat [169-171]. Other studies proposed that glucagon-like-peptide-1 (GLP1), a hormone released by intestinal L- cells, largely mediates the effect of uncarboxylated osteocalcin on insulin secretion. It was shown that osteocalcin administration stimulates the release of GLP1, resulting in improved glucose tolerance and insulin sensitivity. However, this effect is gone following the inactivation of GLP1 receptor. Osteocalcin injection in GLP1 receptor-deficient mice was shown to increase gluconeogenesis, to decrease glucose tolerance, and to promote lipid accumulation [172-174]. On the other hand, one study showed that osteocalcin gene deletion in rats did not impact glucose tolerance and insulin sensitivity [175]. However, the Sprague Dawley genetic background, which is an outbred strain, and the absence of complete and rigorous analysis of metabolic phenotype in these rats could explain this apparently contradictory results. On the other hand, studies supported the endocrine function of osteocalcin in rats either in vitro or in vivo [176-179].

Osteocalcin endocrine functions are mediated through its action on beta cells and peripheral tissues. Based on in vitro and in vivo experiment, the effect of osteocalcin in beta cells and Leydig cells was shown to be mediated through the G-protein coupled receptor family C group 6 member A (GPRC6A). In beta cells, osteocalcin stimulates the ERK signaling pathway,

inhibits voltage-gated potassium and increases calcium accumulation in beta cells [176, 177, 180]. This pathway is important for beta cell proliferation during development and adulthood [181]. In Leydig cells, osteocalcin stimulates cyclic adenosine monophosphate (cAMP) production without altering ERK activation and calcium accumulation [182].

GPRC6A receptor belongs to the family C of G-protein coupled receptors, which are characterized by a long amino-terminal domain. This family includes calcium-sensing receptor (CasR), metabotropic glutamate receptors (mGluR1 to 8), γ -aminobutyric acid receptor 1 and 2 (GABA_BR1 and 2), taste receptors T1R1, T1R2, and T1R3, and seven orphan receptors GPR156, GPR158, GPR179 and GPRC5A-D [183]. Divalent cations and L-amino acid were shown to bind and to activate GPRC6A [184, 185]. Computational modeling predicts that osteocalcin binding involves the 6 amino acids located in its C-terminus, Arg44, Phe45, Tyr46, Gly47, Pro48 and Val 49 [186].

1.3.4.2. Osteocalcin regulates fertility

Besides its role in the regulation of energy metabolism, osteocalcin is also involved in the regulation of male fertility [182]. Oury *et al.* showed that the supernatant of osteoblasts derived from *Ocn*^{-/-} mice failed to stimulate testosterone secretion by Leydig cells, while treatment of Leydig cells with uncarboxylated osteocalcin increased testosterone secretion [182]. Using data collected from the *Ocn*^{-/-} and *Esp*^{-/-} mice, they showed a decrease in the litter number when *Ocn*^{-/-} male were bred to WT female mice compared to WT-WT breeding [182], while *Esp*^{-/-} male mice had bigger litters when bred to WT female mice compared to WT-WT breeding. This is consistent with the fact that *Esp*^{-/-} mice is a model of osteocalcin gain of function [182]. Oury *et al.* also showed that *Ocn*^{-/-} mice had decreased testosterone levels and smaller testes, while *Esp*^{-/-} had an increased level of testosterone and bigger testes [182]. This function of osteocalcin is also mediated through the GPRC6A receptor in Leydig cells, as the activation of GPRC6A signaling pathway by osteocalcin was shown to stimulate testosterone secretion in Leydig cells [182]. The global inactivation of *Gprc6a* coding gene or its specific deletion in Leydig cells recapitulates the fertility phenotype observed in *Ocn*^{-/-} mice [182, 187]. Mechanistically, osteocalcin acts on the GPRC6A to increase cAMP and to mediate the phosphorylation of CREB (cAMP response element

binding protein), a transcription factor that activates the transcription of testosterone producing enzymes (*STAR*, *Cyp11*, *Cyp17* and *3 β -HSD*) (Figure 1-13) [182]. The effect of osteocalcin on testosterone and fertility was shown to be independent of luteinising hormone (LH), a hormone secreted by the pituitary and regulating testosterone biosynthesis [188].

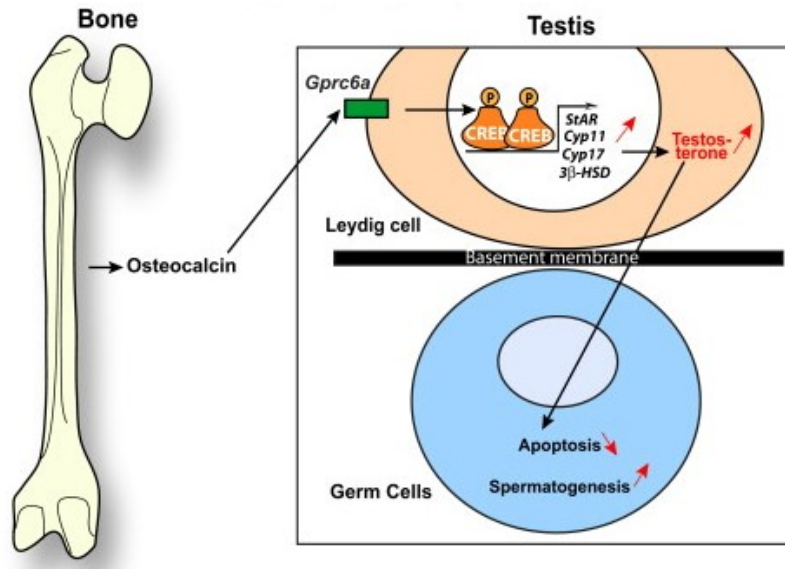


Figure 1-13. Effect of osteocalcin on fertility and testosterone production [182]

Cytochrome P450 family 11 (*Cyp11*); 17 α -steroid hydroxylase (*Cyp17*); Steroidogenic Acute Regulatory (*StAR*); 3 β -hydroxysteroid dehydrogenase (*3 β -HSD*).

1.3.4.3. Osteocalcin effect on brain development and function

A potential endocrine function of osteocalcin in the brain was uncovered by Oury *et al.* in 2013 [189]. They showed that osteocalcin crosses the blood brain barrier, as leptin does. Osteocalcin bound to the ventral tegmental area where dopaminergic neurone are enriched, to the dorsal and median raphe nuclei where serotonergic neurone are enriched and to the CA3 region of hippocampus [189]. Using an osteocalcin deficient mouse model, they showed that osteocalcin deficiency increases anxiety and decreases the exploratory behavior of mice. Mechanistic studies showed that osteocalcin deficient mice have an increase in the expression of glutamate decarboxylase 1 and 2 (*Gad1* and *Gad 2*) in the brainstem, two genes encoding for enzymes involved in gamma amino butyric acid (GABA) biosynthesis [189]. These mice also had

decreased expression of tryptophan hydroxylase-2 (*Tph2*), a gene coding for an essential enzyme involved in serotonin production in the brainstem, and of *Th* which encodes for tyrosine hydroxylase, a dopamine and norepinephrine producing enzyme in the midbrain (Figure 1-14) [189]. This phenotype was rescued following the delivery of uncarboxylated osteocalcin through intracerebroventricular infusion. Osteocalcin crosses the placenta during embryonic development and controls brain development, spatial learning and memory. The absence of maternal osteocalcin leads to an increase in the apoptosis in the hippocampus (Figure 1-14) [189]. Furthermore, osteocalcin supplementation in old mice was also shown to improve memory and to reduce anxiety [190]. Considering the role of insulin in improving cognitive function, it is possible that insulin may contribute to the improved cognitive function observed following osteocalcin injection [191, 192]. Supporting the direct function of osteocalcin on behavior, blood perfusion from young mice to older mice was shown to restore the cognitive function in old mice [193], this effect was blunted following the depletion of osteocalcin in young mice [190]. Furthermore, osteocalcin administration in a Parkinson rat model was shown to improve motor function in these rats [194].

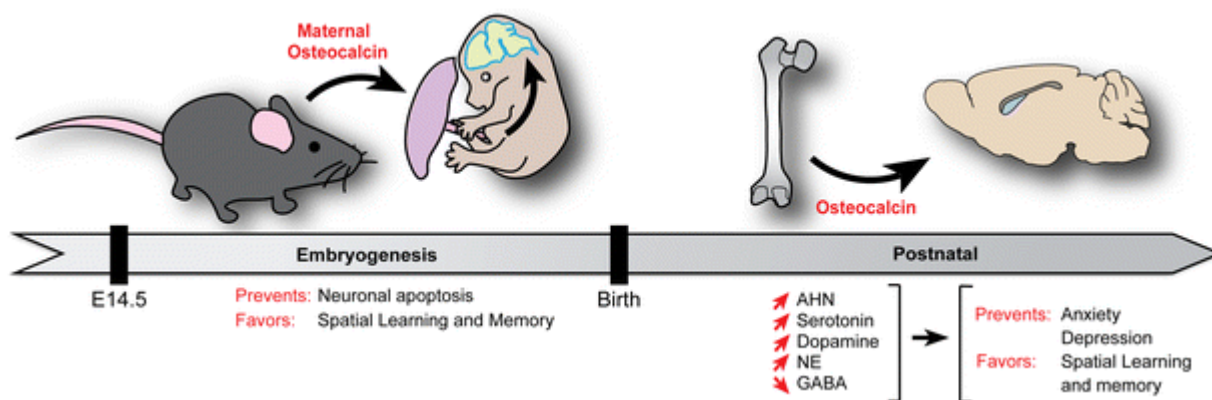


Figure 1-14. Effect of osteocalcin on the brain [195]

In the embryonic stage osteocalcin prevents neuronal apoptosis and favors spatial learning and memory. In postnatal stage osteocalcin improves hippocampal neurogenesis (AHN), increases the production of Norepinephrine (NE), serotonin and dopamine and reduces gamma amino butyric acid (GABA) production.

These functions of osteocalcin in the brain are not mediated through GPRC6A, as inactivation of *Gprc6a* in mice did not recapitulate the phenotype observed in osteocalcin loss of function mice. Genetic evidence showed that GPR158 is the osteocalcin receptor in the brain [190, 196]. GPR158 is an orphan receptor belonging to the family C, which includes GPRC6A, and is expressed in the CA3 region of the hippocampus.

1.3.4.4. Osteocalcin regulates muscle mass and exercise capacity

Osteocalcin serum levels decreases with age in mouse, human, and monkeys [197]. This decrease is associated with a decrease in memory, muscle mass and exercise capacity. Osteocalcin supplementation restores muscle mass in old mice by promoting protein synthesis through an mTOR dependent pathway. Osteocalcin function in muscle is mediated through the GPRC6A receptor, as both osteocalcin deficient mice and the inactivation of GPRC6A in muscle have a decrease in muscle mass [198]. In addition, the reduction of endurance to exercise in old mice, compared to young mice, was restored by supplementation with active osteocalcin [197]. A mechanistic study showed that during exercise osteocalcin improves glucose uptake relying on GLUT4 transporter, it also facilitates the fatty acid uptake and transport to mitochondria through CD36, FATP1, and CPT1B (Figure 1-15) [197]. Osteocalcin stimulates interleukin 6 (IL-6) secretion by the muscle during exercise. However, IL-6 is not required for osteocalcin effect, since its neutralisation using an antibody against IL-6 did not affect osteocalcin function. In response to exercise, muscle secretes IL-6 which signals to osteoblasts through the IL-6 receptor and promotes bone resorption by upregulating RANKL and downregulating OPG expression [197, 199]. IL-6 acts as a feed-forward signal to promote the secretion of osteocalcin during exercise, as the IL-6 knockout mice had a decrease in their serum osteocalcin following exercise compared to control littermates [197].

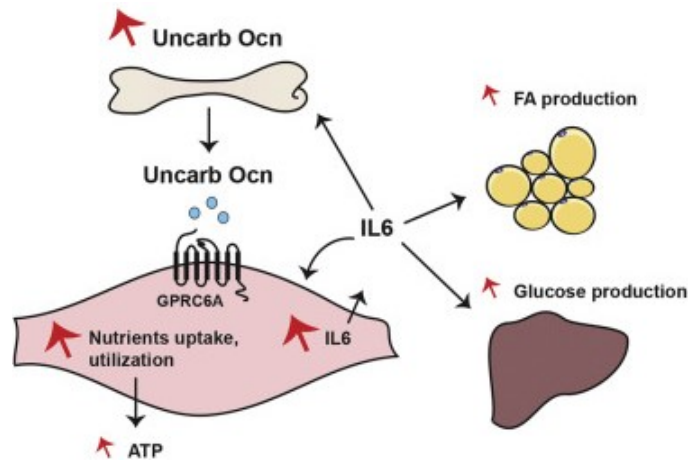


Figure 1-15. Osteocalcin signaling in myofiber and IL-6 feed forward effect

Interleukin 6 (IL-6); Adenosine triphosphate (ATP); Fatty acid (FA); Uncarboxylated osteocalcin (Uncarb Ocn).

1.3.4.5. Osteocalcin regulates the response to acute stress

Osteocalcin improves glucose metabolism, learning, memory, cognition, fertility, exercise capacity and muscle mass. All these functions of osteocalcin are characteristic of bony vertebrate adaptations to the new environment, such as running, hunting and reproduction. In a recent study, Berger *et al.* have shown that osteocalcin is also implicated in acute stress response (ASR), a physiological response to escape from danger [200]. The ASR is characterized by an increase in blood glucose, heart rate and energy expenditure. This response was impaired in osteocalcin- and GPRC6A-, but not Gpr158-deficient mice, showing that osteocalcin signaling through the GPRC6A is required for the ASR response [200]. A mechanistic study showed that upon stimulation with stressors, such as long restraint, electrical shock and 2,4,5-trimethyl thiazoline (TMT), active osteocalcin serum level is increased [200]. However, the ablation of the basolateral amygdala (BLA) abolished the increase in uncarboxylated osteocalcin following stimulation with stressors. The same group showed that the increase in bioactive osteocalcin was not the result of an increase in bone resorption, as osteoclast deficient mice still increased their active osteocalcin level following stimulation with stressor. They also found that the neurotransmitter glutamate is secreted by glutamatergic neurites within the bone under stressor conditions. Glutamate is transported in osteoblasts by GLAST, a glutamate transporter, where it inhibits the gamma-carboxylase enzyme resulting in the secretion of more uncarboxylated active osteocalcin to the

blood circulation. The deletion of GLAST in osteoblasts blunted this effect [200]. The increase in circulating uncarboxylated osteocalcin inhibits the parasympathetic tone by reducing the expression of choline acetyl transferase (*Chat*), choline transporter 1 (*Cht1*) and vesicular acetylcholine transporter 1 (*Vacht1*), which are all required for acetylcholine synthesis and recycling (Figure 1-16) [200].

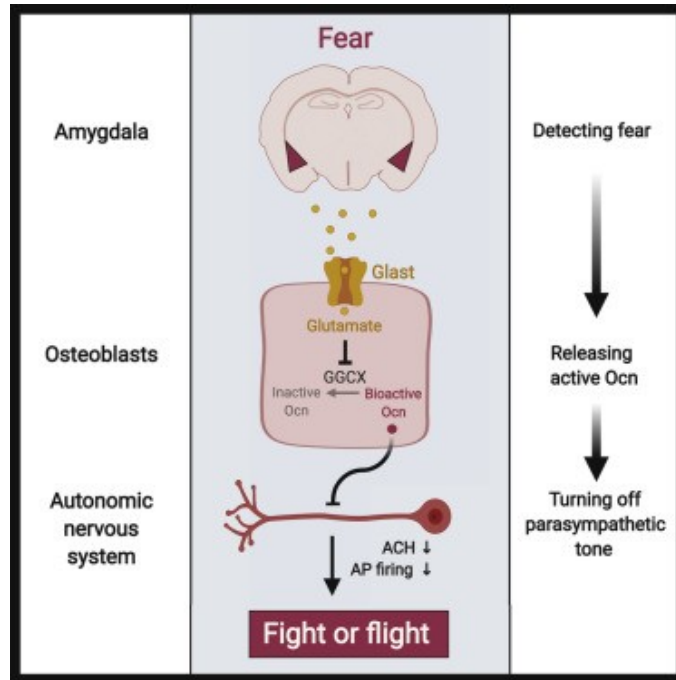


Figure 1-16. Osteocalcin regulation in acute stress response [200]

Osteocalcin (Ocn); Acetylcholine (ACH); Action potential (AP).

1.3.5. Hormonal regulation of osteocalcin in osteoblasts

Osteocalcin synthesis and release are regulated by endocrine factors secreted by peripheral tissues. These factors establish a cross-talk between bone and those tissues. Most of the identified factors act in feed forward mechanisms promoting osteocalcin secretion. For instance, insulin and IL-6 act differentially on bone to promote osteocalcin production. On the other hand, leptin and glucocorticoids were shown to repress this process.

1.3.5.1. Regulation of osteocalcin by Leptin

Leptin is an adipokine inhibiting food intake. Mouse models deficient in Leptin (*ob/ob*) or its receptor (*db/db*) are obese because of the increase in food intake. These mice also have gonadal failure (hypogonadism) and increased bone density [104, 105]. Analysis of *ob/ob* mice at young age, before they develop insulin resistance, showed an increase in their serum insulin levels. Part of this increase was explained by the absence of leptin which was shown to act directly on beta cells and inhibit insulin secretion [201, 202]. However, treatment of islets, derived from *ob/ob* or *db/db* mice, with leptin failed to reduce glucose stimulated insulin secretion, suggesting the presence of an indirect signal regulating insulin secretion in *ob/ob* and *db/db* mice. This indirect signal was found to be osteocalcin. Leptin regulates the sympathetic tone by acting on its receptor in the ventromedial hypothalamic neurons (VMH). Deletion of leptin receptor in VMH, or the deletion of beta-adrenergic receptor 2 (*Adrb2*) in osteoblasts increased serum insulin level while leptin infusion could not rescue this phenotype [203, 204]. Using an *ob/ob* mouse model deficient in *Esp* or *Ocn*, Hinoi *et al.* established that leptin promotes sympathetic tone, which acts through beta-adrenergic receptor 2 in osteoblasts to increase the expression of *Esp*, a negative modulator of osteocalcin [163], resulting in decrease in osteocalcin level and reduced insulin secretion [203-205].

1.3.5.2. Regulation of osteocalcin by insulin

Insulin is secreted by beta cells and was shown to increase the release of active osteocalcin by promoting bone resorption. This mechanism of action was elucidated by Ferron *et al.* and others [158, 206]. Studies on mice deficient in insulin receptor in osteoblasts showed that these mice have a decrease in their active osteocalcin level, a decrease in glucose tolerance, a decrease in beta cells mass and insulin secretion. Consistently, the deletion of FOXO1 in osteoblasts, a downstream target of insulin receptor, improved glucose metabolism by increasing osteocalcin and reducing *Esp* expression [207]. Mechanistic studies showed that insulin receptor signaling in osteoblasts increases FOXO1 phosphorylation and translocation, leading to a decrease in the expression levels of osteoprotegerin (OPG) and an increase in osteoclast function and bone resorption [158].

1.3.5.3. Regulation of osteocalcin by interleukin 6 (IL-6)

Interleukin 6 is both a pro-inflammatory and anti-inflammatory cytokine. During exercise and muscle contraction, transcriptional level of IL-6 in muscle and its circulating level in blood are increased leading to an increase in nutrient utilization [208-211]. Recent studies demonstrated that IL-6 increases exercise capacity through an osteocalcin dependent pathway, as osteocalcin deficient mice have a decrease in endurance during exercise and reduction in IL-6 secretion. During exercise, active osteocalcin and IL-6 levels increase, while the deletion of IL6 impairs the increase in osteocalcin levels. Mera *et al.* showed that IL-6 acts on osteoblasts and it increases the expression of RANKL which activates osteoclast differentiation and bone resorption, a process promoting the release of active osteocalcin [197]. A recent study shows that IL-6 function in osteoblasts is mediated through the interleukin 6 receptor (IL-6R) [199].

1.3.5.4. Osteocalcin regulation by other signals

Uncarboxylated osteocalcin is released during bone resorption due to the acidic pH in the resorption lacuna. Osteogenesis imperfecta, decrease in estrogen and Paget's disease [212-214] are characterized by an increase in osteoclast functions. These conditions are associated with an increase in uncarboxylated osteocalcin serum levels. Osteocalcin is also decreased following glucocorticoid treatment in mice leading to a decrease in energy metabolism [215]. Moreover, estrogen and calcitonin treatments were also shown to decrease serum osteocalcin levels [216, 217]. In humans, glucocorticoid treatment was shown to reduce the uncarboxylated osteocalcin serum levels [218, 219]. This decrease in osteocalcin was associated with insulin resistance [218]. In the next section, osteocalcin endocrine function in human will be further discussed.

1.3.6. Endocrine function of human osteocalcin

Despite the difference in the number of coding genes, i.e., two genes in mouse versus one gene in human, the coding amino acid sequence of mature human osteocalcin shares 65% homology with the mouse protein. More specifically, the glutamic acid residues Glu13, Glu17 and Glu20 in mouse osteocalcin correspond to Glu17, Glu 21 and Glu24 in the human protein. Our

laboratory showed that the increase in the ratio of carboxylated (Gla17) over total osteocalcin (Gla17/tOCN) is associated with increased insulin resistance, suggesting that the function of this modification is conserved between mice and human [154]. Additional genetic and clinical evidence support the conservation of osteocalcin endocrine function in human.

Genetic studies in human identified SNPs and mutations in osteocalcin, *GPRC6A* and *RUNX2* genes, demonstrating the role of human osteocalcin in energy metabolism, fertility and cognitive function. A limited number of studies found polymorphisms in the human osteocalcin gene and associated them with altered glucose homeostasis and body mass index (BMI). The SNP rs34702379 coding for (R94Q) was estimated to increase the diabetes risk and alter glucose homeostasis in African Americans [220]. The C/T HindIII polymorphism was associated with increased BMI in Chinese postmenopausal women [221]. Furthermore, heterozygous mutations in human osteocalcin receptor, *GPRC6A*, were associated with decreased fertility and increased blood glucose and insulin resistance. Oury *et al.* found a substitution mutation F464Y in the human osteocalcin receptor *GRPC6A* in two subjects [188]. The two patients had a decrease in fertility caused by a decrease in sperm viability and low testosterone level. One of the patients presented with high blood glucose. This genetic study supports the role of osteocalcin signaling in the regulation of male fertility in human. An additional study by Nisio *et al.* found a polymorphism in *GPRC6A*, rs2274911, that was associated with insulin resistance and higher blood glucose levels [222]. Patients with cleidocranial dysplasia, a skeletal disease characterized by a defective skull and clavicles caused by mutation in *RUNX2* gene, showed a decline in their cognitive potential [223]. This phenotype was also observed in a mouse model defective in *Runx2* and it was linked to the decrease in serum osteocalcin level, which could also explain the phenotype in human patients [224].

Together, genetics and cross-sectional studies suggests that osteocalcin endocrine functions in regulating energy metabolism, muscle strength, cognition and fertility are conserved in human. The decrease in uncarboxylated osteocalcin serum level, the active form of osteocalcin, or the increase in carboxylated osteocalcin was associated with a higher risk of type two diabetes

and insulin resistance [154, 225, 226]. Metanalysis studies showed that type 2 diabetes patients have a decrease in total serum osteocalcin levels [227], and that increased osteocalcin levels are associated with a reduction in hemoglobin A1C (HbA1c), fasting glucose and HOMA-IR [228]. Additional studies showed that uncarboxylated human osteocalcin is increased with exercise [229, 230] and it correlates with improved muscle strength [231].

1.4. FIBROBLAST GROWTH FACTOR 23 (FGF23)

FGF23 belongs to the family of fibroblast growth factors (FGFs) which comprise 22 members (FGF1-FGF23). FGF's family is divided into three groups: intracellular FGFs, canonical FGFs and hormonal like FGFs [232, 233]. Intracellular FGFs act as downstream signaling molecules independently of FGF receptor. They include the subfamily of FGF13-like (FGF11, 12, 13, 14). Canonical FGFs are extracellular proteins that bind and activate the FGF receptors using heparan sulfate as a cofactor. They act in a paracrine fashion to stimulate cells proliferation and differentiation. This group includes the subfamily of FGF4-like (FGF3, 4, 6), FGF5-like (FGF1, 2, 5), FGF8-like (FGF8, 17, 18), FGF9-like (FGF9, 16, 20) and FGF10-like (FGF7, 10, 22) [232]. The hormonal FGFs compromise the FGF15-like subfamily (FGF15, 21 and 23), which do not have the potential to bind heparan sulfate and instead bind to α -klotho. This feature of FGF15-like prevents its trapping in the ECM and facilitates its circulation through the blood [233].

Fibroblast growth factor (FGF23) belongs to the hormonal FGFs subfamily. It regulates phosphate homeostasis and was originally called "phosphatonin" [234]. Prader *et al.* were the first to propose the existence of circulating factor regulating phosphate wasting [235], a phosphatonin. Evidence from parabiosis experiment and kidney implantation from *Hyp* mice, which are hypophosphatemic due to increased phosphate wasting, further support Prader's proposition [236, 237]. In addition, transplantation of tumor induced osteomalacia from human patients into nude mice induces hypophosphatemia and reduces vitamin D activity [238]. This phosphatonin was finally discovered in 2000 to be FGF23 through genetic analysis of autosomal dominant hypophosphatemic rickets (ADHR) patients [239], a year after it was cloned and characterized by Shimada *et al.* [240].

1.4.1. Phosphorus is an essential element for the body

Phosphorus is the most abundant anion in the body representing 1% of body weight [241]. It is an essential component in many biological molecules and functions, such as synthesis of cell membrane phospholipids and nucleic acid (DNA and RNA), production of adenosine triphosphate (ATP), which is an important factor in cellular metabolism and energy production, the regulation of signaling pathway, the buffering of urine, and the synthesis of hydroxyapatite, the mineral component of bone and teeth [241].

Being an essential element in human physiology, phosphate is tightly regulated to be maintained at steady state. Bone and teeth are the reservoir of phosphate in the body. They represent 85% of phosphate storage. 14% of phosphate is distributed in other tissues while 1% is circulating in the blood [242]. Phosphate homeostasis is maintained through regulation of its intestinal absorption, its urinary excretion and its storage in the bones. Intestinal absorption of phosphate is regulated by 1,25-hydroxyvitamin D (Calcitriol) and parathyroid hormone (PTH) [242, 243]. Through the regulation of bone resorption, PTH also regulates phosphate release from bone [244]. Fibroblast growth factor (FGF23), which regulates phosphate excretion in the kidney, will be discussed in further details in the next section.

1.4.2. FGF23 protein structure and function

The FGF23 gene encodes a 251 amino acids protein in mouse and human. It is a secreted glycoprotein. The first 24 amino acids compose the signal peptide, which is a feature of secreted proteins. The N-terminal region of FGF23 contains the FGF homology domain which allows its binding to the FGF receptor 1 (FGFR 1). The C-terminal peptide harbors the FGF23 co-receptor (α -klotho) binding site.



Figure 1. 1. FGF23 protein structure

FGF23 is mainly expressed in bone [245], it is secreted by osteoblasts and osteocytes. Like other secreted proteins, FGF23 signal peptide is removed by the signal peptidase in the endoplasmic reticulum, releasing the mature FGF23. In circulation, FGF23 exist in two different forms, intact full length FGF23, and C-terminal and N-terminal fragments of FGF23. Full length active FGF23 binds to the FGFR1- α Klotho in the kidney proximal tubule. It reduces the expression of sodium phosphate cotransporter, NaPi2a and NaPi2c, resulting in decreased phosphate reabsorption and increased phosphate excretion (Figure 1-17). Active FGF23 also inhibits vitamin D production in the kidney. It downregulates the expression of *Cyp27b1*, a gene encoding for the 25-hydroxyvitamin D 1- α -hydroxylase, which hydroxylates the inactive 25-hydroxyvitamin D to generate active 1,25-hydroxyvitamin D also known as calcitriol. It also upregulates the expression of *Cyp24a1* gene encoding for the 24-hydroxylase enzyme, the 1,25-hydroxyvitamin D inactivating enzyme [246, 247]. The ablation of FGF23 in mice results in growth retardation, short life span, abnormal bone phenotype and increase renal phosphate reabsorption [248, 249].

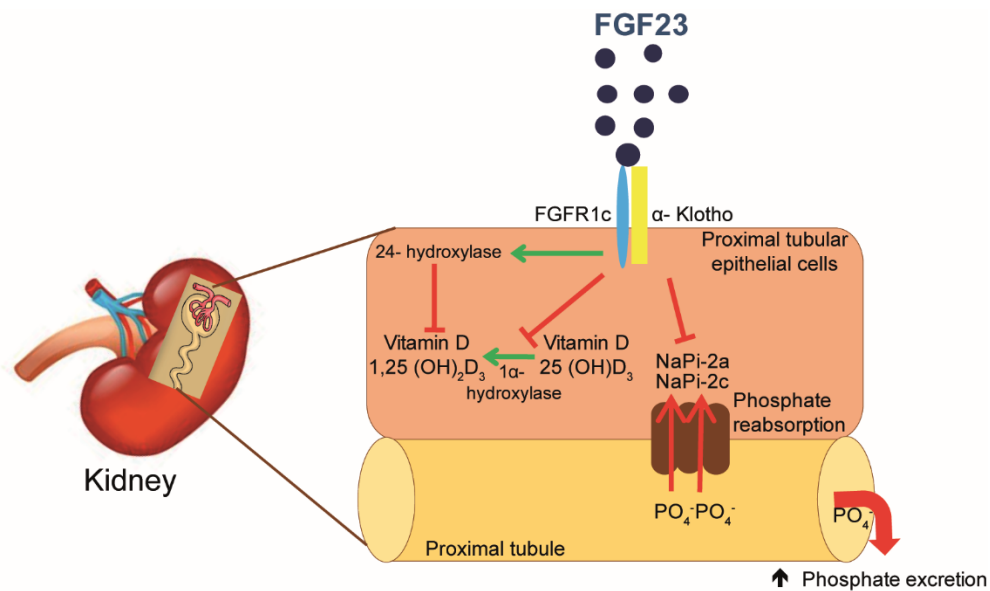


Figure 1-17. Regulation of phosphate reabsorption by FGF23

Phosphate (PO_4^-); fibroblast growth factor receptor 1 (FGFR1c); Sodium phosphate cotransporter 2a and 2c (NaPi-2a and NaPi-2c respectively).

Full length FGF23 possess a proprotein convertases (PCs) cleavage site, 176 Arg-His-Thr-Arg 179. Its cleavage after arginine 179 (Arg 179) releases the N-terminal and C-terminal

fragments of FGF23 and inhibits its endocrine function. Multiple evidences support that full length FGF23 is the active form of this hormone. First, mutations in the FGF23 cleavage site (i.e., R176Q, R179W, R179Q) were detected in autosomal dominant hypophosphatemic rickets (ADHR) patients. This human disease is characterized by an increase in full length active FGF23, a decrease in serum phosphate level and osteomalacia which is a defect in bone mineralisation. Second, a transgenic mouse model overexpressing human FGF23, the implantation of CHO cells expressing FGF23 in nude mice, or the injection of FGF23 recapitulate the ADHR phenotype [240, 246, 247, 250]. On the other hand, the S71G mutation in FGF23 leads to hyperphosphatemic familial tumoral calcinosis (HFTC), a human disease characterized by an increase in endoproteolytic cleavage of full length FGF23, resulting in a decrease in active FGF23 serum level, ectopic calcification and hyperphosphatemia. This is the opposite manifestation of ADHR patients [251]. Despite its importance for FGF23 endocrine function, the identity of the PC(s) involved in the inactivation of this hormone is yet unknown. A question that is addressed in the Chapter V of this thesis.

1.4.3. FGF23 receptor and signaling

FGF23 belongs to the FGFs family, it contains an FGF homology domain which mediates its binding to some FGF receptor such as, FGFR1, FGFR3 and FGFR4. The FGF23 co-receptor α -klotho coding gene was identified in 1997. It encodes a membrane protein composed of two domain the N-terminal domain (KL1) and the C-terminal domain (KL2) (Figure 1-18). These domains have sequence similarity to β -glucosidase enzyme. They are expressed in the kidney, parathyroid gland and brain choroid plexus [252]. Membrane associated α -klotho is shed by ADAM proteases, releasing the soluble klotho (s-klotho) [253]. α -klotho interaction with FGFR1 attributes the specificity of FGF23 signaling to the kidney [254].

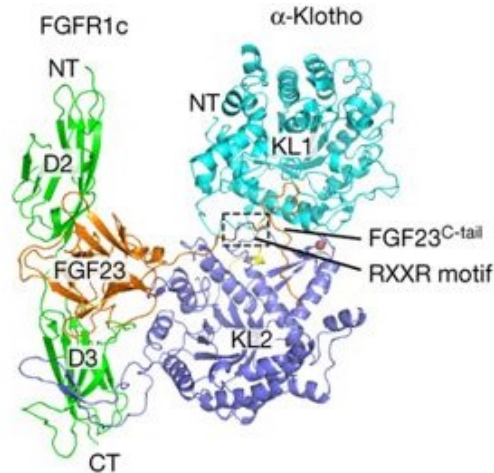


Figure 1-18. Topology of FGF23, FGFR1c and α -klotho interaction [255]

A-klotho N-terminal domain (KL1) and the C-terminal domain (KL2); Cleavage motif RXXR; N-terminal (NT). C-terminal (CT).

Mice deficient in klotho had decreased longevity, ectopic calcification and increased serum active vitamin D and phosphate levels, consistent with the phenotype observed in FGF23 loss-of-function mice [252, 256, 257]. Despite its ability to bind FGFR3 and FGFR4, mice deficient in FGFR3 or FGFR4 and injected with FGF23 develop hypophosphatemia, while FGFR1 deficient mice in the metanephric mesenchyme do not respond to FGF23 injection [258]. These data support that α -klotho-FGFR1 complex is the receptor of FGF23. Studies showed that the signaling pathway of this complex involves the phosphorylation of FGF receptor substrate 2 α and extracellular regulated kinase (ERK) and the increase in early growth response 1 (*Egr-1*) expression [254].

1.4.4. Transcriptional regulation of FGF23

FGF23 is produced and secreted by differentiated osteoblasts and osteocytes. Its production level is regulated at the transcriptional level mainly through the action of vitamin D and PTH. Recent studies showed that FGF23 expression is upregulated under pathological conditions, such as increased aspartate-rich MEPE associated motif (ASARM) peptides, iron deficiency, anemia and inflammation. However, the exact underlying mechanisms are not fully understood.

1.4.4.1. FGF23 regulation by vitamin D

FGF23 inhibits vitamin D production in the kidney. It downregulates expression of the 1,25-hydroxyvitamin D producing enzyme *Cyp27b1* and upregulates the *Cyp24a1* gene encoding for the 24-vitamin D hydroxylase which inhibits 25-hydroxyvitamin D and 1, 25-hydroxyvitamin D. As a feedback mechanism to maintain the vitamin D steady state, vitamin D reduces its own production by increasing FGF23 expression and serum levels. This function of vitamin D is mediated through the vitamin D receptor which then binds to vitamin D response element (VDRE) within the FGF23 promoter [259]. Also, calcium, phosphate and PTH were found to control FGF23 transcription. However, the underlying mechanisms are not clear yet [260, 261].

1.4.4.2. FGF23 regulation by Aspartate-rich Matrix extracellular phosphoglycoprotein associated motif

Aspartate-rich Matrix extracellular phosphoglycoprotein (MEPE) associated motif (ASARM) peptides were found to regulate FGF23 at the transcriptional level. The short integrin binding ligand interacting glycoproteins (SIBLINGs) are expressed in osteocytes and includes MEPE, dentin matrix protein 1 (DMP1), osteopontin (OPN), bone sialoprotein (BSP), and dental sialophosphoprotein (DSPP), which all possess an ASARM motif. DMP1 and MEPE bind to phosphate-regulating neutral endopeptidase (PHEX) through the ASARM motif and inhibit the expression of FGF23. PHEX also binds to the free ASARM peptide and triggers its hydrolysis. In the absence of PHEX, free ASARM peptides are increased in the circulation and it was shown to induce FGF23 expression. Consistent with their functions, loss-of-function mutation in DMP1 and PHEX were found in human patients with hypophosphatemia and osteomalacia [262-264].

1.4.4.3. FGF23 regulation by hypoxia induced factor 1 alpha

Hypoxia induce factor 1 alpha (HIF-1 α) belongs to the family of bHLH transcription factors [265]. In normoxic conditions HIF-1 α is hydroxylated on proline residues and targeted to ubiquitination. In hypoxic conditions HIF-1 α is not hydroxylated and instead activates the transcription of targets gene through interaction with coactivators [266]. Recent studies showed that HIF-1 α bind to the proximal FGF23 promotor and activates FGF23 transcription in tumors

from patients with tumor induced osteomalacia [267]. Furthermore, iron deficiency-induced anemia, which leads to hypoxia and the activation of HIF-1 α expression, was shown to drive hypophosphatemia in an ADHR mouse model (R176Q-FGF23 knock-in) model and human patients by increasing the expression of FGF23 [268]. An additional study showed that inflammation signals, such as interleukin 1 beta (IL-1 β), increases HIF-1 α expression and stabilization resulting in an increase FGF23 expression [269]. The inhibition of HIF-1 α prolyl hydroxylase (HIF-PH) stabilizes HIF-1 α . It was shown to increase the production and cleavage of intact FGF23 via an erythropoietin dependent mechanism [270].

1.4.4.4. FGF23 regulation by Erythropoietin

One interesting phenotype observed in FGF23 null mice is an increase in circulating erythropoietin levels. This increase was associated with an increase in erythropoiesis and hematopoietic stem cells. Erythroid progenitors were shown to express the FGFR1- α -klotho receptor components, where the injection of FGF23 in wild type mice have the opposite effect on erythropoiesis [271]. Further studies showed that bone marrow cells express similar levels of FGF23 compared to bone cells and that erythropoietin injection (EPO) induces FGF23 expression in both compartments [270, 272-275]. Because FGF23 processing is not impaired in normal conditions, EPO injection increases C-terminal FGF23 levels with a very mild effect on full length FGF23. The ablation of bone marrow with carboplatin was shown to reduce the circulating C-terminal FGF23 levels by 40% following EPO injection, showing that bone cells contribute to 60% of EPO induced FGF23 serum level [273]. Consistent with these results in mice, human patients receiving recombinant human EPO have an increase in the total FGF23 levels [274, 275]. A mechanistic study using the HIF-proline hydroxylase inhibitor and anti EPO antibodies showed that EPO induce FGF23 independently of HIF-1 α stabilisation [270].

1.4.5. Regulation of FGF23 by post-translational modifications

Beside its regulation at the transcriptional level, FGF23 protein undergoes three important post-translational modifications that regulate its endocrine functions. These include phosphorylation, *O*-glycosylation and endoproteolytic cleavage (Figure 1-19). Both

phosphorylation and *O*-glycosylation were found to modulate the proteolytic cleavage, at least in vitro. These modifications are important for FGF23 endocrine functions and are implicated in several rare genetic disorders involving FGF23.

1.4.5.1. Proteolytic cleavage

Full length FGF23, the active form of this hormone, possesses a dibasic motif, ¹⁷⁶RHTR₁₇₉. Endoproteolytic cleavage of FGF23 on this motif by a furin-like proprotein convertase releases the N-terminal and C-terminal fragments of FGF23 and inhibits its function (Figure 1-19). Autosomal dominant hypophosphatemic rickets (ADHR) is a human disease caused by mutations in this cleavage site (R176Q, R179W, R179Q) that render FGF23 resistant to cleavage [239, 276]. ADHR patients are characterized by an increase in full length active FGF23, a decrease in serum phosphate levels and osteomalacia, which is a defect in bone mineralisation. In vitro based assays showed that the proprotein convertase furin and the proprotein convertase subtilisin/kexin type 2 and type 5 (PC5) cleaves FGF23 [26, 277], However, the identity of PC involved in FGF23 processing in vivo is still unknown.

1.4.5.2. O-glycosylation

O-glycosylation is a post-translational modification that involves the addition of carbohydrate moieties to serine or threonine residues. This process is initiated by the addition of *N*-acetylgalactosamine catalyzed by the *N*-acetylgalactosaminyltransferase (GalNAc-Ts), a family of 21 members. FGF23 *O*-glycosylation is specifically mediated by the third member, GalNAc-T3, which glycosylates the serine and threonine residues in FGF23 (Figure 1-19). *O*-glycosylation on T178 within the FGF23 cleavage site was shown to reduce its processing in vitro. The genetic ablation of GalNAc-T3 abolishes FGF23 glycosylation and favors FGF23 cleavage [278]. Consequently, mutations in human GalNAc-T3 lead to a human disease known as familial hyperphosphatemic tumoral calcinosis (HFTC) [51]. Additional mutations in FGF23 *O*-glycosylation site, on Serine 71 and serine 129, were also found to cause HFTC [251, 279]. Patients with HFTC are characterized by a decrease in active FGF23 serum level, an increased serum phosphate level and ectopic calcification [51].

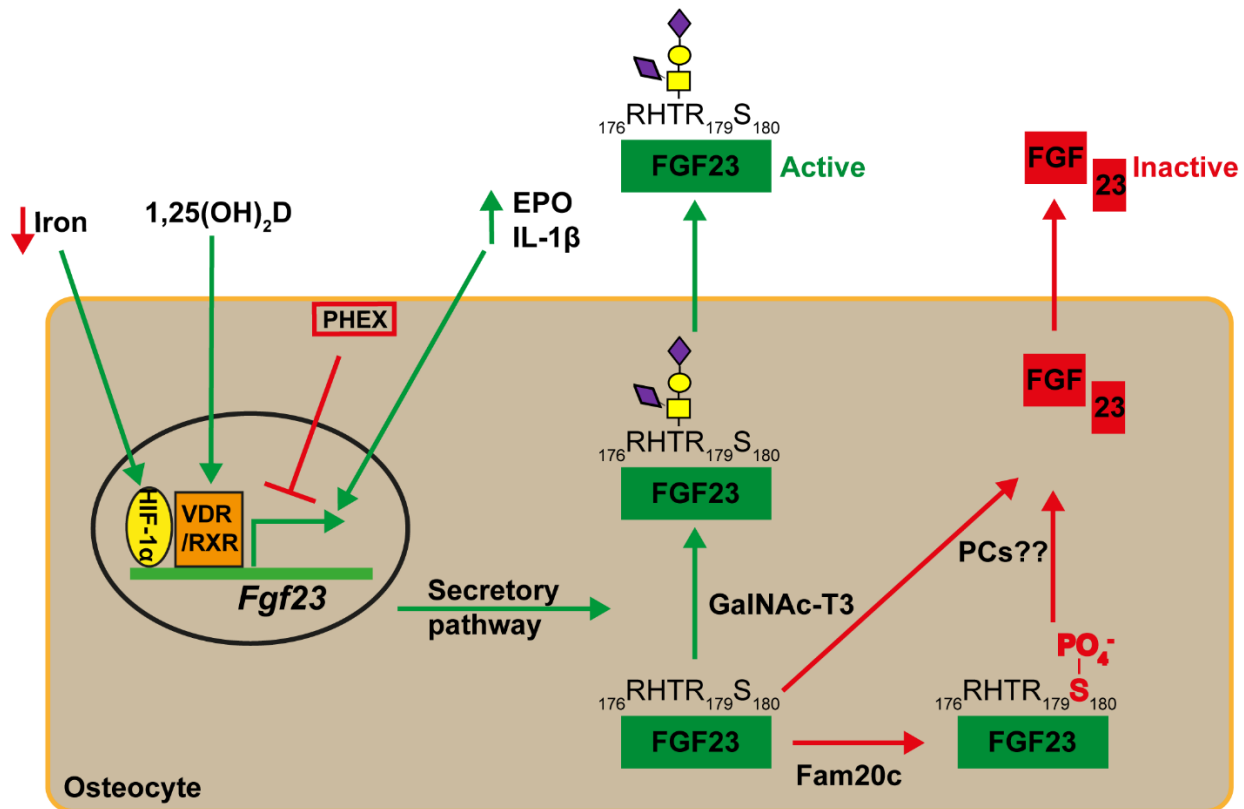


Figure 1-19. Transcriptional and post-translational modifications of FGF23 [280]

Proprotein convertase (PC); *N*-acetylgalactosaminyltransferase 3 (GalNAc-T3); Family with sequence similarity number 20, member C (Fam20c); 1, 25-hydroxyvitamin D (1,25(OH)₂D); Phosphate-regulating neutral endopeptidase (PHEX); Erythropoietin (EPO); Interleukin 1 beta (IL-1β); Arginine, histidine, threonine, arginine, serine (RHTRS); Numbers in subscript represents the amino acid position; Phosphorylation of serine residues (PO₄⁻).

1.4.5.3. Phosphorylation

Family with sequence similarity number 20, member C (FAM20C), a protein kinase located in the Golgi apparatus, phosphorylates proteins in the secretory pathway on a Ser-X-Glu motif. Using whole exome sequencing, FAM20C mutations were found in two siblings. These patients have an increase in urinary phosphate excretion, hypophosphatemia, without developing rickets [281]. *Fam20c* knockout mice are hypophosphatemic and develop osteomalacia as a result of an increase in full length FGF23 [282]. Tagliabracci *et al.* showed that FGF23 phosphorylation on Serine 180 prevent its *O*-glycosylation and favors its proteolytic cleavage in vitro and in cell culture (Figure 1-19) [26].

1.4.6. FGF23 in human disease

Impaired FGF23 serum levels in humans leads to multiple diseases that share similar clinical manifestations. Based on these criteria, these diseases can be divided in two categories. Hypophosphatemia and rickets are characteristic of diseases with high active FGF23 levels, while hyperphosphatemia and ectopic calcification are characteristic of diseases with low active FGF23 levels. These diseases are caused by mutations in FGF23, its receptor and regulator (Table 1. 2.)

Table 1-2. Human diseases associated with FGF23, its receptor and regulators

Increased active FGF23 associated with hypophosphatemia and osteomalacia		
Disease	Mutation	References
Autosomal dominant hypophosphatemic rickets (ADHR)	FGF23 cleavage site mutant	[239, 276]
Autosomal recessive hypophosphatemic rickets (ARHR)	DMP1	[283]
X-linked hypophosphatemia (XLH)	PHEX	[284]
Osteoglophonic dysplasia	FGFR1	[285]
Raine syndrome	FAM20C	[281]
Decrease active FGF23 associated with ectopic calcification and hyperphosphatemia		
Familial hyperphosphatemia tumoral calcinosis	FGF23, GLANT3, α -klotho	[51, 251, 286, 287]

1.4.7. FGF23 in chronic kidney disease

Chronic kidney disease (CKD) is a human disease characterized by kidney dysfunction. As a results of abnormal phosphate excretion, CKD patients have an increase in serum phosphate levels. To counteract this mechanism and reduce serum phosphate, the body responds by increasing FGF23 levels to inhibit phosphate reabsorption and to increase phosphate wasting [288]. Mechanistic studies showed that FGF23 signals through the FGFR4 receptor in the heart and liver in vivo, and through FGFR1 and FGFR2 in the leukocytes in vitro [289-292]. Consequently, CKD patients have higher risk of developing cardiovascular disease and left ventricular hypertrophy, increased risk of infection (bacterial, viral and fungi) and high level of inflammatory cytokines (IL-6, CRP and TNF- α) [292-296] .

2. CHAPTER II

GENERAL HYPOTHESIS

2. CHAPTER II: GENERAL HYPOTHESIS

Bone endocrine functions are mediated at least by two different hormones, osteocalcin and FGF23. These hormones are produced by osteoblasts and osteocytes, which also secrete other paracrine factors to regulate bone homeostasis. Before being secreted by osteoblast and osteocytes, these hormones and factors transit through in the endoplasmic reticulum and trans-Golgi network, the cellular compartments where most of the secreted protein post-translational modifications (PTMs) takes place, such as gamma-carboxylation, glycosylation and proteolytic cleavage.

Osteocalcin cDNA sequence predicts to be synthesized as pre-pro-osteocalcin composed of a signal peptide, a pro-peptide and the mature hormone. Our understanding of osteocalcin regulation by PTMs is limited to its gamma-carboxylation in the endoplasmic reticulum, while its maturation process was never addressed. Considering the lack of knowledge about osteocalcin regulation by PTMS, we **hypothesized** that osteocalcin is subjected to additional PTMs that regulate its gamma-carboxylation and impact its endocrine functions. The main objective of the chapter III and IV of the present theses are:

Chapter III objectives: Identify the endopeptidase(s) involved in osteocalcin maturation, study the impact of this process on osteocalcin gamma-carboxylation and assess its requirement for osteocalcin and bone endocrine function.

Chapter IV objectives: Characterize the role of *O*-glycosylation, a novel PTM in osteocalcin, in the regulation of other osteocalcin modifications and its impact on osteocalcin endocrine function.

FGF23 regulation by PTMs is better understood. It was shown to be subjected to *O*-glycosylation, phosphorylation and endoproteolytic cleavage. The latter modification is critical for FGF23 endocrine function and is regulated by the other two modifications. Despite the importance of FGF23 endoproteolytic cleavage in multiple diseases, the identity of the enzyme(s) involved in the regulation of FGF23 cleavage in vivo is yet unknown. Genetic screening of patient with autosomal dominant hypophosphatemic rickets (ADHR), which have high level of intact FGF23, identified mutations in the proprotein convertase consensus cleavage site that render FGF23 resistant to proteolytic cleavage. Kexin-like proprotein convertase furin and the proprotein convertase subtilisin/kexin type 5 (PC5) were shown to cleave FGF23 in vitro. However, the identity of the PC(s) involved in FGF23 processing was never addressed in vivo. Considering that the subtilisin/kexin like proprotein convertases have similarities in their catalytic site and can redundantly cleaves similar substrates, we **hypothesized** that one or multiple PC(s), including furin and/or PC5, may be responsible of FGF23 cleavage in vivo. The objective of chapter V of the present theses is:

Chapter V objective: Investigate whether furin and/or PC5 are involved in FGF23 processing and address their impact on phosphate homeostasis in vivo.

3. CHAPTER III

**IDENTIFICATION OF PRO-OSTEOCALCIN CONVERTING ENZYME
AND A NOVEL BONE ENDOCRINE FUNCTION**

3.1. HYPOTHESIS AND RELEVANCE

Bone is an endocrine organ regulating glucose and energy metabolism. This function of bone is in part mediated by osteocalcin, a hormone secreted by differentiated osteoblasts, the bone forming cells. Osteocalcin is first synthesized as precursor hormone (pre-pro-osteocalcin), composed of a signal peptide, a propeptide and the mature hormone. Before being secreted by osteoblasts, osteocalcin is gamma-carboxylated on three of its glutamic acid residues in the endoplasmic reticulum, a modification which inhibits its endocrine function in mice and human. However, the function of osteocalcin propeptide and the identity of the endoprotease involved in its removal are not well understood. In the present study, we focused on proprotein convertases (PCs), a family of serine proteases that cleave proteins in the secretory pathways and cell membrane, leading to their activation or inactivation. Using cell-based assays and molecular biology tools, we showed that the proprotein convertase furin cleaves osteocalcin propeptide in its C-terminus motif RLRR independently of its gamma-carboxylation. Using mouse model deficient in furin specifically in osteoblasts, we showed that furin is required for osteocalcin maturation, activation and endocrine function in vivo. Moreover, we discovered that furin in osteoblasts regulates appetite independently of osteocalcin, suggesting the presence of additional bone-derived hormones regulating appetite and controlled by furin.

3.2. FIRST PAPER

Proprotein convertase furin regulates osteocalcin and bone endocrine function

Omar Al Rifai,^{1,2} Jacqueline Chow,¹ Julie Lacombe,¹ Catherine Julien,¹ Denis Faubert,³ Delia Susan-Resiga,⁴ Rachid Essalmani,⁴ John W.M. Creemers,⁵ Nabil G. Seidah,^{4,6,7} and Mathieu Ferron^{1,2,6,7}

¹Integrative and Molecular Physiology Research Unit, Institut de Recherches Cliniques de Montréal (IRCM), Montréal, Québec, Canada.

²Molecular Biology Programs of the Faculty of Medicine, Université de Montréal, Québec, Canada.

³Proteomics Discovery Platform and

⁴Biochemical Neuroendocrinology Research Unit, IRCM, Québec, Canada.

⁵Department of Human Genetics, KU Leuven, Leuven, Belgium.

⁶Department of Medicine, Université de Montréal, Québec, Canada.

⁷Division of Experimental Medicine, McGill University, Montréal, Québec, Canada.

Address correspondence to:

Mathieu Ferron,
Institut de Recherches Cliniques de Montréal,
110 Avenue des Pins O.,
Montréal, Quebec, H2W 1R7, Canada.
Phone: 514.987.5754;
Email: mathieu.ferron@ircm.qc.ca.

Published in the *Journal of Clinical Investigation*. Copied in this thesis with the journal permission

Published in Volume 127, Issue 11 on November 1, 2017

J Clin Invest. 2017;127(11):4104–4117. <https://doi.org/10.1172/JCI93437>.

Copyright © 2017, American Society for Clinical Investigation

Author contributions

MF and JL designed experiments. OAR performed most experiments (Figures 3-1A, 3-1B, 3-1E, 3-2G, 3-4A-C, 3-5C-E, 3-6A-G, 3-7A-D, 3-8A-E, 3-9A-J, 3-10A-E, S3-1 B-I, S3-2 A-L, S3-3 A-H, S3-4 A-C, Table 3-1) with crucial help from JC (genetic and pharmacological studies with primary osteoblasts (Figures 3-1C, 3-1D, 3-3A-E, 3-5A-B), JL (metabolic cages and metabolic tests, Figures 3-8C, 3-8D, 3-9A-J, S3-2 J-L, S3-3 E, F, H), CJ (in vitro PC assay, Figures 3-2A-F, 3-5E, Table 3-1), DF (LC-MS/MS analysis, Figure 3-5E and Table 3-1), and DSR (PC activity, S3-1 A). RE and NGS provided *Pcsk5^{fl/fl}* mice and plasmids. JWC provided *Furin^{fl/fl}* mice. MF and OAR wrote the manuscript with suggestions from JL, JWC, and NGS. All authors discussed the results and commented on the manuscript.

ABSTRACT

Osteocalcin (OCN) is an osteoblast-derived hormone that increases energy expenditure, insulin sensitivity, insulin secretion, and glucose tolerance. The cDNA sequence of OCN predicts that, like many other peptide hormones, OCN is first synthesized as a prohormone (pro-OCN). The importance of pro-OCN maturation in regulating OCN and the identity of the endopeptidase responsible for pro-OCN cleavage in osteoblasts are still unknown. Here, we show that the proprotein convertase furin is responsible for pro-OCN maturation in vitro and in vivo. Using pharmacological and genetic experiments, we also determined that furin-mediated pro-OCN cleavage occurred independently of its γ -carboxylation, a posttranslational modification that is known to hamper OCN endocrine action. However, because pro-OCN is not efficiently decarboxylated and activated during bone resorption, inactivation of furin in osteoblasts in mice resulted in decreased circulating levels of undercarboxylated OCN, impaired glucose tolerance, and reduced energy expenditure. Furthermore, we show that *Furin* deletion in osteoblasts reduced appetite, a function not modulated by OCN, thus suggesting that osteoblasts may secrete additional hormones that regulate different aspects of energy metabolism. Accordingly, the metabolic defects of the mice lacking furin in osteoblasts became more apparent under pair-feeding conditions. These findings identify furin as an important regulator of bone endocrine function.

1. INTRODUCTION

It has been recently established that bone acts as an endocrine organ that secretes at least 3 hormones: fibroblast growth factor 23 (FGF23), lipocalin 2 (LCN2), and osteocalcin (OCN). Bone-forming osteoblasts are the cells that produce OCN, a hormone implicated, among other functions, in the regulation of glucose and energy metabolism (1). Accordingly, when fed a normal diet, *Ocn*-deficient mice (*Ocn*^{-/-}) exhibit reduced glucose tolerance, insulin sensitivity, and circulating insulin levels, as well as decreased energy expenditure and increased fat mass (2). Mechanistic studies conducted in cell cultures and mice showed that OCN improves glucose handling by promoting insulin secretion from β cells (3, 4), by favoring glucose uptake in myofibers (5), and by increasing energy expenditure (6). Studies in mice demonstrated that OCN function in β cells and myofibers is mediated through its binding to the G protein-coupled receptor family C group 6 member A (GPRC6A) (3, 5). This pathway appears to be conserved in humans, since human OCN can bind and activate human GPRC6A (7), while mutations or polymorphisms in human *GPRC6A* are associated with insulin resistance (8, 9).

OCN is a small protein (46 aa in mice and 49 aa in humans) that is uniquely produced by osteoblasts and γ -carboxylated on 3 glutamic acid residues (Glu) before it is secreted. γ -Carboxylation of OCN occurs in the ER and is mediated by γ -glutamyl carboxylase (GGCX), which requires reduced vitamin K as an essential cofactor (10). This posttranslational modification increases the affinity of OCN for hydroxyapatite, the mineral component of bone extracellular matrix (ECM). Hence, the vast majority of OCN secreted by osteoblasts is trapped in bone ECM, in which it constitutes the most abundant noncollagenous polypeptide. Although both γ -carboxylated (Gla) and undercarboxylated (ucOCN) forms of OCN are detected in serum, most *in vitro* and *in vivo* studies concur to indicate that the endocrine function of OCN is fulfilled by ucOCN in mice and humans (3, 4, 11). This has been recently confirmed genetically through the inactivation of *Ggcx* specifically in osteoblasts, which resulted in increased circulating levels of ucOCN and improved glucose tolerance in mice (12). Additional studies showed that osteoclasts, the bone-resorbing cells, are responsible for the partial decarboxylation and activation of OCN present in bone ECM (13, 14). Altogether, these observations suggested a model in which

hormonally inactive γ -carboxylated OCN is produced by osteoblasts and stored in the bone ECM, before being activated and released as ucOCN by osteoclasts during the process of bone resorption.

As is the case for many other peptide hormones, the sequence of *Ocn* cDNA predicts that it is first synthesized as a pre-prohormone composed of a signal peptide, a propeptide, and a mature hormone (Figure 3-1A). The propeptide of other γ -carboxylated proteins such as prothrombin and profactor IX are characterized by a recognition signal for the γ -glutamyl carboxylase (15). However, the importance of the propeptide for the γ -carboxylation and secretion of OCN has never been addressed in vivo. Moreover, it is currently unknown whether removal of the OCN propeptide depends on the γ -carboxylation process. It should be noted that OCN is unique among all known γ -carboxylated proteins, as it is the only one known to be efficiently γ -carboxylated in vitro in the absence of its propeptide (16). These observations raise the question of the function of the OCN propeptide. Last, and as important, the identity of the endopeptidase responsible for processing the OCN prohormone (pro-OCN) and its importance in bone endocrine function remain unknown.

We therefore embarked on a search for the pro-OCN-converting enzyme. For that purpose, we focused on the proprotein convertases (PCs), a series of serine endoproteases that target specific motifs comprising basic residues, such as di-arginine or di-lysine, that are frequently observed in prohormone sequences (17). These enzymes function within the secretory pathway or outside the cell to cleave other proteins, either activating or inactivating them, and have been implicated in the regulation of a myriad of biological processes (18). In particular, the PCs of the subtilisin/kexin type include proprotein convertase 1 (PC1), proprotein convertase 2 (PC2), furin, proprotein convertase 4 (PC4), proprotein convertase 5A and B (PC5A and PC5B), paired basic aa-cleaving enzyme 4 (PACE4), and proprotein convertase 7 (PC7) and play critical functions in several endocrine cells by regulating the maturation and secretion of numerous peptide hormones such as insulin, glucagon, adrenocorticotrophic hormone (ACTH), glucagon-like peptide 1 (GLP-1), and parathyroid hormone (PTH) (18, 19).

Here, we identified furin, using cell-based and genetic arguments, as the endopeptidase responsible for pro-OCN processing in osteoblasts. We also showed in cell culture and in vivo that γ -carboxylation and processing of OCN are 2 independent processes in osteoblasts. The study of mice lacking furin specifically in osteoblasts revealed that proteolysis of pro-OCN is critical for the activation of this hormone. We also found that furin may modulate energy metabolism through OCN-independent pathway(s) affecting appetite.

2. METHODS

Animal models. The *Furin*^{fl/fl} mice were generated by introducing loxP sites upstream and downstream of exon 2 of the *Furin* gene (30). *Ggcx*^{fl/fl} mice were generated by introducing a loxP site upstream of exon 1 and a loxP site downstream of exon 2 of the *Ggcx* gene (12). *Pcsk5*^{fl/fl} mice were generated by introducing loxP sites on each side of *Pcsk5* exon 1 (35). Each of these strains was crossed with *OCN-Cre*–transgenic mice, which express Cre recombinase under the control of a fragment of the human *OCN* promoter (31) and which were previously shown not to display any metabolic anomalies, in order to generate, respectively, *Furin*^{fl/fl} *OCN-Cre* (*Furin*^{osb-/-}), *Ggcx*^{fl/fl} *OCN-Cre* (*Ggcx*^{osb-/-}), and *Pcsk5*^{fl/fl} *OCN-Cre* (*Pcsk5*^{osb-/-}) mice. *Ocn*^{-/-} mice were generated by replacing *Ocn1* (*Bglap1*) and *Ocn2* (*Bglap2*) genes in the mouse *Ocn* cluster with a neomycin resistance cassette through homologous recombination (53). All strains used were backcrossed on a C57BL/6J genetic background more than 10 times and maintained in an IRCM specific pathogen–free animal facility (SPF) under 12-hour dark/12-hour light cycles. Male mice fed a normal chow diet were used in all experiments, unless otherwise noted. Tissue DNA was extracted by standard procedure, and PCR was performed with the genotyping PCR primers listed in Supplemental Table 3-1.

Metabolic analysis. For GTTs, adult male mice fed a normal chow diet were fasted overnight for 16 hours. Blood glucose levels were measured after fasting and at 15, 30, 60, and 120 minutes following i.p. injection with 2 g/kg glucose. In some experiments, mice were fed a 60% high-fat diet (D12331-5I; Research Diets) for 10 weeks starting from 4 weeks of age. In this

case, mice were fasted for 6 hours and injected i.p. with 1 g/kg glucose for the GTT. To measure pancreatic insulin content, pancreas was collected, and insulin was extracted in acid-ethanol as previously described (13). Serum insulin and pancreatic insulin levels were assessed using a commercial insulin ELISA (Merckodia). Serum leptin and LCN2 levels were measured using a mouse leptin ELISA kit (EZML-82K; EMD Millipore) and a mouse lipocalin-2 ELISA kit (MLCN20; R&D Systems), respectively. In the pair-feeding experiment, each mouse was housed in a separate cage. *Furin^{osb-/-}* mice were fed a normal chow diet ad libitum, and food intake was measured and averaged daily. The corresponding amount of food was given to the *Furin^{fl/fl}* mice. Metabolic tests were performed between the third and fourth weeks of pair feeding.

Mouse O₂ consumption, CO₂ release, activity, and food intake were assessed using an 8-chamber Promethion Continuous Metabolic System (Sable Systems International). After a 48-hour acclimation period, O₂ consumption (VO₂) and CO₂ production (VCO₂) data were collected for 72 hours. Heat production was calculated by indirect calorimetry using the following formulas: heat in kcal/hr = 60 × (0.003941 × VO₂ + 0.001106 × VCO₂), where VO₂ and VCO₂ are in units of ml/min. Physical activity was measured using infrared beams connected to the system. Total body fat was measured using a body composition analyzer (echo-MRI) and normalized to body weight.

DNA construct, cell culture, and transfection. Mouse pro-OCN cDNA was cloned into a pIRES2-EGFP-V5 plasmid in EcoRI and AgeI restriction sites. Different OCN mutants were generated by site-directed mutagenesis using specific primers (Supplemental Table 3-1). Primary osteoblasts or Chinese hamster ovary Id1D cells (CHO-Id1D; originating from the M. Krieger laboratory [ref. 54]) were transfected with jetPRIME Reagent (Polyplus transfection). Following an overnight incubation, media were changed to secretion media (FBS-free α MEM plus 2mM L-glutamine for osteoblasts or FBS-free DMEM/F12 for CHO-Id1D cells) supplemented with 22 μ M vitamin K₁ (Sandoz). Twenty-four hours later, media were collected, and cells were lysed in protein lysis buffer (20 mM Tris-HCl, pH 7.4, 150 mM NaCl, 1 mM EDTA, 1 mM EGTA, 1% Triton, 1 mM PMSF, and 1 \times protease inhibitor cocktail) and analyzed by Western blotting. In some

experiments, warfarin (50 μ M; Santa Cruz Biotechnology), D6R (20 μ M; Calbiochem), or Dec-RVKR-CMK (50 μ M; Tocris) was added to the secretion media.

Osteoblast preparation. Primary mouse osteoblasts were isolated from 3-day-old mouse calvariae through serial collagenase (Worthington Biochemical Corp.) digestions as previously described (12). To generate *Furin*^{-/-} or *Pcsk5*^{-/-} osteoblasts, *Furin*^{fl/fl} or *Pcsk5*^{fl/fl} osteoblasts were infected with Cre-GFP-expressing adenovirus (University of Iowa) at 200 MOI per cell. Control osteoblasts were obtained by infecting *Furin*^{fl/fl} or *Pcsk5*^{fl/fl} osteoblasts with GFP-expressing adenovirus. Osteoblast differentiation was induced by supplementing osteoblast culture media (α MEM plus 10% FBS and 2mM L-glutamine) with 5 mM β -glycerophosphate and 100 μ g/ml L-ascorbic acid for 21 days. Bone marrow-derived osteoblasts were prepared as previously described (12). Briefly, long bones of 3 week-old-mice were dissected, and bone marrow cells were flushed with α MEM. Cells were then plated in 6-well plates at a density of 5×10^6 cells per well. After 7 days, media were changed to differentiation media (osteoblast media supplemented with 100 μ g/ml L-ascorbic acid, 5 mM β -glycerophosphate, and 10^{-8} M dexamethasone). After 14 days of differentiation, cells were used for mRNA or protein analysis.

Biochemical studies. For OCN immunoprecipitation, *Furin*^{fl/fl} or *Furin*^{osb-/-} serum was diluted 1:50 with 1 \times PBS containing 1 mM PMSF, and 1 \times protease inhibitor cocktail and incubated overnight at 4°C in the presence of the OCN antibodies indicated in Figure 3-5D, Figure 3-6E, and in Supplemental Figure 3-1F. Protein G agarose beads prewashed with 1 \times PBS were added and incubated for 4 hours at 4°C. Beads were spun down and washed 4 times with 1 \times PBS before Western blot analysis. Proteins were resolved on 15% Tris-tricine SDS-PAGE gel for OCN detection, whereas 7.5% Tris-glycine gel was used for the detection of furin and the insulin receptor. The antibodies used in this study were: anti-OCN (total) polyclonal goat antibody, which recognize aa 26–46 corresponding to mature mouse OCN (55); anti-Gla OCN polyclonal goat antibody, which recognize Gla13 OCN aa 11–26 corresponding to carboxylated mature OCN (55); anti- β -actin (mouse, clone AC-15, A5441; Sigma-Aldrich); anti-V5 (mouse, clone V5-10, V8012; Sigma-Aldrich); anti-furin (rabbit, PA1-062; Thermo Fisher Scientific); anti-insulin receptor β

(mouse, clone L55B10, 3020; New England BioLabs); and anti-LCN2 (goat, AF1857; R&D Systems). Serum and cell supernatant levels of carboxylated, undercarboxylated, and total OCN were measured using ELISAs as described previously (55). Briefly, the Gla ELISA detects OCN only when it is carboxylated on the Glu13 residue. The Glu ELISA quantifies the uncarboxylated form of OCN. The total ELISA detects OCN, whether it is carboxylated or not. OCN measurements in bone homogenate were normalized to total protein content, as assessed by Bradford assay.

GST pro-OCN preparation and in vitro digestion assay. Mouse pro-OCN cDNA (WT or R48A/R49A, i.e., RR/AA mutant) was cloned into pGEX4T3 in BamHI and EcoRI restriction sites (Supplemental Table 3-1). Plasmids were transformed in Rosetta (DE3) pLys S competent bacteria (EMD Millipore), and recombinant GST proteins were purified using glutathione resin (Genscript). Recombinant full-length LCN2 protein was provided by S. Kousteni (Columbia University, New York, NY, USA). The cDNA of the soluble form of various PCs were cloned into the pIRES2-EGFP plasmid and transfected into HEK293 cells (ATCC) using Lipofectamine 2000 (Life Technologies, Thermo Fisher Scientific). Twenty-four hours after transfection, cells were allowed to secrete in serum-free media for twenty-four hours, and supernatant was harvested. PCs were concentrated using centrifugal filters (50-kDa MWCO Amicon; EMD Millipore) and stored in 20% glycerol at -80°C . Kexin-like protease activity was assessed by in vitro cleavage of 100 μM Pyr-RTKR-AMC (Tocris) in PC buffer (25 mM Tris-HCl, pH 7.0, 1 mM CaCl_2 , 1 mM β -mercaptoethanol). Soluble extracellular PACE4 expressed in HEK293 cells revealed no enzymatic activity (data not shown); hence, recombinant soluble PACE4 expressed and purified from insect cells (provided by R. Day, Université de Sherbrooke, Sherbrooke, Canada [ref. 21]) was used for the assay. Pro-GST-OCN or LCN2 in vitro digestions were performed in PC buffer with 200 ng substrate and 0.7 units of PC, and mature OCN was detected by Western blotting using anti-OCN antibodies.

Gene expression. Osteoblasts and calvaria total RNA were isolated using TRIzol Reagent (Invitrogen, Thermo Fisher Scientific). RNAs were reverse transcribed using M-MLV Reverse Transcriptase (Invitrogen, Thermo Fisher Scientific), and real-time quantitative PCR (qPCR) was

performed using SYBR Green qPCR Master Mix (BiMake) and gene-specific primers (see Supplemental Table 3-1). Expression levels were normalized to *Actb* expression levels.

Additional details on the methods used in this study are provided in the supplemental material.

Statistics. Statistical analyses were performed using GraphPad Prism software version 7.03. Results are shown as the mean \pm SEM. For single measurements, an unpaired, 2-tailed Student's *t* test was used, while 1-way ANOVA followed by Bonferroni's post test was used for comparison of more than 2 groups. For repeated measurements (e.g., GTTs and ITTs), a repeated-measures 2-way ANOVA followed by Bonferroni's post test was used. A *P* value of less than 0.05 was considered statistically significant. All experiments were repeated at least 3 times or performed on at least 3 independent animals.

Study approval. All animal use complied with the guidelines of the Canadian Committee for Animal Protection and was approved by IRCM Animal Care Committee.

3. RESULTS

Pro-OCN is cleaved by an intracellular PC. The putative mouse OCN propeptide exhibits a C-terminal motif consisting of 3 basic residues: Arg-Leu-Arg-Arg (**RLRR**⁴⁹), which is highly conserved throughout bony vertebrates (Figure 3-1A). Because this type of basic residue-containing motif represents a consensus recognition site for PCs that is found in many secreted proteins (18), we hypothesized that pro-OCN may be cleaved by 1 or more PCs in osteoblasts. In support of this hypothesis, mutation of the RLRR sequence into ALAA resulted in a molecular shift of the OCN secreted in the culture medium of osteoblast cultures, consistent with retention of the propeptide in the mutated protein (Figure 3-1B). Furthermore, treatment of primary osteoblast cultures with decanoyl-RVKR-chloromethyl ketone (Dec-RVKR-CMK), a cell-permeable inhibitor that blocks all 7 subtilisin/kexin-like PCs, resulted in a similar molecular shift of either endogenous OCN secreted from primary osteoblast cultures or a V5-tagged version transfected in osteoblasts or in CHO-IdID cells (Figure 3-1, C–E). That Dec-RVKR-CMK treatment and the ALAA mutation induced an identical migration shift by SDS-PAGE suggests that the RLRR motif is the

main, if not only, sequence present in pro-OCN that is recognized and cleaved by a PC (Figure 3-1E). Last, treatment of osteoblasts with hexa-D-arginine (D6R), a nonpermeable inhibitor that blocks only extracellular or cell-surface PCs (20), had no impact (Figure 3-1E). Altogether, these results suggest that an intracellular PC in osteoblasts contributes to the conversion of pro-OCN to OCN.

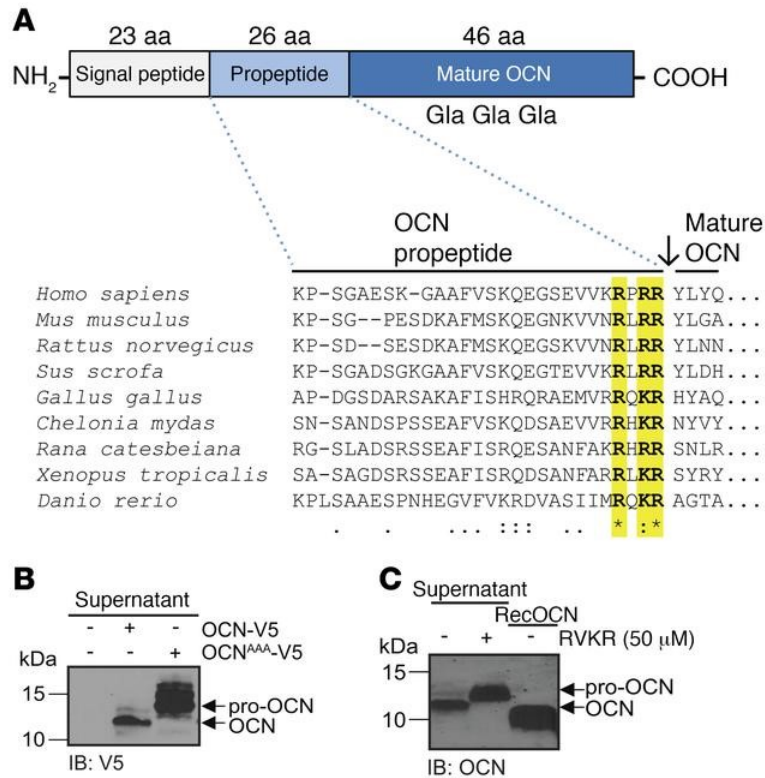


Figure 3-1. PC cleaves pro-OCN at the RXRR motif in osteoblasts. (A) Schematic representation of the pre-pro-OCN protein including the approximate positions of the Gla residues, and amino acid alignment of OCN propeptide sequences from various vertebrate species: the conserved RX(R/K)R motif is highlighted in yellow. Consensus symbols are included below the alignment. A single asterisk indicates a fully conserved residue; a colon indicates a strongly conserved residue; a period indicates moderate or weak conservation. (B) Western blot analysis of cell supernatant from primary osteoblasts transfected with OCN-V5 or an R46A/R48A/R49A OCN mutant (OCN^{AAA}-V5), both tagged at the C-terminal with the V5 epitope. (C) Western blot analysis of endogenous OCN in the cell supernatant from differentiated mouse calvaria osteoblasts treated or not with 50 μM Dec-RVKR-CMK (RVKR).

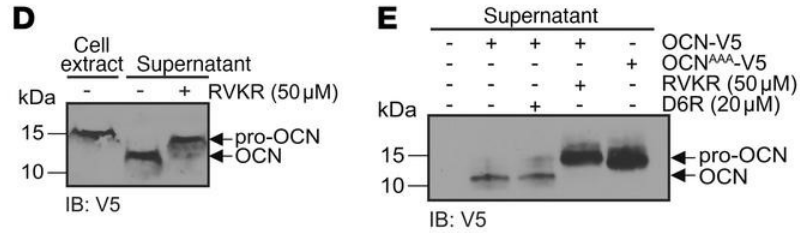


Figure 3-1- continued. A PC cleaves pro-OCN at the RXRR motif in osteoblasts. (D) Western blot analysis of cell supernatant and cell extracts of CHO-IdID cells transfected with OCN-V5 and treated or not with 50 μM Dec-RVKR-CMK. (E) Western blot analysis of the supernatant of primary osteoblasts transfected with OCN-V5 or OCN^{AAA}-V5 and treated or not with 50 μM Dec-RVKR-CMK or 20 μM D6R. IB, immunoblot.

Furin is the PC responsible for pro-OCN cleavage in osteoblasts. In an effort to identify the PC responsible for pro-OCN cleavage in osteoblasts, we first assessed the expression of the 8 subtilisin/kexin-like PCs in this cell type. As shown in Figure 3-2A, mRNAs encoding furin (*Furin*) and PACE4 (*Pcsk6*) were expressed at high levels in this cell type, while mRNAs encoding PC7 (*Pcsk7*) and PC5A (*Pcsk5a*) were detected at lower levels. *Pcsk1*, *Pcsk2*, *Pcsk5b*, and *Pcsk4* mRNAs were either not detectable or expressed at very low levels in osteoblasts. Of note, the expression of both *Furin* and *Pcsk5a* was induced during osteoblast differentiation. Given these results, we next tested the capacity of furin, PC5A, PC7, and PACE4 to cleave pro-OCN in vitro. Recombinant GST–pro-OCN protein produced in bacteria was incubated with the conditioned media of HEK293 cells transfected with either an empty vector or a vector expressing the soluble extracellular enzymatic domains of furin, PC5A, or PC7, or with recombinant soluble PACE4 expressed and purified from insect cells (20, 21). The PC activity of each conditioned media or recombinant PC was measured using an artificial tetrapeptide substrate prior to the assay to ensure that an equal number of enzymatic units was used (see Methods and Supplemental Figure 3-1A; supplemental material available online with this article; <https://doi.org/10.1172/JCI93437DS1>). Furin, PC5A, and PACE4, but not PC7, were able to cleave GST–pro-OCN, releasing mature OCN (Figure 3-2B). We noticed, however, that furin was reproducibly more efficient than were PC5A and PACE4 at cleaving pro-OCN when the incubation was performed for a short period, i.e., 15 minutes (Figure 2B). In addition, further testing revealed that furin could cleave more than 80% of pro-OCN within 30 minutes and in a dose-dependent manner (Figure 3-2, C and D). Since PC5A and PACE4 are known to act primarily on extracellular or plasma membrane–bound substrates, whereas furin acts mainly intracellularly in the secretion pathway (18), these results, combined with the

observation that pro-OCN cleavage in osteoblasts was inhibited by Dec-RVKR-CMK, but not D6R (Figure 3-1E), suggest that pro-OCN is primarily a substrate for furin. Importantly, mutation of the RLRR motif to RLAA completely abrogated the activity of furin toward pro-OCN in vitro (Figure 3-2, E and F), thus demonstrating that furin is cleaving pro-OCN specifically at this dibasic site.

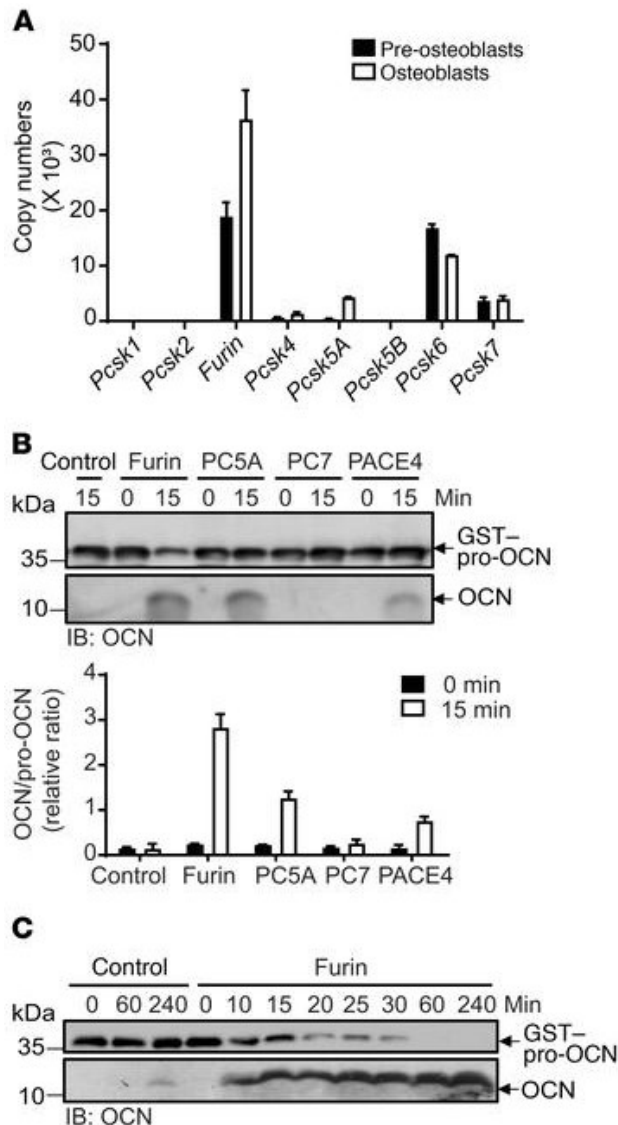


Figure 3-2. Furin cleaves pro-OCN in vitro.

(A) Relative mRNA expression levels of kexin-like PCs in mouse nondifferentiated and differentiated osteoblasts analyzed by qPCR. Copy numbers were calculated from a standard curve prepared from mouse genomic DNA, and samples were normalized using *Actb* as a reference gene ($n = 3$). (B) In vitro processing assay of GST-pro-OCN incubated for 0 or 15 minutes with equal numbers of enzymatic units of furin, PC5A, PC7, and PACE4; released OCN was assessed by Western blotting, and the relative ratio of OCN/GST-pro-OCN from 3 independent experiments was quantified (graph). (C) Time course for processing of GST-pro-OCN by furin, as assessed by Western blotting.

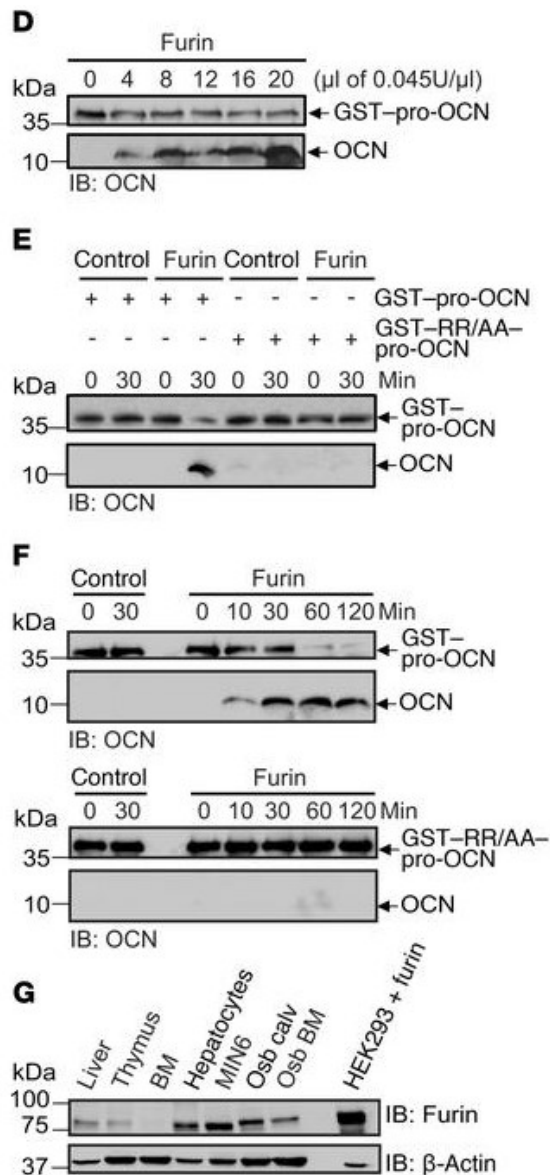


Figure 3-2- continued. Furin cleaves pro-OCN in vitro. (D) In vitro processing assay of GST-pro-OCN with increasing amounts of furin for 60 minutes, as assessed by Western blotting. (E and F) In vitro processing assay of GST-pro-OCN and the R48A/R49A OCN mutant (GST-RR/AA-pro-OCN) by furin for 30 minutes (E) or for various incubation durations (F), as assessed by Western blotting. In B-F, GST-OCN and mature OCN proteins are shown as separate Western blot exposures due to the reduced transfer efficiency of mature OCN (5 kDa) compared with that of GST-pro-OCN (36 kDa). (G) Western blot analyses of furin protein expression in the indicated tissues and cell lines. Osb calv, calvaria-derived osteoblasts; Osb BM, bone marrow-derived osteoblasts; HEK293 + furin, HEK293 cells transfected with human full-length *Furin* cDNA. Results represent the mean \pm SEM.

Consistent with the possibility that it may play an important role in osteoblasts, furin was detected in primary osteoblasts at comparable or higher levels than those observed in hepatocytes, thymus, and MIN6 β cells, where this enzyme is known to have nonredundant functions (Figure 3-2G) (22–24). We therefore next assessed the requirement for furin in pro-OCN maturation in osteoblasts. To that end, *Furin*^{fl/fl} primary osteoblasts were infected with adenovirus expressing either GFP (Ad-GFP) or Cre-GFP (Ad-Cre) to generate control and *Furin*-deficient osteoblasts (hereafter referred to as *Furin*^{-/-} osteoblasts), respectively. *Furin* expression

was significantly reduced in osteoblasts infected with Ad-Cre compared with expression levels in the control (Figure 3-3A). Remarkably, the inactivation of *Furin* in primary osteoblasts was sufficient to induce a molecular shift in the secreted OCN (Figure 3-3B). In contrast, the deletion of *Pcsk5*, the gene encoding PC5A and PC5B, in primary osteoblasts had no impact on the apparent molecular weight of OCN (Figure 3-3, C and D). Moreover, neither Dec-RVKR-CMK nor D6R further affected the apparent molecular weight of OCN in *Furin*-deficient osteoblast cultures (Figure 3-3E), suggesting that secreted OCN retained its propeptide.

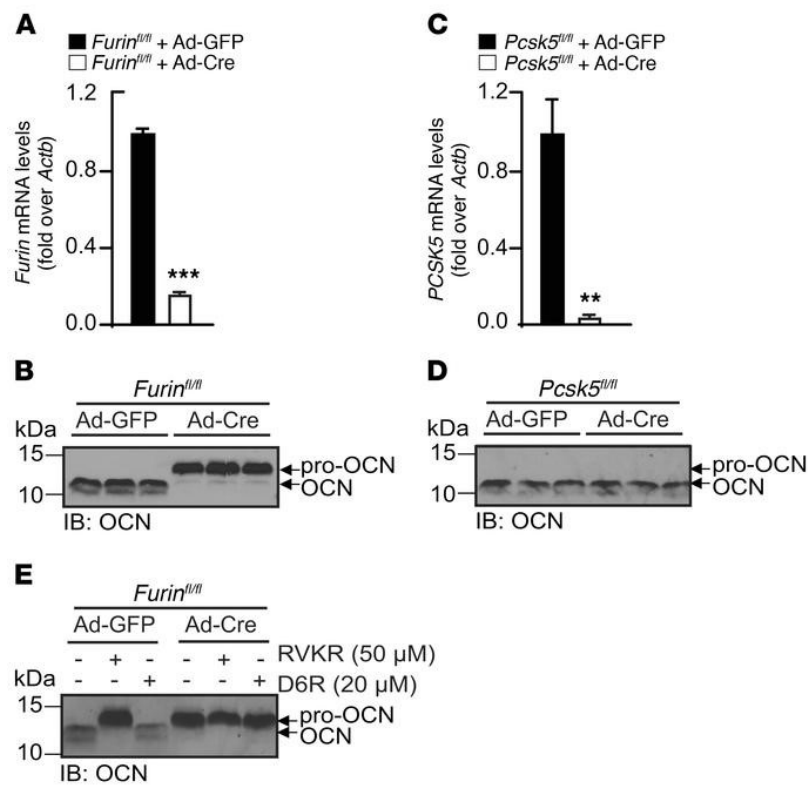


Figure 3-3. Furin but not PC5 is necessary for pro-OCN processing in osteoblasts. (A) Cre-mediated inactivation of *Furin* in *Furin^{fl/fl}* osteoblasts infected with either Ad-GFP (i.e., control osteoblasts) or Ad-Cre (i.e., *Furin^{-/-}* osteoblasts) was assessed by qPCR ($n = 3$). (B) Western blot analysis of secreted OCN from differentiated *Furin^{fl/fl}* osteoblasts infected with either Ad-GFP or Ad-Cre. (C) Cre-mediated inactivation of *Pcsk5* in *Pcsk5^{fl/fl}* osteoblasts infected with either Ad-GFP or Ad-Cre was assessed by qPCR ($n = 3$). (D) Western blot analysis of secreted OCN from differentiated *Pcsk5^{fl/fl}* osteoblasts infected with either Ad-GFP or Ad-Cre. (E) Western blot analysis of secreted OCN from differentiated *Furin^{fl/fl}* mouse calvaria osteoblasts infected with either Ad-GFP or Ad-Cre and treated or not with 50 μ M Dec-RVKR-CMK or 20 μ M D6R. Results represent the mean \pm SEM. ** $P < 0.01$ and *** $P < 0.001$, by unpaired, 2-tailed Student's t test.

To visualize the interaction between furin and pro-OCN, mouse osteoblasts were transfected with a pro-OCN construct in which the propeptide of OCN was tagged with a 3X FLAG epitope at its N-terminus, and the intracellular localization of pro-OCN and furin were assessed by immunofluorescence. As shown in Figure 3-4A, both the FLAG–pro-OCN and the noncleavable mutant (FLAG–pro-OCN^{AAA}) signals overlapped with the furin signal (middle and bottom panels), suggesting colocalization of pro-OCN with furin. However, the FLAG–pro-OCN^{AAA} was more abundant intracellularly than was the FLAG–pro-OCN construct (Figure 3-4A, middle and bottom panels). Quantification of the FLAG–pro-OCN immunofluorescence signal intensity and Western blotting confirmed an increase in the intracellular levels of pro-OCN when the furin cleavage site was mutated (Figure 3-4, B and C). Consistent with the observations made using furin-deficient osteoblasts (Figure 3-3B), FLAG–pro-OCN^{AAA} was still secreted (Figure 3-4C), indicating that retention of the propeptide does not prevent secretion of the protein. Altogether, these in vitro and cell biology experiments support the notion that furin is the primary, if not sole, PC responsible for pro-OCN processing in osteoblasts.

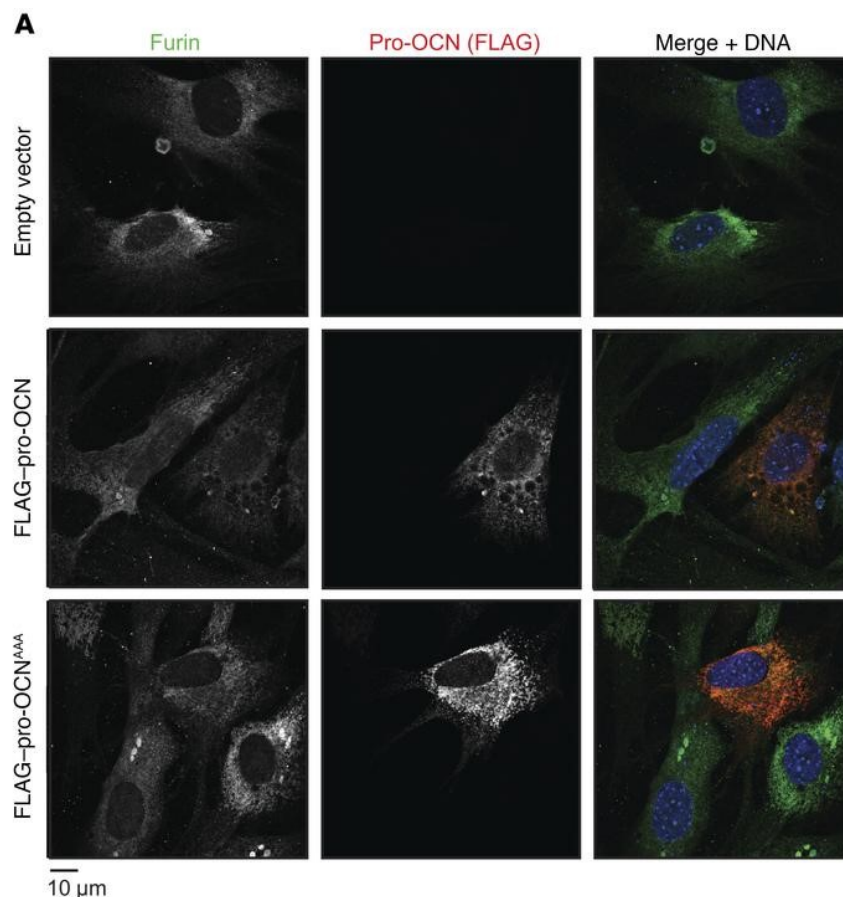


Figure 3-4. Furin and pro-OCN colocalize in osteoblasts.

(A) Representative images of immunofluorescence analyses of primary osteoblasts transfected with FLAG–pro-OCN or the R46A/R48A/R49A FLAG–pro-OCN mutant (FLAG–pro-OCN^{AAA}) expressed from the p3xFLAG-Myc-CMV-23 vector. Furin is shown in green, FLAG (i.e., pro-OCN) in red, and DNA (DAPI) in blue. Scale bar: 10 μm.

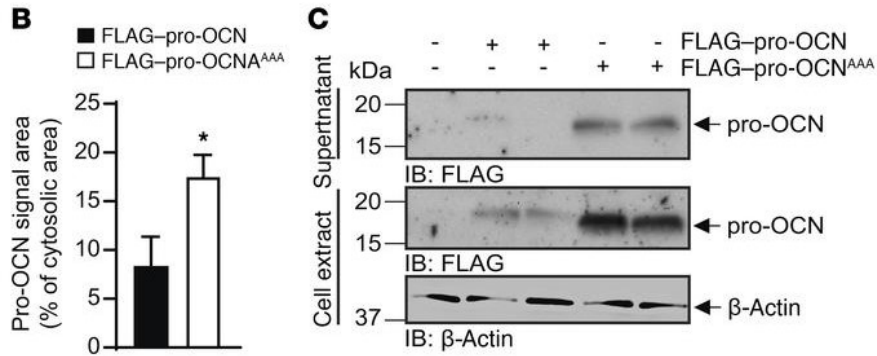


Figure 3-4- continued. Furin and pro-OCN colocalize in osteoblasts. (B) Quantification of the red signal area in primary osteoblasts transfected with either FLAG–pro-OCN ($n = 9$ cells) or FLAG–pro-OCN^{AAA} ($n = 7$ cells). Results represent the mean \pm SEM. * $P < 0.05$, by unpaired, 2-tailed Student’s t test. (C) Western blot analysis of cell supernatant and cell extract from primary osteoblasts transfected with either FLAG–pro-OCN or FLAG–pro-OCN^{AAA}.

Pro-OCN γ -carboxylation and its processing are uncoupled in osteoblasts. In hepatocytes, the cell type in which γ -carboxylation has been the most extensively studied, this posttranslational modification of proteins occurs in the ER (10). Yet furin was shown to be active mainly in the *trans*-Golgi network (TGN) and beyond in several cell types (25, 26), thus suggesting that pro-OCN γ -carboxylation and cleavage by furin might occur sequentially in osteoblasts. To test whether these 2 processes interfere with each other, differentiated osteoblasts were treated with either warfarin, which inhibits γ -carboxylation by blocking vitamin K reduction (10), or with Dec-RVKR-CMK, and pro-OCN processing and γ -carboxylation were assessed. As shown in Figure 3-5A, warfarin efficiently blocked OCN γ -carboxylation, but did not influence its processing. Conversely, treatment with Dec-RVKR-CMK efficiently blocked pro-OCN processing, but had no significant impact on its γ -carboxylation (Figure 3-5B). Similarly, mutation of the 3 OCN glutamic acid (E) residues targeted by γ -carboxylation to aspartic acid (D), a mutation known to prevent this posttranslational modification in prothrombin (27), did not affect the maturation of pro-OCN to OCN in primary osteoblasts (Figure 3-5C). We also assessed the impact of pro-OCN γ -carboxylation on its processing in vivo by studying mice lacking *Ggcx* only in osteoblasts (*Ggcx*^{fl/fl} *OCN-Cre* mice, hereafter referred to as *Ggcx*^{osb-/-} mice) (12). Since the absence of γ -carboxylation prevents OCN from accumulating in the bone ECM in these mice, we evaluated OCN processing in the serum by immunoprecipitation and Western blotting. Although circulating OCN was not γ -carboxylated in *Ggcx*^{osb-/-} mice, its migration was similar to that of OCN from control serum,

indicating that OCN is processed into its mature form *in vivo*, even in the absence of γ -carboxylation (Figure 3-5D).

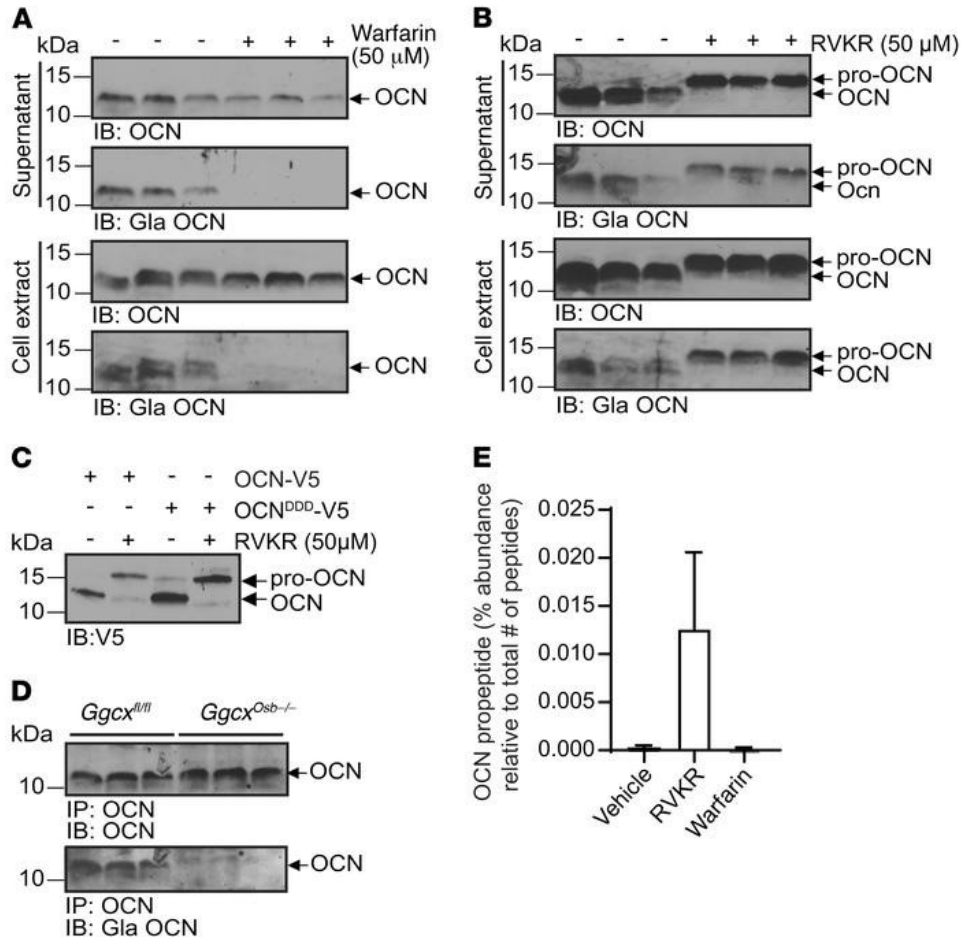


Figure 3-5. Pro-OCN processing and γ -carboxylation occur independently of each other in osteoblasts.

(A and B) Western blot analysis of endogenous total OCN (OCN) and γ -carboxylated OCN (Gla OCN) of cell supernatant and cell extract from differentiated mouse osteoblasts treated or not with 50 μ M warfarin (A) or 50 μ M Dec-RVKR-CMK (RVKR) (B). (C) Western blot analysis of supernatant from osteoblasts transfected with OCN-V5 or the E13D/E17D/E20D OCN-V5 mutant (OCN^{DDD}-V5) and treated or not with 50 μ M Dec-RVKR-CMK. (D) Western blot analysis of OCN immunoprecipitated from the serum of control mice (*Ggcx*^{fl/fl}) and mice lacking γ -carboxylase in osteoblasts (*Ggcx*^{Osb-/-}). Total OCN and γ -carboxylated OCN were assessed by Western blotting. (E) LC-MS/MS analyses of cell supernatant of differentiated mouse osteoblasts treated or not with 50 μ M Dec-RVKR-CMK or 50 μ M warfarin. Quantification of the OCN propeptide area relative to the total peptide area in 3 independent experiments is shown (see also Table 3-1). Results represent the mean \pm SEM.

Finally, we sought to determine more precisely which form(s) of OCN is/are secreted by osteoblasts under normal conditions and when furin-dependent cleavage or γ -carboxylation is inhibited. For that purpose, OCN from differentiated osteoblasts was analyzed by liquid chromatography tandem mass spectrometry (LC-MS/MS) after treatment with vehicle, Dec-RVKR-CMK, or warfarin. Secreted proteins were collected, concentrated, and subjected to digestion by Arg-C, which cleaves proteins following any arginine residues. Hence, if pro-OCN was present in the medium, Arg-C would release an OCN propeptide lacking its last 3 residues, i.e., KPSGPESDKAFMSKQEGNKVVNR. Interestingly, we did not detect this peptide in the supernatant of vehicle- or warfarin-treated osteoblasts, but only in supernatant from osteoblasts treated with the PC inhibitor, together with several N-terminally truncated fragments of OCN propeptide (Table 3-1 and Figure 3-5E). These data further indicate that pro-OCN cleavage is independent of OCN γ -carboxylation and that pro-OCN processing is fully efficient in osteoblasts, as pro-OCN is virtually absent in the medium of vehicle-treated osteoblasts. Last, since OCN propeptide is not detected in the supernatant of osteoblasts in normal conditions, this suggests that the cleaved propeptide is degraded intracellularly and is not secreted. This is consistent with an early study reporting that OCN propeptide was undetectable by radioimmunoassay in human sera or in human osteosarcoma cell supernatant (28).

Table 3-1. LC-MS/MS analyses of cell supernatant of differentiated mouse osteoblasts treated or not with 50 μ M Dec-RVKR-CMK (RVKR) or 50 μ M warfarin

Peptide sequences	Exclusive spectrum count			Average Mascot ion score
	Vehicle	RVKR	Warfarin	
KPSGPESDKAFMSKQEGNKVVNR	0	3	0	35.9
SGPESDKAFMSKQEGNKVVNR	0	7	0	41.8
PESDKAFMSKQEGNKVVNR	0	1	0	29.2
ESDKAFMSKQEGNKVVNR	0	2	0	45.2

Inactivation of Furin in osteoblasts results in impaired pro-OCN processing and decarboxylation in vivo. Our cell culture data indicating that furin is responsible for pro-OCN processing in osteoblasts raised the question of whether furin is also required for pro-OCN processing in vivo. To address this question, we generated mice lacking furin specifically in osteoblasts (*Furin^{fl/fl} OCN-Cre* mice; hereafter referred to as *Furin^{osb-/-}* mice), since mice lacking furin in all cell types died in utero before skeletogenesis was initiated (29). For this purpose, *Furin^{fl/fl}* mice (30) were bred with *OCN-Cre*–transgenic mice, which express the Cre recombinase under the control of the human *OCN* promoter in differentiated osteoblasts (31).

Furin^{osb-/-} mice were born at the expected Mendelian ratios and displayed no overt developmental abnormalities. We confirmed by PCR that recombination at the *Furin* locus occurred only in bone tissues (Figure 3-6A) and that the expression of furin was appreciably reduced in osteoblast cultures derived from bone marrow mesenchymal cells from *Furin^{osb-/-}* mice compared with control osteoblast cultures, both at the mRNA and protein levels (Figure 3-6, B and C, and Supplemental Figure 3-1B). As shown in Figure 3-6D, the inactivation of *Furin* resulted in accumulation of pro-OCN and an absence of mature OCN in bones. Accordingly, OCN was only present in its proform in the serum of *Furin^{osb-/-}* mice (Figure 3-6E). Importantly, and confirming in vivo the observations made in osteoblast cultures, the absence of furin did not affect the level of γ -carboxylation of pro-OCN in the bone ECM, whether it was assessed by Western blotting or ELISA (Figure 3-6, D and F). The insulin receptor precursor (pro-INSR), another protein cleaved by furin and PACE4 in cell culture (32) and involved in the regulation of energy metabolism by osteoblasts (33), was still processed in the bones of *Furin^{osb-/-}* mice and in *Furin^{-/-}* osteoblasts (Supplemental Figure 3-1, C and D). In addition, OCN was still processed when PC5, another PC known to be expressed in osteoblasts (34) and implicated in skeletal development (35), was inactivated in this cell type (Supplemental Figure 3-1E).

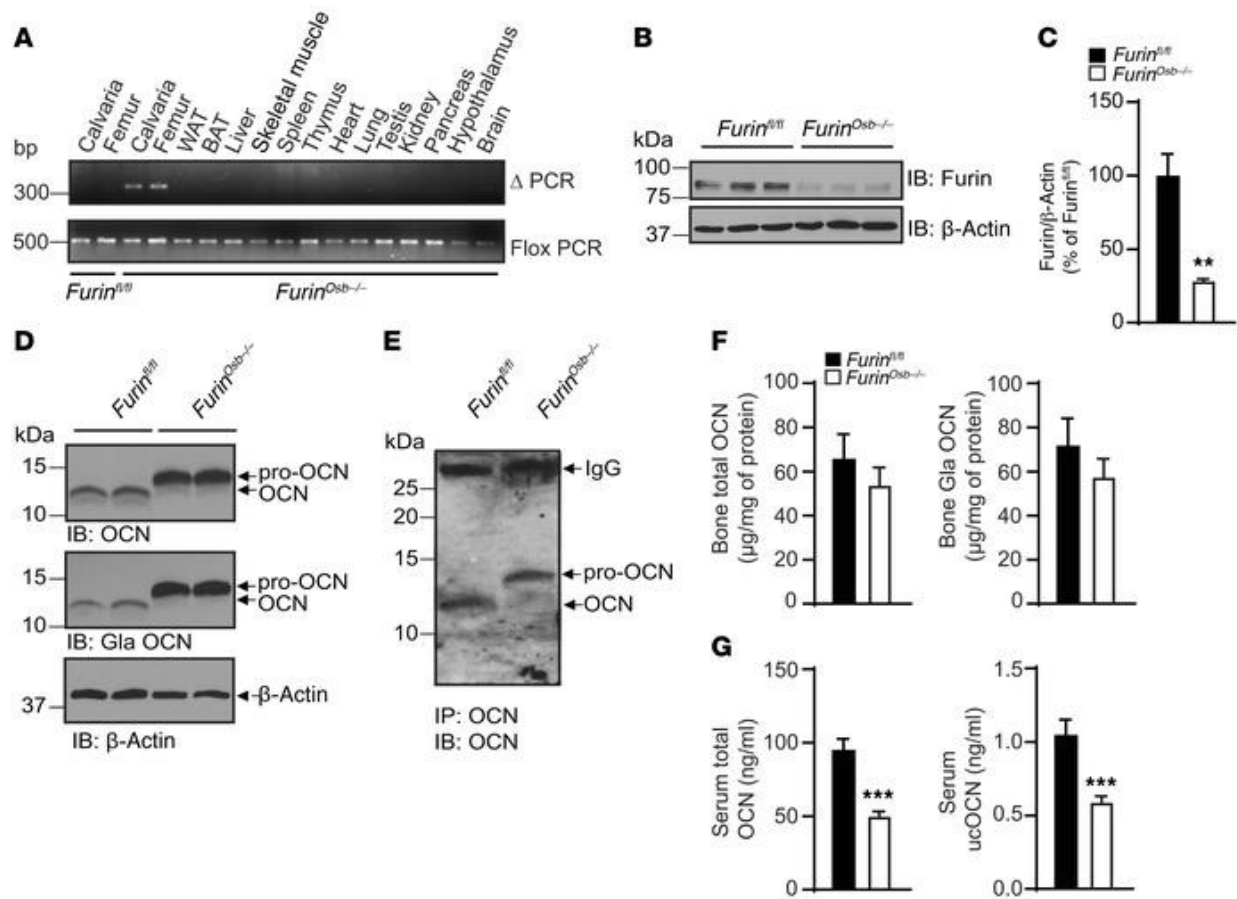


Figure 3-6. Impaired pro-OCN processing in $Furin^{osb/-}$ mice. (A) Detection of the deleted allele (Δ PCR) of *Furin* by PCR on genomic DNA extracted from different tissues. Flox PCR was used as a loading control. WAT, white adipose tissue; BAT, brown adipose tissue. (B) Furin expression in bone marrow–derived osteoblasts from $Furin^{fl/fl}$ or $Furin^{osb/-}$ mice assessed by Western blotting. (C) Quantification of furin protein levels relative to β -actin expressed as a percentage of $Furin^{fl/fl}$. (D) Western blot analysis of total OCN and γ -carboxylated OCN in bone extracts from 9-month-old $Furin^{fl/fl}$ and $Furin^{osb/-}$ mice. (E) Western blot analysis of OCN immunoprecipitated from the serum of $Furin^{fl/fl}$ or $Furin^{osb/-}$ mice. (F) Total and γ -carboxylated OCN ELISA measurements in bone homogenates from 9-month-old $Furin^{fl/fl}$ ($n = 7$) and $Furin^{osb/-}$ ($n = 8$) mice. (G) Total and ucOCN ELISA measurements in serum from 9-month-old $Furin^{fl/fl}$ ($n = 16$) and $Furin^{osb/-}$ ($n = 17$) mice. The ELISAs used in F and G quantify both pro-OCN and mature OCN. Results indicate the mean \pm SEM. ** $P < 0.01$ and *** $P < 0.001$, by unpaired, 2-tailed Student's *t* test.

Interestingly, although total bone OCN content was not reduced in $Furin^{osb/-}$ mice, circulating levels of total and ucOCN were decreased by almost 2-fold when assessed using ELISAs recognizing both OCN and pro-OCN (Figure 3-6G). These reductions were not caused by a difference in the specificity of the antibodies used in the ELISAs, since they similarly recognized pro-OCN or mature OCN under nondenaturing conditions (Supplemental Figure 3-1F). Because carboxylated OCN present in the bone ECM is converted to active ucOCN during the process of

bone resorption (14), we hypothesized that in *Furin^{osb-/-}* mice, pro-OCN was less efficiently decarboxylated and released during bone resorption compared with mature OCN. To test this possibility, RAW 264.7 preosteoclastic cells were cultured on devitalized calvaria bones isolated from control or *Furin^{osb-/-}* mice in the presence or absence of RANKL to induce osteoclast differentiation. When osteoclasts were differentiated on control bones, we could detect the release of both total OCN and ucOCN, whereas when differentiated on bones isolated from *Furin^{osb-/-}* mice, osteoclasts released less total OCN and an undetectable quantity of ucOCN (Figure 3-7A). Importantly, upon tartrate-resistant acid phosphatase (TRAP) staining, osteoclast differentiation did not appear to be impaired on *Furin^{osb-/-}* calvaria compared with control calvaria (Figure 3-7, B and C), and the expression levels of the osteoclast-specific markers *Acp5* and *Cln7* remained unchanged in the bones of *Furin^{osb-/-}* mice compared with levels in their control littermates (Supplemental Figure 3-1G), suggesting that the absence of furin in osteoblasts does not overtly impact osteoclast differentiation.

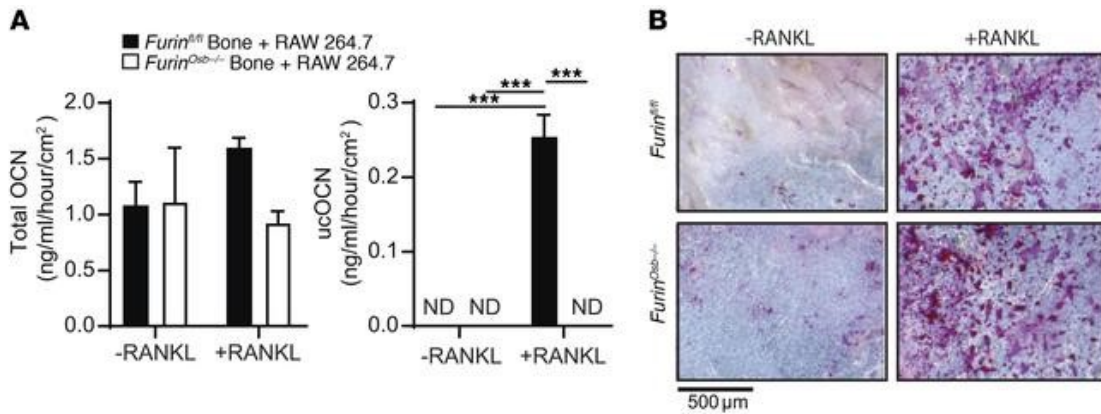


Figure 3-7. Pro-OCN is not efficiently decarboxylated by osteoclasts. (A and B) In vitro resorption assay of devitalized calvaria from *Furin^{fl/fl}* mice ($n = 3$) and *Furin^{osb-/-}* mice ($n = 3$) in the presence of osteoclast-like RAW 246.7 cells, with or without 10 ng/ml RANKL. (A) Total OCN and ucOCN ELISA measurements in the cell culture supernatant. ND, not detected. (B) Representative image of TRAP staining of calvaria. Scale bar: 500 μ m.

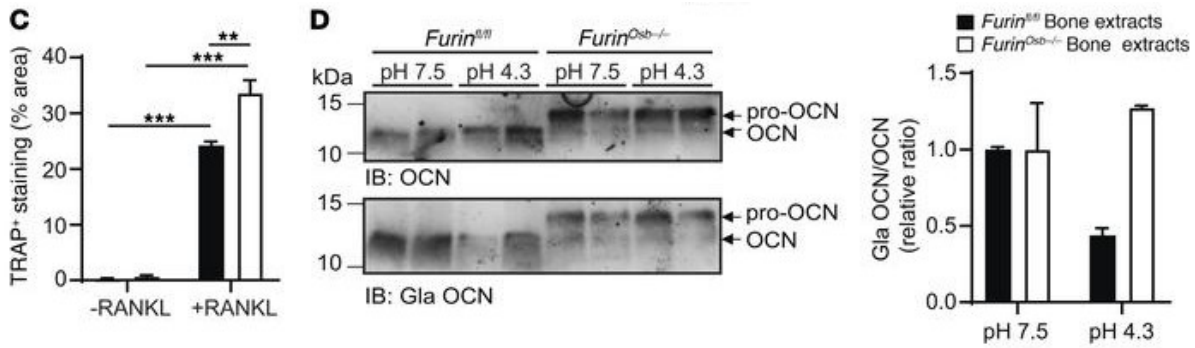


Figure 3-7- continued. Pro-OCN is not efficiently decarboxylated by osteoclasts. (C) Percentage of area with TRAP-positive staining ($n = 3$). (D) Western blot analysis of bone extracts from *Furin^{fl/fl}* and *Furin^{osb-/-}* mice incubated in phosphate-buffered solution at pH 7.5 or pH 4.3 for 14 days at 37°C. Graph shows quantification of the Gla OCN/OCN ratio (representative result from 3 independent experiments). The ELISAs used in A quantify both pro-OCN and mature OCN. Results represent the mean \pm SEM. $**P < 0.01$ and $***P < 0.001$, by 1-way ANOVA followed by Bonferroni's multiple comparisons test.

Previous studies have shown that the acidic pH generated during the process of bone resorption is responsible for OCN decarboxylation (13). Hence, we compared the decarboxylation of mature OCN and pro-OCN following incubation at a pH comparable to that found in the osteoclast resorption lacuna (i.e., pH 4.3). While the OCN contained in control mouse bone extracts was efficiently decarboxylated at pH 4.3, the pro-OCN contained in *Furin^{osb-/-}* mouse bone extracts was not (Figure 3-7D and Supplemental Figure 3-1H). Importantly, anti-Gla OCN and anti-total OCN antibodies could detect mature OCN in control bone extracts, pro-OCN in the *Furin^{osb-/-}* mouse bone extracts, and mature OCN generated following the addition of recombinant furin to the latter extracts (Supplemental Figure 3-1I). Collectively, these results suggest that, in the absence of furin, osteoblasts secrete γ -carboxylated pro-OCN, which, like mature γ -carboxylated OCN, accumulates in the bone ECM. However, pro-OCN is poorly decarboxylated and released during bone resorption, resulting in reduced circulating levels of ucOCN.

Furin in osteoblasts is required to maintain glucose and energy homeostasis. To determine how the absence of pro-OCN cleavage impacts OCN endocrine functions, we next studied glucose metabolism in *Furin^{osb-/-}* mice. Glucose tolerance and serum insulin levels were normal in *Furin^{osb-/-}* mice at 3 and 6 months of age (Supplemental Figure 3-2, A–E). However, at 6 and 9 months of age, there was a significant increase in blood glucose levels under fed conditions in *Furin^{osb-/-}* mice compared with levels in littermate controls (Supplemental Figure 3-2F and Figure 3-8A). In addition, at 9 months of age, *Furin^{osb-/-}* mice also showed reduced glucose tolerance when challenged with a glucose load (Figure 3-8B). Furthermore, in agreement with the fact that ucOCN normally favors insulin secretion by β cells, serum insulin levels were significantly reduced in the fed state in *Furin^{osb-/-}* mice compared with levels in control littermates, while fasting levels were not affected (Figure 3-8C). These results are consistent with higher blood glucose levels in *Furin^{osb-/-}* mice only in fed conditions or during a glucose tolerance test (GTT) (Figure 3-8, A and B). Moreover, and in line with the previously reported positive effect of ucOCN on insulin synthesis by β cells, pancreatic insulin content was also reduced in *Furin^{osb-/-}* mice compared with that detected in control mice (Figure 3-8D). Insulin sensitivity remained normal in *Furin^{osb-/-}* mice at 3, 6, and 9 months of age (Supplemental Figure 3-2, G–I). Finally, challenging 4-week-old *Furin^{osb-/-}* mice with a high-fat, high-sucrose diet for 10 weeks was sufficient to reduce glucose tolerance in younger animals (Figure 3-8E).

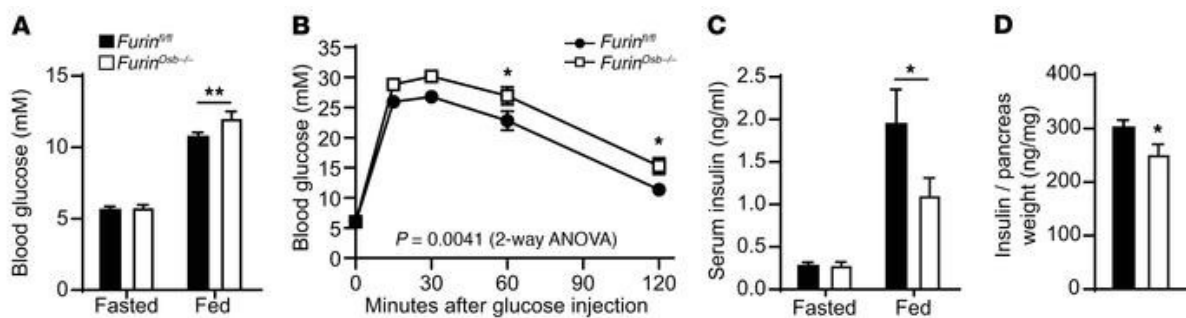


Figure 3-8. Reduced glucose tolerance in *Furin^{osb-/-}* mice. (A) Fasting and fed blood glucose levels in 9-month-old *Furin^{fl/fl}* ($n = 12$) and *Furin^{osb-/-}* ($n = 10$) mice. (B) GTT results for 9-month-old *Furin^{fl/fl}* ($n = 21$) and *Furin^{osb-/-}* ($n = 16$) mice. Mice were fasted for 16 hours and injected i.p. with 2 g/kg glucose. (C) Fasting and fed serum insulin levels in 9-month-old *Furin^{fl/fl}* ($n = 12$) and *Furin^{osb-/-}* ($n = 10$) mice. (D) Pancreas insulin content in 9-month-old *Furin^{fl/fl}* ($n = 10$) and *Furin^{osb-/-}* ($n = 10$) mice.

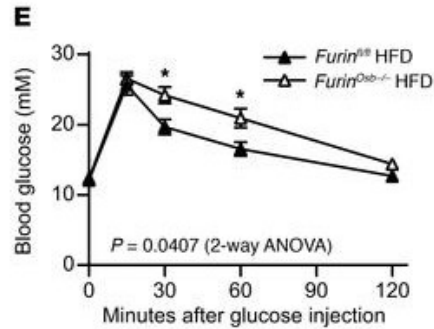


Figure 3-8- continued. Reduced glucose tolerance in *Furin*^{osb-/-} mice. (E) GTT results for 4-month-old *Furin*^{fl/fl} ($n = 8$) and *Furin*^{osb-/-} ($n = 7$) mice after 10 weeks on a high-fat, high-sucrose diet (HFD). Mice were fasted for 6 hours and then injected i.p. with 1 g/kg glucose. Metabolic assessments were performed on male mice fed a normal chow diet (A–D) or a HFD (E). Results represent the mean \pm SEM. * $P < 0.05$ and ** $P < 0.01$, by 2-way ANOVA for repeated measurements with Bonferroni’s multiple comparisons test (A–C and E) or by unpaired, 2-tailed Student’s t test (D).

Since OCN also increases energy expenditure, we assessed the energy balance in control and *Furin*^{osb-/-} mice through indirect calorimetry. At 3 and 6 months of age, chow-fed *Furin*^{osb-/-} mice displayed reduced O₂ consumption and CO₂ production in the dark phase, i.e., when the mice were more active (Figure 3-9, A and B, and Supplemental Figure 3-2, J and K), which resulted in a significant decrease in global energy expenditure (Figure 3-9C and Supplemental Figure 3-2L). We observed no decrease in physical activity in *Furin*^{osb-/-} mice during the dark and light phases (Figure 3-9, D and E), suggesting that the reduced energy expenditure of the *Furin*^{osb-/-} mice was not caused by a diminution in the voluntary movements of these animals. The lower energy expenditure in *Furin*^{osb-/-} mice was associated with an increased epididymal fat pad weight and whole-body fat tissue percentage at 12 months of age compared with control mice, although their body weight was not significantly changed compared with that of their littermate controls, whether the mice were fed a normal chow diet or a high-fat diet (Figure 3-9F and Supplemental Figure 3-3, A–D). Overall, the phenotypic characterization of *Furin*^{osb-/-} mice revealed that furin, through its expression in osteoblasts, plays a role in regulating glucose and energy metabolism. Our findings also support the conclusion that pro-OCN processing by furin is required for the complete activation of this hormone.

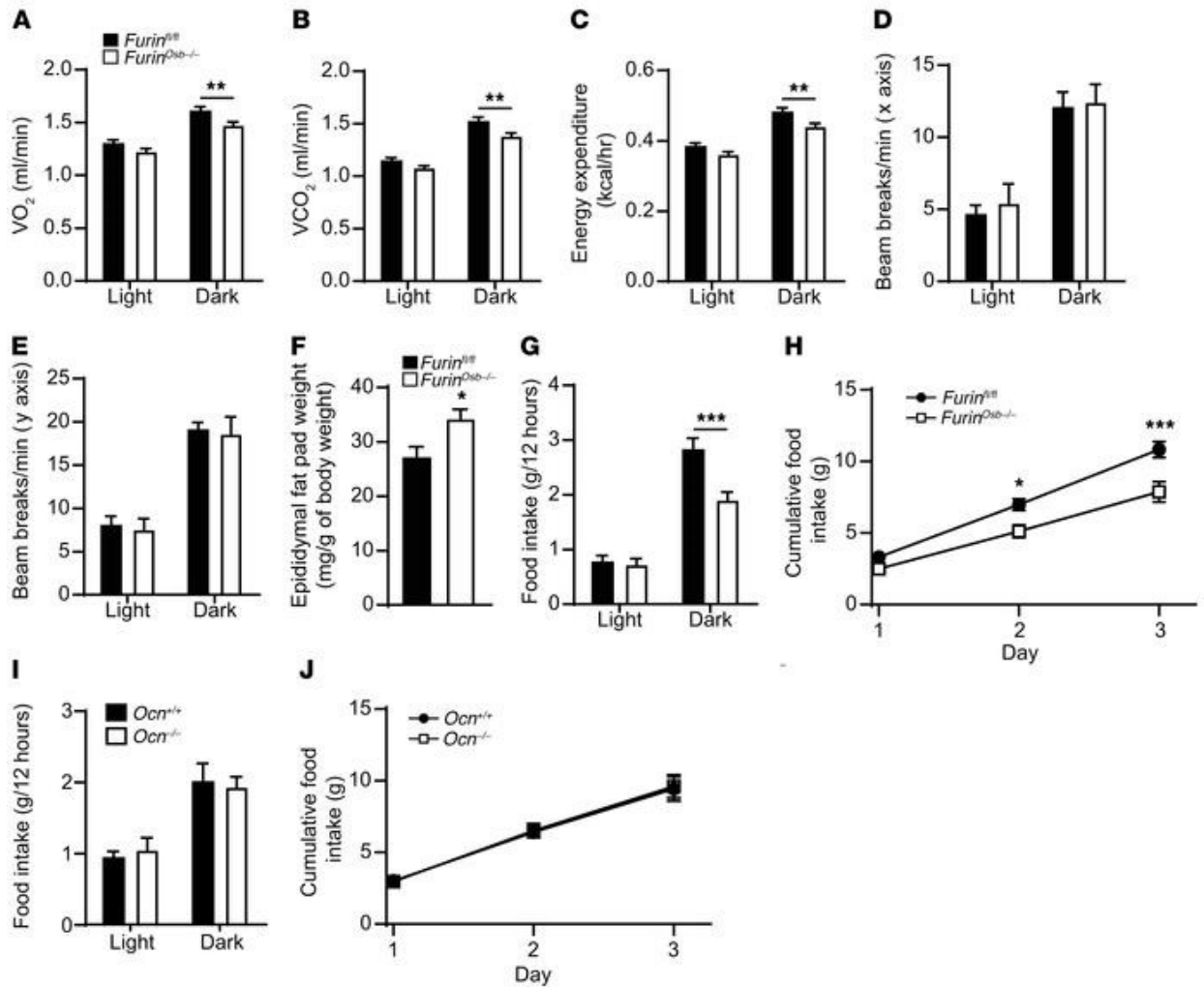


Figure 3-9. Reduced energy expenditure and food intake in *Furin^{osb-/-}* mice. (A–E) Metabolic parameters of 6-month-old *Furin^{fl/fl}* ($n = 11$) and *Furin^{osb-/-}* ($n = 9$) mice. O₂ consumption (A), CO₂ release (B), heat production (energy expenditure) (C), and activity on the x axis (D) and y axis (E). (F) Epididymal fat pad weight normalized to the body weights of 12-month-old *Furin^{fl/fl}* ($n = 12$) and *Furin^{osb-/-}* ($n = 12$) mice fed a normal chow diet. (G–J) Food intake by 6-month-old *Furin^{fl/fl}* ($n = 11$), *Furin^{osb-/-}* ($n = 9$), *Ocn^{+/+}* ($n = 8$), and *Ocn^{-/-}* ($n = 8$) mice. (G and I) Food intake during the light and dark periods. (H and J) Cumulative food intake over a 3-day period. Results represent the mean \pm SEM. * $P < 0.05$, ** $P < 0.01$, and *** $P < 0.001$, by 2-way ANOVA for repeated measurements with Bonferroni’s multiple comparisons test (A–E and G–J) or by unpaired, 2-tailed Student’s t test (F).

Furin regulates appetite through its expression in osteoblasts. *Furin^{osb-/-}* mice are characterized by normal glucose tolerance at 3 and 6 months of age when fed a regular chow diet (Supplemental Figure 3-2, A and D). Moreover, insulin sensitivity, as assessed by insulin tolerance tests (ITTs), was normal in *Furin^{osb-/-}* mice in all the age groups tested (Supplemental Figure 3-2, G–I). This contrasts with *Ocn* inactivation that results in both glucose intolerance and insulin resistance as early as 3 months of age in mice fed a chow diet (2). Likewise, on a chow diet,

Furin^{osb-/-} mice had lower fat accumulation than did *Ocn^{-/-}* mice (Figure 3-9F and ref. 2). Hence, the metabolic phenotypes are delayed or milder in *Furin^{osb-/-}* mice compared with *Ocn^{-/-}* mice. Although several possibilities could explain these differences, one of them is that furin negatively modulates other aspects of energy metabolism independently of OCN. In support of this hypothesis, we observed a significant reduction of approximately 30% in food intake by 6-month-old *Furin^{osb-/-}* mice during the dark phase (Figure 3-9G). Accordingly, cumulative food intake was reduced by approximately 20% over a 3-day period (Figure 3-9H). We found that cumulative food intake was also reduced by approximately 15% in 3-month-old *Furin^{osb-/-}* mice (Supplemental Figure 3-3, E and F). In contrast, *Ocn^{-/-}* animals of the same age (6 months) and genetic background (i.e., C57BL/6J) had normal food intake compared with their WT littermates (Figure 3-9, I and J). Circulating leptin levels were not changed in *Furin^{osb-/-}* mice (Supplemental Figure 3-3G). Collectively, these observations suggest that *Furin^{osb-/-}* mice do not develop insulin resistance as robustly as do *Ocn^{-/-}* mice, in part because of a reduction in calorie intake, a condition shown previously to improve insulin sensitivity in mice (36).

To test this possibility directly, we pair fed 4-month-old control and *Furin^{osb-/-}* mice for 2 to 4 weeks to ensure similar calorie intake in both groups (Supplemental Figure 3-3H) before assessing their glucose tolerance and insulin sensitivity. As shown in Figure 3-10A, *Furin^{osb-/-}* mice were significantly heavier than the pair-fed control mice, and this was associated with an increase in the percentage of whole-body fat tissue (Figure 3-10B). When pair fed with their control littermates, *Furin^{osb-/-}* mice showed higher feeding blood glucose levels and a glucose intolerance phenotype (Figure 3-10, C and D). Finally, under these conditions, the *Furin^{osb-/-}* mice were found to be insulin resistant in comparison with the control mice, as assessed by an ITT (Figure 3-10E). Importantly, most of these phenotypes were not observed at the same age when control and *Furin^{osb-/-}* mice were fed ad libitum (Supplemental Figures 3-2 and 3-3). Since LCN2 was recently identified as a bone-derived hormone regulating appetite (37), we tested whether furin regulates appetite by processing LCN2. However, we found that furin was unable to cleave recombinant LCN2 in vitro and that the apparent molecular weight of LCN2 on Western blotting was not changed in bone extracts from *Furin^{osb-/-}* mice compared with that observed in control bone

extracts (Supplemental Figure 3-4, A and B). Finally, following refeeding, we found that circulating levels of LCN2 were the same in control and *Furin^{osb-/-}* mice (Supplemental Figure 3-4C). Together, these results support the notion that inactivation of furin in osteoblasts produces two distinct effects on energy metabolism: it reduces energy expenditure, glucose tolerance, and insulin sensitivity on one hand, and it decreases appetite on the other hand. The first effect is most likely OCN dependent, while the second one occurs through an OCN and LCN2 independent mechanism.

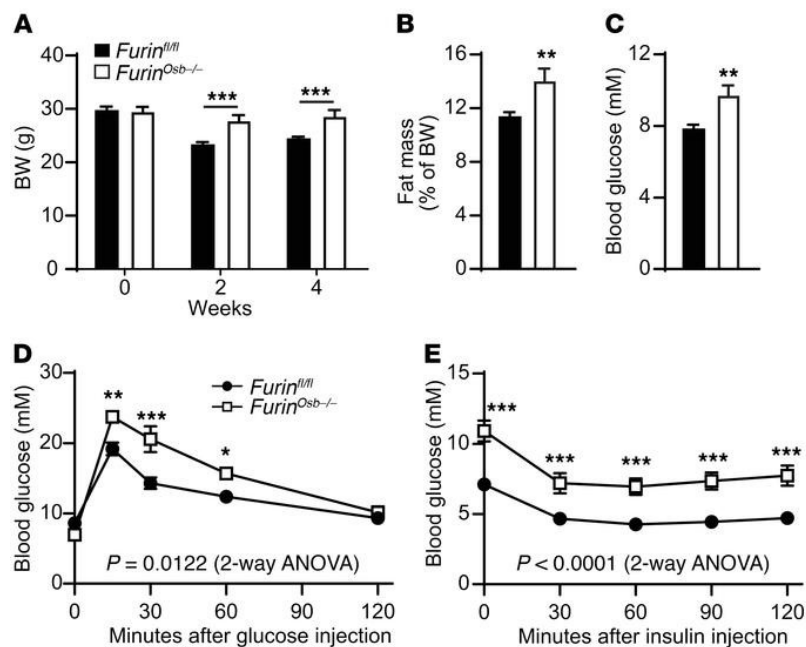


Figure 3-10. Pair feeding reveals a more severe metabolic phenotype in *Furin^{osb-/-}* mice. Metabolic phenotyping of 4-month-old pair-fed *Furin^{fl/fl}* ($n = 12$) and *Furin^{osb-/-}* ($n = 7$) mice. (A) Body weight before initiation of pair feeding (week 0) and after 2 and 4 weeks of pair feeding. (B) Percentage of total fat mass over body weight after 4 weeks of pair feeding. (C) Fed blood glucose measurement after 3 weeks of pair feeding. (D) GTT results after 4 weeks of pair feeding. Mice were fasted for 16 hours and injected i.p. with 2 g/kg glucose. (E) ITT results after 4 weeks of pair feeding. Mice were fasted for 5 hours and injected i.p. with 0.3 U/kg of insulin. Results represent the mean \pm SEM. * $P < 0.05$, ** $P < 0.01$, and *** $P < 0.001$, by 2-way ANOVA for repeated measurements with Bonferroni's multiple comparisons test (A, D, and E) or by unpaired, 2-tailed Student's t test (B and C).

4. DISCUSSION

In this study, we identified furin as the PC responsible for the conversion of pro-OCN to mature OCN in osteoblasts. Our results show that pro-OCN processing regulates the circulating levels of active unOCN, since pro-OCN is less efficiently released and decarboxylated from the bone ECM during the process of bone resorption. Accordingly, mice in which the *Furin* gene is inactivated in osteoblasts only are characterized by metabolic anomalies similar to those reported in *Ocn*-deficient animals. Together, we believe this work identifies a previously undescribed regulatory mechanism of bone endocrine function and shows that OCN activation, as with several other peptide hormones, is dependent on the activity of a specific PC.

Pro-OCN processing is dependent on furin in osteoblasts. With the use of a variety of approaches, we established that, in osteoblasts, pro-OCN maturation is exclusively performed by furin and not by the other members of the PC family. First, in vitro assays showed that pro-OCN is most efficiently processed by furin compared with the 3 other PCs expressed by osteoblasts. Second, inactivation of *Furin* in cultured osteoblasts completely abrogates pro-OCN processing. Third, in mice lacking *Furin* only in osteoblasts, pro-OCN failed to be processed and accumulated in the bone ECM. PC5 is another PC that is required for normal patterning of the axial skeleton through the processing of pro-growth differentiation factor 11 (pro-GDF11) (35). PC5 has been reported to be expressed in osteoblasts and osteocytes, where it may process FGF23, another bone-derived hormone regulating phosphate homeostasis (34). However, our data show that, although PC5A is expressed in primary osteoblasts and cleaves pro-OCN in vitro, the inactivation in this cell type of *Pcsk5*, encoding PC5A and PC5B isoforms, does not affect pro-OCN processing in cell culture or in vivo. PC5A and pro-OCN may not colocalize to the same cellular compartment, as PC5A is activated only after it reaches the cell surface (18).

Since furin deficiency leads to lethality between E10.5 and E11.5, this PC has been implicated in a limited number of postnatal functions so far. Furin was shown to be essential for the maintenance of peripheral immune tolerance through its expression in T lymphocytes (24), to play a role in the granular acidification of pancreatic β cells (23), and to be required for cardiac

development through its expression in endothelial cells (38). In contrast, studies of furin functions in liver showed that it might act redundantly with other PCs in this tissue (22, 30). In the present study, we show that furin is the cognate PC for pro-OCN activation in osteoblasts, providing genuine in vivo evidence for a nonredundant role of furin in this cell type. In classical endocrine cells, prohormones (e.g., proglucagon, proinsulin, and pro-opiomelanocortin) are generally converted to active hormones by either PC1 and/or PC2 (39, 40). Consistent with the notion that the osteoblast is a nonclassical endocrine cell, our data show that both PC1 and PC2 are not expressed in osteoblasts and that instead furin is responsible for pro-OCN conversion. Consequently, although furin was previously shown in cell culture to be responsible for parathyroid hormone (pro-PTH) conversion (41) and in the stepwise generation of growth hormone–releasing hormone (GHRH) together with PC1 (42), our study is the first to our knowledge to reveal the sole requirement for furin in the activation of a specific peptide hormone and to imply that furin has a role in endocrine regulation in vivo.

Processing of OCN is not dependent on its γ -carboxylation. The precursors of other γ -carboxylated proteins, such as thrombin and factor IX, also contain a propeptide that consists of a recognition signal for the γ -glutamyl carboxylase as well as a dibasic motif (RR) in their C-terminus (15). It is thought that processing of the propeptide in γ -carboxylated proteins could depend on their efficient γ -carboxylation (43). Although the OCN propeptide appears to contain a putative γ -glutamyl carboxylase recognition motif (44), mature OCN can be γ -carboxylated in vitro in the absence of its propeptide (16). Through several approaches, including mass spectrometry, we showed that preventing pro-OCN γ -carboxylation, either pharmacologically or genetically, did not affect its processing by furin, thereby establishing that these 2 posttranslational modifications occur independently of each other. In line with our findings, earlier studies reported that inhibition of γ -carboxylation using warfarin in the ROS 17/2.8 rat osteosarcoma cell line caused the intracellular accumulation of pro-OCN, but also the release of mature decarboxylated OCN (45, 46).

Furin in osteoblasts regulates whole-body energy metabolism in part through OCN.

Beyond 9 months of age, *Furin*^{osb-/-} mice display reduced glucose tolerance, decreased serum insulin levels, lower energy expenditure, and increased white adipose tissue mass compared with their control littermates. These phenotypes are consistent with those of *Ocn*^{-/-} mice and support the conclusion that pro-OCN processing by furin is required for the activation of this hormone. Nonetheless, some metabolic anomalies in *Furin*^{osb-/-} mice were delayed or not detected (e.g., insulin resistance) as compared with *Ocn*-deficient mice (2).

Furin^{osb-/-} mice also exhibit reduced food intake, which was not observed in *Ocn*^{-/-} mice. Because reduced calorie intake was shown to improve insulin sensitivity (36), this could explain why glucose intolerance and insulin sensitivity phenotypes are milder in *Furin*^{osb-/-} mice than in *Ocn*^{-/-} mice. Accordingly, pair feeding revealed a more severe glucose intolerance and insulin sensitivity phenotype in the *Furin*^{osb-/-} mice. Interestingly, although OCN appears to be a major mediator of bone endocrine action on energy metabolism, recent findings suggest the existence of additional bone-derived factor(s) implicated in the control of glucose metabolism. For instance, partial ablation of osteoblasts in adult mice resulted in reduced glucose tolerance, hypoinsulinemia, and decreased insulin sensitivity, as observed in *Ocn*^{-/-} mice (47). However, unlike OCN deficiency, osteoblast ablation also results in increased food intake. This earlier work supports the existence of at least 1 additional osteoblast-derived factor negatively regulating appetite and insulin sensitivity. Whether such an osteoblast-derived factor could be processed and possibly inactivated by furin is a possibility with regard to the reduced food intake detected in the *Furin*^{osb-/-} mice. A recent study identified LCN2 as an osteoblast-derived hormone that regulates appetite (37), however, our data suggest that furin does not modulate LCN2 processing or serum levels. Hence, further work will be required to identify the additional osteoblast-derived factor involved in appetite control and to determine how furin regulates its function.

Pro-OCN is less efficiently released during the process of bone resorption. Our cellular and in vivo experiments establish that, in the absence of furin, pro-OCN is not converted to mature OCN, but is still efficiently γ -carboxylated and secreted. These observations suggest that

pro-OCN processing is not required for OCN to be secreted. Similarly, it was previously shown that profactor IX, which can be processed in vitro by furin, is normally secreted in its γ -carboxylated proform in heterologous cells. However, in contrast to mature factor IX, profactor IX was found to be unable to bind phospholipid vesicles in the presence of Ca^{2+} (48). We have previously demonstrated that γ -carboxylation of OCN is absolutely required for its binding to bone ECM, since in mice lacking *Ggcn* in osteoblasts, bones are depleted of OCN (12). In contrast, pro-OCN does accumulate normally in the bones of *Furin^{osb-/-}* mice, suggesting that the propeptide does not prevent binding of the OCN Gla residues to the mineral component of bone ECM. Hence, retention of the propeptide has different effects on the calcium-binding properties of pro-OCN and profactor IX.

Although bone OCN content was normal in *Furin^{osb-/-}* mice, the circulating levels of total and ucOCN were reduced. γ -carboxylated OCN was shown to be partially decarboxylated and activated during the process of bone resorption in a nonenzymatic reaction requiring the acidic pH of the resorption lacuna generated by the osteoclasts (13, 14). Other data presented here show that pro-OCN is less efficiently decarboxylated than is mature OCN during bone resorption and following incubation at pH 4.3, suggesting that the retention of the propeptide protects OCN Gla residues from the effect of the low pH generated by osteoclasts.

What is the role of OCN propeptide if it is not required for OCN γ -carboxylation? The propeptide domain might facilitate the entry of the 96-aa-long pre-pro-OCN in the ER, its cleavage by the signal peptidase, the exit of the 72-aa-long pro-OCN from the ER, and its transport through the secretory pathway until it reaches the TGN, where furin is active (26). In support of this notion, expression of OCN without its propeptide sequence in osteoblasts greatly reduces the amount of mature OCN secreted in the media (El-Rifai and Ferron, unpublished observations). Finally, it was reported that a polypeptide must have a minimum size of at least 50 aa in order to be recognized by the signal recognition particle and threaded through the membrane of the ER (49), making the 46-aa-long OCN too small to be efficiently secreted on its own.

The lumen of the TGN is characterized by an acidic pH, i.e., as low as pH 5.9 in HeLa cells (50). Interestingly, consistent with its preferential action in the TGN, furin is more active in vitro at pH 6 than at pH 7.5 (51). Hence, we can also speculate that the normal function of OCN propeptide could be to protect OCN from undergoing premature decarboxylation while it is transiting through the TGN and the constitutive secretory pathway. Alternatively, the presence of the propeptide may prevent OCN from premature folding in the TGN, since it was reported that OCN can fold in the absence of calcium ions at pH 6 and below (52). Further investigation will be needed to specifically address these possibilities.

In summary, this work provides in vitro and in vivo evidences that the processing of the OCN prohormone by furin regulates the activation and endocrine function of OCN. Moreover, we established that furin in osteoblasts plays an important role in the regulation of energy metabolism by bone through OCN-dependent and -independent mechanisms

Acknowledgments

We are grateful to T.L. Clemens (Johns Hopkins School of Medicine, Baltimore, MD, USA) for providing *OCN-Cre* mice; S. Kousteni (Columbia University, New York, NY, USA) for providing recombinant LCN2; R. Day (Université de Sherbrooke, Sherbrooke, Canada) for providing recombinant PACE4; and A. Prat (IRCM, Montréal, Canada) for her critical reading of the manuscript. This work was supported by funding from the Canada Research Chair program (to MF and NGS); the Fondation J.A. DeSève (to MF); the Canadian Institutes of Health Research (MOP-133652, to MF, and Foundation Scheme Grant 148263, to NGS); and the Natural Sciences and Engineering Research Council of Canada (RGPIN-2016-05213, to MF). OAR received scholarships from the IRCM and the Université de Montréal. JL is a fellow of the Canadian Diabetes Association.

5. REFERENCES

1. Karsenty G, Olson EN. Bone and muscle endocrine functions: unexpected paradigms of inter-organ communication. *Cell*. 2016;164(6):1248–1256.
2. Lee NK, et al. Endocrine regulation of energy metabolism by the skeleton. *Cell*. 2007;130(3):456–469.
3. Pi M, Wu Y, Quarles LD. GPRC6A mediates responses to osteocalcin in β -cells in vitro and pancreas in vivo. *J Bone Miner Res*. 2011;26(7):1680–1683.
4. Sabek OM, Nishimoto SK, Fraga D, Tejpal N, Ricordi C, Gaber AO. Osteocalcin Effect on Human β -Cells Mass and Function. *Endocrinology*. 2015;156(9):3137–3146.
5. Mera P, et al. Osteocalcin Signaling in Myofibers Is Necessary and Sufficient for Optimum Adaptation to Exercise. *Cell Metab*. 2016;23(6):1078–1092.
6. Ferron M, McKee MD, Levine RL, Ducy P, Karsenty G. Intermittent injections of osteocalcin improve glucose metabolism and prevent type 2 diabetes in mice. *Bone*. 2012;50(2):568–575.
7. De Toni L, et al. Osteocalcin and sex hormone binding globulin compete on a specific binding site of GPRC6A. *Endocrinology*. 2016;157(11):4473–4486.
8. Oury F, et al. Osteocalcin regulates murine and human fertility through a pancreas-bone-testis axis. *J Clin Invest*. 2013;123(6):2421–2433.
9. Di Nisio A, et al. The rs2274911 polymorphism in GPRC6A gene is associated with insulin resistance in normal weight and obese subjects. *Clin Endocrinol (Oxf)*. 2017;86(2):185–191.
10. Stafford DW. The vitamin K cycle. *J Thromb Haemost*. 2005;3(8):1873–1878.
11. Bonneau J, et al. Association between osteocalcin gamma-carboxylation and insulin resistance in overweight and obese postmenopausal women. *J Diabetes Complicat*. 2017;31(6):1027–1034.
12. Ferron M, Lacombe J, Germain A, Oury F, Karsenty G. GGCX and VKORC1 inhibit osteocalcin endocrine functions. *J Cell Biol*. 2015;208(6):761–776.
13. Ferron M, et al. Insulin signaling in osteoblasts integrates bone remodeling and energy metabolism. *Cell*. 2010;142(2):296–308.
14. Lacombe J, Karsenty G, Ferron M. In vivo analysis of the contribution of bone resorption to the control of glucose metabolism in mice. *Mol Metab*. 2013;2(4):498–504.
15. Jorgensen MJ, Cantor AB, Furie BC, Brown CL, Shoemaker CB, Furie B. Recognition site directing vitamin K-dependent gamma-carboxylation resides on the propeptide of factor IX. *Cell*. 1987;48(2):185–191.
16. Houben RJ, et al. Osteocalcin binds tightly to the gamma-glutamylcarboxylase at a site distinct from that of the other known vitamin K-dependent proteins. *Biochem J*. 1999;341(Pt 2):265–269.
17. Chrétien M, Mbikay M. 60 YEARS OF POMC: From the prohormone theory to pro-opiomelanocortin and to proprotein convertases (PCSK1 to PCSK9). *J Mol Endocrinol*. 2016;56(4):T49–T62.
18. Seidah NG, Prat A. The biology and therapeutic targeting of the proprotein convertases. *Nat Rev Drug Discov*. 2012;11(5):367–383.
19. Stijnen P, Ramos-Molina B, O’Rahilly S, Creemers JW. PCSK1 mutations and human endocrinopathies: from obesity to gastrointestinal disorders. *Endocr Rev*. 2016;37(4):347–371.

20. Susan-Resiga D, et al. Furin is the major processing enzyme of the cardiac-specific growth factor bone morphogenetic protein 10. *J Biol Chem*. 2011;286(26):22785–22794.
21. Fugère M, et al. Inhibitory potency and specificity of subtilase-like pro-protein convertase (SPC) prodomains. *J Biol Chem*. 2002;277(10):7648–7656.
22. Essalmani R, et al. Furin is the primary in vivo convertase of angiotensin-like 3 and endothelial lipase in hepatocytes. *J Biol Chem*. 2013;288(37):26410–26418.
23. Louagie E, et al. Role of furin in granular acidification in the endocrine pancreas: identification of the V-ATPase subunit Ac45 as a candidate substrate. *Proc Natl Acad Sci U S A*. 2008;105(34):12319–12324.
24. Pesu M, et al. T-cell-expressed proprotein convertase furin is essential for maintenance of peripheral immune tolerance. *Nature*. 2008;455(7210):246–250.
25. Liu G, et al. Cytoskeletal protein ABP-280 directs the intracellular trafficking of furin and modulates proprotein processing in the endocytic pathway. *J Cell Biol*. 1997;139(7):1719–1733.
26. Bresnahan PA, et al. Human fur gene encodes a yeast KEX2-like endoprotease that cleaves pro-beta-NGF in vivo. *J Cell Biol*. 1990;111(6 Pt 2):2851–2859.
27. Ratcliffe JV, Furie B, Furie BC. The importance of specific gamma-carboxyglutamic acid residues in prothrombin. Evaluation by site-specific mutagenesis. *J Biol Chem*. 1993;268(32):24339–24345.
28. Gundberg CM, Clough ME. The osteocalcin propeptide is not secreted in vivo or in vitro. *J Bone Miner Res*. 1992;7(1):73–80.
29. Roebroek AJ, et al. Failure of ventral closure and axial rotation in embryos lacking the proprotein convertase Furin. *Development*. 1998;125(24):4863–4876.
30. Roebroek AJ, et al. Limited redundancy of the proprotein convertase furin in mouse liver. *J Biol Chem*. 2004;279(51):53442–53450.
31. Zhang M, et al. Osteoblast-specific knockout of the insulin-like growth factor (IGF) receptor gene reveals an essential role of IGF signaling in bone matrix mineralization. *J Biol Chem*. 2002;277(46):44005–44012.
32. Kara I, et al. The paired basic amino acid-cleaving enzyme 4 (PACE4) is involved in the maturation of insulin receptor isoform B: an opportunity to reduce the specific insulin receptor-dependent effects of insulin-like growth factor 2 (IGF2). *J Biol Chem*. 2015;290(5):2812–2821.
33. Fulzele K, et al. Insulin receptor signaling in osteoblasts regulates postnatal bone acquisition and body composition. *Cell*. 2010;142(2):309–319.
34. Yamamoto H, et al. Posttranslational processing of FGF23 in osteocytes during the osteoblast to osteocyte transition. *Bone*. 2016;84:120–130.
35. Essalmani R, et al. In vivo functions of the proprotein convertase PC5/6 during mouse development: Gdf11 is a likely substrate. *Proc Natl Acad Sci U S A*. 2008;105(15):5750–5755.
36. Gazdag AC, Dumke CL, Kahn CR, Cartee GD. Calorie restriction increases insulin-stimulated glucose transport in skeletal muscle from IRS-1 knockout mice. *Diabetes*. 1999;48(10):1930–1936.
37. Mosialou I, et al. MC4R-dependent suppression of appetite by bone-derived lipocalin 2. *Nature*. 2017;543(7645):385–390.
38. Kim W, et al. Loss of endothelial furin leads to cardiac malformation and early postnatal death. *Mol Cell Biol*. 2012;32(17):3382–3391.
39. Zhu X, et al. Disruption of PC1/3 expression in mice causes dwarfism and multiple neuroendocrine peptide processing defects. *Proc Natl Acad Sci U S A*. 2002;99(16):10293–10298.

40. Furuta M, et al. Defective prohormone processing and altered pancreatic islet morphology in mice lacking active SPC2. *Proc Natl Acad Sci U S A*. 1997;94(13):6646–6651.
41. Hendy GN, Bennett HP, Gibbs BF, Lazure C, Day R, Seidah NG. Parathyroid hormone is preferentially cleaved to parathyroid hormone by the prohormone convertase furin. A mass spectrometric study. *J Biol Chem*. 1995;270(16):9517–9525.
42. Posner SF, Vaslet CA, Jurofcik M, Lee A, Seidah NG, Nillni EA. Stepwise posttranslational processing of progrowth hormone-releasing hormone (proGHRH) polypeptide by furin and PC1. *Endocrine*. 2004;23(2-3):199–213.
43. Himmelspach M, et al. Recombinant human factor X: high yield expression and the role of furin in proteolytic maturation in vivo and in vitro. *Thromb Res*. 2000;97(2):51–67.
44. Pan LC, Price PA. The propeptide of rat bone gamma-carboxyglutamic acid protein shares homology with other vitamin K-dependent protein precursors. *Proc Natl Acad Sci U S A*. 1985;82(18):6109–6113.
45. Pan LC, Williamson MK, Price PA. Sequence of the precursor to rat bone gamma-carboxyglutamic acid protein that accumulates in warfarin-treated osteosarcoma cells. *J Biol Chem*. 1985;260(25):13398–13401.
46. Nishimoto SK, Price PA. The vitamin K-dependent bone protein is accumulated within cultured osteosarcoma cells in the presence of the vitamin K antagonist warfarin. *J Biol Chem*. 1985;260(5):2832–2836.
47. Yoshikawa Y, et al. Genetic evidence points to an osteocalcin-independent influence of osteoblasts on energy metabolism. *J Bone Miner Res*. 2011;26(9):2012–2025.
48. Bristol JA, Freedman SJ, Furie BC, Furie B. Profactor IX: the propeptide inhibits binding to membrane surfaces and activation by factor XIa. *Biochemistry*. 1994;33(47):14136–14143.
49. Okun MM, Eskridge EM, Shields D. Truncations of a secretory protein define minimum lengths required for binding to signal recognition particle and translocation across the endoplasmic reticulum membrane. *J Biol Chem*. 1990;265(13):7478–7484.
50. Demarex N, Furuya W, D'Souza S, Bonifacino JS, Grinstein S. Mechanism of acidification of the trans-Golgi network (TGN). In situ measurements of pH using retrieval of TGN38 and furin from the cell surface. *J Biol Chem*. 1998;273(4):2044–2051.
51. Anderson ED, VanSlyke JK, Thulin CD, Jean F, Thomas G. Activation of the furin endoprotease is a multiple-step process: requirements for acidification and internal propeptide cleavage. *EMBO J*. 1997;16(7):1508–1518.
52. Isbell DT, Du S, Schroering AG, Colombo G, Shelling JG. Metal ion binding to dog osteocalcin studied by ¹H NMR spectroscopy. *Biochemistry*. 1993;32(42):11352–11362.
53. Ducy P, et al. Increased bone formation in osteocalcin-deficient mice. *Nature*. 1996;382(6590):448–452.
54. Kingsley DM, Kozarsky KF, Hobbie L, Krieger M. Reversible defects in O-linked glycosylation and LDL receptor expression in a UDP-Gal/UDP-GalNAc 4-epimerase deficient mutant. *Cell*. 1986;44(5):749–759.
55. Ferron M, Wei J, Yoshizawa T, Ducy P, Karsenty G. An ELISA-based method to quantify osteocalcin carboxylation in mice. *Biochem Biophys Res Commun*. 2010;397(4):691–696.

6. SUPPLEMENTAL METHODS

LC-MS/MS analyses. Differentiated mouse calvaria osteoblast cells were treated for 20 hours with vehicle, warfarin (50 μ M) or Decanoyl-RVKR-CMK (50 μ M). After treatment, supernatants from control and treated groups were collected and concentrated on a spin column (3 kD MWCO Amicon, EMD Millipore) pre-washed with H₂O. Buffer was then changed to 100 mM ammonium bicarbonate. Concentrated proteins were reduced using 45 mM DTT and digested with Arg-C (Progema). The LC-MS/MS analyses were performed on a LTQ Orbitrap Velos (ThermoFisher Scientific, Bremen, Germany) equipped with a Proxeon nanoelectrospray ion source. The LC column was a C18 reversed phase column packed with a high-pressure packing cell. The buffers used for chromatography were 0.2% formic acid (buffer A) and 100% acetonitrile/0.2% formic acid (buffer B). About 0.6 μ g of each sample was loaded on-column at a flowrate of 600 nL/min and eluted with a 2 slope gradient at a flowrate of 250 nL/min. Buffer B first increased from 2 to 40% in 60 min and then from 40 to 80% in 20 min. LC-MS/MS data acquisition was accomplished using an eleven scan event cycle comprised of a full scan MS for scan event 1 acquired in the Orbitrap. The mass resolution for MS was set to 60,000 (at m/z 400) and used to trigger the nine additional MS/MS events acquired in parallel in the linear ion trap for the top nine most intense ions. Standard proteomics parameters were used for the mass spectrometer. Protein database searches were performed with Mascot 2.5 (Matrix Science) against mouse. The mass tolerances for precursor and fragment ions were set to 10 ppm and 0.6 Da, respectively. The enzyme specified was semi-Arg C and two missed cleavages were allowed. Methionine oxidation and glutamic acid carboxylation were specified as variable modifications.

In vitro bone resorption assay. Calvarias from 9-months old *Furin*^{flox/flox} and *Furin*^{osb^{-/-}} mice were collected and devitalized by 3 cycles of sonication of 10 seconds each in 1X sterile PBS at maximum power and by incubation with 70% ethanol for 72h at 4°C with agitation. Calvarias of each genotype were cut into two equal pieces and cultured in 48-well plates in 100% FBS for 2 hours followed by the addition of DMEM media overnight. At day 0, pre-osteoclastic RAW 264.7 cells (ATCC) were plated on the calvarias at a density of 5000 cells/well in DMEM media supplemented with 10% FBS. At day 1, media was changed to osteoclast differentiation media,

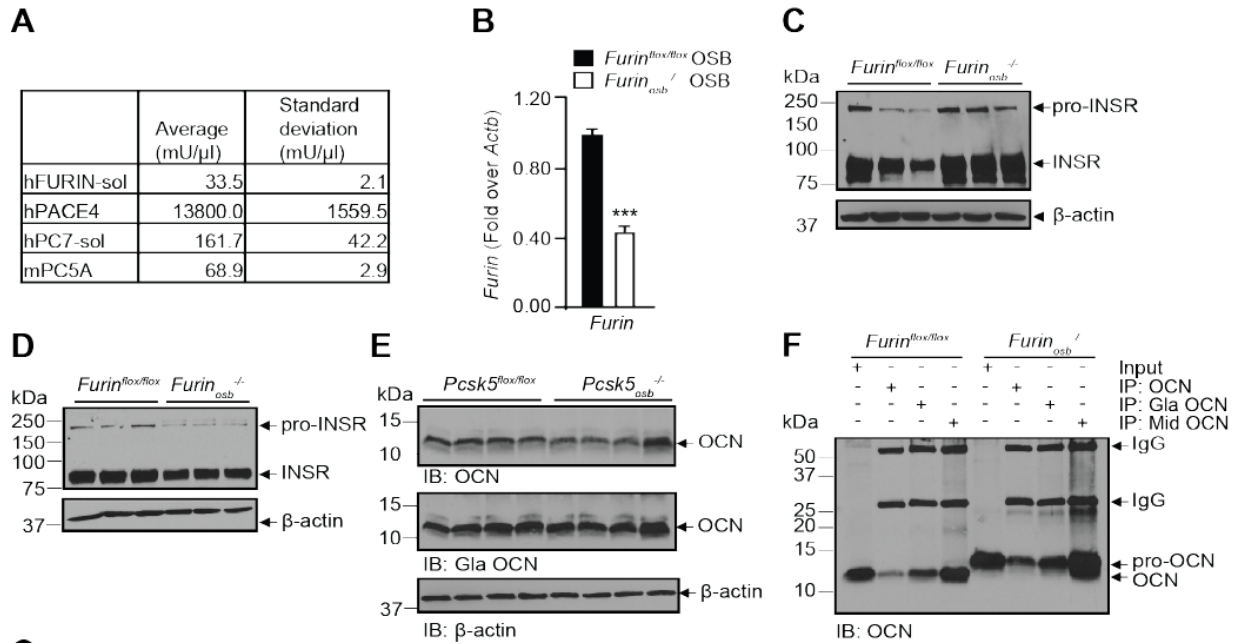
i.e. α MEM containing 10% FBS and supplemented with 10ng/ml of recombinant mouse RANK ligand (R&D). Media was changed at day 3 and 5 of culture. At day 5, media was replaced by 200 μ L of fresh media and collected 24 hours later for OCN measurement by ELISA. Calvarias and osteoclastic cells were fixed in 10% formalin, washed with PBS 1X and stained for tartrate resistant acid phosphatase (TRAP) activity to assess osteoclast differentiation. Images of TRAP staining were taken at RT using a dissecting microscope (Discovery.V12; Carl Zeiss) connected to AxioCam ERc5s camera: objectives were 0.63X and 0.8X motorized zoom. Pictures were taken using the Zen 2012 software (Carl Zeiss). The percentage area of TRAP staining on calvaria and the area of each calvaria was quantified using Image J software. OCN concentration was normalized to surface area of corresponding calvaria of each mouse.

Microscopy. Mouse pro-OCN or R46A/R48A/R49A pro-OCN mutant cDNA was cloned in p3xFLAG-Myc-CMV[™]-23 in Hind III and BamHI restriction sites to generate N-terminally 3xFLAG tagged pro-OCN. Plasmids were transfected in mouse calvaria osteoblasts plated on glass coverslips and cultured in osteoblast medium. Following 24 hours of transfection, cells were fixed in 4% paraformaldehyde for 15 min and permeabilized using 0.1% triton in 1X PBS. Following blocking for 1 hour in 10% Bovine Serum Albumin (BSA) prepared in 1X PBS, the cells were incubated with rabbit anti-FURIN and mouse anti-FLAG primary antibodies (F1804; Sigma Aldrich) overnight at 4°C. After three washes with 1X PBS for 5 min each, cells were incubated with Cy3 anti-mouse (1:1,000) (715-165-150; Jackson Immunoresearch) and Alexa Fluor 488 anti-rabbit (1:1,000) (711-545-152; Jackson Immunoresearch) secondary antibodies for 1 h. Cells were then washed 3 times with 1X PBS, stained with DAPI for 2 min to stain DNA, and mounted on slides with FluorSave reagent (EMD Millipore). Cells were imaged at RT on a confocal microscope (Leica TCS SP8) using a 63X 1.40 Oil CS2 objective with oil Immersol 158F and Leica Application Suite X (LAS X) software. Using image J software the area of red signal of FLAG-pro-OCN and blue signal of the nucleus were quantified after setting up an equal threshold for all conditions. Percentage of FLAG-pro-OCN signal was calculated using this formula:

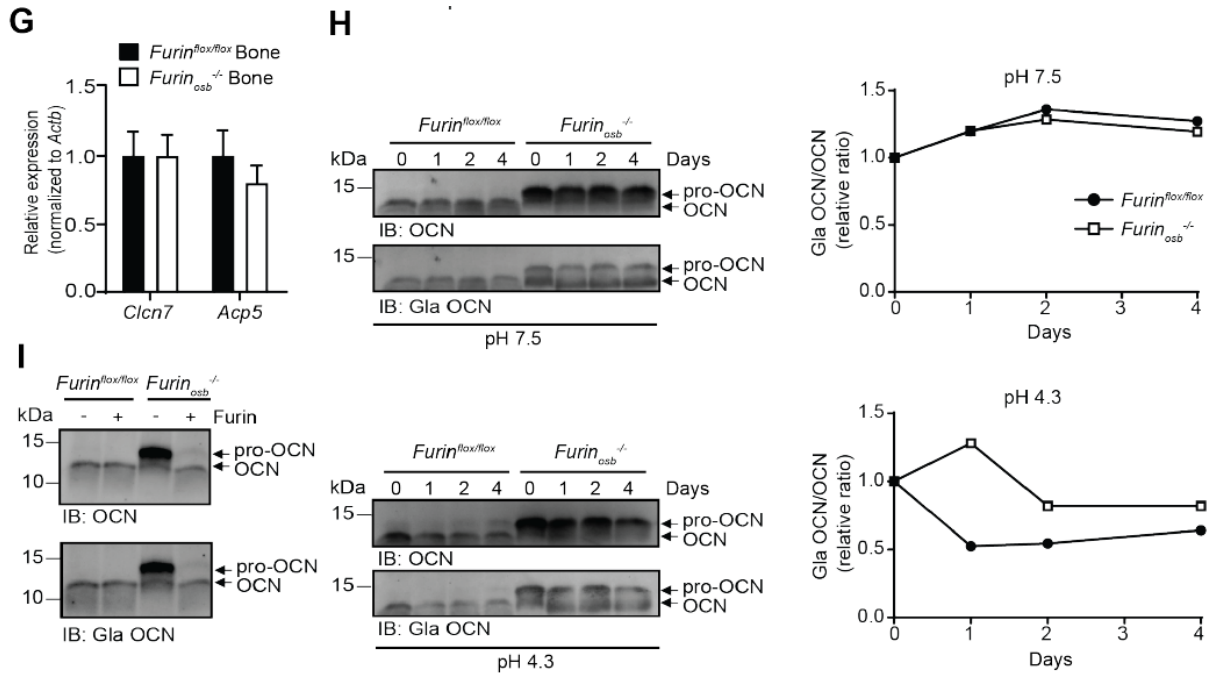
$$\text{Area of FLAG-pro-OCN (\%)} = 100 \times (\text{Area of red signal} / \text{Cytoplasm area})$$

$$\text{Cytoplasm area} = \text{Total cell area} - \text{nucleus area}$$

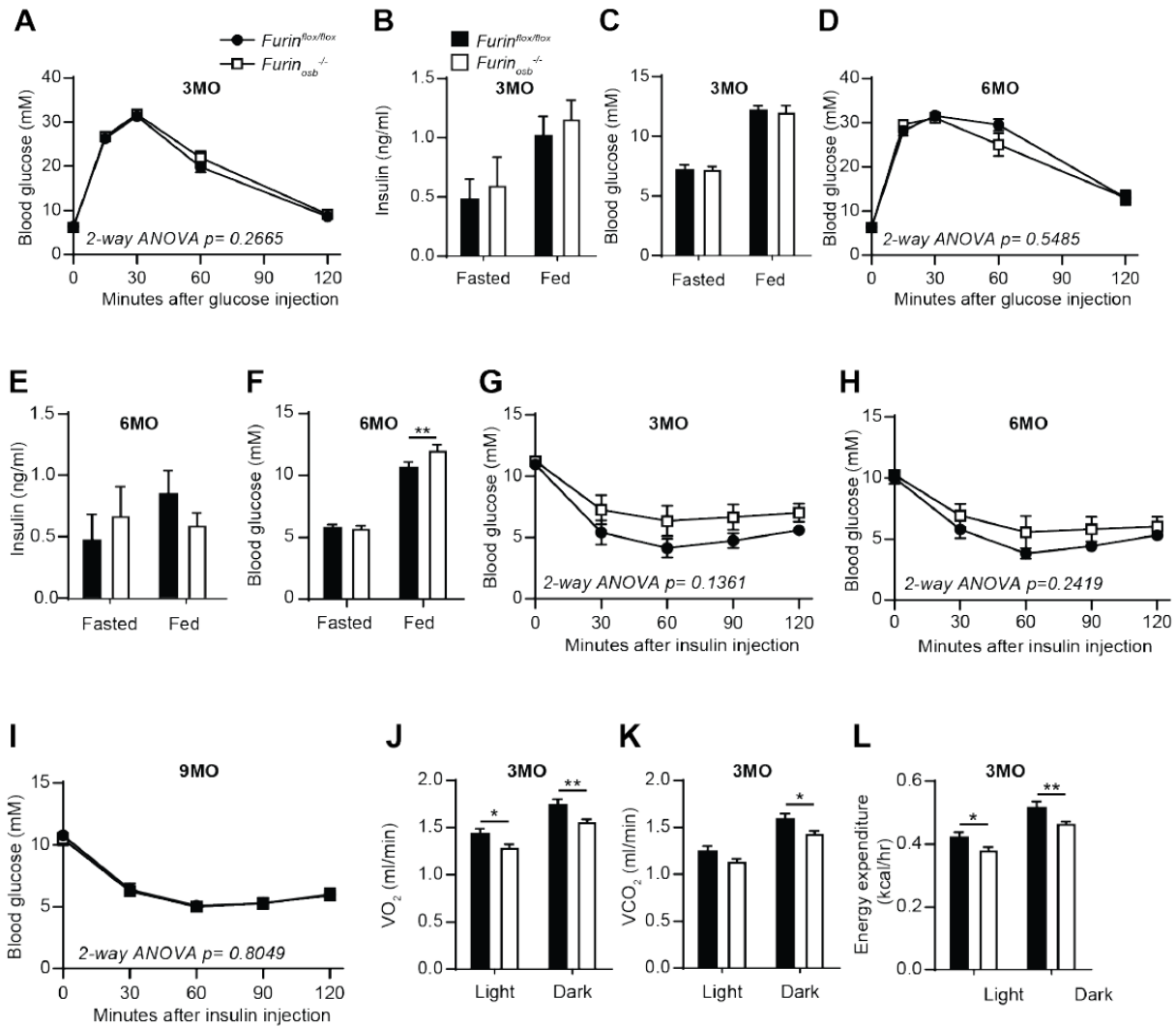
7. SUPPLEMENTAL FIGURES



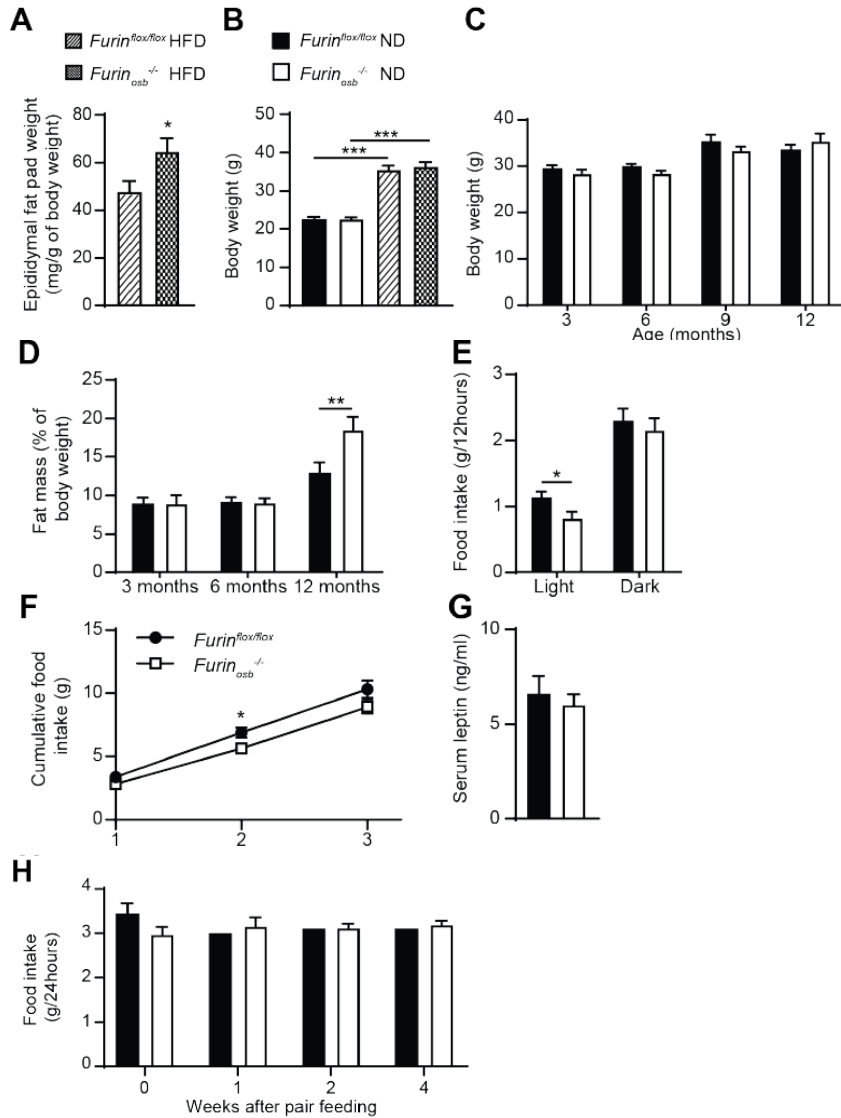
Supplemental Figure 3-1. Biochemical characterization of the *Furin^{osb}^{-/-}* mice. (A) Enzymatic unit activity of different PCs. **(B)** Relative *Furin* expression in bone marrow osteoblasts derived from *Furin^{lox/lox}* and *Furin^{osb}^{-/-}* mice assessed by QPCR (n=3). **(C-D)** Western blot analysis of insulin receptor on bone extracts from *Furin^{lox/lox}* or *Furin^{osb}^{-/-}* mice **(C)** and on cell extracts from bone marrow derived osteoblasts from *Furin^{lox/lox}* or *Furin^{osb}^{-/-}* mice **(D)**. **(E)** Western blot analysis of total (OCN) and β -carboxylated OCN (Gla OCN) on bone extracts from *Pcsk5^{lox/lox}* or *Pcsk5^{osb}^{-/-}* mice. **(F)** OCN immunoprecipitation by the different anti-OCN antibodies used in OCN ELISAs and detection of OCN by Western blotting. Immunoprecipitation was performed on bone extracts from *Furin^{lox/lox}* or *Furin^{osb}^{-/-}* mice



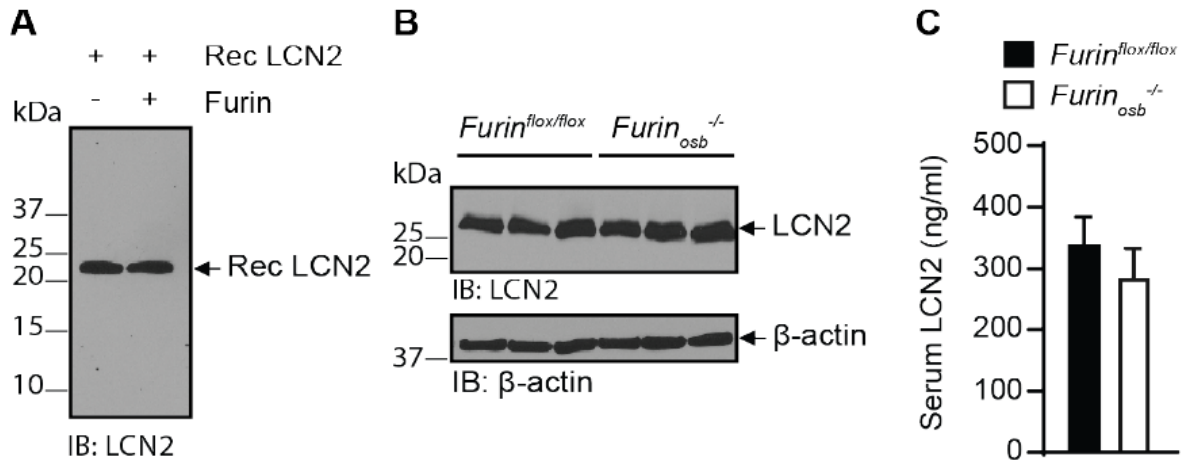
Supplemental Figure 3-1- continued. Biochemical characterization of the *Furin^{osc-/-}* mice. (G) QPCR analysis of *Clcn7* and *Acp5* gene expression in calvaria bone from *Furin^{flx/flx}* or *Furin^{osc-/-}* mice. **(H)** Western blot analyses of in vitro decarboxylation of OCN over 4 days (left panels). Bone extracts from *Furin^{flx/flx}* or *Furin^{osc-/-}* mice were incubated in phosphate buffered solution at pH 7.5 or pH 4.3 during 0-4 days at 37°C. Right panel: Quantification of Gla OCN/OCN ratio. **(I)** In vitro digestion of OCN in bone extract from *Furin^{flx/flx}* and *Furin^{osc-/-}* mice incubated for 1 hour with 1U of FURIN. Released OCN was assessed by Western blot using total OCN and Gla OCN antibodies. Results are given as means \pm SEM. ***, $p < 0.001$ using unpaired two-tailed Student's *t* tests.



Supplemental Figure 3-2. Metabolic phenotype of *Furin^{flox/flox}* and *Furin^{osb^{-/-}}* mice at 3, 6 and 9 months. Glucose metabolism phenotyping of *Furin^{flox/flox}* (n=7-11) and *Furin^{osb^{-/-}}* (n=7-10) mice fed a normal diet at 3 months (A-C) and 6 months (D-F) of age. (A, D) Glucose tolerance test. Mice were fasted for 16 h and injected I.P. with 2g/kg glucose. (B, E) Fasting and fed serum insulin measurements. (C, F) Fasting and fed blood glucose measurements. (G-I) Insulin tolerance test on *Furin^{flox/flox}* and *Furin^{osb^{-/-}}* mice fed a normal diet at 3 (G), 6 (H) and 9 (I) months of age. Mice were fasted for 5h and injected I.P. with 0.75U/kg of insulin. (J-L) Metabolic parameters of 3-month-old *Furin^{flox/flox}* (n=9) and *Furin^{osb^{-/-}}* (n=7) mice. Oxygen consumption (J), carbon dioxide release (K) and heat production (energy expenditure) (L). 3MO: 3-month-old; 6MO: 6-month-old; 9MO: 9-month-old. Results are given as mean \pm SEM. *, $p < 0.05$; **, $p < 0.01$ using 2-way ANOVA for repeated measurements with Bonferroni multiple comparisons testing.



Supplemental Figure 3-3. Reduced energy expenditure and food intake in *Furin^{osb}^{-/-}* mice at 3 months of age. (A) Epididymal fat pad weight normalized to the body weight of *Furin^{lox/flox}* and *Furin^{osb}^{-/-}* mice fed a high fat high sucrose diet (HFD) for 10 weeks. (B) Body weight of *Furin^{lox/flox}* and *Furin^{osb}^{-/-}* mice fed a normal chow diet (ND) or a HFD at 3 months of age. (C) Body weight of *Furin^{lox/flox}* and *Furin^{osb}^{-/-}* mice fed a normal diet at 3, 6, 9 and 12 months of age. (D) Fat mass % to body weight in *Furin^{lox/flox}* and *Furin^{osb}^{-/-}* at 3, 6, 9 and 12 months of age. In panels (A) through (D), n=7-12 mice per group were analyzed. (E and F) Food intake in the light and dark cycle (E) and cumulative food intake over 3 days (F) in *Furin^{lox/flox}* (n=9) and *Furin^{osb}^{-/-}* (n=7) at 3 months of age. (G) Serum leptin levels in 6-month-old *Furin^{lox/flox}* (n=11) and *Furin^{osb}^{-/-}* (n=9) mice fed a normal diet. (H) Average daily food intake in *Furin^{lox/flox}* (n=9) and *Furin^{osb}^{-/-}* (n=7) before initiation of pair feeding (week 0) and after 1, 2 and 4 weeks of pair feeding. Results are shown as mean \pm SEM. *, $p < 0.05$; **, $p < 0.01$; ***, $p < 0.001$ using unpaired two-tailed Student's *t* tests (A), 1-way ANOVA with Bonferroni multiple comparisons testing (B), 2-way ANOVA for non-repeated measurements with Bonferroni multiple comparisons testing (D) or 2-way ANOVA for repeated measurements with Bonferroni multiple comparisons testing (E and F).



Supplemental Figure 3-4. LCN2 is not processed by FURIN in osteoblasts. (A) *In vitro* processing assay of recombinant LCN2 incubated for 1h with FURIN. Released LCN2 was assessed by Western blot. (B) Western blot analysis of LCN2 on bone extracts from *Furin^{flox/flox}* or *Furin^{osb-/-}* mice. (C) Serum LCN2 level in *Furin^{flox/flox}* (n=6) or *Furin^{osb-/-}* (n=6) mice after 16h fasting followed by 2 hours of re-feeding.

Supplemental Table 3-1. List of oligonucleotides used in this study

qPCR primers for gene expression	Sequence (5'-3')	Gene	
Pcsk1-Fw	CCATGCTGCGACTCCTACAA	<i>Pcsk1</i>	
Pcsk1-Rv	TGGAGGGCTTGTGAGCTTT	<i>Pcsk1</i>	
Pcsk2-Fw	TCTAGCAAGCACCCAAAGG	<i>Pcsk2</i>	
Pcsk2-Rv	CTCTGCACATGCTTCAGGGA	<i>Pcsk2</i>	
Furin-Fw	TGTGACGGCTACACCAACAG	<i>Furin</i>	
Furin-Rv	GCTTCTCATTCTGGTTGCCG	<i>Furin</i>	
Pcsk4-Fw	CCCTCCTGTTACACCTGCTG	<i>Pcsk4</i>	
Pcsk4-Rv	TGTGCATGCATGGTTTTGGG	<i>Pcsk4</i>	
Pcsk5A-Fw	AAACCTGGCCGTCGTGATT	<i>Pcsk5 isoforme A</i>	
Pcsk5A-Rv	TGTGCACCTGCATGGTTAGT	<i>Pcsk5 isoforme A</i>	
Pcsk5B-Fw	GGCAGAACCTACCGTGCAT	<i>Pcsk5 isoforme B</i>	
Pcsk5B-Rv	CGATGTCGTCTCATCGTCC	<i>Pcsk5 isoforme B</i>	
Pcsk6-Fw	GGCTGTTCTACCTGTGTCCC	<i>Pcsk6</i>	
Pcsk6-Rv	GGCGACTAGTGATTCAGGGG	<i>Pcsk6</i>	
Pcsk7-Fw	AGATTTGCTGACCCAGAGC	<i>Pcsk7</i>	
Pcsk7-Rv	GAGGAAATCAAGGGCTGCCT	<i>Pcsk7</i>	
Actb-Fw	GACCTCTATGCCAACACAGT	<i>Actb</i>	
Actb-Rv	AGTACTTGCGCTCAGGAGGA	<i>Actb</i>	
Acp5-Fw	AGTCCTGCTTGCCGCTAAC	<i>Acp5</i>	
Acp5-Rv	CCTAAAAGGGGTGAGCCTGG	<i>Acp5</i>	
Clcn7-Fw	GACTGGCTGTGGAAAGGAA	<i>Clcn7</i>	
Clcn7-Rv	TCTCGCTTGAGTGATGTTGACC	<i>Clcn7</i>	
Primers for genotyping	Sequence (5'-3')	Genotype	
Furin flox-Fw	ATGCTCAAGGCCAGAAGATC	<i>Furin +/flox</i>	
Furin delta-Fw	GCTGTATTATTCCGGAGAC	<i>Furin delta</i>	
Furin flox-Rv	AATCTGTTCCCTGCTGAGGA	<i>Furin +/flox & Furin delta</i>	
Ggcx flox-Fw	CCATGTGTCCAAAGCATTCT	<i>Ggcx +/flox</i>	
Ggcx flox-Rv	TCATTGAGTCCTTCCCGAAC	<i>Ggcx +/flox</i>	
Bglap1-Fw	TGGAGTGGTCTCTATGACCT	<i>Ocn +/-</i>	
Neo poly A-Fw	TTCTTGACCCTGGAAGGTG	<i>Ocn +/-</i>	
Bglap2-Fw	TTGTGCTGGGGTGGTTTCTG	<i>Ocn +/-</i>	
Bglap2-Rv	AGCCTTCCCCAACCCCTATT	<i>Ocn +/-</i>	
Pcsk5 flox-Fw	CAGAATTGCTGTGCTCTGGA	<i>Pcsk5 +/flox</i>	
Pcsk5 flox-Rv	GTATTGGCATTTCCTCAGC	<i>Pcsk5 +/flox</i>	
Cre-Fw	GCGGTCTGGCAGTAAAACTATC	<i>OC-Cre</i>	
Cre-Rv	GTGAAACAGCATTGCTGTCACTT	<i>OC-Cre</i>	
Il-2-Fw	CTAGGCCACAGAATTGAAAGATCT	<i>OC-Cre</i>	
Il-2-Rv	GTAGGTGGAATTCTAGCATCATCC	<i>OC-Cre</i>	
Primers for mutagenesis	Sequence (5'-3')	Mutation	
mOcn R48A/R49A-Fw	gtgaacagactcGCgGCctacctggagc	R48A/R49A	
mOcn R48A/R49A-Rv	gctccaaggtagGCcGCgagctgttcac	R48A/R49A	
mOcn R46A/R48A/R49A-Fw	aggtagtgaaacGCactcgcgccta	R46A/R48A/R49A	
mOcn R46A/R48A/R49A-Rv	taggcgcgagtgcgttcactacct	R46A/R48A/R49A	
Primers for cloning	Sequence (5'-3')	Cloning vector	Restriction site included
Hind III pro Fw	attaaaagcctaagcccagggccctgagtct	in p3xFLAG-Myc-CMV [™] -23	Hind III
mOcn BamHI Rv	attaaggatccaatagtgataccgtagatgcg	in p3xFLAG-Myc-CMV [™] -23	BamHI
EcoRI pro Fw	aattgaattccaccatgaggacctctctc	pIRES2-EGFP-V5	EcoRI
mOcn AgeI Rv	aattaccggtaatagtgataccgtagatgcg	pIRES2-EGFP-V5	AgeI
OCN aa 24 BamHI F	ttaaGGATCCaagcccagggccctgagtc	pGEX4T3	BamHI
OCN aa 95 EcoRI R	ttaaGAATTCctaaatagtgataccatagatg	pGEX4T3	EcoRI

4. CHAPTER IV

**OSTEOCALCIN *O*-GLYCOSYLATION: A MOUSE SPECIFIC POST-
TRANSLATIONAL MODIFICATION REGULATING ITS HALF-LIFE**

4.1. HYPOTHESIS AND RELEVANCE

Using proteomics analysis on osteocalcin secreted by differentiated osteoblasts, we discovered that its subjected to *O*-glycosylation, a novel osteocalcin modification. Protein *O*-glycosylation occurs in the Golgi apparatus and involved the addition of carbohydrates moiety to serine or threonine residues. This modification was shown to regulate the endoproteolytic cleavage of protein in the secretory pathways, such as FGF23 and angiopoietin-like protein 3. In the present study we investigated the role of this modification in the regulation of other osteocalcin modifications and its impact on osteocalcin endocrine functions in vivo. We showed that osteocalcin *O*-glycosylation occurs on the serine 8 of mature mouse protein independently of its gamma-carboxylation and processing. We also found that this modification increases mouse osteocalcin half-life in plasma ex vivo and in vivo. Moreover, *O*-glycosylation is a mouse specific modification which does not occur in human or any other species. The *O*-glycosylation site of mouse osteocalcin, serine 8, corresponds to the tyrosine 12 in the human sequence. A Y12S mutation was sufficient to *O*-glycosylates human osteocalcin and increases its half-life in plasma ex vivo. These findings contribute to our understanding of the differences between mouse and human osteocalcin. They also provide a tool to improve human osteocalcin half-life in future therapeutic applications of osteocalcin in human diseases.

4.2. SECOND PAPER

The half-life of the bone-derived hormone osteocalcin is regulated through O-glycosylation in mice, but not in humans

Omar Al Rifai^{1,2}, Catherine Julien¹, Denis Faubert³, Yoshiki Narimatsu⁴, Henrik Clausen⁴ and Mathieu Ferron^{1,2,6,5.*}

1. Molecular physiology research unit, Institut de Recherches Cliniques de Montréal, Montréal, Québec H2W 1R7, Canada
2. Programme de biologie moléculaire, Université de Montréal, Québec H3T 3J7, Canada
3. Proteomics Platform, Institut de Recherches Cliniques de Montréal, Montréal, H2W 1R7, Québec, Canada
4. University of Copenhagen, Faculty of Health Sciences, Copenhagen Center for Glycomics, Departments of Cellular and Molecular Medicine and Odontology, Blegdamsvej 3, Copenhagen, Denmark
5. Département de Médecine, Université de Montréal, Québec, Canada
6. Division of Experimental Medicine, McGill University, Montréal, Québec H3A 1A3, Canada

* *Corresponding author:*

Mathieu Ferron, PhD
Institut de Recherches Cliniques de Montréal
110 Ave. des Pins O.
Montréal, QC,
H2W 1R7, Canada
Phone: 1-514-987-5754
Email: mathieu.ferron@ircm.qc.ca
Supported by grants from CIHR and NSERC

Manuscript in preparation, which will be submitted to *Elife* in March 2020

Author contributions

MF and OAR designed experiments. OAR performed most experiments (Figures 4-1B-G, 4-2A, 4-2C-F, 4-3A-G, 4-4A-H, S4-1 A, S4-2 A-G, Table S4-1, Table S4-3, Table S 4-4), with crucial help from CJ (Top down on osteocalcin from differentiated osteoblasts, Table S4-2), DF (LC-MS/MS analysis, Figure 4-1H, 4-3A-B, 4-4E-F, Table S4-2 and Table S4-3), YN (Experiment in *Cosmc*^{-/-} and *Galnt*^{-/-} cells, Figure 4-1A, 4-2B). MF and OAR wrote the manuscript with suggestions from HC. All authors discussed the results and commented on the manuscript.

ABSTRACT

Osteocalcin (OCN) is an osteoblast-derived hormone favoring insulin secretion by pancreatic beta-cells and insulin sensitivity in peripheral tissue. Here, we uncover *O*-glycosylation as a novel post-translational modification (PTM) present on mouse OCN. We identified serine 8 (S8) as the *O*-glycosylation site and showed that OCN *O*-glycosylation occurs independently of its carboxylation and processing by furin, two other PTMs regulating this hormone. Yet, *O*-glycosylated OCN is more stable in plasma ex vivo and has an increased half-life in circulation in vivo, when compared to its non-*O*-glycosylated counterpart. Remarkably, the residue corresponding to S8 is a tyrosine (Y12) in human OCN, which is not *O*-glycosylated. The Y12S mutation is sufficient to produce *O*-glycosylated human OCN and to increase its half-life in plasma compared to normal human OCN. These findings reveal an important species difference in OCN regulation, which may explain why serum concentrations of OCN are higher in mice than in humans.

1. INTRODUCTION

Osteocalcin (OCN) is a peptide hormone secreted by osteoblasts, the bone forming cells, and which regulates glucose and energy metabolism by promoting beta cells proliferation and insulin secretion, and by improving insulin sensitivity [1, 2]. Beside its regulation of energy metabolism, OCN is also involved in male's fertility by promoting testosterone synthesis by Leydig cells [3], in muscle adaptation to exercise by improving glucose and fatty acid uptake in myocytes [4], and in acute stress response through the inhibition of post-synaptic parasympathetic neurons [5]. In addition, OCN whose circulating level decreases with age, might act as an anti-geronic circulating factor preventing age-related cognitive decline and muscle wasting [6-8]. The G protein coupled receptor family C group 6 member A (GPRC6A) mediates OCN function in beta cells, muscles, and testis [1, 3, 4], while G protein coupled receptor 158 (Gpr158) mediates its function in the brain [6, 9].

Within the bone tissue, OCN undergoes a series of post-translational modifications that are critical for the regulation of its endocrine functions. Prior to its secretion, in the osteoblast endoplasmic reticulum, the OCN precursor (pro-OCN) is gamma-carboxylated on three glutamic acid residues (Glu) by the vitamin K-dependent gamma-glutamyl carboxylase [10]. In the trans-Golgi network, pro-OCN is next cleaved by the proprotein convertase furin releasing mature carboxylated OCN (Gla-OCN) [11]. The presence of the negatively charged Gla residues allows Gla-OCN to bind hydroxyapatite the mineral component of the bone extracellular matrix (ECM). It is during bone resorption that Gla-OCN is decarboxylated through a non-enzymatic process involving the acidic pH generated by the osteoclasts, ultimately leading to the release of bioactive uncarboxylated OCN (ucOCN) in the circulation [12, 13]. The conclusion that ucOCN represents the bioactive form of this protein in rodents is supported by cell-based assays, mouse genetics and in vivo studies [reviewed in [14]].

The role of OCN in the regulation of glucose metabolism appears to be conserved in humans, since human OCN can bind and activate human GPRC6A [15], and promotes beta-cell proliferation and insulin synthesis in human islets [16], while mutations or polymorphisms in

human GPRC6A are associated with insulin resistance [17, 18]. In addition, several cross-sectional and observational studies have detected an association between OCN or ucOCN and insulin sensitivity or the risk of developing T2D in various human populations [reviewed in [19-21, 31].

Nevertheless, some important species divergences exist between mice and humans with regard to OCN biology. First, only 30 out of the 46 amino acids (i.e., 65%) composing mature mouse OCN are conserved in human OCN. This is in striking contrast with other peptide hormones involved in the control of energy metabolism such as leptin and insulin whose respective sequence display up to 85% conservation between mouse and human. Second, the circulating concentrations of OCN, even though decreasing with age in both species, are 5 to 10 time higher in mice than in humans throughout life span [4] (see also Supplementary table 4-1). These observations led us to postulate the existence in mouse OCN of a species-specific post-translational modification (PTM) increasing its half-life in circulation.

Here, using proteomics and cell-based assays, we uncover *O*-glycosylation as a novel post-translational modification unique to mouse OCN, and showed that this modification increases mouse OCN half-life in plasma ex vivo and in vivo. In contrast, human OCN does not contain the *O*-glycosylation site found in the mouse protein and consequently is not naturally glycosylated. Yet, a single point mutation in human OCN is sufficient to elicit its *O*-glycosylation and to increase its half-life in plasma.

2. MATERIAL AND METHODS

Animal models. The *Furin*^{fl/fl} and *Furin*^{osb-/-} mice were generated by breeding *Furin*^{fl/fl} with *OCN-Cre*–transgenic mice that express Cre recombinase under the control of human OCN promoter as described previously [11]. *Ocn*^{-/-} mice were generated using homologous recombination to replace *Ocn1* (*Bglap1*) and *Ocn2* (*Bglap2*) genes in the mouse *Ocn* cluster with a neomycin resistance cassette [22]. All strains used in this study were backcrossed on a C57BL/6J genetic background more than 10 times and maintained under 12-hour dark/12-hour light cycles

in a specific pathogen-free animal facility (SPF) at IRCM. Male mice were used in all experiments, and they were fed a 18% normal chow diet.

DNA constructs. Mouse pro-OCN cDNA was cloned into the pIRES2-EGFP-V5 plasmid in EcoRI and AgeI cloning sites. SST/AAA pro-OCN, STT/AAA pro-OCN and 6ST/6A pro-OCN mutant were purchased originally from GeneArts. pcDNA3 human pre-pro-OCN cDNA was originally purchased from GenScript. Each construct was used as PCR template for amplification and to introduce EcoRI and AgeI cloning sites and cloned in pIRES2-EGFP-V5 plasmid. Point mutations in mouse pro-OCN (S5A; S8A, T15A) and Y12S in human pro-OCN were generated by site directed mutagenesis using specific primer (Supplementary table 4-5).

The cDNA coding of the Fc and hinge region of human immunoglobulin flanked with HindIII-BamHI restriction sites was amplified using standard PCR and pTT5-Fc1_CTL vector as template [23]. The PCR product was cloned in pcDNA3.1-myc-His B in HindIII-BamHI cloning site, generating the pcDNA3.1-Fc-hinge-myc-His vector. cDNA coding for Thrombin-hOCN (Y12S) was generated using pIRES2-EGFP-hOCN (Y12S)-V5 as template, to which thrombin (Thr) cleavage site was added at the N-terminus and BglII-EcoRI restriction site were introduced by standard PCR amplifications. Thr-hOCN (Y12S) product was cloned in the pcDNA3.1-Fc-hinge-myc-His vector. The generated vector pcDNA3.1-Fc-hinge-Thr-hOCN (Y12S) is an expression vector of human OCN fusion protein composed of the Fc and hinge region of human IgG1, thrombin cleavage site and human OCN (Y12S). Mouse and human OCN fused to Fc were generated following the same procedure and using different primers.

Cell culture and transfection. Primary osteoblasts were prepared following the previously described protocol [10]. In brief, calvariae were collected from 3 days old mice and washed with 1× PBS, digested in the digestion solution (α MEM, 0.1 mg/ml collagenase type 2 (Worthington Biochemical Corporation) and 0.00075% trypsin). The first two digestions last for 10 minutes and they were discarded. The next two 30 minutes digestions were collected, centrifuged and cultured in α MEM supplemented with 10% FBS, penicillin and streptomycin (PS), and L-glutamine.

Culture media was supplemented with 5 mM β -glycerophosphate and 100 μ g/ml L-ascorbic acid to induce osteoblasts differentiation and it was replaced every 2 days for 21 days.

Primary osteoblasts were transfected using jetPRIME Reagent (Polypus transfection). After an overnight incubation, media were changed to secretion media (FBS-free α MEM plus 2mM L-glutamine, PS). After 24 hours of secretion, media were collected, and cells were lysed in protein lysis buffer (20 mM Tris-HC, pH 7.4, 150 mM NaCl, 1 mM EDTA, 1 mM EGTA, 1% Triton, 1 mM PMSF, and 1 \times protease inhibitor cocktail) and analyzed by Western blotting. In some experiments, osteoblasts were treated with the gamma-carboxylation inhibitor warfarin (50 μ M; Santa Cruz Biotechnology), or the *N*-Acetylgalactosaminyltransferase inhibitor GalNAc-bn (2 mM, Sigma) and the proprotein convertase inhibitor Dec-RVKR-CMK (50 μ M, Tocris), combined with 22 μ M vitamin K₁ (Sandoz).

Chinese hamster ovary (CHO) cells, originally purchased from ATCC, and Chinese hamster ovary IdID cells (CHO-IdID; originating from the M. Krieger laboratory [24]) were cultured in DMEM-F12 containing PS and 5% FBS for CHO cells or 3% FBS for CHO-IdID cells and transfected using lipofectamin 2000 reagent (Life technology) following standard protocol. Secretion was performed in DMEM-F12 media supplemented with PS and 22 μ M VK₁. In some experiments, CHO-IdID culture, transfection and secretion media was supplemented with 0.1 mM galactose and/or 1 mM *N*-acetylgalactosamine (GalNAc) to rescue the *O*-glycosylation defect as previously reported [24].

Human embryonic kidney cells HEK 293 were originally purchased from ATCC. *COSMC* knockout HEK 293 cells and *GALNTs* deficient HEK293 cells were generated using zing finger nuclease (ZFN) gene editing and ZFN constructs targeting *COSMC* or specific *GALNTs* genes as described previously [25-29]. Cells were transfected using lipofectamine 2000 reagent and secretion was performed over 24 hours in EMEM supplemented with PS and 22 μ M VK₁. In some experiments, HEK 293 cells were treated with warfarin, or GalNAc-bn and Dec-RVKR-CMK combined with 22 μ M vitamin K₁.

For Western blot analysis, proteins were resolved on 15% Tris-tricine gel and blotted overnight with indicated antibody. Antibody used in this study are: anti-V5 (mouse, clone V5-10, V8012; Sigma-Aldrich), anti- β -actin (mouse, clone AC-15, A5441; Sigma-Aldrich), anti-GFP (mouse, clones 7.1 and 13.1, 11814460001; Sigma), anti-Gla OCN goat antibody which recognize amino acids 11-26 of carboxylated mature OCN and anti-CTERM OCN goat antibody which recognize amino acids 26-46 of mature mouse OCN [30].

In vitro de-glycosylation assay. Flushed mouse femur and tibia from C57BL/6J were homogenized in lysis buffer (20 mM Tris-HCl, pH 7.4, 150 mM NaCl, 1 mM EDTA, 1 mM EGTA, 1% Triton, 1 mM PMSF, and 1 \times protease inhibitors cocktail). Tissue homogenates were then centrifuged for 10 minutes at 4000 rpm to remove tissue debris. In vitro de-glycosylation assay was performed on 10 μ g of bone homogenate. Briefly, proteins were denatured in denaturing buffer at 95°C for 5 min and incubated with *O*-glycosidase and neuraminidase for 4 hours at 37°C following the NEB kit protocol (NEB; E0540S). Samples were resolved on 15% Tris-tricine SDS-PAGE gel and blotted using anti-CTERM OCN goat antibody.

Top-down LC-MS/MS analysis MS analysis of OCN in osteoblasts supernatant and on bone extract. Flushed femur and tibia from wild type mice were homogenized in lysis buffer containing (20 mM Tris-HCl, pH 7.4, 150 mM NaCl, 1 mM EDTA, 1 mM EGTA, 1% Triton, 1 mM PMSF, and 1 \times protease inhibitors cocktail). 100 μ g of protein homogenate was diluted in 1,6 ml of 100 mM phosphate buffer pH 7.4 and incubated overnight at 4°C with anti-CTERM OCN antibody. After overnight incubation, samples were centrifuged at 10000 rpm for 10 minutes, supernatant was incubated with protein-G agarose beads pre-washed with 1X PBS. After for 4 hours of agitation at 4°C, beads were spun down, washed twice with 1X PBS and three times with 50 mM Ammonium Bicarbonate pH 8. OCN was then eluted with 100 μ l of 0.5 M NH₄OH, snap frozen in liquid nitrogen and evaporated under vacuum using speedvac concentrator (Thermo scientific, savant SPD131DDA).

Samples were diluted in 25% ACN 0.3%TFA and loaded onto a 50x4.6 mm PLRP-S 300A column (Agilent Technologies) connected to an Accela pump (Thermo Scientific) and a RTC autosampler (Pal systems). The buffers used for chromatography were 0.1% formic acid (buffer A) and 100% acetonitrile/0.1% formic acid (buffer B). Proteins and peptides were eluted with a two slopes gradient at a flowrate of 120 μ L/min. Solvent B first increased from 12 to 50% in 4.5 min and then from 50 to 70% in 1.5 min. The HPLC system was coupled to a Q Exactive mass spectrometer (Thermo Scientific) through an electrospray Ion Source. The spray and S-lens voltages were set to 3.6 kV and 60 V, respectively. Capillary temperature was set to 225 °C. Full scan MS survey spectra (m/z 600-2000) in profile mode were acquired in the Orbitrap with a resolution of 70,000 with a target value at 3e6. The 4 most intense protein/peptide ions were fragmented in the HCD collision cell and analyzed in the Orbitrap with a target value at 5e5 and a normalized collision energy at 33. Data processing protocol: The identification of the different forms of OCN was performed by manual denovo sequencing.

Galnts expression in osteoblasts. RNA was extracted from non-differentiated and differentiated calvariae osteoblasts using Trizol reagent (Invitrogen, Thermo Fisher Scientific) following standard protocol. RNA was treated with DNase I, and reverse transcribed using poly dT primer, random primers and MMLV reverse transcriptase (Invitrogen). QPCR was performed on a standard of genomic DNA and cDNA products using specific primers (Supplementary primer list) and ViiA-7 QPCR machine. *Galnts* gene copy number were calculated using the genomic DNA standard curve and they were normalized to *Actb* expression level.

Production mouse and human OCN fused to the Fc region of human immunoglobulin. Human embryonic kidney cells HEK 293 were originally purchased from ATCC. To generated stable clone expressing glycosylated human and mouse OCN, HEK 293 were transfected with pcDNA3.1-Fc-hinge-Thr-hOCN (Y12S) and pcDNA3.1-Fc-hinge-Thr-OCN respectively using lipofectamine 2000 reagent. Following 48 hours of transfection, cells were trypsinized and resuspended in sorting buffer containing (1X sterile PBS, 2% FBS and 1 mM EDTA). Cells were sorted 5-10 cells/well in 96 well plates containing the selection media (EMEM, 10% FBS supplemented with

G418 sulfate [500 µg/ml; multicell]). Following two weeks of selection, single clones start to appear and the expression of mouse and human OCN was assessed using ELISA assay described in the following sections. Clones that express high level of OCN were amplified and frozen.

Purification of mouse and human OCN fused to the Fc region of human immunoglobulin.

TM102F12 clone expressing IgFc- mouse OCN fusion protein and 22H5 clone expressing IgFc-human OCN fusion protein were cultured in triple layers 175cm² flasks. After reaching 100% confluency, cells were kept to secrete in secretion media (EMEM media supplemented with 1% FBS and 10 µM warfarin to block gamma-carboxylation) for 72 hours. Secretion media was collected, filtered with 0.45 µm filter, and media was buffered 10X Binding buffer (0.2 M phosphate buffer, pH 7). Cell supernatant was then loaded into protein A affinity column (HiTrap protein A high performance, GE29-0485-76) using liquid chromatography system (GE AKTA Prime Plus). Column were then washed with 20 ml 1X binding buffer (0.02 M phosphate buffer, pH 7) and 5 ml of filtered 1X PBS. To release OCN from the column, OCN fusion protein was digested with thrombin (27-0846-01, GE healthcare) and eluted with 1X PBS, thrombin was subsequently removed using benzamidine sepharose (17-5123-10, GE healthcare). Fc region was then eluted from column using acetate buffer pH 3 and buffered with 1M Tris pH 9. Mouse and human OCN purity were assessed using Coomassie staining and MS analysis compared to a purified uncarboxylated non-O-glycosylated mouse or human ucOCN respectively. Mouse glycosylated OCN (O-Gly ucOCN) was quantified using ELISA assay as described previously [30]. Human glycosylated OCN (O-Gly uchOCN) measurements was performed using human ucOCN ELISA developed in our laboratory [31]. Briefly, ELISA plate was coated overnight at room temperature (RT) with 2µg/ml of human Glu OCN antibody (mouse, 4B6 clone recognize human ucOCN) prepared in 1X ELISA coating buffer (ImmunoChemistry Technologies). ELISA plate was then washed twice with wash buffer (1X PBS, 0.05% tween) and blocked with blocking buffer (3% FA free BSA in 1X PBS) for 4 hours at RT. Assay buffer (3% FA free BSA in 1X PBS), standards and samples were loaded and incubated overnight at 4°C. Following the incubation, ELISA plate was washed 6 times with wash buffer, incubated with 1µg/ml of human OCN antibody coupled to HRP (mouse, 4C5 clone recognize C-terminal of hOCN) for 1 hour with shaking at RT. After another 6

washes with the wash buffer, plate was tapped firmly and TMB substrate was added. Fifteen minutes later, HCl was added to stop the reaction and absorbance was measured at 450nm using an ELISA plate reader.

Ex vivo and in vivo half-life assays. The mouse OCN ex vivo half-life assays were performed on plasma (lithium heparin) collected from four independent *Ocn*^{-/-} mice. Glycosylated OCN and non-glycosylated OCN, produced in bacteria as previously [2], were incubated in plasma at 37°C and OCN level was measured at indicated time points using the total mouse OCN ELISA assay described previously [30]. Human OCN half-life assay was performed ex vivo using *Ocn*^{-/-} mice plasma as well and human OCN was measured using the ucOCN ELISA described above. In some experiment, plasma was heat inactivated for 30 minutes at 56°C, or treated with 10 mM EDTA which inhibits metalloproteases, protease inhibitor cocktail EDTA free (PI) (7X, Roche) which inhibit serine proteases and cysteine proteases, Phenylmethylsulfonyl Fluoride (PMSF, 1 mM, Sigma) which inhibit serine proteases and cysteine proteases, 4-benzenesulfonyl fluoride hydrochloride (AEBSF, 2.5 mM, Sigma) which inhibit serine proteases, cysteine proteases, plasmin and plasma kallikrein, Pepstatin A (Pep A, 10 µM, Sigma) which inhibits aspartic proteases (pepsin, cathepsin D, renin, chymosin), 50 µM RVKR which inhibits proprotein convertases, or benzamidine sepharose (BAM) which inhibits serine proteases, trypsin and trypsin like proteases).

For the in vivo half-life assay, *Ocn*^{-/-} male mice were injected intraperitoneally with 40ng/g or 80 ng/g of mouse *O*-glycosylated ucOCN or non-*O*-glycosylated ucOCN, serum OCN level was analyzed at indicated time points using total mouse OCN ELISA. In all the ex vivo and in vivo study, mouse or human proteins were prepared in saline solution containing 3.5% BSA as a carrier.

3. RESULTS

Mouse OCN is O-glycosylated on a single serine residue. We measured the level of circulating OCN in wildtype mice at different ages (2 weeks, 4 weeks, 13 weeks and 60 weeks) and compared the values with the reported serum levels of OCN at corresponding life phases in humans (Supplementary table 4-1). This analysis reveals that serum OCN level is five- to ten-time lower in humans than in mice throughout life span. One potential explication for these observations could be that mouse OCN is retained longer in circulation because of a mouse-specific protein modification increasing its half-life. Because, OCN gamma-carboxylation and pro-OCN cleavage site are conserved between mouse and human, we decided to search for additional PTMs present in mouse OCN and characterize their impact on OCN half-life.

For that purpose, OCN was immunoprecipitated from the supernatant of primary mouse osteoblast cultures and from mouse bone protein extracts using polyclonal goat antibodies recognizing its C-terminus region [30], and characterized without any proteolysis by reverse-phase HPLC followed by mass spectrometry (MS) and tandem mass spectrometry (MS/MS). This analysis revealed that the most abundant OCN forms have a monoisotopic mass ranging from 5783.68 to 6190.74 Da which exceeds the predicted mass of 5243.45 Da (Supplementary table 4-2 and 4-3). According to the various monoisotopic mass observed, we could predict that this difference could be explained by the presence of a single *O*-linked glycan adduct composed of one N-acetylgalactosamine (GalNAc), one galactose (Gal) and one or two N-Acetylneuraminic acid (NANA).

Using multiple approaches, we next established that mouse OCN is indeed subjected to *O*-glycosylation in cells and in vivo. First, OCN apparent molecular weight is reduced in HEK293 cells lacking COSMC (core 1 β 3-Gal-T-specific molecular chaperone), a protein essential to the addition of Gal on the *O*-linked GalNAc (Figure 4-1A) [26]. Second, when expressed in CHO-IdID cells which have defective UDP-Gal/UDP-GalNAc 4-epimerase and are hence deficient in *O*-glycosylation [24], OCN apparent molecular weight is also reduced compared to the same protein expressed in the parental CHO cell line (Figure 4-1B). Importantly and as expected, Gal and GalNAc

supplementation rescued the *O*-glycosylation defect of CHO-IdID and restored the molecular shift in the secreted OCN. Third, treatment of primary osteoblasts with GalNAc-bn an inhibitor of *N*-acetylgalactosaminyltransferases (GalNAc-Ts), the enzyme responsible for initiating *O*-glycosylation, decreases the apparent molecular weight of the OCN secreted in the media (Figure 4-1C). Finally, treatment of mouse bone extracts with neuraminidase and *O*-glycosidase, which remove respectively NANA, and core 1 and core 3 *O*-linked disaccharide, also decreases the apparent molecular weight of endogenous OCN (Figure 4-1D).

We next aimed to determine on which of these residue(s) OCN is glycosylated. Mature mouse OCN contains 3 serine (S) and 3 threonine (T) residues (Figure 4-1E), the two types of amino acids on which *O*-glycosylation can occur [32]. Mutating all serine and threonine residues into alanine abrogates OCN glycosylation in primary mouse osteoblasts. Further mutagenesis studies revealed that the *O*-glycosylation site resides within the N-terminal part of the protein, i.e., on S5, S8 or T15 (Figure 4-6B). Single amino acid mutagenesis allowed the identification of S8 as the *O*-glycosylation site of OCN in osteoblasts (Figure 4-1G), a result consistent with the MS/MS analysis of OCN isolated from bone which also suggested that this residue is the *O*-glycosylation site (Figure 4-1H). Together these results demonstrate that mouse OCN is *O*-glycosylated on a single serine residue in cell culture and *in vivo*.

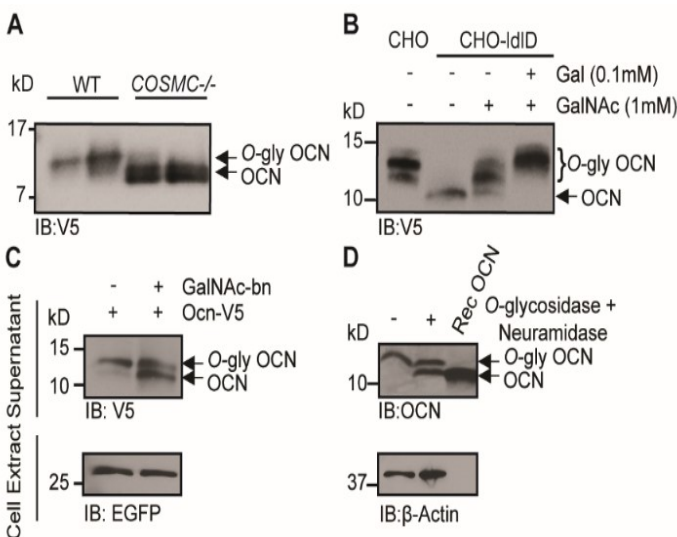


Figure 4-1. OCN is *O*-glycosylated *in vitro* and *in vivo* on Serine 8. **A)** Western blot analysis on the supernatant of HEK293 (WT) and HEK293_{sc} (COSMC^{-/-}) transfected with mouse OCN-V5. **B)** Western blot analysis on the supernatant of CHO and CHO-IdID cells transfected with mouse OCN-V5, CHO-IdID cells were treated or not with 0.1 mM Gal (Galactose) and/or 1 mM GalNAc (*N*-acetylgalactosamine). **C)** Western blot analysis on the supernatant of osteoblasts transfected with mouse OCN-V5 and treated or not with 2 mM of GalNAc-bn. **D)** Western blot analysis of OCN deglycosylation assay. Bone extract of C57B6J mice were treated or not with *O*-glycosidase and neuraminidase for 4 hours at 37°C and analyzed by western blot using OCN antibody.

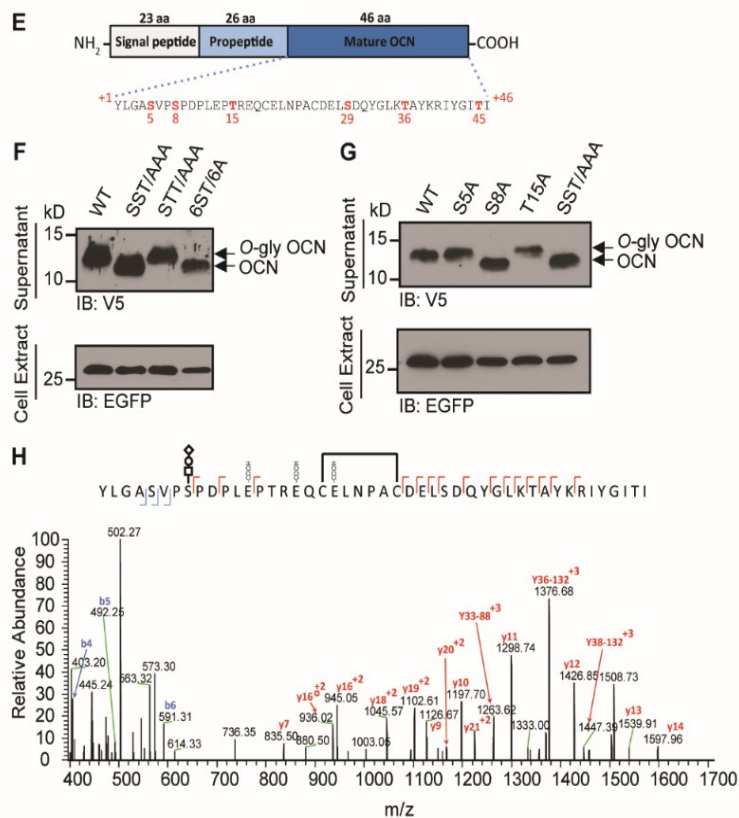


Figure 4-1- continued. OCN is O-glycosylated in vitro and in vivo on Serine 8. E) Amino acid sequence of mouse pre-pro-OCN. **F and G)** Western blot analysis on the supernatant of osteoblasts transfected with WT or different mutant of mouse OCN-V5. **F)** SST/AAA mutant (Serine 5, Serine 8 and Threonine 15 were mutated to Alanine), STT/AAA (Serine 29, Threonine 36 and Threonine 45 were mutated to Alanine), 6ST/6A (Serine 5, Serine 8, Threonine 15, Serine 29, Threonine 36 and Threonine 45 were mutated to Alanine). **G)** S5A (Serine 5 were mutated to Alanine), S8A (Serine 8 were mutated to Alanine), T15A (Threonine 15 were mutated to Alanine), SST/AAA mutant (Serine 5, Serine 8 and Threonine 15 were mutated to Alanine). **H)** Annotated HCD MS/MS spectrum of a modified form of OCN (HexNAc-Hex-NANA + 3 Gla + S-S) pulled down from the bone homogenate of C57B6J mice. The precursor m/z value is 1180.95003 (M+5H)⁺⁵ and mass accuracy with the annotated OCN modified form is 4.6 ppm.

Several polypeptide N-acetylgalactosaminyltransferases (GalNAc-Ts) redundantly O-glycosylates OCN independently of its gamma carboxylation and processing. Protein O-glycosylation is initiated by the transfer of a N-acetylgalactosamine (GalNAc) to a serine or threonine residue, a reaction taking place in the Golgi and catalyzed by N-acetylgalactosaminyltransferases (GalNAc-Ts) a family of enzymes comprising 19 different members in mice [32]. Quantitative PCR on mRNA isolated from undifferentiated and differentiated primary mouse osteoblasts revealed that several GalNAc-Ts are expressed in this cell type, with *Galnt1* and *Galnt2* being the most strongly expressed ones (Figure 4-2A). We noticed that S8A mutation abrogates OCN O-glycosylation in HEK293 cells and in primary osteoblasts, but not in CHO cells (Figure 4-1G and data not shown). GalNAc-T3 and GalNAc-T6 are known to be expressed in HEK293 but not in CHO [33, 34], and our data shows they are also expressed in primary mouse osteoblasts and strongly induced during osteoblast differentiation. Although these observations suggest one or both of these enzymes may be involved in OCN O-glycosylation, the inactivation of *GALNT3* and/or *GALNT6* genes failed to alter OCN O-

glycosylation in HEK293 (Figure 4-2B). Since *GALNT1*, *GALNT2* and *GALNT3* are also highly expressed in osteoblasts, we also inactivated these three genes and assessed the impact on OCN *O*-glycosylation. This manipulation partially abolished OCN glycosylation (Figure 4-2B), suggesting that these three GalNAc-Ts may redundantly initiate the *O*-glycosylation of OCN.

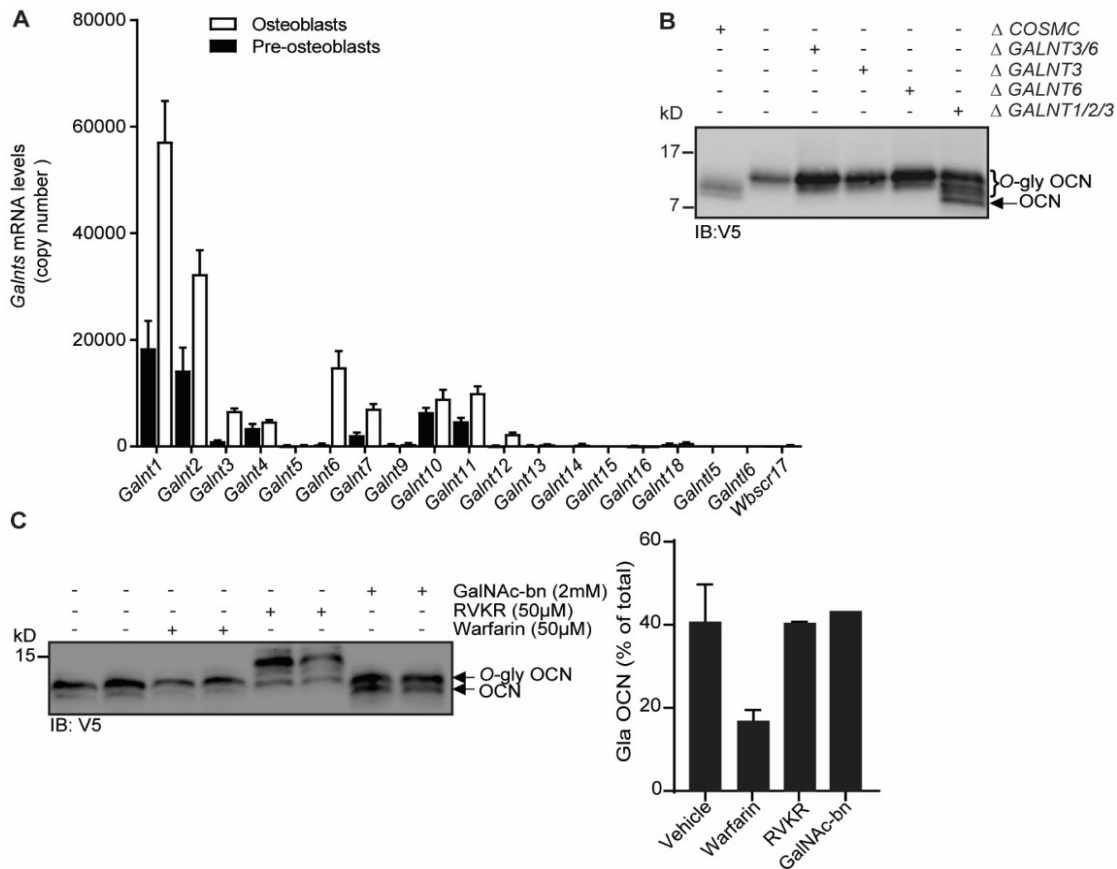


Figure 4-2. Multiple *N*-acetylgalactosaminyltransferase (GalNAc-Ts) *O*-glycosylate OCN and this process is independent of its processing and γ -carboxylation. **A) *Galnts* expression in pre-osteoblasts (undifferentiated) and osteoblasts (differentiated), results are represented as copy number of *Galnts* normalized to *Actb*. **B**) Western blot analysis of OCN in HEK293 deficient in specific GalNAc-Ts. OCN-V5 were transfected in HEK293_{sc}, HEK293, or *GALNTs* deficient HEK293; Cell supernatant was analysed by western blot using anti V5 antibody. **C**) Western blot analysis on the supernatant of osteoblasts transfected with mouse OCN-V5 and treated or not with 2 mM of GalNAc-bn, 50 μ M warfarin or 50 μ M RVKR (left panel), and percentage of carboxylated OCN to total OCN measured by ELISA (right panel).**

Processing of pro-OCN by the proprotein convertase furin and its gamma-carboxylation are two post-translational modifications regulating OCN endocrine function [10, 11]. We

therefore next aimed to test whether OCN *O*-glycosylation can interfere with its gamma-carboxylation or processing, or vice versa. Pharmacological inhibition of gamma-carboxylation or furin, using warfarin or Dec-RVKR-CMK (RVKR) respectively, did not impact OCN *O*-glycosylation in cell culture (Figure 4-2C). Similarly, inhibition of OCN *O*-glycosylation through GalNAc-bn treatment or the S8A mutation did not significantly affect its processing or its gamma-carboxylation (Figure 4-2C-E and Supplementary figure 4-1A). We also tested whether OCN processing may influences its *O*-glycosylation in vivo. As shown in Figure 4-2F, both mature OCN present in control bones and pro-OCN present in furin-deficient bones are de-glycosylated by neuraminidase and *O*-glycosidase, indicating that pro-OCN is normally *O*-glycosylated in absence of processing by furin. Altogether, these results support the notion that OCN *O*-glycosylation is not influenced by the carboxylation status or by endoproteolysis by furin. Moreover, blocking *O*-glycosylation do not prevent the processing of pro-OCN by furin.

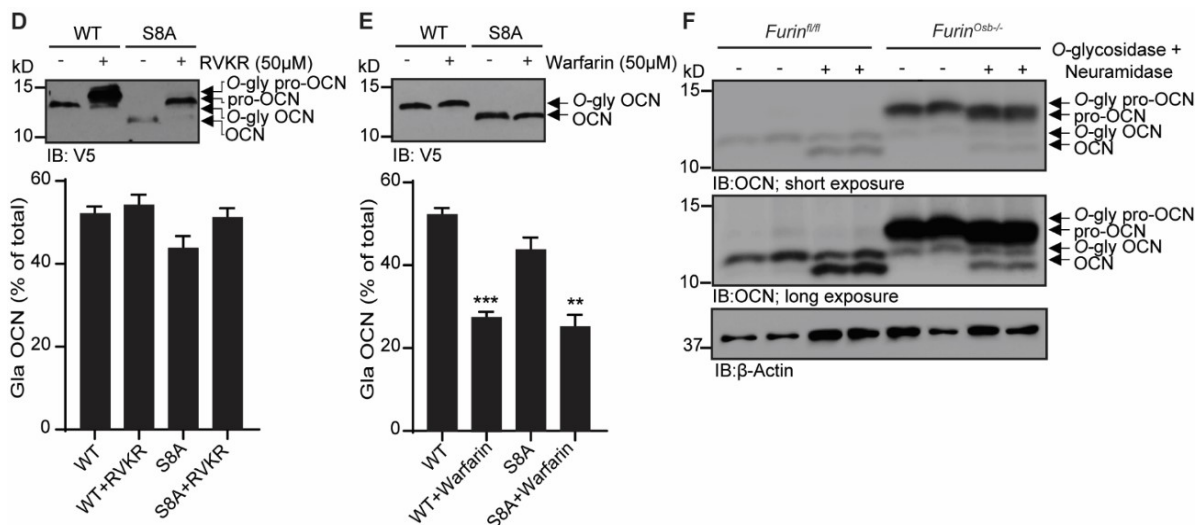


Figure 4-2- continued. Multiple *N*-acetylgalactosaminyltransferase (GalNAc-Ts) *O*-glycosylate OCN and this process is independent of its processing and γ -carboxylation.

D) Western blot analysis on the supernatant of osteoblasts transfected with WT mouse OCN-V5 or S8A mouse OCN-V5 and treated with 50 μM RVKR (upper panel), and percentage of carboxylated OCN to total OCN measured by ELISA (lower panel). **E)** Western blot analysis on the supernatant of osteoblasts transfected with WT mouse OCN-V5 or S8A mouse OCN-V5 and treated with 50 μM warfarin (upper panel), and percentage of carboxylated OCN to total OCN measured by ELISA (lower panel). **F)** Western blot analysis of OCN deglycosylation assay on bone extract from *Furin^{fl/fl}* and *Furin^{Osb/-}* mice. Bone extract were treated or not with *O*-glycosidase and neuraminidase for 4 hours at 37°C and analyzed by western blot using OCN antibody.

Glycosylated mouse OCN has increased half-life in plasma ex vivo and in vivo. The results presented above suggest that *O*-glycosylation is not regulating the processing of pro-OCN by furin or the secretion of mature OCN by osteoblasts. Glycosylation can also increase the half-life of some proteins in the circulation by preventing proteolytic degradation [35, 36]. We therefore tested the half-life in mouse plasma of glycosylated and non-glycosylated mouse uncarboxylated OCN (ucOCN), produced and purified from HEK293 cells and bacteria respectively (Figure 4-3A, B and supplementary figure 4-2 A and B). *Ocn*^{-/-} plasma, which is depleted of endogenous OCN was used in these experiments. Non-glycosylated ucOCN has a half-life of ~120 minutes when incubated in plasma at 37°C, while *O*-glycosylated ucOCN (O-gly ucOCN) is stable for more than 5 hours in the same condition (Figure 4-3C). The stability of the non-glycosylated ucOCN was restored when incubated in heat inactivated plasma at 37°C or at 4°C (Figure 4-3D), suggesting that non-*O*-glycosylated OCN decline involves an enzymatic dependent process, potentially a protease. However, none of the tested protease inhibitors (EDTA which inhibits metalloproteases, phenylmethylsulfonyl fluoride (PMSF) and EDTA free protease inhibitor (PI) which inhibit serine proteases and cysteine proteases, 4-benzenesulfonyl fluoride hydrochloride (AEBSF) which additionally to PMSF inhibits plasmin and plasma kallikrein, Pepstatin A (Pep A) which inhibits aspartic proteases (pepsin, cathepsin D, renin, chymosin), RVKR which inhibits proprotein convertases and benzamidine sepharose (BAM) which inhibits serine proteases, trypsin and trypsin like proteases), could rescue non-*O*-glycosylated ucOCN half-life (Supplementary figure 4-2 C and D) suggesting that it is degraded by a specific proteases that is resistant to this inhibitor, such as prolyl peptidase.

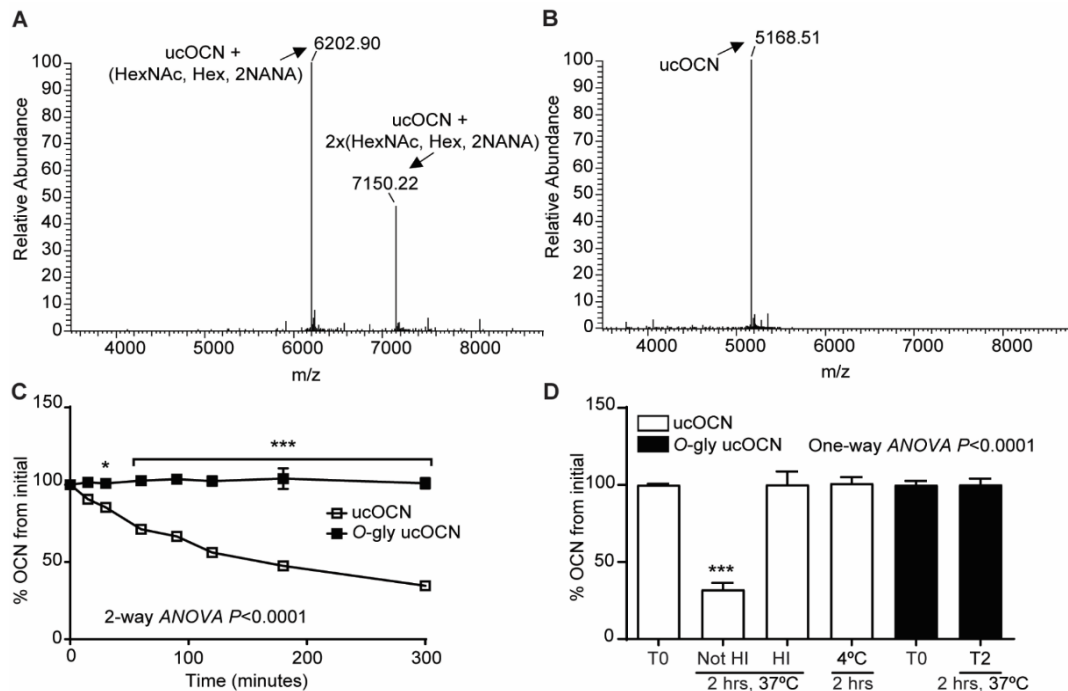


Figure 4-3. OCN O-glycosylation increases its half-life ex vivo and in vivo. A and B) Annotated HCD MS/MS spectrum of purified *O*-glycosylated mouse OCN (*O*-gly ucOCN) (**A**) and purified non-*O*-glycosylated mouse OCN (ucOCN) (**B**). HexNAc: *N*-acetylhexosamine; Hex: Hexose; NANA: *N*-acetylneuraminic acid. **C and D)** Ex vivo half-life of *O*-glycosylated mouse OCN (*O*-gly ucOCN) and non-*O*-glycosylated mouse OCN (ucOCN) in OCN deficient mice (*Ocn*^{-/-}) heparin plasma (n=3-4 plasma), OCN levels were measured at the indicated time points using total OCN ELISA assay. *O*-gly ucOCN and ucOCN were incubated in normal plasma at 37°C over 5 hours (**C**). *O*-gly ucOCN or ucOCN were incubated in plasma for 2 hours at 37°C in different condition or at 4°C. T2: 2 hours in normal plasma; HI: heat inactivated plasma (**D**).

We next examined the half-life of *O*-glycosylated and non-glycosylated mouse ucOCN in vivo by injecting an equal dose (40ng/g) of each of these proteins in *Ocn*^{-/-} mice. In fed mice, the maximum serum level of ucOCN reached after 30 minutes of injection was 1.5 times higher with the glycosylated protein compared to the non-glycosylated form (Figure 4-3E). Moreover, glycosylated ucOCN is detected in the serum up to 2 hours following the injection and it is further increased with 80ng/g of injection, while non-glycosylated ucOCN is two time less detected after 2 hours and slightly increased with the higher dose (Figure 4-3F). In fasted animals, the maximum serum concentrations of ucOCN is reduced at 30 min compared to the level reached in fed animals, regardless of glycosylation status (Figure 4-3G). However, the level of glycosylated ucOCN remains higher compare to the non-glycosylated form for the following 90 minutes. These results establish that *O*-glycosylation increase the half-life of mouse OCN protein ex vivo and in vivo.

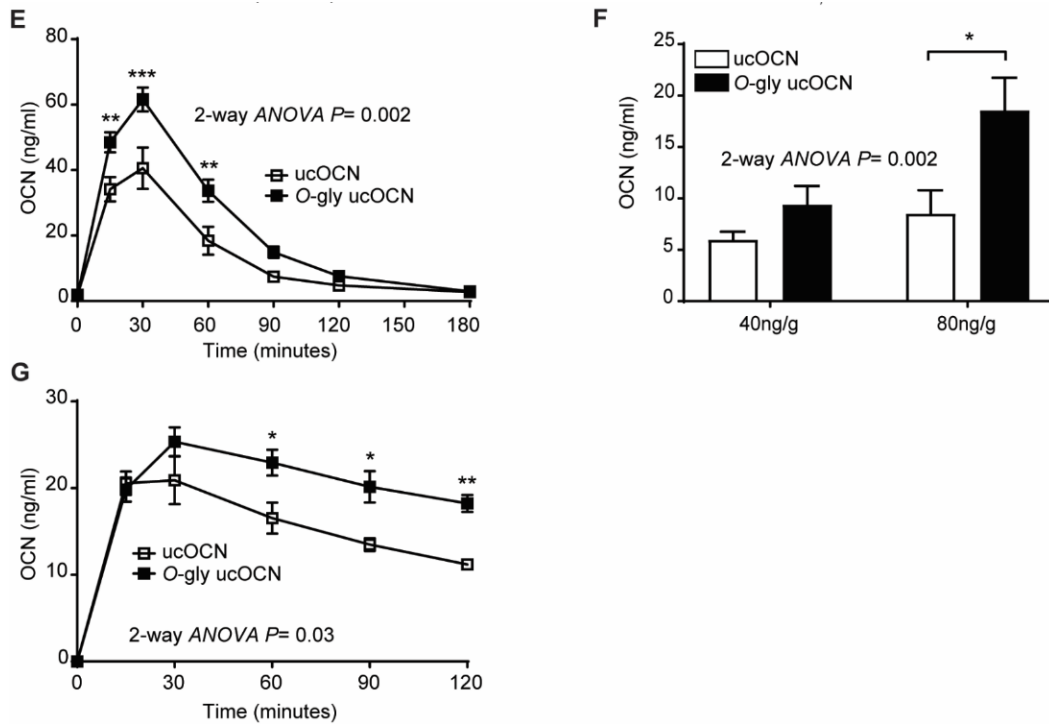


Figure 4-3- continued. OCN O-glycosylation increases its half-life ex vivo and in vivo. E and F In vivo half-life of O-glycosylated OCN (O-gly ucOCN) and non-O-glycosylated OCN (ucOCN) in fed condition. O-gly ucOCN (n=9 mice) or ucOCN (n=9 mice) were injected intraperitoneally (I.P) in OCN deficient male mice (*Ocn*^{-/-}) at a dose of 40ng/g and serum was collected at the indicated time points (**E**). O-gly ucOCN (n=4 mice) or ucOCN (n=4 mice) were injected intraperitoneally (I.P) in OCN deficient male mice (*Ocn*^{-/-}) at a dose of 40ng/g and 80ng/g serum was collected at 120 minutes (**F**). **G** In vivo half-life of O-glycosylated OCN (O-gly ucOCN) and non-O-glycosylated OCN (ucOCN) in fasting condition. OCN deficient male mice (*Ocn*^{-/-}) were fasted for 16 hours, O-gly ucOCN (n=5 mice) or ucOCN (n=5 mice) were injected intraperitoneally (I.P) at a dose of 40ng/g and serum was collected at the indicated time points. OCN measurements were performed using total OCN ELISA assay. Results are given as mean \pm SEM. *, $p < 0.05$; **, $p < 0.01$; ***, $p < 0.001$ using 2-way ANOVA for repeated measurements with Bonferroni multiple comparisons testing.

Human OCN is not glycosylated. Sequence alignment revealed that the residue corresponding to S8 in the mouse protein is a tyrosine (Y12) in human OCN (Figure 4-4A). In addition, human OCN does not contain any serine or threonine residues and migrates at a lower molecular weight compared to mouse OCN when transfected in osteoblasts (Figure 4-4B), supporting the notion that the human OCN is not O-glycosylated. Remarkably, introduction of a single serine residue (Y12S mutation) in the human protein is sufficient to induce its O-glycosylation in osteoblasts as visualized by Western blot (Figure 4-4C). In contrast, introducing a leucine at the same position (Y12L) did not alter human OCN apparent molecular weight, suggesting this tyrosine residue is not normally subjected to O-glycosylation. Since the apparent molecular weight of both native and Y12S human OCN are increased following treatment with

RVKR, we concluded that O-glycosylation does not affect human OCN processing by furin (Figure 4-4D). These results establish that human OCN is not normally subjected to O-glycosylation, but that a single amino acid change (Y12S) suffice to induce its O-glycosylation in osteoblasts.

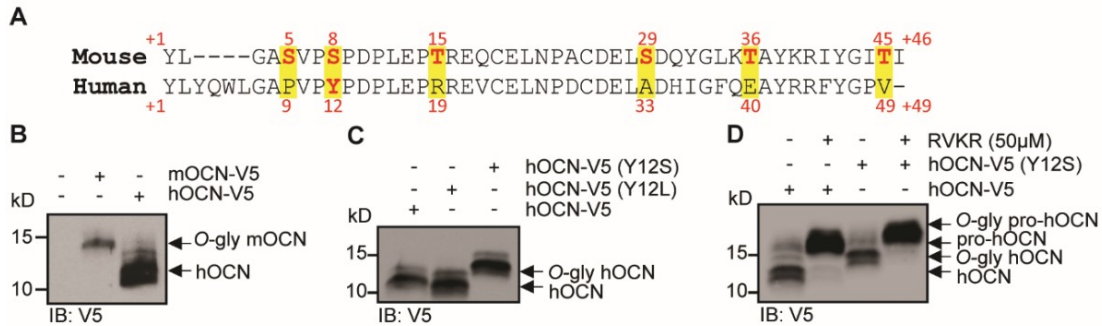


Figure 4-4. Human OCN O-glycosylation increases its half-life ex vivo. **A)** Amino acid alignment of mouse and human OCN, highlighted residue represents the alignment of mouse OCN O-glycosylation site with corresponding amino acid in human OCN. **B)** Western Blot analysis on the supernatant of osteoblasts transfected with human OCN-V5 and mouse OCN-V5. **C and D)** Western Blot analysis on the supernatant of osteoblasts transfected with wild type human OCN (hOCN-V5), tyrosine to leucine (Y12L) or tyrosine to serine (Y12S) hOCN-V5 mutants (**C**) and treated or not with 50 µM RVKR (**D**).

Because O-glycosylation impacts mouse ucOCN half-life in plasma, we next aimed to determine whether this PTM has a similar effect on human ucOCN. To that end, we produced and purified Y12S O-glycosylated human ucOCN from HEK293 and compared its purity and molecular weight to non-O-glycosylated human OCN by LC-MS, MS/MS and SDS-PAGE (Figure 4-4E-F and supplementary figure 4-2 E and F). These proteins were then incubated in *Ocn*^{-/-} mouse plasma at 37°C and the concentration of OCN was monitored over time using a specific ELISA assay [31]. As shown in Figure 4-4G, this assay revealed that non-glycosylated human ucOCN level decline by 50% within 180 min, the concentration of the O-glycosylated version remains stable over the course of the experiment (5 hours). As observed with the mouse protein, human ucOCN degradation was only inhibited when the plasma was heat inactivated or incubated at 4°C (Figure 4-4H and supplementary figure 4-2G), suggesting that glycosylation protect mouse and human ucOCN from degradation through a similar enzymatic mechanism.

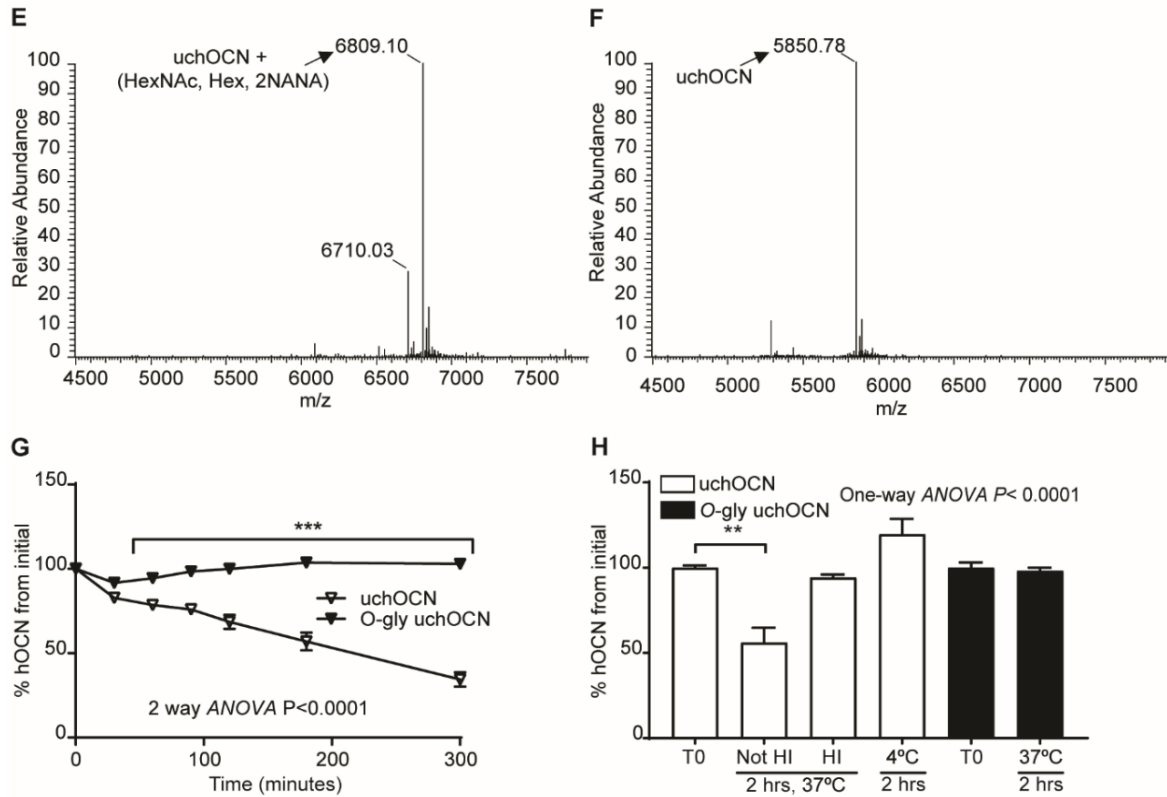


Figure 4-4- continued. Human OCN O-glycosylation increases its half-life ex vivo. E and F) Annotated HCD MS/MS spectrum of purified O-glycosylated human OCN (O-gly uchOCN) (**E**) and purified non-O-glycosylated human OCN (uchOCN) (**F**). HexNAc: N-acetylhexosamine; Hex: Hexose; NANA: N-acetylneuraminic acid. **G and H)** Ex vivo half-life of O-glycosylated human OCN (O-Gly uchOCN) and non-O-glycosylated human OCN (uchOCN). **G)** O-Gly uchOCN and uchOCN were incubated in normal plasma of OCN deficient mice (*Ocn*^{-/-}) (n=4 plasma) for 5 hours. **F)** O-Gly uchOCN and uchOCN were incubated in plasma for 2 hours at 37°C in different condition or at 4°C. T2: 2 hours in normal plasma; HI: heat inactivated plasma. uchOCN levels were measured at the indicated time points using total OCN ELISA assay. Results are given as mean \pm SEM. **, $p < 0.01$; ***, $p < 0.001$ using 2-way ANOVA for repeated measurements with Bonferroni multiple comparisons testing.

4. DISCUSSION

In this study we identified *O*-glycosylation as a novel PTM regulating ucOCN half-life in the circulation. Although, *O*-glycosylation is present in mouse but not human OCN, we also showed that *O*-glycosylation of human OCN by means of a single amino acid change improves its half-life in plasma ex vivo. This finding might have important implication for the future use of recombinant ucOCN as a therapeutic agent in humans.

Numerous secreted proteins are subjected to mucine type *O*-glycosylation, a PTM which occurs in the Golgi apparatus and involves several steps [27, 32]. *O*-glycosylation initiation is catalyzed by the GalNAc-Ts enzyme, a family of 21 enzymes, which form the core 1 glycan by the addition of a GalNAc residue to the hydroxyl group of a serine or threonine [32]. This core 1 is further elongated by the addition of different glycan residues leading to multiple cores [32]. However, the specific protein sequence(s) targeted by each of the GalNAc-Ts remain poorly characterized, with the exception of GalNAc-T1, GalNAc-T2 and GalNAc-T10 [37, 38]. Here, we found that mouse OCN is *O*-glycosylated on serine 8 which is located within the amino acid sequence SVPSPDP. Interestingly, this sequence strongly matches the consensus site previously defined for GalNAc-T1 and GalNAc-T2 [38]. In particular, the presence of proline residues in position -1, +1 and +3 has been shown to be determinant in the recognition of peptide substrates by GalNAc-T1 and GalNAc-T2. Nevertheless, the inactivation of GalNAc-T1, 2 and 3 only partially abolishes mouse OCN *O*-glycosylation in HEK 293 cells, suggesting that OCN may be a substrate of other GalNAc-Ts.

O-glycosylation was shown to interfere with the endoproteolysis of several hormones and receptors [25, 29, 39-42]. This appears not to be the case for OCN as its *O*-glycosylation does not interfere with its processing in vitro and in vivo. In other proteins, such as leptin and erythropoietin, glycosylation adducts were shown to increase protein stability and half-life in circulation [43-47]. Our data demonstrated that *O*-glycosylated mouse ucOCN has a longer half-life compared to non-*O*-glycosylated ucOCN in plasma ex vivo and in the circulation in vivo. In the mouse OCN ELISA assay [30] we used to monitor OCN half-life, the capture antibody is directed

against the central part of OCN (i.e., amino acids 11 to 26), while the detection antibody recognizes the C-terminal region (i.e., amino acids 25-46). We can therefore predict that the disappearance of non-*O*-glycosylated ucOCN in plasma is most likely due to proteolytic cleavage by one or several plasma proteases targeting OCN between residues 11 and 46. Additional studies showed that sialic acid residues, in the glycosylation adducts, increase the protein charge resulting in a decrease in the liver and renal clearance [48, 49]. N-glycosylation of follicle stimulating hormone (FSH) and human interferon alpha (hIFN- α) increase their sialic acid content, reduce their renal clearance and increase their serum half life [45, 47, 48, 50, 51]. Additional study on interleukin-3 (IL-3) suggested that N-glycosylated IL-3 is trapped in tissue resulting in a decrease IL-3 clearance. Since OCN clearance was previously shown to occur through the kidney, liver and bone [52], we can suppose that OCN glycosylation adducts, which contains sialic acid, protects OCN against degradation and decrease its renal clearance.

In the present study, we show that human OCN is not subjected to *O*-glycosylation and that consequently it has reduced half-life in plasma. The *O*-glycosylation sequence “SVPSPDP” of mouse OCN is almost perfectly conserved in the human protein, except for the amino acids corresponding to S5 and S8, which are replaced by a proline (P9) and a tyrosine (Y12) in human OCN (i.e., “PVPPYPDP”). Remarkably, we could introduce *O*-glycosylation into human OCN by a single amino acid change (Y12S). *O*-glycosylated human OCN is retained in mouse plasma *ex vivo* like the glycosylated mouse protein, potentially explaining why circulating level of OCN in 1 to 6 months old mice is 5-10 time higher than the levels measured in young or adult human [10, 30, 53, 54] (Supplemental table 4-1). Of note, in the human gene the codon encoding Y12 could, in theory, be converted to a serine codon by mean of a single base variant (i.e., TAC to TCC). However, such single-nucleotide polymorphism (SNP) creating an *O*-glycosylation site at residue 12 has not been reported yet in human (Supplementary table 4-4 and gnomMAD).

It remains unknown if the increased half-life of *O*-glycosylated ucOCN will result in improved biological activity *in vivo*, even though it does so for other proteins [45, 46, 55]. Moreover, although it is currently not known if *O*-glycosylation ucOCN is active in mice, a few

evidences suggest it could be the case. First, our data shows that mouse OCN is endogenously *O*-glycosylated in vivo and that more than 95% of OCN, including the ucOCN fraction, is *O*-glycosylated in bone, in osteoblast supernatant and in serum, suggesting that the bioactive form of OCN is *O*-glycosylated in vivo in mice. Second, bacterially produce mouse ucOCN, which is not *O*-glycosylated, was previously shown to be bioactive in cell-based assay and in vivo [2, 4, 6, 7], suggesting that *O*-glycosylation is not required for ucOCN activity in mice. Moreover, based on the crystal structure of bovine OCN and the alignment of bovine and mouse OCN, *O*-glycosylation occurs in the N-terminal region of the helix 1, where the Gla /Glu residues are located [56, 57]. Computational analysis predicts the C-terminal residues (RFYGPV) of bovine OCN to be responsible of OCN binding to the GPRC6A receptor [58], suggesting that OCN glycosylation does not impact OCN binding.

In summary, this work identified *O*-glycosylation as a previously unrecognized OCN PTM regulating its half-life in circulation in mice. This modification is not conserved in human yet introducing *O*-glycosylation in human ucOCN also increases its half-life in plasma. These findings reveal an important difference between mouse and human OCN biology. They also provide an approach to increase recombinant human OCN half-life in vivo and might be relevant for the future development of OCN-based therapies for human diseases.

5. ACKNOWLEDGEMENTS

We thank Dr. Nabil Seidah for his critical reading of the manuscript and for providing reagents as well as the CHO and CHO-Idld cells. This work was supported by funding from the Canada Research Chair program (M.F.), the Canadian Institutes of Health Research (M.F., MOP-133652 and PJT-159534) and the Natural Sciences and Engineering Research Council of Canada (RGPIN-2016-05213, to MF). OAR received scholarships from IRCM and FRQS.

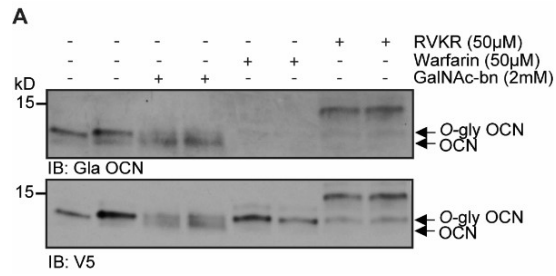
6. REFERENCES

1. Pi, M., Y. Wu, and L.D. Quarles, *GPRC6A mediates responses to osteocalcin in beta-cells in vitro and pancreas in vivo*. *J Bone Miner Res*, 2011. **26**(7): p. 1680-3.
2. Ferron, M., et al., *Intermittent injections of osteocalcin improve glucose metabolism and prevent type 2 diabetes in mice*. *Bone*, 2012. **50**(2): p. 568-75.
3. Oury, F., et al., *Osteocalcin regulates murine and human fertility through a pancreas-bone-testis axis*. *J Clin Invest*, 2015. **125**(5): p. 2180.
4. Mera, P., et al., *Osteocalcin Signaling in Myofibers Is Necessary and Sufficient for Optimum Adaptation to Exercise*. *Cell Metab*, 2016. **23**(6): p. 1078-1092.
5. Berger, J.M., et al., *Mediation of the Acute Stress Response by the Skeleton*. *Cell Metab*, 2019. **30**(5): p. 890-902 e8.
6. Khrimian, L., et al., *Gpr158 mediates osteocalcin's regulation of cognition*. *J Exp Med*, 2017. **214**(10): p. 2859-2873.
7. Mera, P., et al., *Osteocalcin is necessary and sufficient to maintain muscle mass in older mice*. *Mol Metab*, 2016. **5**(10): p. 1042-1047.
8. Oury, F., et al., *Maternal and offspring pools of osteocalcin influence brain development and functions*. *Cell*, 2013. **155**(1): p. 228-41.
9. Kosmidis, S., et al., *RbAp48 Protein Is a Critical Component of GPR158/OCN Signaling and Ameliorates Age-Related Memory Loss*. *Cell Rep*, 2018. **25**(4): p. 959-973 e6.
10. Ferron, M., et al., *GGCX and VKORC1 inhibit osteocalcin endocrine functions*. *J Cell Biol*, 2015. **208**(6): p. 761-76.
11. Al Rifai, O., et al., *Proprotein convertase furin regulates osteocalcin and bone endocrine function*. *J Clin Invest*, 2017. **127**(11): p. 4104-4117.
12. Ferron, M., et al., *Insulin signaling in osteoblasts integrates bone remodeling and energy metabolism*. *Cell*, 2010. **142**(2): p. 296-308.
13. Lacombe, J., G. Karsenty, and M. Ferron, *In vivo analysis of the contribution of bone resorption to the control of glucose metabolism in mice*. *Mol Metab*, 2013. **2**(4): p. 498-504.
14. Mera, P., M. Ferron, and I. Mosialou, *Regulation of Energy Metabolism by Bone-Derived Hormones*. *Cold Spring Harb Perspect Med*, 2018. **8**(6).
15. De Toni, L., et al., *Osteocalcin and Sex Hormone Binding Globulin Compete on a Specific Binding Site of GPRC6A*. *Endocrinology*, 2016. **157**(11): p. 4473-4486.
16. Sabek, O.M., et al., *Osteocalcin Effect on Human beta-Cells Mass and Function*. *Endocrinology*, 2015. **156**(9): p. 3137-46.
17. Di Nisio, A., et al., *The rs2274911 polymorphism in GPRC6A gene is associated with insulin resistance in normal weight and obese subjects*. *Clin Endocrinol (Oxf)*, 2017. **86**(2): p. 185-191.
18. Oury, F., et al., *Osteocalcin regulates murine and human fertility through a pancreas-bone-testis axis*. *J Clin Invest*, 2013. **123**(6): p. 2421-33.
19. Ferron, M. and J. Lacombe, *Regulation of energy metabolism by the skeleton: Osteocalcin and beyond*. *Arch Biochem Biophys*, 2014. **561C**: p. 137-146.
20. Lin, X., et al., *Undercarboxylated Osteocalcin: Experimental and Human Evidence for a Role in Glucose Homeostasis and Muscle Regulation of Insulin Sensitivity*. *Nutrients*, 2018. **10**(7).
21. Bonneau, J., et al., *Association between osteocalcin gamma-carboxylation and insulin resistance in overweight and obese postmenopausal women*. *J Diabetes Complications*, 2017. **31**(6): p. 1027-1034.

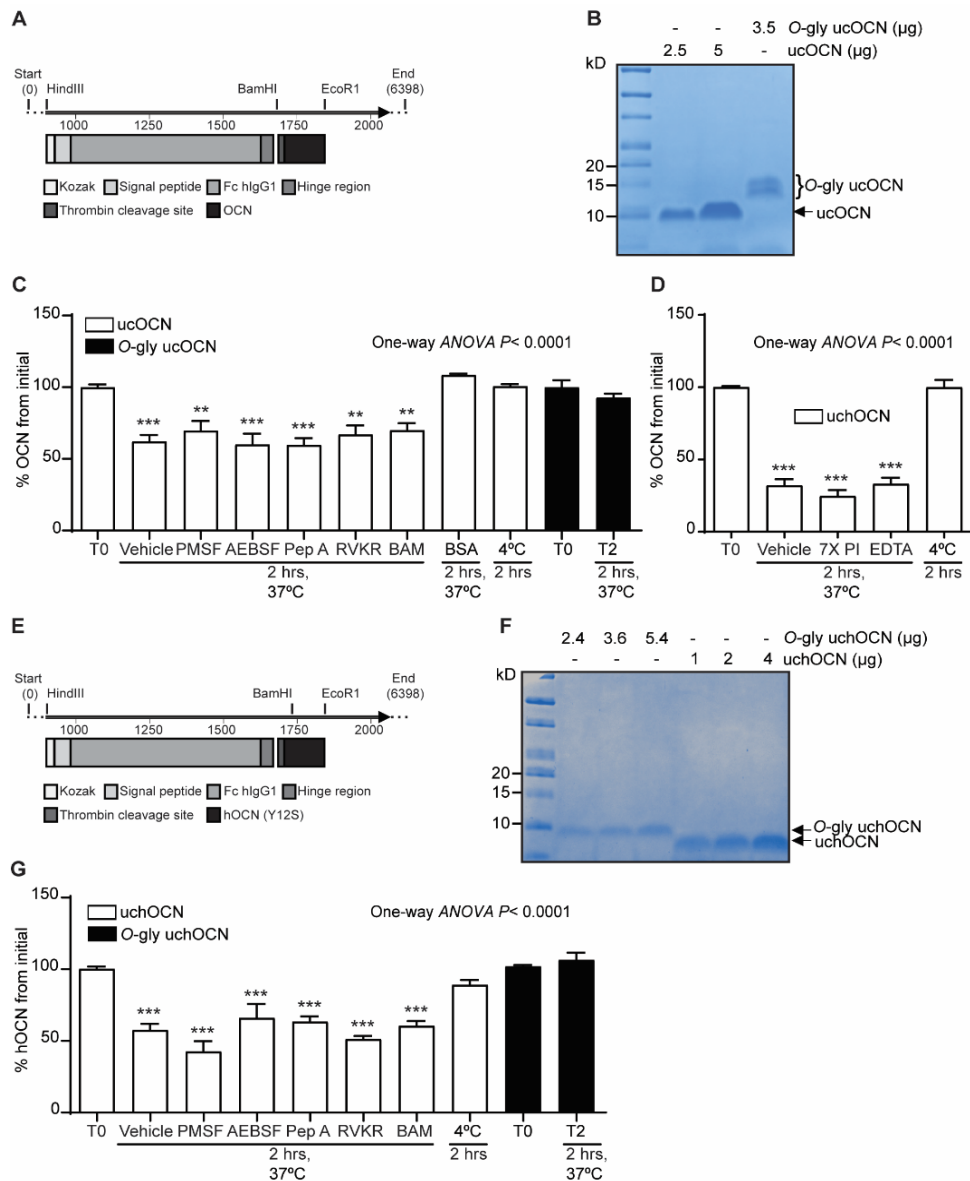
22. Ducey, P., et al., *Increased bone formation in osteocalcin-deficient mice*. *Nature*, 1996. **382**(6590): p. 448-52.
23. Saavedra, Y.G., J. Zhang, and N.G. Seidah, *PCSK9 prosegment chimera as novel inhibitors of LDLR degradation*. *PLoS One*, 2013. **8**(8): p. e72113.
24. Kingsley, D.M., et al., *Reversible defects in O-linked glycosylation and LDL receptor expression in a UDP-Gal/UDP-GalNAc 4-epimerase deficient mutant*. *Cell*, 1986. **44**(5): p. 749-59.
25. Goth, C.K., et al., *A systematic study of modulation of ADAM-mediated ectodomain shedding by site-specific O-glycosylation*. *Proc Natl Acad Sci U S A*, 2015. **112**(47): p. 14623-8.
26. Schjoldager, K.T., et al., *Probing isoform-specific functions of polypeptide GalNAc-transferases using zinc finger nuclease glycoengineered SimpleCells*. *Proc Natl Acad Sci U S A*, 2012. **109**(25): p. 9893-8.
27. Steentoft, C., et al., *Precision mapping of the human O-GalNAc glycoproteome through SimpleCell technology*. *EMBO J*, 2013. **32**(10): p. 1478-88.
28. Steentoft, C., et al., *Mining the O-glycoproteome using zinc-finger nuclease-glycoengineered SimpleCell lines*. *Nat Methods*, 2011. **8**(11): p. 977-82.
29. Goth, C.K., et al., *Site-specific O-Glycosylation by Polypeptide N-Acetylgalactosaminyltransferase 2 (GalNAc-transferase T2) Co-regulates beta1-Adrenergic Receptor N-terminal Cleavage*. *J Biol Chem*, 2017. **292**(11): p. 4714-4726.
30. Ferron, M., et al., *An ELISA-based method to quantify osteocalcin carboxylation in mice*. *Biochem Biophys Res Commun*, 2010. **397**(4): p. 691-6.
31. Lacombe, J., et al., *Measurement of bioactive osteocalcin in humans using a novel immunoassay reveals association with glucose metabolism and beta-cell function*. *Am J Physiol Endocrinol Metab* 2020.
32. Bennett, E.P., et al., *Control of mucin-type O-glycosylation: a classification of the polypeptide GalNAc-transferase gene family*. *Glycobiology*, 2012. **22**(6): p. 736-56.
33. Xu, X., et al., *The genomic sequence of the Chinese hamster ovary (CHO)-K1 cell line*. *Nat Biotechnol*, 2011. **29**(8): p. 735-41.
34. Hintze, J., et al., *Probing the contribution of individual polypeptide GalNAc-transferase isoforms to the O-glycoproteome by inducible expression in isogenic cell lines*. *J Biol Chem*, 2018. **293**(49): p. 19064-19077.
35. Sola, R.J. and K. Griebenow, *Effects of glycosylation on the stability of protein pharmaceuticals*. *J Pharm Sci*, 2009. **98**(4): p. 1223-45.
36. Bernard, B.A., K.M. Yamada, and K. Olden, *Carbohydrates selectively protect a specific domain of fibronectin against proteases*. *J Biol Chem*, 1982. **257**(14): p. 8549-54.
37. Perrine, C.L., et al., *Glycopeptide-preferring polypeptide GalNAc transferase 10 (ppGalNAc T10), involved in mucin-type O-glycosylation, has a unique GalNAc-O-Ser/Thr-binding site in its catalytic domain not found in ppGalNAc T1 or T2*. *J Biol Chem*, 2009. **284**(30): p. 20387-97.
38. Gerken, T.A., et al., *Identification of common and unique peptide substrate preferences for the UDP-GalNAc:polypeptide alpha-N-acetylgalactosaminyltransferases T1 and T2 derived from oriented random peptide substrates*. *J Biol Chem*, 2006. **281**(43): p. 32403-16.
39. Kato, K., et al., *Polypeptide GalNAc-transferase T3 and familial tumoral calcinosis. Secretion of fibroblast growth factor 23 requires O-glycosylation*. *J Biol Chem*, 2006. **281**(27): p. 18370-7.

40. May, P., et al., *Differential glycosylation regulates processing of lipoprotein receptors by gamma-secretase*. J Biol Chem, 2003. **278**(39): p. 37386-92.
41. Schjoldager, K.T. and H. Clausen, *Site-specific protein O-glycosylation modulates proprotein processing - deciphering specific functions of the large polypeptide GalNAc-transferase gene family*. Biochim Biophys Acta, 2012. **1820**(12): p. 2079-94.
42. Schjoldager, K.T., et al., *O-glycosylation modulates proprotein convertase activation of angiotensin-like protein 3: possible role of polypeptide GalNAc-transferase-2 in regulation of concentrations of plasma lipids*. J Biol Chem, 2010. **285**(47): p. 36293-303.
43. Vegarud, G. and T.B. Christensen, *Glycosylation of Proteins: a new method of enzyme stabilization*. Biotechnol Bioeng, 1975. **17**(9): p. 1391-7.
44. Wang, C., et al., *Influence of the carbohydrate moiety on the stability of glycoproteins*. Biochemistry, 1996. **35**(23): p. 7299-307.
45. Runkel, L., et al., *Structural and functional differences between glycosylated and non-glycosylated forms of human interferon-beta (IFN-beta)*. Pharm Res, 1998. **15**(4): p. 641-9.
46. Elliott, S., et al., *Enhancement of therapeutic protein in vivo activities through glycoengineering*. Nat Biotechnol, 2003. **21**(4): p. 414-21.
47. Creus, S., et al., *Human FSH isoforms: carbohydrate complexity as determinant of in-vitro bioactivity*. Mol Cell Endocrinol, 2001. **174**(1-2): p. 41-9.
48. Wide, L., *The regulation of metabolic clearance rate of human FSH in mice by variation of the molecular structure of the hormone*. Acta Endocrinol (Copenh), 1986. **112**(3): p. 336-44.
49. Morell, A.G., et al., *The role of sialic acid in determining the survival of glycoproteins in the circulation*. J Biol Chem, 1971. **246**(5): p. 1461-7.
50. Perlman, S., et al., *Glycosylation of an N-terminal extension prolongs the half-life and increases the in vivo activity of follicle stimulating hormone*. J Clin Endocrinol Metab, 2003. **88**(7): p. 3227-35.
51. Weenen, C., et al., *Long-acting follicle-stimulating hormone analogs containing N-linked glycosylation exhibited increased bioactivity compared with o-linked analogs in female rats*. J Clin Endocrinol Metab, 2004. **89**(10): p. 5204-12.
52. Farrugia, W. and R.A. Melick, *Metabolism of osteocalcin*. Calcif Tissue Int, 1986. **39**(4): p. 234-8.
53. Hannemann, A., et al., *Reference intervals for serum osteocalcin concentrations in adult men and women from the study of health in Pomerania*. BMC Endocr Disord, 2013. **13**: p. 11.
54. Cioffi, M., et al., *Serum osteocalcin in 1634 healthy children*. Clin Chem, 1997. **43**(3): p. 543-5.
55. Baudys, M., et al., *Physical stabilization of insulin by glycosylation*. J Pharm Sci, 1995. **84**(1): p. 28-33.
56. Malashkevich, V.N., S.C. Almo, and T.L. Dowd, *X-ray crystal structure of bovine 3 Glu-osteocalcin*. Biochemistry, 2013. **52**(47): p. 8387-92.
57. Dowd, T.L., et al., *The three-dimensional structure of bovine calcium ion-bound osteocalcin using 1H NMR spectroscopy*. Biochemistry, 2003. **42**(25): p. 7769-79.
58. Pi, M., et al., *Evidence for Osteocalcin Binding and Activation of GPRC6A in beta-Cells*. Endocrinology, 2016. **157**(5): p. 1866-80.

7. SUPPLEMENTARY FIGURES



Supplemental Figure 4-1. Mouse OCN O-glycosylation occurs independently of its carboxylation and processing in HEK293. A) Western blot analysis on the supernatant of HEK293 transfected with mouse OCN-V5 and treated or not with 2 mM of GalNAc-bn, 50 μ M warfarin or 50 μ M RVKR.



Supplemental Figure 4-2. Different protease inhibitor failed to rescue non-glycosylated mouse and human ucOCN degradation.

A) Construct map of pcDNA3.1-Fc-hinge-Thr-OCN used to produce mouse OCN fusion protein. **B)** Coomassie staining of purified *O*-glycosylated mouse OCN (*O*-gly ucOCN) compared to non-*O*-glycosylated mouse OCN (ucOCN). **C and D)** Ex vivo half-life of *O*-glycosylated mouse OCN (*O*-gly ucOCN) and non-*O*-glycosylated mouse OCN (ucOCN) in OCN deficient mice (*Ocn*^{-/-}) heparin plasma (n=3-4 plasma). *O*-gly ucOCN and ucOCN was incubated for 2 hours in normal plasma at 37°C or 4°C and treated or not with protease inhibitors. **C)** T2: 2 hours in normal plasma; PMSF: 1 mM phenylmethylsulfonyl fluoride; AEBSF: 2.5 mM 4-benzenesulfonyl fluoride hydrochloride; Pep A: 10 μM Pepstatin A; RVKR: 50 μM Dec-RVKR-CMK; BAM: Benzamidine Beads, or incubated in 3.5% BSA (bovine serum albumin prepared in saline solution), **D)** EDTA (10 mM); 7X PI: protease inhibitor cocktail EDTA free. **E)** Construct map of pcDNA3.1-Fc-hinge-Thr-hOCN (Y12S) used to produce *O*-glycosylated human OCN fusion protein. **F)** Coomassie staining of purified *O*-glycosylated human OCN (*O*-gly uchOCN) compared to non-*O*-glycosylated human OCN (uchOCN). **G)** Ex vivo half-life of *O*-glycosylated human OCN (*O*-gly uchOCN) and non-*O*-glycosylated OCN (uchOCN) in OCN deficient mice (*Ocn*^{-/-}) heparin plasma (n=3-4 plasma). *O*-gly uchOCN and uchOCN were incubated for 2 hours in normal plasma at 37°C or 4°C and treated or not with protease inhibitors. T2: 2 hours in normal plasma; PMSF: 1 mM phenylmethylsulfonyl fluoride; AEBSF: 2.5 mM 4-benzenesulfonyl fluoride hydrochloride; Pep A: 10 μM Pepstatin A; RVKR: 50 μM Dec-RVKR-CMK; BAM: Benzamidine Beads.

8. SUPPLEMENTAL TABLES

Supplemental Table 4-1. OCN serum levels in mice and human at different age

Age mice/human	OCN serum levels (ng/ml)	
	Mice [mean \pm SD (n)]	Humans* [mean \pm SD (n)]
2 weeks/ 1 year old	1369.7 \pm 146.69 (8)	62.9 \pm 8.14 (43)
4 weeks/ [11-13] years old	617.2 \pm 192.5 (5)	74.1 \pm 8.88 (41)
13 weeks/ [25-29] years old	252.2 \pm 7.96 (4)	21 \pm 6.29 (49)
60 weeks/ [50-54] years old	50 \pm 7.18 (4)	13.5 \pm 6.3 (127)

*Anke Hannemann et al, *BMC Endocr Disord.* 2013. Michele Gioffi et al, *Clinical Chemistry.* 1997

Supplemental Table 4-2. The monoisotopic mass and relative abundance of the different OCN forms detected in the supernatant of differentiated osteoblasts

Monoisotopic mass range	Relative abundance (%)	Most probable modification	Most probable oligosaccharide
O-glycosylated OCN	84.89		
5767.6961	4.80	Glycosylation	HexNAc, Hex, NANA
5783.6801	0.25	Glycosylation+ Oxidation	HexNAc, Hex, NANA
5855.6676	4.60	Glycosylation+2x Gla	HexNAc, Hex, NANA
5899.7161	3.16	Glycosylation+ 3x Gla	HexNAc, Hex, NANA
5915.6386 - 5968.5796	5.51	Glycosylation+ 3x Gla+ Oxidation	HexNAc, Hex, NANA
6058.7916	24.48	Glycosylation	HexNAc, Hex, 2x NANA
6074.7766- 6096.7409	3.49	Glycosylation+ Oxidation	HexNAc, Hex, 2x NANA
6102.7681	7.89	Glycosylation+ 1x Gla	HexNAc, Hex, 2x NANA
6146.7609	23.97	Glycosylation+ 2x Gla	HexNAc, Hex, 2x NANA
6190.8061- 6214.7278	6.72	Glycosylation+ 3x Gla	HexNAc, Hex, 2x NANA
Non O-glycosylated OCN	16.12		
5127.4676	3.03	OCN + 1 S-S + Oxidation	NA
5171.4301	1.85	OCN + 1 S-S + 1 Gla + Oxidation	NA
5199.4446	2.08	OCN + 1S-S + 2x Gla	NA
5215.4296	8.50	OCN + 1S-S + 2x Gla + Oxidation	NA
5259.4204	0.66	OCN + 1S-S + 3x Gla + Oxidation	NA

Supplemental Table 4-3. The monoisotopic mass and relative abundance of the different OCN forms detected in the supernatant of differentiated osteoblasts

Monoisotopic mass range	Relative abundance (%)	Most probable modification	Most probable oligosaccharide
O-glycosylated OCN	99%		
5855.6676	0.54%	Glycosylation+ 2x Gla	HexNAc, Hex, NANA
5899.7161	7.43%	Glycosylation+ 3x Gla	HexNAc, Hex, NANA
5915.6386-6122.7026	38.08%	Glycosylation+ 3x Gla + Oxidation	HexNAc, Hex, NANA
6146.7609-6162.7991	3.02%	Glycosylation+ 2x Gla	HexNAc, Hex, 2xNANA
6190.8061	4.49%	Glycosylation+ 3x Gla	HexNAc, Hex, 2xNANA
6206.8016-6441.7636	45.12%	Glycosylation+ 3x Gla + Oxidation	HexNAc, Hex, 2xNANA
Non O-glycosylated OCN	1.00%		
5259.4204	0.93%	3x Gla	NA

Mouse aa#	52 53	54 55 56 57 58 59	60 61 62 63 64 65 66 67 68 69	70 71 72 73 74 75 76 77 78 79 80 81 82 83 84 85 86 87 88 89 90 91 92 93 94 95 96 97	Total aa #
Mouse	Y L - - -	G A S V P S	P L E P T R E Q C E L N P A C D E L S D Q Y G L K T A Y K R I Y G I T		45
Human aa#	52 53	54 55 56 57 58 59 60 61 62 63 64 65 66 67 68 69 70 71 72 73 74 75 76 77 78 79 80 81 82 83 84 85 86 87 88 89 90 91 92 93 94 95 96 97 98 99 100 101			49
Human	Y L Y Q W L G A P V P Y P D P L E P R E V C E L N P D C D E L A D H I G F Q E A Y R R F Y G P V				
Human GLY (Y63S)			S		
rs1241667190			*		Codon 1
rs144327492			*		3
rs748979663			P		2
rs914139584			S		2
rs375784952			L		2
rs775628553			E		3
rs115631152			K		1
rs1337844551			D		3
rs371279016			V		2
rs890794648			R		1
rs1324827756			V		1
rs1440598170			S		2
rs369228193			S		2
rs1239256735			S		1
rs1280961571			*		1
rs1411074866			G		2
rs1166726363			D		3
rs778330457			C		2
rs34702397			W		1
rs200610507			Q		2
rs777313170			C		1
rs777313170			H		2
rs535838505			P		2
rs756750489			Y		2
rs756750490			S		1
rs778444804			R		1
rs182971055			L		1
					2

Supplemental Table 4-5. Primer List

Primer name	Sequence 5'-3'
mOCN-For-EcoRI	AATTGAATTCgCcaccatgaggaccctctctc
mOCN-Rev-Stop-AgeI	AATTACCGGTctaataagtataccgtagatg
mOCN-Rev-AgeI	AATTACCGGTaatagtataccgtagatgcg
mOCN-T15A-For	CTG GAG CCC GCC CGG GAG CAG
mOCN-T15A-Rev	ctg ctc ccg ggc ggg ctc cag
mOCNSTT-stop-Age1-Rev	AATTACCGGTctaataagcgataccgtagatg
mOCNSTT-Age1-Rev	AATTACCGGTaatagcgataccgtagatgcg
mOCN-S5A-For	5'-taccttggagccGcCgtcccagccca-3'
mOCN-S5A-Rev	5'-tgggctggggacggcgctccaagga-3'
mOCN-S8A-For	5'-gcctcagtcgccGcccagatcccctg-3'
mOCN-S8A-Rev	5'-caggggatctggggcggggactgaggc-3'
hOCN-EcoRI-For	aattgaattgccaccatgagagccctcacactct
hOCN-AgeI-Rev	aatt accggt gaccgggccgtagaagcg
hOCN-Stop-AgeI-Rev	aatt accggt ctgaccgggcccgtagaag
hOCN-R19T-For	cccctggagcccACgagggagggtgtgt
hOCN-R19T-Rev	acacacctccctcgtgggctccagggg
hOCN-Y12S-For	gccccagtccccAGcccggatcccctg
hOCN-Y12S-Rev	caggggatccgggctggggactggggc
hOCN-P11S-For	ggagccccagtcTcctaccggatccc
hOCN-P11S-Rev	gggatccgggtaggAgactggggctcc
HindIII-FchIgG1 -For	AATTAAGCTTGCCACCATGGAGTTTGGGCTG
BamHI-FchIgG1-Rev	AATTGGATCTGGGCACGGTGGGCATGTG
BamHI-Thrombin-mOCN-For	AATTggatccCTGGTTCGCGTGGATCTtacctggagcctcagtc
EcoRI-mOCN-Rev	AATTGAATTCctaataagtataccgtagatg
BglII-Thrombin-hOCN-For	AATTtagatctCTGGTTCGCGTGGATCTtacctgtatcaatggctgg
EcoRI-hOCN-Rev	AATTGAATTCtagaccgggcccgtagaagcgc
GalnT1-For	GCAGCATGTGAACAGCAATCA
GalnT1-Rev	GCTGAGGTAGCCCAGTCAATC
GalnT2-For	GGCAACTCCAACTGCGACA
GalnT2-Rev	TCAACAACTGGGCCGGTG
GalnT3-For	ACTTAGTGCCATGTGACGCA
GalnT3-Rev	GGGTTTCTGCAGCGTTCTA
GalnT4-For	CAAACTGCCCAAAGACGG
GalnT4-Rev	CGCTCTGCTGCTAGCCTATT
GalnT5-For	CCCTGAACTGGCTGCTTGT
GalnT5-Rev	ATGGAGAGAAATTCAGTCAGCAA
GalnT6-For	CCAGCTCTGGCTGTTTGTCTA

GalnT6-Rev	TTGGGCCAAGTAGCATGTGA
GalnT7-For	GCACAGGTTTACGCACATCA
GalnT7-Rev	TTCCAGGCGGTTTTAGTCC
GalnT9-For	CAACTTTGGGCTGCGGTTAG
GalnT9-Rev	CCCACATTGCTCTTGGGTCT
GalnT10-For	GGAGTACCGCCACCTCTCAG
GalnT10-Rev	AGGTCCCAGGCAATTTTGGT
GalnT11-For	GGCTGTACCAAGTGCCGTT
GalnT11-Rev	GCAGGCATGACAAAACCAGG
GalnT12-For	ACAACGGCTTTGCACCATAC
GalnT12-Rev	ACACTCTTGTGACACCCAGC
GalnT13-For	CTGGCAATGTGGAGTTCTT
GalnT13-Rev	AATTCATCCATCCACTTCTGC
GalnT14-For	TCTTTCCGAGTGTGGATGTGT
GalnT14-Rev	CCCATCGGGGAAAACATAAGGA
GalnT15-For	CTGCGGTGGCTCTGTTGAAA
GalnT15-Rev	CTGGGATGTGCCTGTAGAAGG
GalnT16-For	TGGTGACCAGCAAATGTCAGA
GalnT16-Rev	TCCGGTCGAAATGTGAGGAG
GalnT18-For	CAGAAGTGCTCGGGACAACA
GalnT18-Rev	TTGGCTCTCCCTCTCAGACT
Galnt15-For	AGTGAGCGCGTGGAATTAAG
Galnt15-Rev	AGATTTGTCTGTGGTGCGA
Wbscr17-For	CTTAGGTGCTCTGGGGACCA
Wbscr17-Rev	TGTACAAGCTGCTCTTGACCT
Galnt16-For	ACCGAGACTAGCAGTTCCT
Galnt16-Rev	GTCATGCGCTCTGTTCCAC

5. CHAPTER V

**FURIN IN OSTEOLASTS REGULATES FGF23 PROCESSING AND
BONE MASS ACCRUAL**

5.1. HYPOTHESIS AND RELEVANCE

FGF23 endocrine functions are mediated through the full length intact FGF23, the active form of this hormone. Its endoproteolytic cleavage negatively controls its endocrine functions by releasing the N-terminal and C-terminal fragments. Mutations in the FGF23 cleavage site that render FGF23 resistant to endoproteolytic cleavage were found in autosomal dominant hypophosphatemic rickets (ADHR) patients. This disease is characterised by an increase in intact FGF23 serum levels, hypophosphatemia and osteomalacia. FGF23 cleavage motif, RHTR, is a consensus cleavage site for proprotein convertases. Furin and the proprotein convertase subtilisin/kexin type 5 (PC5) were shown to cleaves FGF23 in vitro. However, the identity of the PC(s) involved in FGF23 processing in vivo remains unknown. In the present study we address this question using mice deficient in furin and/or in PC5 specifically in osteoblasts and osteocytes. We found that furin, but not PC5, is partially responsible of FGF23 processing under physiological conditions. Moreover, the absence of furin impairs FGF23 processing under iron deficiency condition, but not following erythropoietin or interleukin 1 beta injections, which stimulate FGF23 production and processing. Our data suggest that beside furin additional PC(s), excluding PC5, redundantly cleave FGF23 in vivo.

5.2. THIRD PAPER

Genetic analysis of the contribution of the proprotein convertases furin and PC5 in the regulation of FGF23 in vivo

Omar Al Rifai^{1,2}, Rachid Essalmani³, John W.M. Creemers⁴, Nabil G. Seidah³ and Mathieu Ferron^{1,2,5,6#}

¹ Unité de recherche en physiologie moléculaire, Institut de Recherches Cliniques de Montréal, Montréal, Québec H2W 1R7, Canada

² Programme de biologie moléculaire, Université de Montréal, Québec H3T 3J7, Canada

³ Unité de recherche en biochimie neuroendocrinienne, Institut de Recherches Cliniques de Montréal, Montréal, Québec H2W 1R7, Canada

⁴ Department of Human Genetics, KU Leuven, Herestraat 49, B-3000 Leuven, Belgium

⁵ Département de Médecine, Université de Montréal, Québec H3T 3J7, Canada

⁶ Division of Experimental Medicine, McGill University, Montréal, Québec H3A 1A3, Canada

Correspondence to:

Mathieu Ferron, PhD

Institut de Recherches Cliniques de Montréal

110 Ave. des Pins O.

Montréal, QC,

H2W 1R7, Canada

Phone: 514-987-5754

Email: mathieu.ferron@ircm.qc.ca

Manuscript in preparation, which will be submitted to a bone or endocrinology specialized journal (e.g., *Journal of Bone and Mineral Research* or *Endocrinology*)

Author contributions

MF and OAR designed experiments. OAR performed all the experiments. RE and NGS provided *Pcsk5^{fl/fl}* mice. JWC provided *Furin^{fl/fl}* mice. MF and OAR wrote the manuscript. All authors discussed the results and commented on the manuscript.

ABSTRACT

Fibroblast growth factor 23 is a hormone secreted by terminally differentiated osteoblasts and osteocytes which negatively regulates phosphate reabsorption in the kidney proximal tubule. FGF23 endocrine functions are mediated through the intact full-length protein. Endoproteolytic cleavage of intact FGF23 at the R₁₇₆HTR₁₇₉ motif, a consensus cleavage sequence for the proprotein convertases (PCs), releases the C-terminal and the N-terminal fragment and inactivates FGF23 endocrine function. Mutation in FGF23 cleavage site rendering FGF23 resistant to cleavage leads to Autosomal Dominant Hypophosphatemic Rickets (ADHR), a human disease characterized by an increase in serum intact FGF23, increased phosphate excretion, hypophosphatemia, and osteomalacia. Processing of FGF23 is also regulated in specific physiological conditions such as low or high phosphate diets, iron deficiency, and increased circulating erythropoietin or interleukin 1 beta (IL-1 β). Furin and PC5 were shown to process FGF23 in vitro. Yet, despite the importance of endoproteolysis in FGF23 regulation, the PC(s) involved in FGF23 cleavage in vivo remain unknown. In the present study, we assessed FGF23 processing and phosphate metabolism in mice lacking either or both furin and PC5 in osteoblasts and osteocytes (*Furin^{osb}-/-*, *Pcsk5^{osb}-/-* or *Furin;Pcsk5^{osb}-/-*). Our data showed that furin deficient mice have a 25% increase in intact FGF23 while they maintained normal phosphate levels on normal and low phosphate diet. In conditions of iron deficiency, FGF23 processing is impaired in the mice lacking furin in osteoblasts and osteocytes, while it is normally processed in control mice. In contrast, FGF23 is normally processed following erythropoietin or IL-1 β injections in mice lacking furin or both furin and PC5. Our data suggest that furin is partially responsible of FGF23 cleavage in vivo under normal physiological conditions, and that other PCs, besides PC5, may redundantly cleave FGF23 in osteocytes.

1. INTRODUCTION

Fibroblast growth factor 23 (FGF23) is a bone-derived hormone (i.e., osteokine) secreted by terminally differentiated cell of the osteoblast lineage (osteocytes). It plays a fundamental role in phosphate and vitamin D metabolism in particular through a direct action on the kidney [1, 2]. FGF23 signals through the FGF receptors (FGFRs) where its specific role in the kidney is mediated via an interaction between FGFR1 and the co-receptor α -klotho [3]. FGFR1/ α -klotho signaling in the kidney proximal tubule suppresses the transcription of *Slc34a1* and *Slc34a3*, the genes encoding for the sodium phosphate co-transporters NaPi2A and NaPi2C respectively, resulting in increased urinary phosphate excretion and decreased serum phosphate levels. In addition, FGF23 reduces the 1,25-dihydroxyvitamin D₃ (Calcitriol) level by reducing the expression of vitamin D producing enzyme coding gene *Cyp27b1* and increasing the expression of vitamin D inactivating enzyme coding gene *Cyp24a1* [4-7]. These functions of FGF23 are mediated through full-length intact FGF23. Endoproteolytic cleavage of FGF23 at the basic motif R₁₇₆HTR₁₇₉, a consensus cleavage site for proprotein convertases (PCs), inactivates FGF23 by releasing the N-terminus and the C-terminus fragments.

The physiological level of intact over processed FGF23 is tightly regulated in part through various post-translational modifications of amino acids surrounding the PC cleavage site in FGF23. The *O*-glycosylation of threonine 178 (T₁₇₈) by the *N*-acetylgalactosaminyltransferase 3 (GalNAc-T3) inhibits FGF23 processing [8-10]. FGF23 *O*-glycosylation is in turn reduced when the serine 180 (S₁₈₀) is phosphorylated by Fam20c, a kinase residing in the Golgi [11]. Impaired FGF23 glycosylation caused by a defective GalNAc-T3 or mutation in FGF23 glycosylation sites cause an increase in FGF23 processing and subsequent decrease in active FGF23 serum level. These molecular defects lead to familial tumoral calcinosis (FTC), a human disease characterised by hyperphosphatemia and heterotopic calcification [8-10]. On the other hand, autosomal dominant hypophosphatemic rickets (ADHR) and X-linked hypophosphatemic rickets (XLH) are human diseases caused by mutations in the FGF23 cleavage site and PHEX protein respectively. ADHR and XLH patients develop hypophosphatemia and osteomalacia due to the increased level of active intact FGF23 [12, 13]. Iron deficiency, erythropoietin treatment or interleukin-1 beta (IL-

1β) were shown to stimulate FGF23 production [14-19]. The increase in FGF23 production increases intact FGF23 levels in ADHR conditions, but not in normal conditions as it is properly processed.

The proprotein convertases furin and PC5 were shown to cleave FGF23 in vitro [20] while inactivation of *FURIN* in the human osteosarcomas U2-OS cell line impaired the cleavage of ectopically expressed FGF23 [11]. Yet, despite the importance of FGF23 cleavage in the pathology of several human diseases, the identity of the enzyme(s) responsible for FGF23 endoproteolysis in vivo remains undetermined. In the present study we assessed the requirement of furin and PC5 for FGF23 processing and phosphate metabolism in vivo. We showed that furin inactivation in the osteoblast lineage results in increased intact FGF23 under normal diet and low phosphate diet, while it totally impairs FGF23 cleavage under iron deficiency condition. The injection of erythropoietin or interleukin-1-beta increases FGF23 serum level, while it still properly cleaved in the absence of furin or both furin and PC5 in vivo. Together, our data suggest that furin is involved in FGF23 cleavage in vivo, but that other PC(s), excluding PC5, might redundantly be implicated in this process.

2. MATERIALS AND METHODS

Mice model. *Furin*^{flox/flox} and *Pcsk5*^{flox/flox} mice were generated by introducing loxP site flanking exon 2 of furin gene and exon 1 of Pcsk5 gene as described previously [21, 22]. To generate conditional knockout of furin (*Furin*^{osb-/-}) or PC5 (*Pcsk5*^{osb-/-}) in osteoblasts/osteocytes, *Furin*^{flox/flox} and *Pcsk5*^{flox/flox} were crossed with hOCN-Cre transgenic mice, which express the Cre-recombinase under the control of human osteocalcin promoter [23]. *Furin*; *Pcsk5*^{osb-/-} mice are deficient in both *Furin* and *Pcsk5* in osteoblasts/osteocytes, they were generated by breeding *Furin*^{osb-/-} and *Pcsk5*^{flox/flox} colonies. All mice were backcrossed at least 10 times with the C57B6J genetic background, they were maintained at the IRCM pathogen free animal facility on 12h light/dark cycle and fed a normal chow diet. In some indicated experiments mice were fed with synthetic diet to induce iron or phosphate deficiency. For iron deficiency challenge, after weaning at 21 days old, mice were fed either with normal diet or iron deficient diet (Research diet, Ain-

76A modified rodent diet, D09070102i) in combination with bleeding equivalent to one blood capillary every two weeks. For phosphate challenge, mice were fed for 5 days on normal phosphate diet (Teklad custom diet, TD. 98243, 0.6% phosphorus), then divided to two groups. The first group was maintained for one more week on 0.6% PI diet while the second group was fed on phosphate deficient diet (Teklad custom diet, TD. 86128, 0.02% phosphorus). In other set of experiment normal diet fed mice were injected with Erythropoietin (Eperex:) or IL-1 β (Stem cells).

Serum biochemistry. Intact and C-terminal FGF23 measurements were performed on EDTA plasma collected from mice under fed condition. Intact FGF23 ELISA and C-terminal FGF23 plasma levels were quantified using intact and C-terminal FGF23 from Quidel (Immutopics, cat#: 60-6800 and cat#: 60-6300 respectively). At the experiment end point, mice were anesthetized, and serum was collected by heart puncture. Serum phosphate level was determined using the phosphorus assay kit (Sekisui cat#:117-30). For urine phosphate measurements, urine was collected over 3 days, phosphate level was normalized to Creatinine measured using Creatinine assay from Quidel (MicroVue, cat#: 8009).

RNA extraction. Liver, kidney, bone and bone marrow RNA was extracted using the standard protocol previously described by *Chomczynski et al* [24]. cDNA was generated by RNA reverse transcription using M-MLV Reverse Transcriptase (Invitrogen, Thermo Fisher Scientific). Quantitative real-time PCR (qPCR) was performed using specific primers (Supplemental table 5-1) and SYBR Green qPCR Master Mix (BiMake). Expression levels were normalized to *Actb* expression levels.

Von Kossa / Van Gieson staining. Mice were collected and fixed in 10% formalin for 24 hours, following which the buffer is switched to 70% ethanol. Lumbar vertebrae were collected and dehydrated by gradual increase of ethanol %. Vertebrae were then embedded in methyl methacrylate resin as described previously [25]. Following embedding, vertebrae were sectioned

at 7- μ m sections and stained with Von kossa/ Van Gieson and images were analysed using the Osteomeasure analysis system (Osteometrics, Atlanta, GA).

3. RESULTS

Furin inactivation in osteoblasts and osteocytes partially impairs FGF23 cleavage, but decreases phosphate excretion. In order to investigate the role of furin in the regulation of FGF23 processing in vivo, we generated mice in which the *Furin* gene was specifically inactivated in osteoblasts and osteocytes (*Furin^{osb}-/-*) by breeding *Furin^{flox/flox}* mice with *hOCN-Cre* transgenic animals which express the Cre recombinase under the control of human osteocalcin promoter [23]. When fed a normal chow diet (0,7% Pi), 4-month-old *Furin^{osb}-/-* displayed a significant ~25% increase in intact FGF23 (Figure 5-1A). However, this moderate increase did not significantly alter the expression of the genes encoding sodium phosphate co-transporters *Slc34a1* and *Slc34a3* or of the vitamin D producing enzyme *Cyp27b1* and vitamin D inactivating enzyme *Cyp24a1* (Figure 5-1B). Consequently, these mice maintained normal phosphate levels and histological analysis did not reveal presence of osteomalacia (Figure 5-1 C and D).

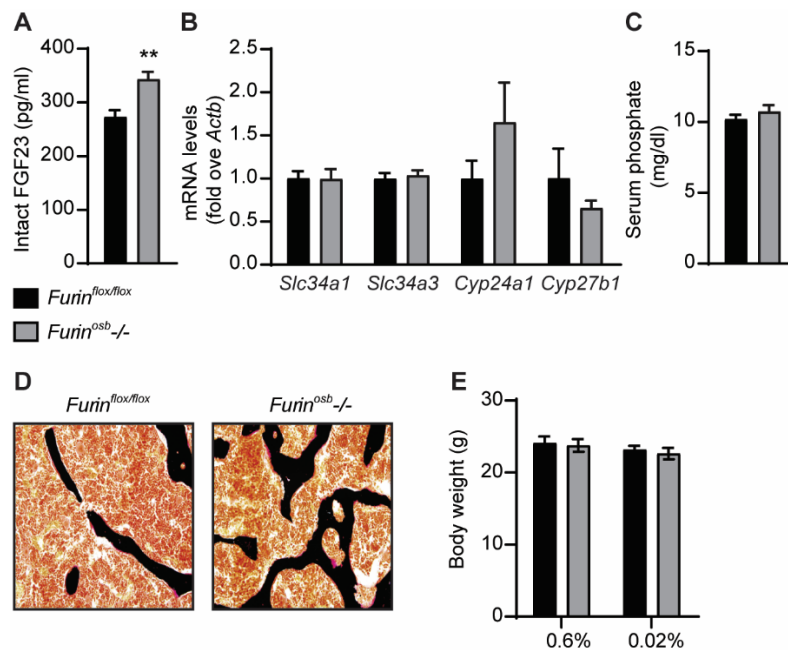


Figure 5-1. Increased FGF23 level and reduced phosphate excretion in *Furin^{osb}-/-* mice. FGF23 and phosphate levels in *Furin^{flox/flox}* (n=6) and *Furin^{osb}-/-* (n=6) fed on normal chow diet (A-D). Intact FGF23 levels in plasma (A). FGF23 target genes expression in kidney (B). Serum phosphate level (C). Von Kossa staining on vertebrae (D).

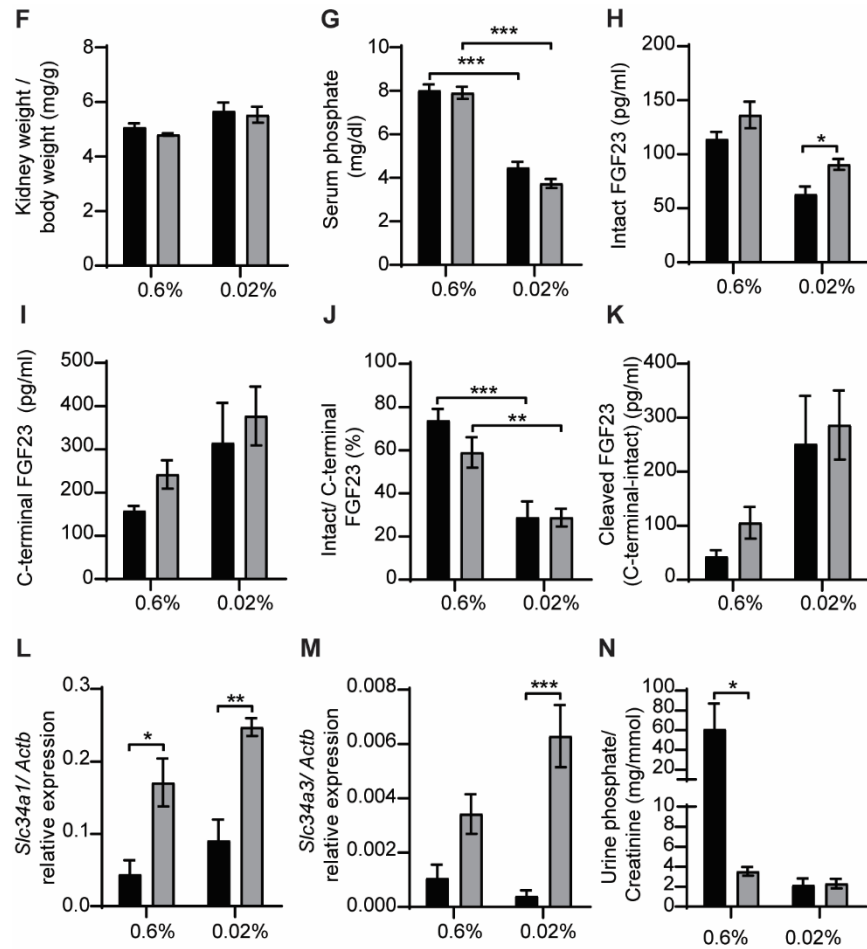


Figure 5-1- continued. Increased FGF23 level and reduced phosphate excretion in *Furin^{osb}-/-* mice. FGF23 and phosphate parameters in *Furin^{lox/lox}* (n=6) and *Furin^{osb}-/-* (n=6-7) fed on normal phosphate diet (0.6%) or low phosphate diet (0.02%) (E-N). Body weight (E). Kidney weight normalize to body weight (F). Serum phosphate levels (G). FGF23 plasma measurements, intact FGF23 (H). C-terminal FGF23 (I), % of intact over C-terminal FGF23 (J) and cleaved FGF23 levels, calculated by subtracting C-terminal from intact FGF23 level (K). Expression levels of Sodium phosphate cotransporter in kidney, *Slc34a1* expression (L) and *Slc34a3* expression (M). (N) Urine phosphate measurements normalized to Creatinine. Results represent the mean \pm SEM. * $P < 0.05$, ** $P < 0.01$, and *** $P < 0.001$, by Student T-test or 2-way ANOVA for non repeated measurements with Bonferroni's multiple comparisons test.

Serum phosphate level is a powerful regulator of FGF23 and previous studies has shown that in mice fed a low phosphate diet the serum level of intact FGF23 is reduced and the intact over C-terminal FGF23(Total FGF23) ratio is decreased, presumably due to the action of a PC [26-28]. We therefore next assessed if hypophosphatemia could be induced in *Furin^{osb}-/-* mice under low phosphate dietary intake. Feeding control and *Furin^{osb}-/-* mice normal phosphate diet (i.e., 0.6% Pi) or low-phosphate diet (0.02% Pi) did not affected body weight or kidney weight (Figure 5-1 E and F). As expected, serum phosphate level decreased significantly in both control and

Furin^{osb}-/- mice fed low phosphate deficient diet (Figure 5-1G). Interestingly, under low dietary phosphate, *Furin^{osb}-/-* mice tend to have a lower serum phosphate level compared to control mice, although this did not reach statistical significance. *Furin^{osb}-/-* mice on normal diet had >25% increase in intact and C-terminal (total) FGF23, while maintaining normal intact/C-terminal FGF23 ratio compared to control littermates (Figure 5-1H-J). Interestingly, the amount of cleaved FGF23 (i.e., C-terminal FGF23 minus intact FGF23) was increased in *Furin^{osb}-/-* on normal phosphate diet, suggesting cleavage of FGF23 even in absence of furin (Figure 5-1K). *Furin^{osb}-/-* mice also displayed increase expression of the sodium phosphate transporter *Slc34a1* and *Slc34a3* genes compared to control group (Figure 5-1 L and M). In addition, *Furin^{osb}-/-* mice on normal phosphate diet showed a decrease in urinary phosphate compared to control littermate (Figure 5-1N). Challenging the mice for one week on phosphate deficient diet reduced urinary phosphate in control mice but not in *Furin^{osb}-/-* mice, as these mice maintained a low urinary phosphate observed on normal phosphate diet (Figure 5-1N). Together these results show that inactivation of the *Furin* in the osteoblast lineage results only in a modest increase in intact FGF23 in physiological conditions.

Impact of iron deficiency on FGF23 processing and phosphate metabolism in absence of furin in osteoblast and osteocytes. Our data showed that *Furin^{osb}-/-* mice have a modest 25% increase in intact FGF23 under normal physiological conditions. It was previously reported that mice with an ADHR mutation (R176Q) in the *Fgf23* gene did not develop hypophosphatemia unless they were fed a low-iron diet [15]. We therefore next tested the impact of iron-deficiency, induced by feeding the mice a low-iron diet in combination with repeated tail bleedings (i.e., 70 μ l every other week) for 14 weeks, on FGF23 and phosphate metabolism in control and *Furin^{osb}-/-* mice. Both genotypes maintained normal growth curves in these conditions as compared to mice fed the control diet, but they developed iron deficiency as reflected by the decrease in hepcidin (*Hamp*) expression and the increase in transferrin receptor (*Tfrc*) expression in liver (Figure 5-2A-C). Consequently and as previously reported [15], both control and *Furin^{osb}-/-* mice displayed an increase in *Fgf23* gene expression in bone (Figure 5-2D). However, iron-deficiency resulted in increased C-terminal FGF23 only in control mice, although both genotypes showed an

increase in intact FGF23 (Figure 5-2 E and F). Consistent with an essential role for furin in cleaving this hormone, FGF23 processing appears to be totally impaired in *Furin^{osb-/-}* mice under conditions of iron deficiency as these mice maintained a 1:1 ratio (i.e., 100%) of intact over C-terminal FGF23 and very low level of cleaved FGF23 (Figure 5-2 G and H). Yet, despite this near complete inhibition in FGF23 processing, *Furin^{osb-/-}* mice displayed a paradoxical increase in serum phosphate level compared to the control littermates under iron deficiency (Figure 5-2I). Together these results suggest that furin is responsible for FGF23 processing under iron deficiency.

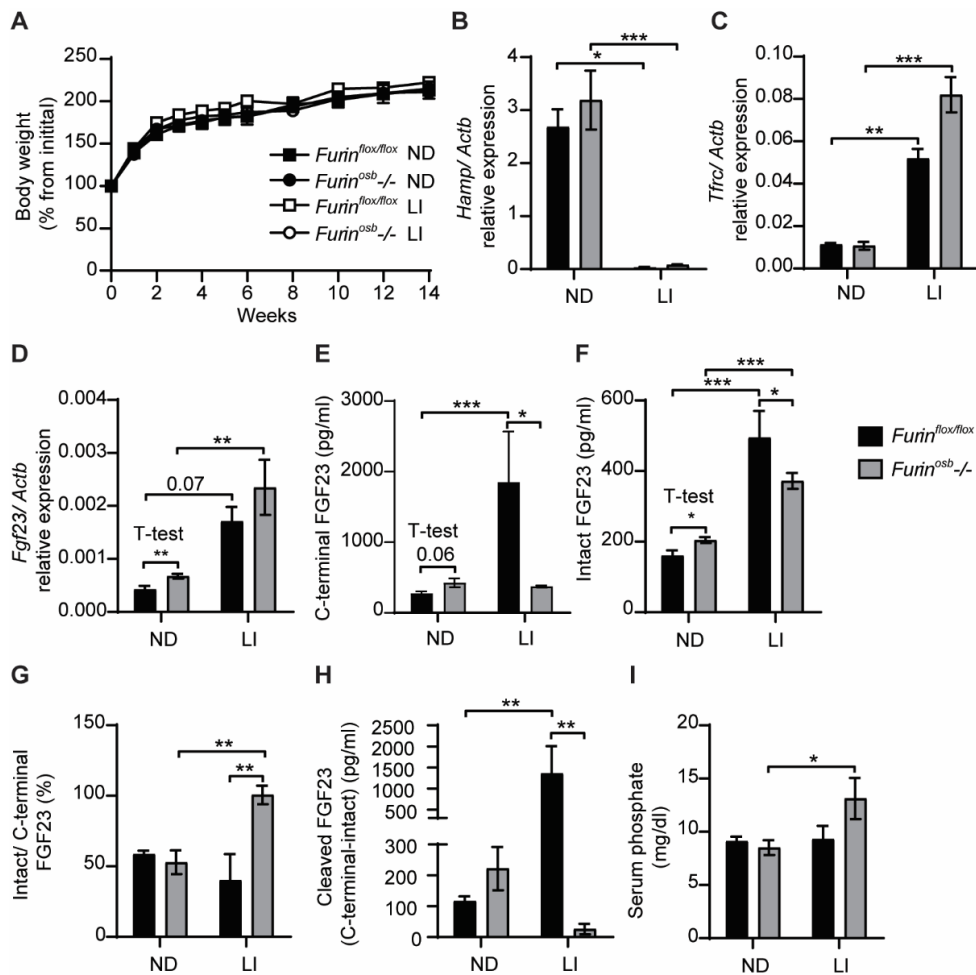


Figure 5-2. Impaired FGF23 processing and hyperphosphatemia in *Furin^{osb-/-}* mice following iron restriction. *Furin^{lox/lox}* (n=3-5) and *Furin^{osb-/-}* (n=7-8) fed on normal chow diet (ND) or low iron diet (LI). (A) Body weight growth curve represented as % body weight relative to initial body weight. (B-C) Iron deficiency target gene expression in liver. Heparin expression “*Hamp*” (B), Transferrin receptor expression “*Tfrc*” (C). (D) *Fgf23* expression in long bone. (E-H) Plasma FGF23 measurements. C-terminal FGF23 (E), intact FGF23 (F), % of intact over C-terminal FGF23 (G) and cleaved FGF23 levels, calculated by subtracting C-terminal from intact FGF23 level (H). (I) Serum phosphate levels. Results represent the mean ± SEM. **P* < 0.05, ***P* < 0.01, and ****P* < 0.001, by student T-test or 2-way ANOVA for non repeated measurements with Bonferroni’s multiple comparisons test.

Normal FGF23 processing in absence of furin in osteoblasts/osteocytes following rhEPO and IL-1 β injections. Recent studies showed that erythropoietin and interleukin 1 beta (IL-1 β), which are increased under anemic and inflammation conditions respectively, are two potent inducers of FGF23 at the transcriptional and protein level [16-19, 29, 30]. Such pathological conditions may also contribute to the onset of ADHR phenotype [16-19, 30]. Human recombinant erythropoietin (rhEPO) is widely used as a treatment for patient suffering from anemia and it was shown to correlate with the increase in total FGF23 circulating level in mice and human [17-19, 29-31]. Additional genetic studies in mice suggested that osteocytes are one contributor of the circulating FGF23 following rhEPO injection [30, 32]. Importantly, in normal rodents, most (i.e., >80%) of the circulating FGF23 is in its cleaved form following rhEPO or IL-1 β injections, explaining why the animals maintain normal phosphate level in face of elevated FGF23 expression [16, 17, 19]. It was suggested that the activity of one or multiple PC is required to maintain FGF23 in its inactive form in these particular conditions [16, 17]. We therefore next tested the impact of furin deficiency in osteoblasts and osteocytes on FGF23 processing following 6h of a single injection of rhEPO or IL-1 β .

Because of discrepancy in the doses of rhEPO used in the literature to induce FGF23 in rodents [17-19, 29, 30], we first tested if two relatively low doses (i.e., 300U/kg and 3000U/kg) of rhEPO were sufficient to induce the expression of two known EPO target genes erythroferrone (*Erfe*) and erythropoietin receptor (*Epor*) in bone and bone marrow of wild type C57BL/6J mice (Figure 5-3A-D). Both doses also robustly induced the expression of *Fgf23* in both tissues in the same animals (Figure 5-3 E and F). We next assessed the effect of the same treatment in control and *Furin^{osb}-/-* mice. Circulating level of total (C-terminal) FGF23 was increased in a dose dependent manner by rhEPO, while intact FGF23 was modestly changed regardless of the genotype (Figure 5-3 G and H). The ratio of intact over C-terminal FGF23 was decreased, while the cleaved FGF23 was increased more than 10-fold and to the same extent in both control and *Furin^{osb}-/-* mice (Figure 5-3 I and J), suggesting that in this context FGF23 is normally processed even in absence of furin in osteoblasts and osteocytes.

Control and *Furin^{osb}*^{-/-} mice were also administered a single dose of IL-1 β (50ng/g), a treatment which was previously shown to induce *Fgf23* expression in bone and to raise total FGF23 circulating level within a few hours [16]. FGF23 measurements showed that 6h following the injection of IL-1 β in both control and *Furin^{osb}*^{-/-} mice the level of total (C-terminal) FGF23 increased by more than 30-fold, while intact FGF23 is increased by less than 10-fold (Figure 5-3K and L). Regardless of the genotype, the plasma concentration of intact over C-terminal FGF23 is decreased and the cleaved FGF23 following IL-1 β injection is also increased more than 10 times (Figure 5-3 M and N). Together, these data show that FGF23 is efficiently processed following rhEPO or IL-1 β injections in absence of furin in osteoblast and osteocytes.

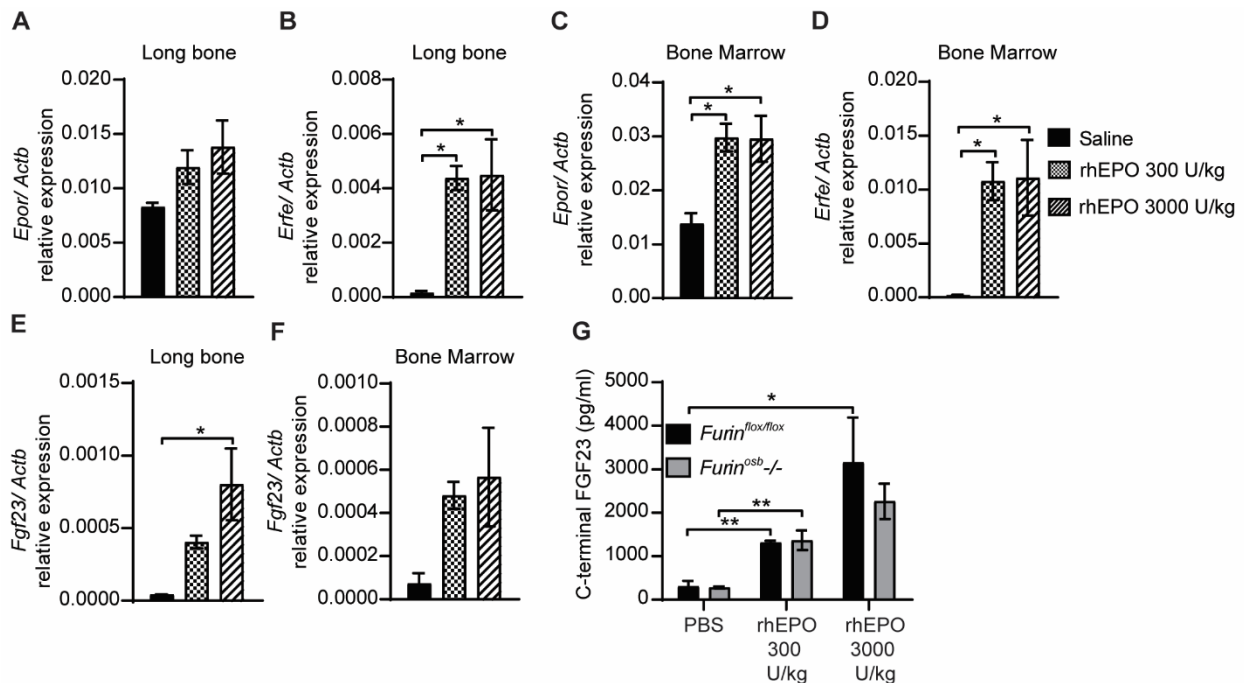


Figure 5-3. FGF23 is normally processed following rhEPO and IL-1 β injection. Genes expression in long bone (A, B and E) and bone marrow (C, D and F) of C57B6J mice at 6 hours following the injection of saline (n=4), 300 U/kg (n=4), and 3000 U/kg (n=4) of rhEPO. Erythropoietin receptor “*Epor*” (A and C), Erythroferrone “*Erfe*” (B and D), and FGF23 “*Fgf23*” (E and F).

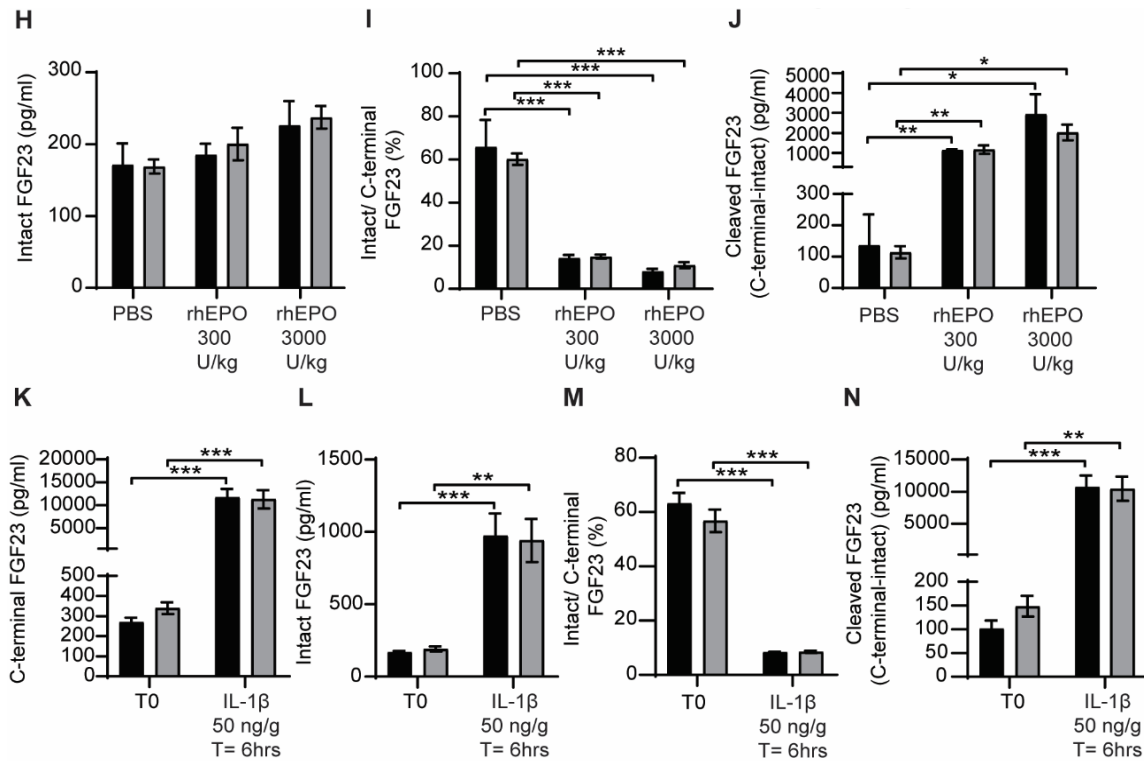


Figure 5-3- continued. FGF23 is normally processed following rhEPO and IL-1 β injection. Plasma FGF23 measurements in *Furin^{flox/flox}* (n=3) and *Furin^{osb-/-}* (n=3) following 6 hours of the injection of PBS, 300 U/kg, and 3000 U/kg of rhEPO. C-terminal FGF23 (G), intact FGF23 (H), % of intact over C-terminal FGF23 (I) and cleaved FGF23 levels, calculated by subtracting C-terminal from intact FGF23 level (J). (K and N) Plasma FGF23 measurements in *Furin^{flox/flox}* (n=4) and *Furin^{osb-/-}* (n=4) at time T0 and 6 hours following the injection of 50 ng/g IL-1 β . C-terminal FGF23 (K), intact FGF23 (L), % of intact over C-terminal FGF23 (M) and cleaved FGF23 levels, calculated by subtracting C-terminal from intact FGF23 level (N). Results represent the mean \pm SEM. * $P < 0.05$, ** $P < 0.01$, and *** $P < 0.001$, by one-way ANOVA (A-F), 2-way ANOVA for non repeated measurements (G-J) or for repeated measurements (K-N) with Bonferroni's multiple comparisons test.

Effect of combined PC5 and furin genetic ablation in the osteoblast lineage on FGF23 processing in vivo. The data presented above suggests that under physiological condition furin is partially responsible of FGF23 cleavage, while under iron deficiency, furin may be a major contributor to the processing of FGF23. Remarkably, FGF23 was normally processed following rhEPO or IL-1 β injection in *Furin^{osb-/-}* mice, suggesting a context dependent redundancy between furin and another PC. PC5 can cleave FGF23 in vitro and is expressed in differentiated osteoblasts and in osteocytes [20, 33]. To address whether PC5 contributes to FGF23 processing in vivo, we generated mice in which *Pcsk5*, the gene encoding PC5, was inactivated specifically in osteoblasts and osteocytes (*Pcsk5^{osb-/-}* mice) by breeding *Pcsk5^{fl/fl}* mice with *hOCN-Cre* transgenic animals. When fed a normal chow diet, the circulating level of intact FGF23 and serum phosphate in the

Pcsk5^{osb}-/- mice was indistinguishable from control littermates (Figure 5-4 A and B). Von Kossa/van Gieson staining on non-decalcified bone sections failed to reveal any sign of osteomalacia in these mice (Figure 5-4C), suggesting that PC5 in the osteoblast lineage is dispensable for the regulation of FGF23 and phosphate level in vivo.

Finally, we tested if PC5 and furin may redundantly cleave FGF23 in vivo. For this purpose, we generated mice lacking specifically both furin and PC5 in osteoblasts and osteocytes (*Furin;Pcsk5^{osb}-/-* mice). Osteoblast-specific inactivation of furin and PC5 resulted in a modest increase in circulating intact FGF23 when the mice were fed normal or low phosphate diet (Figure 5-4D). A single injection of rhEPO (300U/kg) increased total (C-terminal) FGF23 by almost 10-fold, while intact FGF23 levels were only moderately increased in control and *Furin;Pcsk5^{osb}-/-* mice (Figure 5-4E-F). Consequently, intact over C-terminal FGF23 was equally decreased and the cleaved FGF23 was equally increased more than 10 times in both genotypes following rhEPO injection (Figure 5-4 G and H). Together, these results show that FGF23 is still efficiently processed in vivo even in the context of combined genetic ablation of furin and PC5 in osteoblasts and osteocytes.

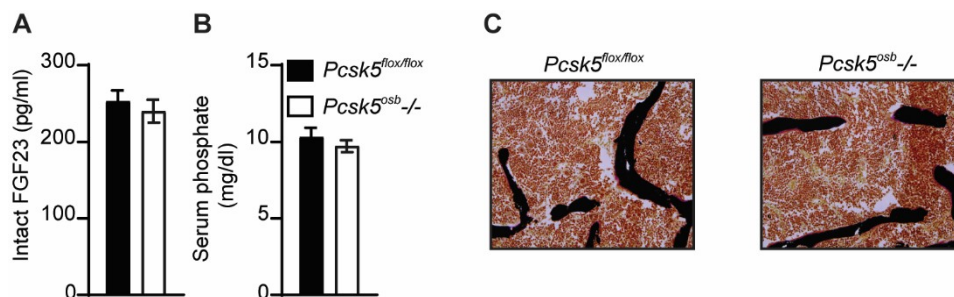


Figure 5-4. PC5 inactivation did not impair FGF23 processing. Plasma intact FGF23 (A) and serum phosphate levels (B) in *Pcsk5^{flox/flox}* (n=6) and *Pcsk5^{osb}-/-* (n=7) fed on normal diet. (C) Von Kossa staining of vertebrae of *Pcsk5^{flox/flox}* and *Pcsk5^{osb}-/-*.

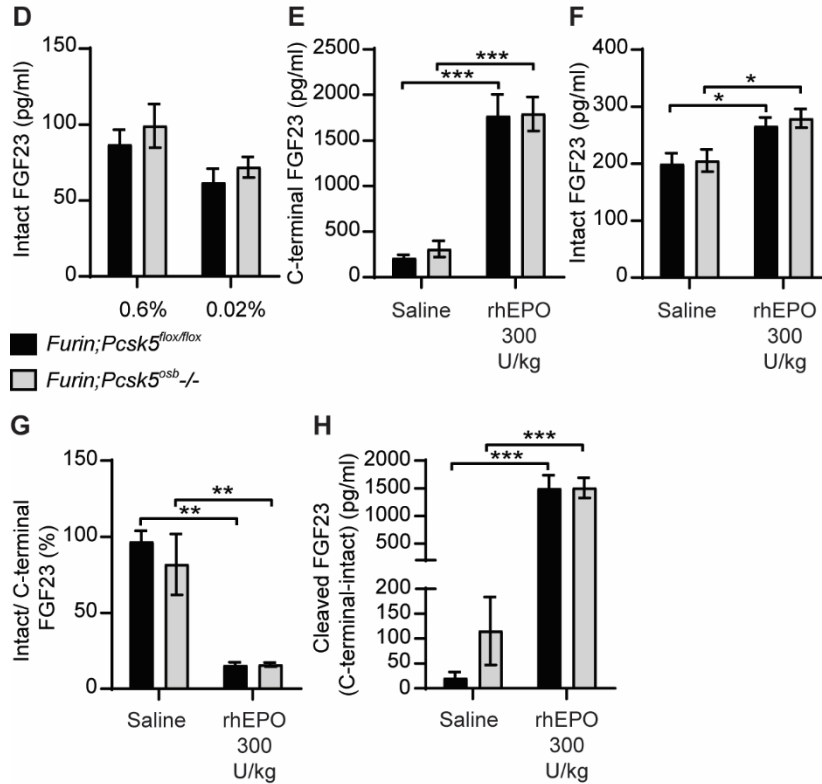


Figure 5-4- continued. PC5 inactivation did not impair FGF23 processing. Plasma intact FGF23 in *Furin;Pcsk5^{flox/flox}* (n=7-8) and *Furin;Pcsk5^{osb-/-}* (n=8) fed on normal phosphate diet (0.6%) or low phosphate diet (0.02%) (D). (E and G) Plasma FGF23 measurements in *Furin;Pcsk5^{flox/flox}* (n=4) and *Furin;Pcsk5^{osb-/-}* (n=4) following 6 hours of the injection of saline and 300 U/kg of rhEPO. C-terminal FGF23 (E), intact FGF23 (F) and cleaved FGF23 levels, calculated by subtracting C-terminal from intact FGF23 level (G). Results represent the mean \pm SEM. * $P < 0.05$ and *** $P < 0.001$, by 2-way ANOVA for non repeated measurements with Bonferroni's multiple comparisons test.

4. DISCUSSION

More than 20 years ago mutations in a putative proprotein convertase (PC) target sequence within human FGF23 were found to cause ADHR. Yet, the identity of the specific PCs involved in FGF23 cleavage in vivo remained elusive. Taking advantage of floxed alleles of *Furin* and *Pcsk5*, and using the *hOCN-Cre* transgenic mice, we generated mice lacking furin and/or PC5 specifically in osteoblasts and osteocytes and assessed the role of these two enzymes in regulating FGF23 processing in vivo. We provide evidence suggesting that furin, but not PC5, partially regulates FGF23 processing in vivo under normal condition. We also exposed the mice to different challenges that were shown to contribute to the regulation of FGF23. Our data showed that FGF23 processing is completely mediated by furin under iron deficiency conditions.

The requirement of furin for FGF23 processing appears to be context-dependent, since FGF23 is still properly cleaved following rhEPO or IL-1 β injection in absence of furin and PC5. Our results therefore suggest that additional PC(s) may redundantly cleave FGF23 in vivo.

When mice were fed standard chow diet, the modest increase in circulating intact FGF23 in *Furin^{osb}-/-* mice was not sufficient to cause hypophosphatemia and osteomalacia. We first interpreted this result as being consistent with the observation that ADHR patients show variable age of onset and penetrance of the disease [34]. Since iron deficiency was shown to positively correlate with FGF23 circulating levels in ADHR patient and to induce hypophosphatemia and osteomalacia in mice carrying an ADHR mutation [14, 15], we challenged control and furin deficient mice with iron deprivation. However, furin deficient mice did not develop hypophosphatemia and in fact displayed higher serum phosphate level despite a near complete impairment of FGF23 cleavage.

The results obtained in the context of iron deficiency raised the question whether under normal condition FGF23 is redundantly cleaved by another enzyme which is repressed following iron deficiency. To clarify whether FGF23 cleavage by furin is context specific, we injected controls and furin deficient mice with rhEPO or IL-1 β . These two circulating proteins are secreted in response to anemia and inflammation respectively [16, 35], and were shown to induce FGF23 secretion in bone and bone marrow cells in rodents [16-19, 29, 30]. Ablation of marrow cells with carboplatin in mice, suggest that osteoblasts and osteocytes may contribute up to ~60% of the increase in circulating FGF23 in response to rhEPO injections [30]. In our own study, despite a strong increase in their circulating total (C-terminal) FGF23 level following rhEPO or IL-1 β injection, *Furin^{osb}-/-* mice did not show a concurrent increase in intact FGF23. These results provide additional credence to the notion that furin is not the only PC involved in FGF23 processing in vivo. We also tested the possibility that PC5 may cleave FGF23 in osteoblasts and osteocytes. Our results showed that FGF23 and serum phosphate levels were not changed in the mice lacking PC5 in these cells specifically. Finally, we tested the possibility that PC5 compensates for the absence of furin and redundantly cleaves FGF23. Yet, mice deficient in both enzymes in

the osteoblast lineage are comparable to furin deficient mice in term of FGF23 circulating levels under physiological condition and following rhEPO injection. Together, our data support that beside furin additional PCs, excluding PC5, redundantly cleaves FGF23 in vivo. We previously showed that *Pcsk6* encoding for the paired basic amino acid cleaving enzyme 4 (PACE4) and *Pcsk7* encoding for PC7 are expressed in osteoblasts [33]. These PCs also belong the subtilisin/kexin PC family and share the minimal consensus cleavage site required for furin and PC5 [36], suggesting that these PCs may redundantly cleave FGF23 in vivo.

The FGF23 processing in *Furin^{osb-/-}* is context specific: it is totally impaired under iron deficiency but not following rhEPO or IL-1 β injection, suggesting the presence of two different mechanisms of FGF23 regulation. Iron deficiency was previously shown to increase FGF23 expression through the stabilisation of the hypoxia induced factor 1 alpha (HIF1 α), a transcription factor that is activated on low oxygen condition [37]. Moreover, the rise in IL-1 β levels was found to increase both *Hif1 α* expression and nuclear localization. HIF1 α inhibition reduced IL-1 β effect on FGF23 and increased intact FGF23 levels [16] possibly by repressing the expression of furin which was shown to be enhanced by HIF1 α in vitro [38]. On the other hand, treatment with Hif1 α prolyl hydroxylase (HIF-PH) inhibitor, which stabilize HIF1 α , increase the cleavage of intact FGF23. An additional study showed that the effect of HIF-PH inhibitor on FGF23 is dependent on erythropoietin [18]. Taking in consideration that erythropoietin increases FGF23 production in bone and bone marrow, this suggests that FGF23 is produced from the two compartments in *Furin^{osb-/-}* mice following a single dose injection of rhEPO or IL-1 β , while it is mainly coming from bone under iron deficiency condition.

In conclusion, these findings provide genetic evidence that furin in osteoblasts is partially responsible of FGF23 processing in vivo. Our data also showed that FGF23 cleavage is differentially regulated depending on the physiological context. Under iron deficiency furin is completely responsible of this process, while following rhEPO and IL-1 β single injection multiple or different PCs may be involved in FGF23 processing. Alternately, the increase in cleaved FGF23 following rhEPO and IL-1 β injection could be derived from non-osteoblastic cells such as bone

marrow. Future research is needed to address the identity of the additional enzyme involved in FGF23 processing and whether bone marrow compensates for the impaired FGF23 processing in bone.

5. REFERENCES

1. Meyer, R.A., Jr., M.H. Meyer, and R.W. Gray, *Parabiosis suggests a humoral factor is involved in X-linked hypophosphatemia in mice*. J Bone Miner Res, 1989. **4**(4): p. 493-500.
2. Miyauchi, A., et al., *Hemangiopericytoma-induced osteomalacia: tumor transplantation in nude mice causes hypophosphatemia and tumor extracts inhibit renal 25-hydroxyvitamin D 1-hydroxylase activity*. J Clin Endocrinol Metab, 1988. **67**(1): p. 46-53.
3. Urakawa, I., et al., *Klotho converts canonical FGF receptor into a specific receptor for FGF23*. Nature, 2006. **444**(7120): p. 770-4.
4. Larsson, T., et al., *Transgenic mice expressing fibroblast growth factor 23 under the control of the alpha1(I) collagen promoter exhibit growth retardation, osteomalacia, and disturbed phosphate homeostasis*. Endocrinology, 2004. **145**(7): p. 3087-94.
5. Shimada, T., et al., *FGF-23 is a potent regulator of vitamin D metabolism and phosphate homeostasis*. J Bone Miner Res, 2004. **19**(3): p. 429-35.
6. Shimada, T., et al., *Targeted ablation of Fgf23 demonstrates an essential physiological role of FGF23 in phosphate and vitamin D metabolism*. J Clin Invest, 2004. **113**(4): p. 561-8.
7. Shimada, T., et al., *FGF-23 transgenic mice demonstrate hypophosphatemic rickets with reduced expression of sodium phosphate cotransporter type IIa*. Biochem Biophys Res Commun, 2004. **314**(2): p. 409-14.
8. Benet-Pages, A., et al., *An FGF23 missense mutation causes familial tumoral calcinosis with hyperphosphatemia*. Hum Mol Genet, 2005. **14**(3): p. 385-90.
9. Ichikawa, S., et al., *Genetic rescue of glycosylation-deficient Fgf23 in the Galnt3 knockout mouse*. Endocrinology, 2014. **155**(10): p. 3891-8.
10. Topaz, O., et al., *Mutations in GALNT3, encoding a protein involved in O-linked glycosylation, cause familial tumoral calcinosis*. Nat Genet, 2004. **36**(6): p. 579-81.
11. Tagliabracci, V.S., et al., *Dynamic regulation of FGF23 by Fam20C phosphorylation, GalNAc-T3 glycosylation, and furin proteolysis*. Proc Natl Acad Sci U S A, 2014. **111**(15): p. 5520-5.
12. Consortium, A., *Autosomal dominant hypophosphataemic rickets is associated with mutations in FGF23*. Nat Genet, 2000. **26**(3): p. 345-8.
13. Nesbitt, T., et al., *Crosstransplantation of kidneys in normal and Hyp mice. Evidence that the Hyp mouse phenotype is unrelated to an intrinsic renal defect*. J Clin Invest, 1992. **89**(5): p. 1453-9.
14. Imel, E.A., et al., *Iron modifies plasma FGF23 differently in autosomal dominant hypophosphatemic rickets and healthy humans*. J Clin Endocrinol Metab, 2011. **96**(11): p. 3541-9.
15. Farrow, E.G., et al., *Iron deficiency drives an autosomal dominant hypophosphatemic rickets (ADHR) phenotype in fibroblast growth factor-23 (Fgf23) knock-in mice*. Proc Natl Acad Sci U S A, 2011. **108**(46): p. E1146-55.
16. David, V., et al., *Inflammation and functional iron deficiency regulate fibroblast growth factor 23 production*. Kidney Int, 2016. **89**(1): p. 135-46.
17. Hanudel, M.R., et al., *Effects of erythropoietin on fibroblast growth factor 23 in mice and humans*. Nephrol Dial Transplant, 2018.
18. Flamme, I., et al., *FGF23 expression in rodents is directly induced via erythropoietin after inhibition of hypoxia inducible factor proline hydroxylase*. PLoS One, 2017. **12**(10): p. e0186979.

19. Daryadel, A., et al., *Erythropoietin stimulates fibroblast growth factor 23 (FGF23) in mice and men*. Pflugers Arch, 2018. **470**(10): p. 1569-1582.
20. Yamamoto, H., et al., *Posttranslational processing of FGF23 in osteocytes during the osteoblast to osteocyte transition*. Bone, 2016. **84**: p. 120-30.
21. Essalmani, R., et al., *In vivo functions of the proprotein convertase PC5/6 during mouse development: Gdf11 is a likely substrate*. Proc Natl Acad Sci U S A, 2008. **105**(15): p. 5750-5.
22. Roebroek, A.J., et al., *Limited redundancy of the proprotein convertase furin in mouse liver*. J Biol Chem, 2004. **279**(51): p. 53442-50.
23. Zhang, M., et al., *Osteoblast-specific knockout of the insulin-like growth factor (IGF) receptor gene reveals an essential role of IGF signaling in bone matrix mineralization*. J Biol Chem, 2002. **277**(46): p. 44005-12.
24. Chomczynski, P. and N. Sacchi, *The single-step method of RNA isolation by acid guanidinium thiocyanate-phenol-chloroform extraction: twenty-something years on*. Nat Protoc, 2006. **1**(2): p. 581-5.
25. Chappard, D., et al., *Bone embedding in pure methyl methacrylate at low temperature preserves enzyme activities*. Acta Histochem, 1987. **81**(2): p. 183-90.
26. Bon, N., et al., *Phosphate-dependent FGF23 secretion is modulated by Pit2/Slc20a2*. Mol Metab, 2018. **11**: p. 197-204.
27. Yu, X., et al., *Genetic dissection of phosphate- and vitamin D-mediated regulation of circulating Fgf23 concentrations*. Bone, 2005. **36**(6): p. 971-7.
28. Perwad, F., et al., *Dietary and serum phosphorus regulate fibroblast growth factor 23 expression and 1,25-dihydroxyvitamin D metabolism in mice*. Endocrinology, 2005. **146**(12): p. 5358-64.
29. Toro, L., et al., *Erythropoietin induces bone marrow and plasma fibroblast growth factor 23 during acute kidney injury*. Kidney Int, 2018. **93**(5): p. 1131-1141.
30. Clinkenbeard, E.L., et al., *Erythropoietin stimulates murine and human fibroblast growth factor-23, revealing novel roles for bone and bone marrow*. Haematologica, 2017. **102**(11): p. e427-e430.
31. Coe, L.M., et al., *FGF-23 is a negative regulator of prenatal and postnatal erythropoiesis*. J Biol Chem, 2014. **289**(14): p. 9795-810.
32. Clinkenbeard, E.L., et al., *Conditional Deletion of Murine Fgf23: Interruption of the Normal Skeletal Responses to Phosphate Challenge and Rescue of Genetic Hypophosphatemia*. J Bone Miner Res, 2016. **31**(6): p. 1247-57.
33. Al Rifai, O., et al., *Proprotein convertase furin regulates osteocalcin and bone endocrine function*. J Clin Invest, 2017. **127**(11): p. 4104-4117.
34. Imel, E.A., S.L. Hui, and M.J. Econs, *FGF23 concentrations vary with disease status in autosomal dominant hypophosphatemic rickets*. J Bone Miner Res, 2007. **22**(4): p. 520-6.
35. Jelkmann, W., *Regulation of erythropoietin production*. J Physiol, 2011. **589**(Pt 6): p. 1251-8.
36. Seidah, N.G. and A. Prat, *The biology and therapeutic targeting of the proprotein convertases*. Nat Rev Drug Discov, 2012. **11**(5): p. 367-83.
37. Clinkenbeard, E.L., et al., *Neonatal iron deficiency causes abnormal phosphate metabolism by elevating FGF23 in normal and ADHR mice*. J Bone Miner Res, 2014. **29**(2): p. 361-9.

38. McMahon, S., et al., *Hypoxia-enhanced expression of the proprotein convertase furin is mediated by hypoxia-inducible factor-1: impact on the bioactivation of proproteins*. J Biol Chem, 2005. **280**(8): p. 6561-9.

6. SUPPLEMENTAL TABLE

Supplemental Table 5-1. Primer list

Primer	Sequence 5'-3'
Actin beta-Fw	GAC CTC TAT GCC AAC ACA GT
Actin beta-Rv	AGT ACT TGC GCT CAG GAG GA
Slc34a1-Fw	GCATCCTACTGTGGTACCCG
Slc34a1-Rv	CAGCAAACCAGCGGTACTTG
Slc34a3-Fw	CCTTTGGACTTTCCTGGCA
Slc34a3-Rv	GATGGTCGGTGTTGTTGCAG
Hamp-Fw	AGAGCTGCAGCCTTTGCAC
Hamp-Rv	GAGGTCAGGATGTGGCTCTA
Tfrc-Fw	TAAATCCCCGTTGTTGAGG
Tfrc-Rv	CAGGACAGCTTCCTCCATT

6. CHAPTER VI

DISCUSSION

The work presented in this thesis shows for the first time that the proprotein convertase furin is a pleiotropic regulator of osteoblast and osteocyte functions. Here we demonstrate that furin in osteoblasts and osteocytes regulates glucose and energy metabolism through two independent mechanisms. First, it mediates pro-osteocalcin maturation which is required for osteocalcin endocrine function. Second, it controls appetite independently of osteocalcin, suggesting the presence of additional osteokines that regulate appetite and are controlled by furin. We also showed that furin cleavage of FGF23 *in vivo* is context specific and that furin is required for proper bone mass accrual. Moreover, in the present thesis we describe for the first times that mouse osteocalcin is subjected to *O*-glycosylation, a species-specific modification. We also show that osteocalcin *O*-glycosylation increases its half-life *ex vivo* and *in vivo*. This discovery led us to generate a modified *O*-glycosylated human osteocalcin, which has a longer half-life in circulation, providing a potential tool to improve human osteocalcin bioactivity in future therapeutic applications for human diseases. This chapter will discuss the outcomes of this thesis, its significance in clinical studies and future therapeutic application, and the perspectives for the different projects.

6.1. OSTEOCALCIN PROTEOLYTIC CLEAVAGE AND *O*-GLYCOSYLATION REGULATES ITS ENDOCRINE FUNCTIONS

Uncarboxylated osteocalcin was shown to be the bioactive form of this hormone *in vitro*, *ex vivo*, and *in vivo*. Osteocalcin regulation by gamma-carboxylation is a well-studied process, as the enzyme and cofactors involved in this process are well characterized. Despite the importance of protein PTMs in the regulation of secreted hormones, our knowledge of additional osteocalcin modifications was limited. Hence, we decided to study the regulation of osteocalcin by PTMs. Osteocalcin was predicted to be synthesized as a pre-pro-protein, its signal peptide being removed by the signal peptidases in the endoplasmic reticulum [140, 141]. However, the mechanism and the enzyme(s) involved in osteocalcin propeptide removal were never investigated. Proprotein convertases are involved in endoproteolytic cleavage of proteins in secretory pathway, such as proopiomelanocortin (POMC), proglucagon, proinsulin, bone morphogenic protein 10 (BMP10), and angiopoietin-like 3 [297-301]. Consistent with this role, in

the present thesis we describe for the first time an in vivo role of PCs in osteoblasts. We identified furin as the pro-osteocalcin converting enzyme which cleaves osteocalcin propeptide in its C-terminus at the basic motif “RLRR” (Figure 6-1) independently of osteocalcin gamma-carboxylation. In addition, we discovered that osteocalcin is subjected to *O*-glycosylation, a specific modification that occurs on serine 8 of mouse osteocalcin and is not present in human or any other species (Figure 6-1). Our data showed that pro-osteocalcin processing by furin and its *O*-glycosylation are independent of each other and of osteocalcin gamma-carboxylation. We also demonstrated that osteocalcin processing is required for its proper decarboxylation and release during bone resorption [302]. The impaired osteocalcin processing in *Furin^{osb}/-* mice decreases the serum uncarboxylated osteocalcin, impairs glucose tolerance and reduces insulin secretion and energy expenditure [302]. In addition, we found that *O*-glycosylated osteocalcin is the most abundant form in mice. It represents 99% of osteocalcin in the bone of wild type mice. Computational modelling predicts the C-terminal amino acids of osteocalcin as the binding site to the GPRC6A receptor [186]. As *O*-glycosylation occurs in the N-terminal part of osteocalcin, it is likely that it does not affect its receptor binding capacity. Moreover, uncarboxylated non-*O*-glycosylated osteocalcin produced in bacteria was shown to be active in vivo [167, 171, 173]. Together, this evidence suggests that osteocalcin *O*-glycosylation may not be required for its endocrine function.

Protein glycosylation was shown to increase the stability and half-life of other proteins, such as interferon beta, follicle stimulating hormone, leptin and erythropoietin [303-305]. Likewise, we found that *O*-glycosylated osteocalcin has a longer half-life compared to its non-*O*-glycosylated form ex vivo and in vivo. Our data showed that the decrease in the half-life of non-*O*-glycosylated osteocalcin can be inhibited by heat inactivation ex vivo. Interestingly, mouse osteocalcin *O*-glycosylation occurs within a proline rich sequence VPSPDP, suggesting that this process might prevent osteocalcin proteolysis near these residues. Prolyl peptidase is a family of proteases that cleaves after proline residues at the N-terminal or C-terminal of protein [306]. Some members of this family, such as peptidyl proteases and prolyl oligopeptidases are not inhibited using the inhibitors screened in Chapter IV.

Together, these findings emphasize the importance of osteocalcin maturation and activation by furin for its endocrine functions and the requirement of osteocalcin *O*-glycosylation for a longer half-life in circulation. Some of these modifications are conserved in human osteocalcin and they will be discussed in the next paragraph.

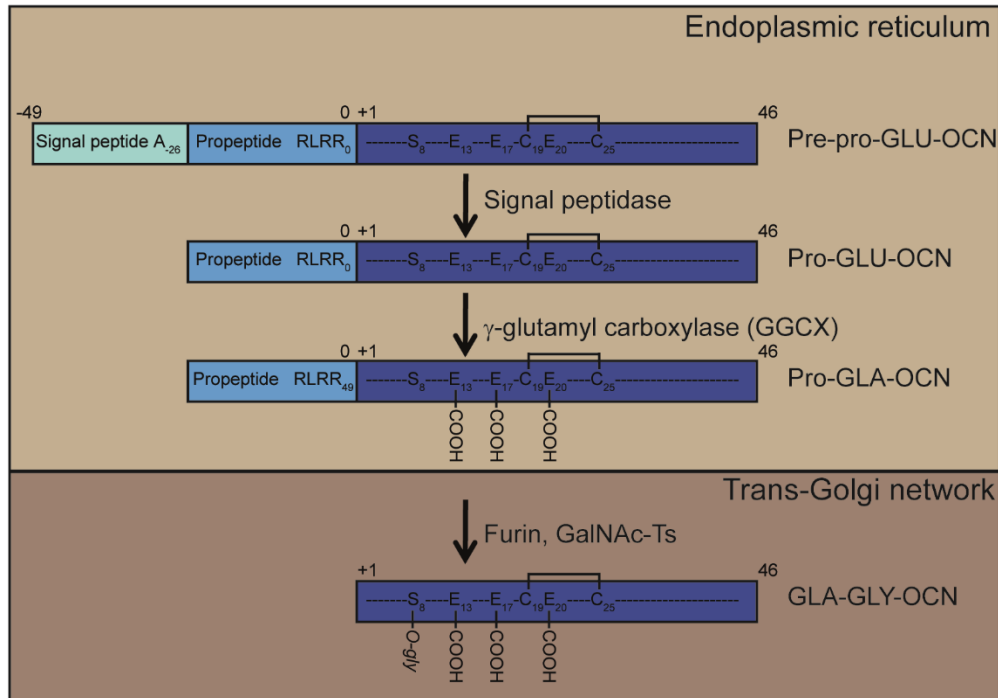


Figure 6-1. Mouse osteocalcin post-translational modifications

Amino acid residues: serine (S), glutamic acid (E), cysteine (C), arginine (R), leucine (L). Prep-pro-GLU-OCN, uncarboxylated osteocalcin precursor. Pro-GLU-OCN, uncarboxylated osteocalcin precursor after the removal of signal peptide. Pro-GLA-OCN, carboxylated osteocalcin precursor without the signal peptide. GLA-GLY-OCN, mature uncarboxylated *O*-glycosylated osteocalcin. COOH, carboxy group on glutamic acid residues (E). *O*-gly, *O*-glycosylation site.

6.1.1. Post-translational modifications in human osteocalcin

Mouse osteocalcin is subjected to three different PTMs: the gamma-carboxylation of its glutamic acid residues Glu13, Glu17 and Glu20 which inhibits its endocrine function, the proteolytic cleavage of its pro-peptide which is required for its maturation and activity, and the *O*-glycosylation of the serine residue 8 which increases its half-life in circulation. In human,

osteocalcin gamma-carboxylation occurs on the glutamic acid residues Glu17, Glu 21, and Glu24. Carboxylated osteocalcin positively correlates with insulin resistance in human [154]. In the present thesis we provide evidence supporting that osteocalcin proteolytic cleavage is conserved in human. Amino acid sequence alignment of the mouse and human osteocalcin showed that the furin cleavage site RLRR of the mouse protein corresponds to the RPRR in human osteocalcin. Using osteoblasts transfected with human osteocalcin as a model, we showed that treatment with PC inhibitor blocks human osteocalcin processing in these cells. On the other hand, we showed that *O*-glycosylation is limited to mouse osteocalcin, as human osteocalcin does not contain any serine or threonine residues. *O*-glycosylation in mouse osteocalcin occurs on the serine residue 8 within a suggested GalNAc-Ts recognition sequence SVPSPDP, where proline residue at position -1, +1 and +3 were shown to be essential for GalNAc-Ts activity [49]. This sequence is conserved in human while serine residue is substituted by a tyrosine in the human sequence PVPY12PDP. Moreover, we showed that a single amino acid mutation Y12S is sufficient to introduce *O*-glycosylation and increases human osteocalcin half-life ex vivo. Nevertheless, the substitution mutation Y12S was never described in human osteocalcin single-nucleotide polymorphism (SNP) database. Considering the importance of these modifications for human osteocalcin endocrine functions, in the next paragraph we will discuss their significance for future clinical studies.

6.1.2. Significance of human osteocalcin modifications in clinical studies

Most of the clinical studies addressing human osteocalcin function analysed the total serum levels of osteocalcin. These studies showed an association between osteocalcin forms and metabolic syndrome, exercise and muscle strength. For example, the decrease in uncarboxylated osteocalcin serum levels, the active form of osteocalcin, or the increase in carboxylated osteocalcin were positively associated with the risk of type 2 diabetes and insulin resistance [154, 225, 226, 307-309]. Total osteocalcin was negatively associated with diabetes risk and positively associated with reduction in HbA1c, fasting glucose and homeostatic model assessment of insulin resistance (HOMA-IR) [227, 228, 309]. Additional studies showed that uncarboxylated human osteocalcin is increased with exercise and is positively correlated with improved muscle strength

[229-231]. At the genotype-phenotype correlation, few genetic studies identified SNPs in osteocalcin and GPRC6A genes, these SNPs were associated with increased diabetes risk and infertility [188, 220-222] (introduced in the Chapter I).

In this thesis, we showed that osteocalcin pro-peptide cleavage by furin is conserved between mice and human. As this process is required for osteocalcin endocrine functions in mouse, we looked for SNPs in the osteocalcin cleavage site and in furin to better understand their impacts on osteocalcin biology in human. Revising the human osteocalcin SNPs database (NCBI), we found SNPs within the human pro-osteocalcin cleavage site R₄₈PRR₅₁, rs371474888, rs941161941, rs758769877, rs757750903, and rs1324662623, while these SNPs occur at low frequency and there is no literature about their clinical significance (Table 6.1).

Table 6-1. SNPs in human osteocalcin cleavage site (R₄₈PRR₅₁)

SNP	Mutation	Amino acid change	Frequency
rs371474888	Missense	Arg48Ser	0.00003 (GnomAD)
rs941161941	Missense	Pro49Ser	0.000032 (TOPMED)
rs758769877	Missense	Arg50Gly	0.000017 (ExAC)
rs757750903	Missense	Arg51Cys	0.000016 ((TOPMED)
rs1324662623	Missense	Arg51His	0.000008 (TOPMED)

In line with the metabolic defect observed in *Furin^{osb}*^{-/-} mice, some reports support a role of furin in energy metabolism. For example, genetic screening in Japanese individuals identified the rs17514846 SNP in *FURIN* to be associated with metabolic syndrome and a large scale genetic analysis identified *FURIN* gene to be associated with increased risk of coronary artery disease in human [310, 311]. However, it was also reported that increase in furin serum level is a predictive factor for developing type 2 diabetes [312]. One genetic study in a Chinese population with insulin resistance failed to show an association between common furin SNPs and insulin resistance [313]. However, none of these studies addressed osteocalcin serum levels or looked for pro-osteocalcin in circulation. Under physiological conditions, osteocalcin propeptide was not detected in vitro and in blood circulation of adults [314, 315], while in one paper they could detect osteocalcin

propeptide in children [315]. Only mature full-length or fragments of carboxylated and uncarboxylated osteocalcin are detected in human serum [316]. Fragments of mature osteocalcin were shown to be released during bone resorption and were also found excreted in urine [317, 318]. In abnormal conditions, such as patients with mutation in human pro-osteocalcin cleavage site or heterozygous mutation in the furin gene, it will be inappropriate to look only for circulating osteocalcin level, as the current available ELISA does not discriminate between mature and pro-osteocalcin [319]. Moreover, our data showed that uncarboxylated human osteocalcin ELISA recognizes equally the non-glycosylated human osteocalcin and the *O*-glycosylated forms. Considering the increased half-life of glycosylated human osteocalcin, which can also be detected by the available ELISA assays, high serum osteocalcin level may be also attributed to mutations in human osteocalcin that induce its *O*-glycosylation. By unraveling the human osteocalcin post-translational modifications, it will be more informative to combine genetic screening and osteocalcin measurements to address more precisely the contribution of osteocalcin in human biology.

6.2. FURIN IN OSTEOBLASTS REGULATES BONE ENDOCRINE FUNCTION INDEPENDENTLY OF OSTEOCALCIN.

The deletion of furin in osteoblasts in *Furin^{osb}/-* mice impaired osteocalcin processing. However, these mice recapitulated only some of the metabolic phenotypes observed in the osteocalcin loss-of-function mouse model [163, 302]. We could explain this phenotype by the caloric restriction due to the decrease in appetite in these mice (Figure 6-2), as caloric restriction was shown to improve glucose handling, energy metabolism and gluconeogenesis [320-322]. Consistent with the impact of caloric restriction on the gluconeogenesis and using the pyruvate tolerance test, we showed that *Furin^{osb}/-* mice have an increase in gluconeogenesis on normal chow diet and high fat high sucrose diet (Annex figure 8-1 A and B). In addition, we showed that pair feeding of control mice renders the metabolic phenotype of *Furin^{osb}/-* mice more apparent as it appears at a younger age, concomitant with insulin resistance and increase in fat accumulation [302]. Supporting our data, other studies showed that osteoblast ablation in mice resulted in an increased blood glucose, decreased glucose tolerance, reduced insulin secretion

and insulin sensitivity, increased energy expenditure, decreased gonadal fat and increased appetite. Osteocalcin injection in these mice corrected the defect in glucose handling and insulin secretion, but only partially rescued the insulin resistance phenotype. Moreover, osteocalcin injection failed to rescue the increase in energy expenditure, the decrease in gonadal fat and the increase in appetite observed in osteoblasts-deficient mice [130]. These results suggest that osteoblasts regulate energy metabolism and food intake independently of osteocalcin. An additional study by the same group showed that lipocalin-2 derived from bone regulates glucose and energy metabolism by suppressing appetite [132]. However, we showed in our study that lipocalin-2 serum level was not changed in *Furin^{osb}-/-* mice and that it is not processed by furin in vitro and in vivo. Together these data suggest that furin in osteoblasts regulates appetite independently of osteocalcin and lipocalin-2 [302]. Consistent with the presence of additional osteokines regulating energy metabolism (Figure 6-2), mechanical loading on osteocytes was shown to decrease fat mass by reducing food intake. This mechanism was shown to occur independently of the known bone derived hormone, osteocalcin, lipocalin-2, sclerostin and FGF23 [131]. Sclerostin is secreted by osteocytes and its inactivation in mice was shown to reduce fat mass, improve glucose tolerance and insulin sensitivity, and prevent insulin resistance following diet-induced obesity, however, no change in food intake was observed in these mice [323]. Sclerostin serum level was not measured in the *Furin^{osb}-/-* mice. Based on the furin substrate cleavage site, mouse sclerostin amino acid sequence possess at least two possible furin cleavage site “KTRTQR” and “RYTR” which are also conserved in human [13, 324, 325].

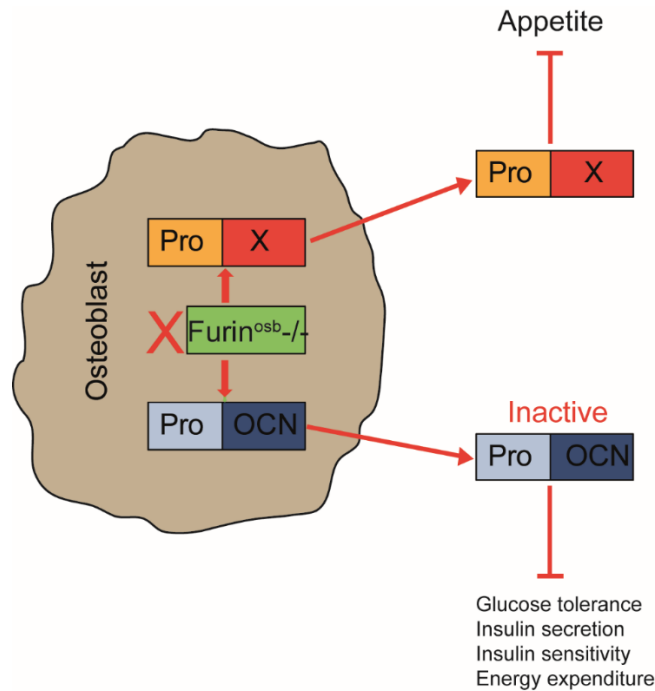


Figure 6-2. Furin in osteoblasts regulates whole body energy metabolism

Pro OCN is the osteocalcin precursor. Pro X is the precursor theoretical hormone (X).

The regulation of appetite by furin in osteoblasts could be also indirect through the effect of hormones derived from tissues other than bone, such as adipose tissue, stomach, intestine and bone marrow. For instance, leptin is an adipokine that inhibits food intake. In *Furin^{osb-/-}* mice, leptin serum level was not changed [302]. Studies also showed that ghrelin and glucagon-like-peptide 1 (GLP1) administration increases and decreases food intake respectively [326, 327]. An additional study showed that the deletion of brain-derived neurotrophic factor (BDNF) in bone marrow reduces glucose tolerance and increases food intake and insulin secretion [328]. Its administration in *db/db* mice improve energy expenditure, insulin content and lower blood glucose [329]. Interestingly, BDNF was shown to be expressed in osteoblasts and to be cleaved by furin in vitro [330, 331] and by PC7 in the hippocampus and amygdala in vivo [332]. However, the hypothesis that BDNF might be a possible target of furin in osteoblasts was never tested.

6.3. FURIN IN OSTEOBLASTS AND OSTEOCYTES PARTIALLY MEDIATES FGF23 ENDOPROTEOLYTIC CLEAVAGE.

Currently there is no direct evidence demonstrating the role of a specific PC in FGF23 cleavage in vivo. In vitro assays showed that furin and PC5 are involved in FGF23 processing [26, 277]. PC1 and PC2 were also found to cleave FGF23 in vitro. However, based on our data PC1 and PC2 are not expressed in osteoblasts (see Chapter V) [302]. To identify the PC(s) involved in FGF23 processing in vivo, we generated mice deficient in furin and/or PC5 in osteoblasts/osteocytes using human osteocalcin cre (*hOCN-Cre*) [206].

Our study showed that *Furin* inactivation in osteoblasts increased intact FGF23 by 25% but did not cause hypophosphatemia and osteomalacia. This phenotype is consistent with what was observed in the ADHR mouse model (R176Q-FGF23 knock-in). These mice did not develop hypophosphatemia and osteomalacia unless they were challenged on low iron diet [268]. Moreover, mice treated with the PC inhibitor, DecRVKR-CMK, showed a similar increase in intact FGF23 to what we observe in *Furin^{osb}-/-* mice [269]. ADHR patients have different age of onset and penetrance of the disease [333]. Iron deficiency, erythropoietin treatment and interleukin-1 beta were shown to stimulate the mRNA and protein levels of FGF23, which is still 100% processed in normal conditions. However, this increase significantly affects ADHR patients, as FGF23 is not properly processed, resulting in an increase in intact FGF23 [268, 269, 273, 333, 334]. Therefore, we decided to challenge the *Furin^{osb}-/-* mice with these conditions and investigate their impact on intact FGF23 cleavage and phosphate homeostasis. Iron deficiency induced FGF23 expression in control and *Furin^{osb}-/-* mice. However, only in control mice was total FGF23 (C-terminal FGF23) significantly increased. Interestingly, compared to normal diet, *Furin^{osb}-/-* mice on low iron diet showed a complete impairment of FGF23 processing, while they had an increase in serum phosphate level. Despite the increase in the expression of vitamin D activating enzyme *Cyp27b1* in *Furin^{osb}-/-* mice on normal chow diet, its expression level was decreased following iron deficiency (Annex figure 8-2 D). Moreover, *Furin^{osb}-/-* mice on iron deficient conditions had an increase in the expression of vitamin D inhibiting enzyme (*Cyp24a1*) and a decrease in the expression of sodium phosphate co-transporter (*Slc34a3*) compared to the mice on normal chow

diet (Annex figure 8-2 A and C). These results are consistent with the impaired FGF23 processing in *Furin^{osb}/-* mice on iron deficiency condition. However, since the increase in 1,25-hydroxyvitamin D and phosphate serum level was shown to increase intact FGF23, it could be possible that the complete impairment of FGF23 processing in *Furin^{osb}/-* mice is secondary and not completely due to the absence of furin. rhEPO or IL-1 β injections in control and *Furin^{osb}/-* mice significantly increased total FGF23 (C-terminal FGF23) while intact protein levels were not affected, suggesting that FGF23 processing is not completely impaired in *Furin^{osb}/-* mice. Next, we tested whether PC5 could be the FGF23 converting enzyme in normal conditions or in the absence of furin. PC5 inactivation in osteoblasts and osteocytes did not alter intact FGF23 levels and a slight increase in intact FGF23 was observed in furin/PC5 deficient mice. rhEPO injection induces total FGF23 (C-terminal FGF23) in mice deficient in both furin and PC5, while intact FGF23 is not induced to the same extent as total FGF23. This raise the question of whether C-terminal FGF23 has a longer half-life following rhEPO or IL-1 β injection. However, David *et al.* showed that C-terminal FGF23 has the same half-life when injected alone or in combination with IL-1 β [269]. In addition, another study showed that C-terminal and intact FGF23 has the same half-life in the serum of tumor induced osteomalacia patients [335]. The outcome of these experiments supports the conclusion that furin is partially responsible for FGF23 processing in vivo under physiological conditions, while its absence completely abrogates FGF23 processing under iron deficiency condition. This partial loss of FGF23 processing raises multiple questions. First, are there other sources of FGF23 that are induced when FGF23 processing is impaired in osteoblasts and osteocytes, masking the furin or PC5 deficient mouse phenotype? Second, how could we explain the 25% increase in intact FGF23 in *Furin^{osb}/-* mice? Finally, what is the identity of the PC involved in FGF23 processing?

6.3.1. Other possible sources of FGF23

Two important studies by Clinkenbeard *et al.* support that osteoblasts and osteocytes are the main source of circulating FGF23 [273, 336]. First, using mice harboring one inactivated allele of FGF23, they conditionally deleted the second allele using *Col2.3-Cre* or *Dmp1-cre* to allow the deletion of FGF23 in early osteoblasts and osteocytes. The outcome of this study showed that

osteoblasts and osteocytes contribute to 50-60% of circulating FGF23 under physiological conditions, which also reflects the deletion efficiency shown with these Cre. However, following high phosphate diet, the increase in intact FGF23 was reduced by 70%, which means that osteoblasts and osteocytes are responsible for the physiological response following high phosphate intake [336]. On the other hand, using *Col2.3-Cre* they deleted FGF23 in *Hyp* mice, a mouse model of X-linked hypophosphatemia. The deletion of FGF23 in osteoblasts and osteocytes of *Hyp* mice reduces the circulating level of intact FGF23 by almost 90%, emphasizing that these cells are the main source of FGF23 in the *Hyp* mouse model. This result is consistent with the specific expression of *Phex* gene in osteoblasts and osteocytes [336, 337]. In a second study published by the same group and using carboplatin to ablate hematopoietic cells, they showed that bone cells contribute approximately 40% of circulating FGF23 following rhEPO treatment [273]. Taking in consideration these published data, we would expect at least a 60% increase of circulating intact FGF23 in *Furin^{osb}/-* mice following rhEPO and IL-1 β injection, but this is not the case. Our data collected from the iron deficiency challenge, rhEPO and IL-1 β injection suggest bone marrow as a possible source of FGF23 in *Furin^{osb}/-* mice.

The data presented in this thesis showed that control and *Furin^{osb}/-* mice on iron deficient diet showed an increase in transferrin receptor (*Tfrc*) expression and a decrease in hepcidin gene (*Hamp*) expression in liver, reflecting iron deficiency in these tissues. However, these mice maintained normal serum iron levels (Annex figure 8-3A) and they initially had an increase in transferrin receptor (*Tfrc*) expression in long bone and kidney on normal diet. The *Tfrc* gene expression was not induced in the kidney of these mice following iron deficiency (Annex figure 8-3C), suggesting that these mice already developed a mechanism to resist for iron deficiency probably due to the reduction in iron uptake caused by the decrease in appetite in these mice. Consistent with the role of iron supplementation in curing ADHR complications in human patients [338, 339], this could explain why FGF23 production at the protein level was not increased in *Furin^{osb}/-* mice under iron deficient condition. Erythropoietin injection was shown to induce FGF23 at the mRNA and protein level. In *Furin^{osb}/-* mice erythropoietin (*Epo*) gene expression was not significantly affected (Annex figure 8-3D). These mice also had normal hematocrit and

properly respond to repetitive rhEPO injection by increasing their hematocrit compared to control littermates (Annex figure 8-4A). Single rhEPO injection increases *Fgf23* expression after 6 hours (Chapter V) while repetitive rhEPO injection does not change *Fgf23* expression and serum phosphate assessed after 24 hours of the last injection (Annex figure 8-4 B and C). Interestingly, despite the similar increase in *Fgf23* expression in the long bone of control and *Furin^{osb}-/-* mice on iron deficiency, only control mice had a significant increase in total FGF23 serum level (Chapter V), suggesting that there are other sources of FGF23 production. As rhEPO injection increases *Fgf23* expression in long bone and bone marrow, it would be possible that bone marrow is the main source of FGF23 following rhEPO or IL-1 β injection in *Furin^{osb}-/-* mice. To clearly address whether hematopoietic cells are a primary source of FGF23 in the absence of furin in osteoblasts and osteocytes, we are currently generating mice that are deficient in furin in osteoblasts and osteocytes and/or in hematopoietic cells by breeding *Furin^{osb}-/-* mice with *Furin^{flox/flox};Vav-Cre*. The *Vav-Cre* express the Cre recombinase under the control of the *Vav* promoter, allowing the deletion of furin in fetal and adult hematopoietic stem cells (HSC). FGF23 serum level will be compared between the different genotypes at steady state and following rhEPO injection.

6.3.2. Metabolic phenotype and the increase in FGF23 in *Furin^{osb}-/-* mice

Recent studies have been focussing on the relationship between diabetes and FGF23. Diabetes complications contribute to the development of cardiovascular disease, retinopathy, nephropathy, vision loss and Alzheimer's [340]. Consistent with the diabetic complications observed in human, wild type mice on high fat diet showed an increase in blood pressure, albuminuria, renal alteration and a decrease in food intake [341]. Additional studies in mice showed that HFD, which cause insulin resistance in mice, increases FGF23, and that insulin suppresses the increase in FGF23 in streptozotocin (STZ) treated mice, a model of type 1 diabetes [342, 343]. Moreover, human studies in patients with and without chronic kidney disease showed a positive association between FGF23 and insulin resistance, while maintaining normal phosphate level [344, 345], whereas in healthy subjects FGF23 negatively correlates with the serum insulin level [343, 346]. Furthermore, the injection of C-terminal FGF23 was shown to reduce diabetes

nephropathy complications in mice [347], and to rescue hypophosphatemia through the inhibition of FGFR1/ α -klotho signaling in rats [348].

In addition to the metabolic phenotype observed in furin deficient mice [302], these mice have a decrease in urinary phosphate on a normal phosphate diet, an increase in serum phosphate level on iron deficient diet (Chapter V and annex figure 8-3A) and maintain normal *Tfrc* expression in kidney following iron deficiency. The increase in FGF23 and hyperphosphatemia could reflect possibly defective kidney function which could be caused by the mild metabolic defects in these mice [288]. It also suggests the presence of a direct or indirect mechanism regulating phosphate reabsorption in the kidney independently of FGF23. However, further analysis of kidney function is required to confirm this observation.

6.3.3. The possible identity of the convertase(s) involved in FGF23 processing

Our data showed that furin is partially responsible for FGF23 inactivation *in vivo* and excludes PC5 from redundantly cleaving FGF23. This raises the question of whether additional PCs, beside furin, are implicated in this process. A mouse model of X-linked hypophosphatemia (i.e., *Hyp* mice), which has increased levels of intact FGF23, showed a decrease in PC2 and its chaperon protein 7B2 in bone [349]. The same study showed that treatment with Hexa-D-arginine (D6R), an extracellular PCs inhibitor which cannot cross the cell membrane, improves the bone phenotype of *Hyp* mice by normalizing the FGF23 expression and circulating level. This effect was explained by the increase in PC2, 7B2 and BMP1-mediated DMP1 cleavage following treatment with D6R [349]. Another study by the same group showed that PC5, furin and PC2 colocalize with FGF23 in the trans-Golgi network in an osteocyte cell line (IDG-SW3), while FGF23 is not localized in the acidic compartment required for proPC2 activation, supporting that furin and/or PC5 cleaves FGF23 in the differentiated SW3 cells [277]. Additional studies by Tagliabracci *et al.* showed that, when coexpressed with FGF23 in osteosarcoma model (U2OS), furin efficiently cleaves intact FGF23 compared to PC1 and PC2, whereas furin inactivation in these cells totally abolished FGF23 processing [26]. Our data and other reports showed that PC2 is not expressed in undifferentiated and differentiated osteoblasts, however, we could detect significant expression

of furin, PACE4 and PC7 [277, 302, 350]. As these PCs belong to the same subtilisin/kexin family and share similarities in their consensus cleavage site, it is possible that furin, PACE4 and PC7 redundantly mediate FGF23 processing in vivo. Mice deficient in PACE4 or PC7 are viable, and we are planning to assess FGF23 and phosphate serum levels in these mice at steady state and following rhEPO or IL-1 β injection.

6.4. FURIN BUT NOT PC5 REGULATES BONE MASS ACCRUAL

As discussed in the introduction, the inactivation of furin in mice is embryonically lethal at E10.5, while the inactivation of PC5 gene in mice leads among other phenotype to patterning and mineralization defects and mice died at E18.5 [36, 37]. The specific deletion of PC5 in osteoblast/osteocytes using *hOCN-cre* did not affect any of the tested bone parameters, suggesting that although PC5 may be required for skeleton patterning it is not essential for osteoblasts and osteocytes function (Annex figure 8-5). Supporting this hypothesis, the inactivation of PC5 in osterix positive osteoprogenitor in adults using *Osx-Cre* resulted in a decrease in bone mineral density (Annex figure 8-5). On the other hand, furin inactivation in osteoblasts and osteocytes using *hOCN-cre* resulted in poor cortical bone quality. Using micro-CT analysis, we showed that these mice had a 15% decrease in the cortical thickness at the femur midshaft and a significant increase in trabecular bone parameters (Annex figure 8-6A). These mice also had a decrease in femur and tibia length (Annex figure 8-6 B and C), a decrease in load force to fracture, stiffness and bone mineral density (Annex figure 8-6 A, C and D). Histological analysis on the vertebrae and long bone of *Furin^{osb}-/-* mice showed an increase in trabecular bone with no sign of defective mineralization (Annex figure 8-7 A-C). This bone phenotype observed in *Furin^{osb}-/-* mice suggests the presence of multiple factors that differentially regulate trabecular and cortical bone separately. This bone phenotype could be explained in part by impaired bone remodelling, a process that involves bone resorption by osteoclasts and bone formation by osteoblasts. Our data showed a decrease in mineralization capacity and alkaline phosphatase activity in bone marrow derived osteoblasts from *Furin^{osb}-/-* mice, which suggests a decrease in osteoblast progenitors or their differentiation capacity (Annex figure 8-8 A and B). Bone remodeling process is tightly regulated by paracrine factors secreted by osteoblasts and

osteocytes such as, OPG, RANKL, BMPs, Jagged/Notch, WNT, TGF- β , sclerostin and others. Many of these paracrine signals are potential furin substrates and regulate bone mass. *Notch1* and *Notch2* inactivation in osteocytes results in increased trabecular bone and decreased cortical thickness similar to what is observed in *Furin^{osb}-/-* mice [351]. Sclerostin, BMP2, BMP3, BMP4, BMP6 and Jagged1 inactivation in mice resulted in some of the bone defects observed in *Furin^{osb}-/-* mice [352-355]. Moreover, furin was shown to cleave proteins that affect directly or indirectly bone ECM components. For instance, in vitro based evidence showed that furin cleaves matrix extracellular phosphoglycoprotein precursor (MEPE), 7B2 which also controls dentin matrix protein (DMP1), bone morphogenic protein 1 (BMP1) and matrix metalloproteinase 2 (MMP2) which harbor protease activity required for bone ECM formation [349, 356-361]. These substrates can contribute to the mineralization defect observed in *Furin^{osb}-/-* mice.

In addition to the direct effect of furin inactivation in osteoblasts on bone mass accrual through the regulation of osteoblast paracrine and endocrine factors, the metabolic defects in these mice may also contribute to the observed bone phenotype. Insulin resistance is associated with increased bone mass, while caloric restriction is linked to decreased bone mass [362-364]. Devlin *et al.* showed a decrease in bone quality, reduced trabecular and cortical bone parameter, following 6 and 12 weeks of caloric restriction in mice [363]. Moreover, leptin suppresses food intake and bone formation, whereas the inactivation of leptin or leptin receptor increase bone formation [104, 105]. Even though leptin is not changed in *Furin^{osb}-/-* mice, these mice have reduced food intake which may contribute indirectly to the bone phenotype. The reduction in food intake not only reflects a reduction in caloric intake, but also a reduction in mineral uptake such as calcium and phosphate, which are the mineral components of bone.

6.5. IMPACT ON FUTURE THERAPEUTIC APPLICATIONS

In the present thesis, we showed that furin is a pleiotropic regulator of osteoblast and osteocyte function. It regulates glucose and energy metabolism by mediating pro-osteocalcin maturation and by regulating appetite independently of osteocalcin. Furin in osteoblasts and osteocytes also regulates bone mass accrual. Its inactivation in these cells increases trabecular

bone parameters and decrease cortical thickness, whereas the underlying mechanism possibly involve the uncoupling of bone remodeling. Moreover, these mice, on purified normal phosphate diet, showed a decrease in phosphate excretion and an increase in sodium phosphate cotransporters while FGF23 was slightly increased, suggesting that furin in osteoblasts and osteocytes may regulate phosphate metabolism independently of FGF23. This regulatory mechanism could be indirect or directly through the secretion of other phosphatonin(s) regulated by furin. The underlying mechanism by which furin in osteoblasts and osteocytes regulates bone mass accrual and phosphate excretion remains unclear, however, targeting furin in osteoblasts and osteocytes may have beneficial effects for patient with osteoporotic bone diseases, hypophosphatemia and hyperphosphatemia, such as X-linked hypophosphatemic rickets, human familiar tumoral calcinosis (HFTC) and osteogenesis imperfecta.

Osteogenesis imperfecta (OI) is a human disease characterized by increased bone fragility and concurrent fractures [365, 366]. The main causative disease factor is the poor quality and quantity of type 1 collagen mainly caused by dominant mutations in collagen type 1 alpha 1 (*Col1a1*) and collagen type 1 alpha 2 (*Col1a2*) coding gene which impairs collagen structure, post-translational modification, and folding. Additional mutations were also found in proteins that interact with type 1 collagen. OI patients are classified based on their clinical manifestation ranging from mild, moderate, progressive and severe deformities which are lethal [365, 366]. Different mouse models harboring mutations in collagen develop OI-like phenotype. These mice are characterized by bone fragility, decreased trabecular bone and cortical thickness, and increased bone resorption [367-370]. In addition to these bone defects, genetic OI mice have decreased in body weight and fat mass. This phenotype was attributed to the increase in bone resorption and the release in uncarboxylated osteocalcin [213]. Bisphosphonate is a widely used drug for the treatment of OI patients as it reduces bone resorption [365, 366]. Studies in mice showed that sclerostin antibody can ameliorate the bone phenotype in OI mice with mutations in the alpha-2 chain of type I procollagen coding gene, but not in OI mice model having mutation in the splice donor of collagen alpha1 type I [371, 372]. Considering the metabolic and bone phenotype observed following the inactivation of furin in osteoblasts and osteocytes, the

inhibition of furin in OI patients could be beneficial to correct the metabolic phenotype by inhibiting osteocalcin function and improving the bone phenotype by uncoupling bone remodelling.

Another important outcome of our study is the discovery of mouse osteocalcin *O*-glycosylation and its role in improving osteocalcin half-life in plasma. Uncarboxylated osteocalcin (ucOCN) produced in bacteria or purified from bovine bone was previously used in the metabolic study in vivo. In both sources, osteocalcin is not *O*-glycosylated, and was used at doses ranging from 0.3-30 ng/g of mouse body weight [167, 171]. These doses are relatively high, as they were delivered via daily IP injection or osmotic pump over at least a one-month period. Moreover, some other studies used higher dose (100-500 ng/g) to observe the effect of osteocalcin on muscle mass, exercise capacity and cognitive function [190, 197, 198]. By extrapolating the doses used to treat the mice to kilograms and considering the same osteocalcin pharmacokinetics between human and mice, we can predict a daily injected dose ranging from 150-250 µg to treat a human subject with a 50-80 kg of body weight. However, the use of *O*-glycosylated human osteocalcin could improve its half-life in plasma and provide a tool to reduce the dose, the frequency and to change the route of osteocalcin administration (oral, intravenous, subcutaneous) in future therapeutic applications.

6.6. FUTURE PERSPECTIVES

1. Elucidating the different osteocalcin modifications and their impact on osteocalcin biology provides knowledge for better diagnosis of osteocalcin-dependent diseases. Based on our findings, clinical studies aiming to address osteocalcin function in humans should not only be based on osteocalcin serum measurements but should also consider the genetic screening of osteocalcin and its regulators. Moreover, we found that mouse osteocalcin is subjected to *O*-glycosylation, a modification that is not conserved in human and increase osteocalcin half-life in vitro and in vivo. We also showed that human osteocalcin *O*-glycosylation increases its half-life in plasma. Mouse *O*-glycosylated osteocalcin represents 99% of total osteocalcin in the bone, suggesting that it is the active form of this hormone in vivo. However, this was not experimentally

validated. Therefore, future investigations should focus on investigating the therapeutic benefits of glycosylated mouse osteocalcin in mouse models and to test the half-life of glycosylated human osteocalcin in primate model, such as monkey. Furthermore, the identity of the peptidase involved in osteocalcin degradation remains unknown. Since osteocalcin *O*-glycosylation occurs within a proline rich sequence SVPSPDP. It is possible that osteocalcin is degraded by a member of the prolyl peptidase family and that *O*-glycosylation creates a steric hinderance to block or reduce this process. If we can prove this hypothesis using a prolyl peptidase inhibitor such as Talabostat, the production of osteocalcin harboring mutation in these proline residues (i.e., mutation to glycine, alanine, leucine) may increase its half-life in circulation.

2. Demonstrating that furin in osteoblasts and osteocytes is partially responsible for FGF23 processing opened the question of whether the bone marrow may compensate for the impaired FGF23 processing in osteoblast and osteocytes. To address this question, we are currently generating a mouse model that is deficient in furin simultaneously in hematopoietic cells, osteoblasts and osteocytes using *Vav*-Cre and *hOCN*-Cre. However, it is still possible that multiple PCs cleave FGF23 in vivo. PC7 and PACE4 belong to the same family as furin and PC5. It was never tested whether they cleave FGF23 in vitro or in vivo. Future investigations aim to assess FGF23 and phosphate serum level in PACE4 and PC7 deficient mice in steady state and following rhEPO or IL-1 β injection. Furthermore, using general PCs inhibitors, such as hexapeptide D-arginine (D6R) and decanoyl RVKR-chloromethyl ketone (RVKR-cmk) in *Furin^{osb}*^{-/-} mice, we can assess whether multiple PCs, beside furin, act together to cleave FGF23 in vivo.

3. Unraveling the novel osteokine secreted by furin deficient mice will help to identify the secreted factors involved in the regulation of appetite and phosphate excretion. Future investigation could aim to identify these osteokines using proteomics approaches. The “TAILS” or N-terminomic technique is a novel approach that will allow the detection of the protein’s N-terminus [373, 374]. This technique could be applied to the bone homogenate or osteoblasts derived from control and *Furin^{osb}*^{-/-} mice, allowing the comparison of the protein’s N-terminus between the two genotypes and uncovering novel furin substrates. To determine whether bone

remodelling is impaired in *Furin^{osb}-/-* mice, dynamic bone histology using calcein double labeling will allow the measurement of bone formation rate and mineral apposition rate. In addition, bone resorption and osteoclasts activity should be assessed. It will be also interesting to study fracture healing in these mice.

4. Investigating the possible therapeutic potential of furin inhibition for the treatment of osteogenesis imperfecta (OI), X-linked hypophosphatemic rickets (XLH) and human familial tumoral calcinosis (HFTC) is feasible. This question can be addressed by breeding mouse model of mild OI (Brtl mice), XLH mice model (*Hyp mice*) or HFTC mouse model (*Galnt3^{-/-}*) with *Furin^{osb}-/-* mice. Following which complete phenotype characterization will be performed and compared between the different genotypes

5. Induced pluripotent cells (iPSCs) can be used as a model to study PCs function in human. Understanding human disease through translational research in animal models impacted the standards of clinical diagnosis and treatment of many diseases, such as diabetes, obesity, osteoporosis and others. However, these advances created a gap in how to translate the knowledge gained from animal models to human applications. To fill these gaps and to reduce the cost of clinical trials, researchers and pharmaceutical companies tend to use patient derived induced pluripotent stem cells iPSCs as a powerful *in vitro* model of human disease. These cells are a great tool for precise diagnosis, drug screening and potential prediction of side effects of certain treatments. The proprotein convertases furin and PC5 have significant clinical importance, as the deletion of their coding genes in mice is embryonic lethal and only few studies addressed their roles in tissue specific knockout mouse models. Consistent with its importance in mouse development, in the present thesis we present data supporting the significant role of furin in osteoblasts and osteocytes. On the other hand, although PC5 deficient mice show a patterning defects, the deletion of PC5 in pre-osteoblasts, osteoblasts and osteocytes failed to recapitulate those defects observed in full body inactivation. This result suggests that the skeletal defect is happening earlier in development, a question that can be addressed in mouse by inactivating PC5 in the osteochondral progenitor using *Prrx1*-Cre. However, it will be interesting to address the

physiological and pathological functions of these two critical PCs using a human model. To realize this goal, CRISPR-Cas9 technology and advancements in iPSCs reprogramming provide a tool to generate iPSCs-deficient in these specific PCs. Afterwards, their ability to differentiate into different cell types, in 2D and 3D culture, can be compared to the parental cells. Moreover, gene regulation and the secretome of differentiated cells at specific stages can be assessed using genomic and proteomics approaches. Combining these approaches allows better understanding of the role of these two PCs in tissue development, the crosstalk between the cells at different stage of differentiation and the identification of new targets that are relevant to human disease.

7. REFERENCES

1. Manning, G., et al., *The protein kinase complement of the human genome*. Science, 2002. **298**(5600): p. 1912-34.
2. Shi, Y., *Serine/threonine phosphatases: mechanism through structure*. Cell, 2009. **139**(3): p. 468-84.
3. Alonso, A., et al., *Protein tyrosine phosphatases in the human genome*. Cell, 2004. **117**(6): p. 699-711.
4. Rawlings, N.D., A.J. Barrett, and R. Finn, *Twenty years of the MEROPS database of proteolytic enzymes, their substrates and inhibitors*. Nucleic Acids Res, 2016. **44**(D1): p. D343-50.
5. Klein, T., et al., *Proteolytic Cleavage-Mechanisms, Function, and "Omic" Approaches for a Near-Ubiquitous Posttranslational Modification*. Chem Rev, 2018. **118**(3): p. 1137-1168.
6. Levy, G.G., D.G. Motto, and D. Ginsburg, *ADAMTS13 turns 3*. Blood, 2005. **106**(1): p. 11-7.
7. Chang, C. and Z. Werb, *The many faces of metalloproteases: cell growth, invasion, angiogenesis and metastasis*. Trends Cell Biol, 2001. **11**(11): p. S37-43.
8. Nishimura, Y., T. Kawabata, and K. Kato, *Identification of latent procathepsins B and L in microsomal lumen: characterization of enzymatic activation and proteolytic processing in vitro*. Arch Biochem Biophys, 1988. **261**(1): p. 64-71.
9. van der Westhuyzen, D.R., W. Gevers, and G.A. Coetzee, *Cathepsin-D-dependent initiation of the hydrolysis by lysosomal enzymes of apoprotein B from low-density lipoproteins*. Eur J Biochem, 1980. **112**(1): p. 153-60.
10. Olsson, F., et al., *Characterization of intermediate steps in amyloid beta (Abeta) production under near-native conditions*. J Biol Chem, 2014. **289**(3): p. 1540-50.
11. McArthur, K. and B.T. Kile, *Apoptotic Caspases: Multiple or Mistaken Identities?* Trends Cell Biol, 2018. **28**(6): p. 475-493.
12. Seemuller, E., et al., *Proteasome from Thermoplasma acidophilum: a threonine protease*. Science, 1995. **268**(5210): p. 579-82.
13. Rawlings, N.D., et al., *MEROPS: the peptidase database*. Nucleic Acids Res, 2008. **36**(Database issue): p. D320-5.
14. Page, M.J. and E. Di Cera, *Serine peptidases: classification, structure and function*. Cell Mol Life Sci, 2008. **65**(7-8): p. 1220-36.
15. Krishnaswamy, S., K.C. Jones, and K.G. Mann, *Prothrombinase complex assembly. Kinetic mechanism of enzyme assembly on phospholipid vesicles*. J Biol Chem, 1988. **263**(8): p. 3823-34.
16. Greenberg, C.S., et al., *Cleavage of blood coagulation factor XIII and fibrinogen by thrombin during in vitro clotting*. J Clin Invest, 1985. **75**(5): p. 1463-70.
17. Fuller, R.S., A. Brake, and J. Thorner, *Yeast prohormone processing enzyme (KEX2 gene product) is a Ca²⁺-dependent serine protease*. Proc Natl Acad Sci U S A, 1989. **86**(5): p. 1434-8.
18. Fuller, R.S., R.E. Sterne, and J. Thorner, *Enzymes required for yeast prohormone processing*. Annu Rev Physiol, 1988. **50**: p. 345-62.
19. Seidah, N.G. and A. Prat, *The biology and therapeutic targeting of the proprotein convertases*. Nat Rev Drug Discov, 2012. **11**(5): p. 367-83.

20. Malide, D., et al., *Electron microscopic immunocytochemical evidence for the involvement of the convertases PC1 and PC2 in the processing of proinsulin in pancreatic beta-cells.* J Histochem Cytochem, 1995. **43**(1): p. 11-9.
21. Thomas, G., *Furin at the cutting edge: from protein traffic to embryogenesis and disease.* Nat Rev Mol Cell Biol, 2002. **3**(10): p. 753-66.
22. Nour, N., et al., *The cysteine-rich domain of the secreted proprotein convertases PC5A and PACE4 functions as a cell surface anchor and interacts with tissue inhibitors of metalloproteinases.* Mol Biol Cell, 2005. **16**(11): p. 5215-26.
23. Pullikotil, P., et al., *The proprotein convertase SKI-1/S1P: alternate translation and subcellular localization.* J Biol Chem, 2007. **282**(37): p. 27402-13.
24. Anderson, E.D., et al., *The ordered and compartment-specific autoproteolytic removal of the furin intramolecular chaperone is required for enzyme activation.* J Biol Chem, 2002. **277**(15): p. 12879-90.
25. Roebroek, A.J., et al., *Limited redundancy of the proprotein convertase furin in mouse liver.* J Biol Chem, 2004. **279**(51): p. 53442-50.
26. Tagliabracci, V.S., et al., *Dynamic regulation of FGF23 by Fam20C phosphorylation, GalNAc-T3 glycosylation, and furin proteolysis.* Proc Natl Acad Sci U S A, 2014. **111**(15): p. 5520-5.
27. Kim, W., et al., *Loss of endothelial furin leads to cardiac malformation and early postnatal death.* Mol Cell Biol, 2012. **32**(17): p. 3382-91.
28. Roebroek, A.J., et al., *Failure of ventral closure and axial rotation in embryos lacking the proprotein convertase Furin.* Development, 1998. **125**(24): p. 4863-76.
29. Constam, D.B. and E.J. Robertson, *Tissue-specific requirements for the proprotein convertase furin/SPC1 during embryonic turning and heart looping.* Development, 2000. **127**(2): p. 245-54.
30. Jiao, K., et al., *An essential role of Bmp4 in the atrioventricular septation of the mouse heart.* Genes Dev, 2003. **17**(19): p. 2362-7.
31. Pesu, M., et al., *T-cell-expressed proprotein convertase furin is essential for maintenance of peripheral immune tolerance.* Nature, 2008. **455**(7210): p. 246-50.
32. Vahatupa, M., et al., *T-cell-expressed proprotein convertase FURIN inhibits DMBA/TPA-induced skin cancer development.* Oncoimmunology, 2016. **5**(12): p. e1245266.
33. Essalmani, R., et al., *In vivo evidence that furin from hepatocytes inactivates PCSK9.* J Biol Chem, 2011. **286**(6): p. 4257-63.
34. Louagie, E., et al., *Role of furin in granular acidification in the endocrine pancreas: identification of the V-ATPase subunit Ac45 as a candidate substrate.* Proc Natl Acad Sci U S A, 2008. **105**(34): p. 12319-24.
35. Essalmani, R., et al., *Deletion of the gene encoding proprotein convertase 5/6 causes early embryonic lethality in the mouse.* Mol Cell Biol, 2006. **26**(1): p. 354-61.
36. Essalmani, R., et al., *In vivo functions of the proprotein convertase PC5/6 during mouse development: Gdf11 is a likely substrate.* Proc Natl Acad Sci U S A, 2008. **105**(15): p. 5750-5.
37. Szumska, D., et al., *VACTERL/caudal regression/Currarino syndrome-like malformations in mice with mutation in the proprotein convertase Pcsk5.* Genes Dev, 2008. **22**(11): p. 1465-77.

38. Szumska, D., et al., *Pcsk5 is required in the early cranio-cardiac mesoderm for heart development*. BMC Dev Biol, 2017. **17**(1): p. 6.
39. Sun, X., et al., *The proprotein convertase PC5/6 is protective against intestinal tumorigenesis: in vivo mouse model*. Mol Cancer, 2009. **8**: p. 73.
40. Nothaft, H. and C.M. Szymanski, *Protein glycosylation in bacteria: sweeter than ever*. Nat Rev Microbiol, 2010. **8**(11): p. 765-78.
41. Johansen, P.G., R.D. Marshall, and A. Neuberger, *Carbohydrates in protein. 3 The preparation and some of the properties of a glycopeptide from hen's-egg albumin*. Biochem J, 1961. **78**: p. 518-27.
42. Burda, P. and M. Aebi, *The dolichol pathway of N-linked glycosylation*. Biochim Biophys Acta, 1999. **1426**(2): p. 239-57.
43. Kelleher, D.J. and R. Gilmore, *An evolving view of the eukaryotic oligosaccharyltransferase*. Glycobiology, 2006. **16**(4): p. 47R-62R.
44. Herscovics, A., *Importance of glycosidases in mammalian glycoprotein biosynthesis*. Biochim Biophys Acta, 1999. **1473**(1): p. 96-107.
45. Helenius, A. and M. Aebi, *Roles of N-linked glycans in the endoplasmic reticulum*. Annu Rev Biochem, 2004. **73**: p. 1019-49.
46. Stanley, P., H. Schachter, and N. Taniguchi, *N-Glycans*, in *Essentials of Glycobiology*, nd, et al., Editors. 2009: Cold Spring Harbor (NY).
47. Narimatsu, Y., et al., *An Atlas of Human Glycosylation Pathways Enables Display of the Human Glycome by Gene Engineered Cells*. Mol Cell, 2019. **75**(2): p. 394-407 e5.
48. Bennett, E.P., et al., *Control of mucin-type O-glycosylation: a classification of the polypeptide GalNAc-transferase gene family*. Glycobiology, 2012. **22**(6): p. 736-56.
49. Gerken, T.A., et al., *Identification of common and unique peptide substrate preferences for the UDP-GalNAc:polypeptide alpha-N-acetylgalactosaminyltransferases T1 and T2 derived from oriented random peptide substrates*. J Biol Chem, 2006. **281**(43): p. 32403-16.
50. Perrine, C.L., et al., *Glycopeptide-preferring polypeptide GalNAc transferase 10 (ppGalNAc T10), involved in mucin-type O-glycosylation, has a unique GalNAc-O-Ser/Thr-binding site in its catalytic domain not found in ppGalNAc T1 or T2*. J Biol Chem, 2009. **284**(30): p. 20387-97.
51. Topaz, O., et al., *Mutations in GALNT3, encoding a protein involved in O-linked glycosylation, cause familial tumoral calcinosis*. Nat Genet, 2004. **36**(6): p. 579-81.
52. Harris, R.J. and M.W. Spellman, *O-linked fucose and other post-translational modifications unique to EGF modules*. Glycobiology, 1993. **3**(3): p. 219-24.
53. Endo, T., *Mammalian O-mannosyl glycans: Biochemistry and glycopathology*. Proc Jpn Acad Ser B Phys Biol Sci, 2019. **95**(1): p. 39-51.
54. Kjellen, L. and U. Lindahl, *Proteoglycans: structures and interactions*. Annu Rev Biochem, 1991. **60**: p. 443-75.
55. Spiro, R.G., *Characterization and quantitative determination of the hydroxylysine-linked carbohydrate units of several collagens*. J Biol Chem, 1969. **244**(4): p. 602-12.
56. Smythe, C. and P. Cohen, *The discovery of glycogenin and the priming mechanism for glycogen biogenesis*. Eur J Biochem, 1991. **200**(3): p. 625-31.

57. J. Gordon Betts, K.A.Y., James A. Wise, Eddie Johnson, Brandon Poe, Dean H. Kruse, Oksana Korol, Jody E. Johnson, Mark Womble, Peter DeSaix *Anatomy and Physiology* 2013, Houston, Texas OpenStax
58. Linsenmayer, T.F., et al., *Collagen types IX and X in the developing chick tibiotarsus: analyses of mRNAs and proteins*. *Development*, 1991. **111**(1): p. 191-6.
59. Hall, B.K. and T. Miyake, *All for one and one for all: condensations and the initiation of skeletal development*. *Bioessays*, 2000. **22**(2): p. 138-47.
60. Ducy, P., et al., *Osf2/Cbfa1: a transcriptional activator of osteoblast differentiation*. *Cell*, 1997. **89**(5): p. 747-54.
61. Karsenty, G. and E.F. Wagner, *Reaching a genetic and molecular understanding of skeletal development*. *Dev Cell*, 2002. **2**(4): p. 389-406.
62. Karsenty, G., H.M. Kronenberg, and C. Settembre, *Genetic control of bone formation*. *Annu Rev Cell Dev Biol*, 2009. **25**: p. 629-48.
63. Komori, T., et al., *Targeted disruption of Cbfa1 results in a complete lack of bone formation owing to maturational arrest of osteoblasts*. *Cell*, 1997. **89**(5): p. 755-64.
64. Howard, T.D., et al., *Mutations in TWIST, a basic helix-loop-helix transcription factor, in Saethre-Chotzen syndrome*. *Nat Genet*, 1997. **15**(1): p. 36-41.
65. el Ghouzzi, V., et al., *Mutations of the TWIST gene in the Saethre-Chotzen syndrome*. *Nat Genet*, 1997. **15**(1): p. 42-6.
66. Bialek, P., et al., *A twist code determines the onset of osteoblast differentiation*. *Dev Cell*, 2004. **6**(3): p. 423-35.
67. Jones, D.C., et al., *Regulation of adult bone mass by the zinc finger adapter protein Schnurri-3*. *Science*, 2006. **312**(5777): p. 1223-7.
68. Koga, T., et al., *NFAT and Osterix cooperatively regulate bone formation*. *Nat Med*, 2005. **11**(8): p. 880-5.
69. Nakashima, K., et al., *The novel zinc finger-containing transcription factor osterix is required for osteoblast differentiation and bone formation*. *Cell*, 2002. **108**(1): p. 17-29.
70. Lassot, I., et al., *ATF4 degradation relies on a phosphorylation-dependent interaction with the SCF(betaTrCP) ubiquitin ligase*. *Mol Cell Biol*, 2001. **21**(6): p. 2192-202.
71. Yang, X. and G. Karsenty, *ATF4, the osteoblast accumulation of which is determined post-translationally, can induce osteoblast-specific gene expression in non-osteoblastic cells*. *J Biol Chem*, 2004. **279**(45): p. 47109-14.
72. Yang, X., et al., *ATF4 is a substrate of RSK2 and an essential regulator of osteoblast biology; implication for Coffin-Lowry Syndrome*. *Cell*, 2004. **117**(3): p. 387-98.
73. Gully, J.C., et al., *Up-regulation of activating transcription factor 4 induces severe loss of dopamine nigral neurons in a rat model of Parkinson's disease*. *Neurosci Lett*, 2016. **627**: p. 36-41.
74. Sun, X., et al., *ATF4 protects against neuronal death in cellular Parkinson's disease models by maintaining levels of parkin*. *J Neurosci*, 2013. **33**(6): p. 2398-407.
75. Yang, J., et al., *DJ-1 modulates the unfolded protein response and cell death via upregulation of ATF4 following ER stress*. *Cell Death Dis*, 2019. **10**(2): p. 135.
76. Dobрева, G., et al., *SATB2 is a multifunctional determinant of craniofacial patterning and osteoblast differentiation*. *Cell*, 2006. **125**(5): p. 971-86.

77. Chandhoke, T.K., et al., *Osteopenia in transgenic mice with osteoblast-targeted expression of the inducible cAMP early repressor*. Bone, 2008. **43**(1): p. 101-109.
78. Yu, V.W., et al., *FIAT represses ATF4-mediated transcription to regulate bone mass in transgenic mice*. J Cell Biol, 2005. **169**(4): p. 591-601.
79. Yu, V.W., J. El-Hoss, and R. St-Arnaud, *FIAT inhibition increases osteoblast activity by modulating Atf4-dependent functions*. J Cell Biochem, 2009. **106**(1): p. 186-92.
80. Yu, V.W., C. Gauthier, and R. St-Arnaud, *FIAT represses bone matrix mineralization by interacting with ATF4 through its second leucine zipper*. J Cell Biochem, 2008. **105**(3): p. 859-65.
81. Hekmatnejad, B., et al., *SUMOylated alphaNAC potentiates transcriptional repression by FIAT*. J Cell Biochem, 2014. **115**(5): p. 866-73.
82. Baek, W.Y. and J.E. Kim, *Transcriptional regulation of bone formation*. Front Biosci (Schol Ed), 2011. **3**: p. 126-35.
83. St-Jacques, B., M. Hammerschmidt, and A.P. McMahon, *Indian hedgehog signaling regulates proliferation and differentiation of chondrocytes and is essential for bone formation*. Genes Dev, 1999. **13**(16): p. 2072-86.
84. Ohbayashi, N., et al., *FGF18 is required for normal cell proliferation and differentiation during osteogenesis and chondrogenesis*. Genes Dev, 2002. **16**(7): p. 870-9.
85. Wu, X., W. Shi, and X. Cao, *Multiplicity of BMP signaling in skeletal development*. Ann N Y Acad Sci, 2007. **1116**: p. 29-49.
86. Day, T.F., et al., *Wnt/beta-catenin signaling in mesenchymal progenitors controls osteoblast and chondrocyte differentiation during vertebrate skeletogenesis*. Dev Cell, 2005. **8**(5): p. 739-50.
87. Glass, D.A., 2nd, et al., *Canonical Wnt signaling in differentiated osteoblasts controls osteoclast differentiation*. Dev Cell, 2005. **8**(5): p. 751-64.
88. Hill, T.P., et al., *Canonical Wnt/beta-catenin signaling prevents osteoblasts from differentiating into chondrocytes*. Dev Cell, 2005. **8**(5): p. 727-38.
89. Cui, Y., et al., *Lrp5 functions in bone to regulate bone mass*. Nat Med, 2011. **17**(6): p. 684-91.
90. Yadav, V.K., et al., *Lrp5 controls bone formation by inhibiting serotonin synthesis in the duodenum*. Cell, 2008. **135**(5): p. 825-37.
91. Feng, X. and S.L. Teitelbaum, *Osteoclasts: New Insights*. Bone Res, 2013. **1**(1): p. 11-26.
92. Hohmann, E.L., et al., *Innervation of periosteum and bone by sympathetic vasoactive intestinal peptide-containing nerve fibers*. Science, 1986. **232**(4752): p. 868-71.
93. Bjurholm, A., *Neuroendocrine peptides in bone*. Int Orthop, 1991. **15**(4): p. 325-9.
94. Wang, L., et al., *Substance P stimulates bone marrow stromal cell osteogenic activity, osteoclast differentiation, and resorption activity in vitro*. Bone, 2009. **45**(2): p. 309-20.
95. Brakspear, K.S. and D.J. Mason, *Glutamate signaling in bone*. Front Endocrinol (Lausanne), 2012. **3**: p. 97.
96. Laketic-Ljubojevic, I., et al., *Functional characterization of N-methyl-D-aspartic acid-gated channels in bone cells*. Bone, 1999. **25**(6): p. 631-7.
97. Taylor, A.F., *Osteoblastic glutamate receptor function regulates bone formation and resorption*. J Musculoskelet Neuronal Interact, 2002. **2**(3): p. 285-90.

98. Genever, P.G. and T.M. Skerry, *Regulation of spontaneous glutamate release activity in osteoblastic cells and its role in differentiation and survival: evidence for intrinsic glutamatergic signaling in bone*. FASEB J, 2001. **15**(9): p. 1586-8.
99. Gray, C., et al., *Glutamate does not play a major role in controlling bone growth*. J Bone Miner Res, 2001. **16**(4): p. 742-9.
100. Kawase, T. and D.M. Burns, *Calcitonin gene-related peptide stimulates potassium efflux through adenosine triphosphate-sensitive potassium channels and produces membrane hyperpolarization in osteoblastic UMR106 cells*. Endocrinology, 1998. **139**(8): p. 3492-502.
101. Bjurholm, A., et al., *Neuroendocrine regulation of cyclic AMP formation in osteoblastic cell lines (UMR-106-01, ROS 17/2.8, MC3T3-E1, and Saos-2) and primary bone cells*. J Bone Miner Res, 1992. **7**(9): p. 1011-9.
102. Ballica, R., et al., *Targeted expression of calcitonin gene-related peptide to osteoblasts increases bone density in mice*. J Bone Miner Res, 1999. **14**(7): p. 1067-74.
103. Schinke, T., et al., *Decreased bone formation and osteopenia in mice lacking alpha-calcitonin gene-related peptide*. J Bone Miner Res, 2004. **19**(12): p. 2049-56.
104. Ducy, P., et al., *Leptin inhibits bone formation through a hypothalamic relay: a central control of bone mass*. Cell, 2000. **100**(2): p. 197-207.
105. Takeda, S., et al., *Leptin regulates bone formation via the sympathetic nervous system*. Cell, 2002. **111**(3): p. 305-17.
106. Turner, R.T., et al., *Peripheral leptin regulates bone formation*. J Bone Miner Res, 2013. **28**(1): p. 22-34.
107. Burguera, B., et al., *Leptin reduces ovariectomy-induced bone loss in rats*. Endocrinology, 2001. **142**(8): p. 3546-53.
108. Hamrick, M.W., *Leptin, bone mass, and the thrifty phenotype*. J Bone Miner Res, 2004. **19**(10): p. 1607-11.
109. Franz-Odenaal, T.A., B.K. Hall, and P.E. Witten, *Buried alive: how osteoblasts become osteocytes*. Dev Dyn, 2006. **235**(1): p. 176-90.
110. Candelieri, G.A., F. Liu, and J.E. Aubin, *Individual osteoblasts in the developing calvaria express different gene repertoires*. Bone, 2001. **28**(4): p. 351-61.
111. Paic, F., et al., *Identification of differentially expressed genes between osteoblasts and osteocytes*. Bone, 2009. **45**(4): p. 682-92.
112. Bonewald, L.F., *The amazing osteocyte*. J Bone Miner Res, 2011. **26**(2): p. 229-38.
113. Armstrong, V.J., et al., *Wnt/beta-catenin signaling is a component of osteoblastic bone cell early responses to load-bearing and requires estrogen receptor alpha*. J Biol Chem, 2007. **282**(28): p. 20715-27.
114. Bonewald, L.F. and M.L. Johnson, *Osteocytes, mechanosensing and Wnt signaling*. Bone, 2008. **42**(4): p. 606-15.
115. Kramer, I., et al., *Osteocyte Wnt/beta-catenin signaling is required for normal bone homeostasis*. Mol Cell Biol, 2010. **30**(12): p. 3071-85.
116. Aguirre, J.I., et al., *Osteocyte apoptosis is induced by weightlessness in mice and precedes osteoclast recruitment and bone loss*. J Bone Miner Res, 2006. **21**(4): p. 605-15.
117. Nakashima, T., et al., *Evidence for osteocyte regulation of bone homeostasis through RANKL expression*. Nat Med, 2011. **17**(10): p. 1231-4.

118. Xiong, J., et al., *Osteocyte-derived RANKL is a critical mediator of the increased bone resorption caused by dietary calcium deficiency*. Bone, 2014. **66**: p. 146-54.
119. Lacey, D.L., et al., *Osteoprotegerin ligand is a cytokine that regulates osteoclast differentiation and activation*. Cell, 1998. **93**(2): p. 165-76.
120. Wijenayaka, A.R., et al., *Sclerostin stimulates osteocyte support of osteoclast activity by a RANKL-dependent pathway*. PLoS One, 2011. **6**(10): p. e25900.
121. Yasuda, H., et al., *Osteoclast differentiation factor is a ligand for osteoprotegerin/osteoclastogenesis-inhibitory factor and is identical to TRANCE/RANKL*. Proc Natl Acad Sci U S A, 1998. **95**(7): p. 3597-602.
122. Ushach, I. and A. Zlotnik, *Biological role of granulocyte macrophage colony-stimulating factor (GM-CSF) and macrophage colony-stimulating factor (M-CSF) on cells of the myeloid lineage*. J Leukoc Biol, 2016. **100**(3): p. 481-9.
123. Felix, R., et al., *Synthesis of membrane- and matrix-bound colony-stimulating factor-1 by cultured osteoblasts*. J Cell Physiol, 1996. **166**(2): p. 311-22.
124. Li, X., et al., *Sclerostin binds to LRP5/6 and antagonizes canonical Wnt signaling*. J Biol Chem, 2005. **280**(20): p. 19883-7.
125. Maeda, K., et al., *Wnt5a-Ror2 signaling between osteoblast-lineage cells and osteoclast precursors enhances osteoclastogenesis*. Nat Med, 2012. **18**(3): p. 405-12.
126. Moverare-Skrtic, S., et al., *Osteoblast-derived WNT16 represses osteoclastogenesis and prevents cortical bone fragility fractures*. Nat Med, 2014. **20**(11): p. 1279-88.
127. Hu, K. and B.R. Olsen, *Osteoblast-derived VEGF regulates osteoblast differentiation and bone formation during bone repair*. J Clin Invest, 2016. **126**(2): p. 509-26.
128. Maes, C., et al., *Increased skeletal VEGF enhances beta-catenin activity and results in excessively ossified bones*. EMBO J, 2010. **29**(2): p. 424-41.
129. Wang, Y., et al., *The hypoxia-inducible factor alpha pathway couples angiogenesis to osteogenesis during skeletal development*. J Clin Invest, 2007. **117**(6): p. 1616-26.
130. Yoshikawa, Y., et al., *Genetic evidence points to an osteocalcin-independent influence of osteoblasts on energy metabolism*. J Bone Miner Res, 2011. **26**(9): p. 2012-25.
131. Jansson, J.O., et al., *Body weight homeostat that regulates fat mass independently of leptin in rats and mice*. Proc Natl Acad Sci U S A, 2018. **115**(2): p. 427-432.
132. Mosialou, I., et al., *MC4R-dependent suppression of appetite by bone-derived lipocalin 2*. Nature, 2017. **543**(7645): p. 385-390.
133. Stenflo, J., et al., *Vitamin K dependent modifications of glutamic acid residues in prothrombin*. Proc Natl Acad Sci U S A, 1974. **71**(7): p. 2730-3.
134. Price, P.A., et al., *Characterization of a gamma-carboxyglutamic acid-containing protein from bone*. Proc Natl Acad Sci U S A, 1976. **73**(5): p. 1447-51.
135. Hauschka, P.V., J.B. Lian, and P.M. Gallop, *Direct identification of the calcium-binding amino acid, gamma-carboxyglutamate, in mineralized tissue*. Proc Natl Acad Sci U S A, 1975. **72**(10): p. 3925-9.
136. Hauschka, P.V. and S.A. Carr, *Calcium-dependent alpha-helical structure in osteocalcin*. Biochemistry, 1982. **21**(10): p. 2538-47.
137. Desbois, C. and G. Karsenty, *Osteocalcin cluster: implications for functional studies*. J Cell Biochem, 1995. **57**(3): p. 379-83.

138. Ducy, P. and G. Karsenty, *Two distinct osteoblast-specific cis-acting elements control expression of a mouse osteocalcin gene*. Mol Cell Biol, 1995. **15**(4): p. 1858-69.
139. Schinke, T. and G. Karsenty, *Characterization of *Osf1*, an osteoblast-specific transcription factor binding to a critical cis-acting element in the mouse Osteocalcin promoters*. J Biol Chem, 1999. **274**(42): p. 30182-9.
140. Pan, L.C. and P.A. Price, *The propeptide of rat bone gamma-carboxyglutamic acid protein shares homology with other vitamin K-dependent protein precursors*. Proc Natl Acad Sci U S A, 1985. **82**(18): p. 6109-13.
141. Hauschka, P.V., et al., *Osteocalcin and matrix Gla protein: vitamin K-dependent proteins in bone*. Physiol Rev, 1989. **69**(3): p. 990-1047.
142. Hoang, Q.Q., et al., *Bone recognition mechanism of porcine osteocalcin from crystal structure*. Nature, 2003. **425**(6961): p. 977-80.
143. Dowd, T.L., et al., *The three-dimensional structure of bovine calcium ion-bound osteocalcin using 1H NMR spectroscopy*. Biochemistry, 2003. **42**(25): p. 7769-79.
144. Malashkevich, V.N., S.C. Almo, and T.L. Dowd, *X-ray crystal structure of bovine 3 Glu-osteocalcin*. Biochemistry, 2013. **52**(47): p. 8387-92.
145. Romberg, R.W., et al., *Inhibition of hydroxyapatite crystal growth by bone-specific and other calcium-binding proteins*. Biochemistry, 1986. **25**(5): p. 1176-80.
146. Lian, J.B., M. Tassinari, and J. Glowacki, *Resorption of implanted bone prepared from normal and warfarin-treated rats*. J Clin Invest, 1984. **73**(4): p. 1223-6.
147. Ducy, P., et al., *Increased bone formation in osteocalcin-deficient mice*. Nature, 1996. **382**(6590): p. 448-52.
148. Murshed, M., et al., *Extracellular matrix mineralization is regulated locally; different roles of two gla-containing proteins*. J Cell Biol, 2004. **165**(5): p. 625-30.
149. Furie, B. and B.C. Furie, *The molecular basis of blood coagulation*. Cell, 1988. **53**(4): p. 505-18.
150. Stenflo, J. and J.W. Suttie, *Vitamin K-dependent formation of gamma-carboxyglutamic acid*. Annu Rev Biochem, 1977. **46**: p. 157-72.
151. Berkner, K.L., et al., *Purification and identification of bovine liver gamma-carboxylase*. Proc Natl Acad Sci U S A, 1992. **89**(14): p. 6242-6.
152. Lacombe, J., et al., *VKOR paralog VKORC1L1 supports vitamin K-dependent protein carboxylation in vivo*. JCI Insight, 2018. **3**(1).
153. Lacombe, J. and M. Ferron, *VKORC1L1, An Enzyme Mediating the Effect of Vitamin K in Liver and Extrahepatic Tissues*. Nutrients, 2018. **10**(8).
154. Bonneau, J., et al., *Association between osteocalcin gamma-carboxylation and insulin resistance in overweight and obese postmenopausal women*. J Diabetes Complications, 2017. **31**(6): p. 1027-1034.
155. Ferron, M., et al., *GGCX and VKORC1 inhibit osteocalcin endocrine functions*. J Cell Biol, 2015. **208**(6): p. 761-76.
156. Engelke, J.A., et al., *Vitamin K-dependent carboxylase: utilization of decarboxylated bone Gla protein and matrix Gla protein as substrates*. Biochim Biophys Acta, 1991. **1078**(1): p. 31-4.

157. Lacombe, J., G. Karsenty, and M. Ferron, *In vivo analysis of the contribution of bone resorption to the control of glucose metabolism in mice*. Mol Metab, 2013. **2**(4): p. 498-504.
158. Ferron, M., et al., *Insulin signaling in osteoblasts integrates bone remodeling and energy metabolism*. Cell, 2010. **142**(2): p. 296-308.
159. Legroux-Gerot, I., et al., *Bone loss associated with anorexia nervosa*. Joint Bone Spine, 2005. **72**(6): p. 489-95.
160. Misra, M. and A. Klibanski, *The neuroendocrine basis of anorexia nervosa and its impact on bone metabolism*. Neuroendocrinology, 2011. **93**(2): p. 65-73.
161. Riggs, B.L., S. Khosla, and L.J. Melton, 3rd, *A unitary model for involutional osteoporosis: estrogen deficiency causes both type I and type II osteoporosis in postmenopausal women and contributes to bone loss in aging men*. J Bone Miner Res, 1998. **13**(5): p. 763-73.
162. Riggs, B.L. and L.J. Melton, 3rd, *Involutional osteoporosis*. N Engl J Med, 1986. **314**(26): p. 1676-86.
163. Lee, N.K., et al., *Endocrine regulation of energy metabolism by the skeleton*. Cell, 2007. **130**(3): p. 456-69.
164. Mauro, L.J., et al., *Identification of a hormonally regulated protein tyrosine phosphatase associated with bone and testicular differentiation*. J Biol Chem, 1994. **269**(48): p. 30659-67.
165. Yunker, L.A., et al., *The tyrosine phosphatase, OST-PTP, is expressed in mesenchymal progenitor cells early during skeletogenesis in the mouse*. J Cell Biochem, 2004. **93**(4): p. 761-73.
166. Ferron, M., et al., *Osteocalcin differentially regulates beta cell and adipocyte gene expression and affects the development of metabolic diseases in wild-type mice*. Proc Natl Acad Sci U S A, 2008. **105**(13): p. 5266-70.
167. Ferron, M., et al., *Intermittent injections of osteocalcin improve glucose metabolism and prevent type 2 diabetes in mice*. Bone, 2012. **50**(2): p. 568-75.
168. Zhang, X.L., et al., *Uncarboxylated osteocalcin ameliorates hepatic glucose and lipid metabolism in KKAy mice via activating insulin signaling pathway*. Acta Pharmacol Sin, 2019.
169. Otani, T., et al., *Signaling pathway for adiponectin expression in adipocytes by osteocalcin*. Cell Signal, 2015. **27**(3): p. 532-44.
170. Zhou, B., et al., *Osteocalcin reverses endoplasmic reticulum stress and improves impaired insulin sensitivity secondary to diet-induced obesity through nuclear factor-kappaB signaling pathway*. Endocrinology, 2013. **154**(3): p. 1055-68.
171. Sabek, O.M., et al., *Osteocalcin Effect on Human beta-Cells Mass and Function*. Endocrinology, 2015. **156**(9): p. 3137-46.
172. Mizokami, A., et al., *Osteocalcin induces release of glucagon-like peptide-1 and thereby stimulates insulin secretion in mice*. PLoS One, 2013. **8**(2): p. e57375.
173. Mizokami, A., et al., *Oral administration of osteocalcin improves glucose utilization by stimulating glucagon-like peptide-1 secretion*. Bone, 2014. **69**: p. 68-79.
174. Mizokami, A., et al., *GLP-1 signaling is required for improvement of glucose tolerance by osteocalcin*. J Endocrinol, 2019.

175. Lambert, L.J., et al., *Increased trabecular bone and improved biomechanics in an osteocalcin-null rat model created by CRISPR/Cas9 technology*. *Dis Model Mech*, 2016. **9**(10): p. 1169-1179.
176. Gao, J., et al., *The PLC/PKC/Ras/MEK/Kv channel pathway is involved in uncarboxylated osteocalcin-regulated insulin secretion in rats*. *Peptides*, 2016. **86**: p. 72-79.
177. Gao, J., et al., *Inhibition of voltage-gated potassium channels mediates uncarboxylated osteocalcin-regulated insulin secretion in rat pancreatic beta cells*. *Eur J Pharmacol*, 2016. **777**: p. 41-8.
178. Kover, K., et al., *Osteocalcin protects pancreatic beta cell function and survival under high glucose conditions*. *Biochem Biophys Res Commun*, 2015. **462**(1): p. 21-6.
179. Huang, L., et al., *Osteocalcin Improves Metabolic Profiles, Body Composition and Arterial Stiffening in an Induced Diabetic Rat Model*. *Exp Clin Endocrinol Diabetes*, 2017. **125**(4): p. 234-240.
180. Pi, M., Y. Wu, and L.D. Quarles, *GPRC6A mediates responses to osteocalcin in beta-cells in vitro and pancreas in vivo*. *J Bone Miner Res*, 2011. **26**(7): p. 1680-3.
181. Wei, J., et al., *Osteocalcin promotes beta-cell proliferation during development and adulthood through Gprc6a*. *Diabetes*, 2014. **63**(3): p. 1021-31.
182. Oury, F., et al., *Endocrine regulation of male fertility by the skeleton*. *Cell*, 2011. **144**(5): p. 796-809.
183. Clemmensen, C., et al., *The GPCR, class C, group 6, subtype A (GPRC6A) receptor: from cloning to physiological function*. *Br J Pharmacol*, 2014. **171**(5): p. 1129-41.
184. Faure, H., et al., *Molecular determinants of non-competitive antagonist binding to the mouse GPRC6A receptor*. *Cell Calcium*, 2009. **46**(5-6): p. 323-32.
185. Pi, M., et al., *Identification of a novel extracellular cation-sensing G-protein-coupled receptor*. *J Biol Chem*, 2005. **280**(48): p. 40201-9.
186. Pi, M., et al., *Evidence for Osteocalcin Binding and Activation of GPRC6A in beta-Cells*. *Endocrinology*, 2016. **157**(5): p. 1866-80.
187. Pi, M., et al., *GPRC6A null mice exhibit osteopenia, feminization and metabolic syndrome*. *PLoS One*, 2008. **3**(12): p. e3858.
188. Oury, F., et al., *Osteocalcin regulates murine and human fertility through a pancreas-bone-testis axis*. *J Clin Invest*, 2013. **123**(6): p. 2421-33.
189. Oury, F., et al., *Maternal and offspring pools of osteocalcin influence brain development and functions*. *Cell*, 2013. **155**(1): p. 228-41.
190. Khrimian, L., et al., *Gpr158 mediates osteocalcin's regulation of cognition*. *J Exp Med*, 2017. **214**(10): p. 2859-2873.
191. Ott, V., et al., *Intranasal administration of insulin to the brain impacts cognitive function and peripheral metabolism*. *Diabetes Obes Metab*, 2012. **14**(3): p. 214-21.
192. Novak, V., et al., *Enhancement of vasoreactivity and cognition by intranasal insulin in type 2 diabetes*. *Diabetes Care*, 2014. **37**(3): p. 751-9.
193. Villeda, S.A., et al., *Young blood reverses age-related impairments in cognitive function and synaptic plasticity in mice*. *Nat Med*, 2014. **20**(6): p. 659-63.
194. Guo, X.Z., et al., *Osteocalcin Ameliorates Motor Dysfunction in a 6-Hydroxydopamine-Induced Parkinson's Disease Rat Model Through AKT/GSK3beta Signaling*. *Front Mol Neurosci*, 2018. **11**: p. 343.

195. Chamouni, A., C. Schreiweis, and F. Oury, *Bone, brain & beyond*. Rev Endocr Metab Disord, 2015. **16**(2): p. 99-113.
196. Kosmidis, S., et al., *RbAp48 Protein Is a Critical Component of GPR158/OCN Signaling and Ameliorates Age-Related Memory Loss*. Cell Rep, 2018. **25**(4): p. 959-973 e6.
197. Mera, P., et al., *Osteocalcin Signaling in Myofibers Is Necessary and Sufficient for Optimum Adaptation to Exercise*. Cell Metab, 2016. **23**(6): p. 1078-1092.
198. Mera, P., et al., *Osteocalcin is necessary and sufficient to maintain muscle mass in older mice*. Mol Metab, 2016. **5**(10): p. 1042-1047.
199. Chowdhury, S., et al., *Muscle derived interleukin-6 increases exercise capacity by signaling in osteoblasts*. J Clin Invest, 2020.
200. Berger, J.M., et al., *Mediation of the Acute Stress Response by the Skeleton*. Cell Metab, 2019.
201. Covey, S.D., et al., *The pancreatic beta cell is a key site for mediating the effects of leptin on glucose homeostasis*. Cell Metab, 2006. **4**(4): p. 291-302.
202. Morioka, T., et al., *Disruption of leptin receptor expression in the pancreas directly affects beta cell growth and function in mice*. J Clin Invest, 2007. **117**(10): p. 2860-8.
203. Hinoi, E., et al., *An Osteoblast-dependent mechanism contributes to the leptin regulation of insulin secretion*. Ann N Y Acad Sci, 2009. **1173 Suppl 1**: p. E20-30.
204. Hinoi, E., et al., *The sympathetic tone mediates leptin's inhibition of insulin secretion by modulating osteocalcin bioactivity*. J Cell Biol, 2008. **183**(7): p. 1235-42.
205. Kalra, S.P., M.G. Dube, and U.T. Iwaniec, *Leptin increases osteoblast-specific osteocalcin release through a hypothalamic relay*. Peptides, 2009. **30**(5): p. 967-73.
206. Zhang, M., et al., *Osteoblast-specific knockout of the insulin-like growth factor (IGF) receptor gene reveals an essential role of IGF signaling in bone matrix mineralization*. J Biol Chem, 2002. **277**(46): p. 44005-12.
207. Rached, M.T., et al., *FoxO1 expression in osteoblasts regulates glucose homeostasis through regulation of osteocalcin in mice*. J Clin Invest, 2010. **120**(1): p. 357-68.
208. Febbraio, M.A. and B.K. Pedersen, *Contraction-induced myokine production and release: is skeletal muscle an endocrine organ?* Exerc Sport Sci Rev, 2005. **33**(3): p. 114-9.
209. Keller, C., et al., *Transcriptional activation of the IL-6 gene in human contracting skeletal muscle: influence of muscle glycogen content*. FASEB J, 2001. **15**(14): p. 2748-50.
210. Pedersen, B.K. and M.A. Febbraio, *Muscle as an endocrine organ: focus on muscle-derived interleukin-6*. Physiol Rev, 2008. **88**(4): p. 1379-406.
211. Steensberg, A., et al., *Production of interleukin-6 in contracting human skeletal muscles can account for the exercise-induced increase in plasma interleukin-6*. J Physiol, 2000. **529 Pt 1**: p. 237-42.
212. Harslof, T., et al., *The Effect of Treatment With PTH on Undercarboxylated Osteocalcin and Energy Metabolism in Hypoparathyroidism*. J Clin Endocrinol Metab, 2015. **100**(7): p. 2758-62.
213. Boraschi-Diaz, I., et al., *Metabolic phenotype in the mouse model of osteogenesis imperfecta*. J Endocrinol, 2017. **234**(3): p. 279-289.
214. Papapoulos, S.E., et al., *Serum osteocalcin in Paget's disease of bone: basal concentrations and response to bisphosphonate treatment*. J Clin Endocrinol Metab, 1987. **65**(1): p. 89-94.

215. Brennan-Speranza, T.C., et al., *Osteoblasts mediate the adverse effects of glucocorticoids on fuel metabolism*. J Clin Invest, 2012. **122**(11): p. 4172-89.
216. Morrison, N.A., et al., *1,25-dihydroxyvitamin D-responsive element and glucocorticoid repression in the osteocalcin gene*. Science, 1989. **246**(4934): p. 1158-61.
217. Oury, F., *A crosstalk between bone and gonads*. Ann N Y Acad Sci, 2012. **1260**: p. 1-7.
218. Parker, L., et al., *Glucocorticoid-Induced Insulin Resistance in Men Is Associated With Suppressed Undercarboxylated Osteocalcin*. J Bone Miner Res, 2019. **34**(1): p. 49-58.
219. Prummel, M.F., et al., *The course of biochemical parameters of bone turnover during treatment with corticosteroids*. J Clin Endocrinol Metab, 1991. **72**(2): p. 382-6.
220. Das, S.K., N.K. Sharma, and S.C. Elbein, *Analysis of osteocalcin as a candidate gene for type 2 diabetes (T2D) and intermediate traits in Caucasians and African Americans*. Dis Markers, 2010. **28**(5): p. 281-6.
221. Xu, H., et al., *Association analysis of genetic polymorphisms and potential interaction of the osteocalcin (BGP) and ER-alpha genes with body mass index (BMI) in premenopausal Chinese women*. Acta Pharmacol Sin, 2010. **31**(4): p. 455-60.
222. Di Nisio, A., et al., *The rs2274911 polymorphism in GPRC6A gene is associated with insulin resistance in normal weight and obese subjects*. Clin Endocrinol (Oxf), 2017. **86**(2): p. 185-191.
223. Takenouchi, T., et al., *Progressive cognitive decline in an adult patient with cleidocranial dysplasia*. Eur J Med Genet, 2014. **57**(7): p. 319-21.
224. Khrimian, L., A. Obri, and G. Karsenty, *Modulation of cognition and anxiety-like behavior by bone remodeling*. Mol Metab, 2017. **6**(12): p. 1610-1615.
225. Razny, U., et al., *Carboxylated and undercarboxylated osteocalcin in metabolic complications of human obesity and prediabetes*. Diabetes Metab Res Rev, 2017. **33**(3).
226. Diaz-Lopez, A., et al., *Reduced serum concentrations of carboxylated and undercarboxylated osteocalcin are associated with risk of developing type 2 diabetes mellitus in a high cardiovascular risk population: a nested case-control study*. J Clin Endocrinol Metab, 2013. **98**(11): p. 4524-31.
227. Liu, C., et al., *Association between Serum Total Osteocalcin Level and Type 2 Diabetes Mellitus: A Systematic Review and Meta-Analysis*. Horm Metab Res, 2015. **47**(11): p. 813-9.
228. Kunutsor, S.K., T.A. Apekey, and J.A. Laukkanen, *Association of serum total osteocalcin with type 2 diabetes and intermediate metabolic phenotypes: systematic review and meta-analysis of observational evidence*. Eur J Epidemiol, 2015. **30**(8): p. 599-614.
229. Kim, Y.S., et al., *The effects of aerobic exercise training on serum osteocalcin, adipocytokines and insulin resistance on obese young males*. Clin Endocrinol (Oxf), 2015. **82**(5): p. 686-94.
230. Lin, C.F., et al., *Acute effects of plyometric jumping and intermittent running on serum bone markers in young males*. Eur J Appl Physiol, 2012. **112**(4): p. 1475-84.
231. Levinger, I., et al., *Undercarboxylated osteocalcin, muscle strength and indices of bone health in older women*. Bone, 2014. **64**: p. 8-12.
232. Itoh, N. and D.M. Ornitz, *Evolution of the Fgf and Fgfr gene families*. Trends Genet, 2004. **20**(11): p. 563-9.

233. Itoh, N. and D.M. Ornitz, *Functional evolutionary history of the mouse Fgf gene family*. Dev Dyn, 2008. **237**(1): p. 18-27.
234. Econs, M.J. and M.K. Drezner, *Tumor-induced osteomalacia--unveiling a new hormone*. N Engl J Med, 1994. **330**(23): p. 1679-81.
235. Prader, A., et al., *[Rickets following bone tumor]*. Helv Paediatr Acta, 1959. **14**: p. 554-65.
236. Meyer, R.A., Jr., M.H. Meyer, and R.W. Gray, *Parabiosis suggests a humoral factor is involved in X-linked hypophosphatemia in mice*. J Bone Miner Res, 1989. **4**(4): p. 493-500.
237. Nesbitt, T., et al., *Crosstransplantation of kidneys in normal and Hyp mice. Evidence that the Hyp mouse phenotype is unrelated to an intrinsic renal defect*. J Clin Invest, 1992. **89**(5): p. 1453-9.
238. Miyauchi, A., et al., *Hemangiopericytoma-induced osteomalacia: tumor transplantation in nude mice causes hypophosphatemia and tumor extracts inhibit renal 25-hydroxyvitamin D 1-hydroxylase activity*. J Clin Endocrinol Metab, 1988. **67**(1): p. 46-53.
239. Consortium, A., *Autosomal dominant hypophosphataemic rickets is associated with mutations in FGF23*. Nat Genet, 2000. **26**(3): p. 345-8.
240. Shimada, T., et al., *Cloning and characterization of FGF23 as a causative factor of tumor-induced osteomalacia*. Proc Natl Acad Sci U S A, 2001. **98**(11): p. 6500-5.
241. Farrow, E.G. and K.E. White, *Recent advances in renal phosphate handling*. Nat Rev Nephrol, 2010. **6**(4): p. 207-17.
242. Moe, S.M., *Disorders involving calcium, phosphorus, and magnesium*. Prim Care, 2008. **35**(2): p. 215-37, v-vi.
243. Quarles, L.D., *Endocrine functions of bone in mineral metabolism regulation*. J Clin Invest, 2008. **118**(12): p. 3820-8.
244. Parfitt, A.M., *The actions of parathyroid hormone on bone: relation to bone remodeling and turnover, calcium homeostasis, and metabolic bone disease. Part IV of IV parts: The state of the bones in uremic hyperparathyroidism--the mechanisms of skeletal resistance to PTH in renal failure and pseudohypoparathyroidism and the role of PTH in osteoporosis, osteopetrosis, and osteofluorosis*. Metabolism, 1976. **25**(10): p. 1157-88.
245. Yoshiko, Y., et al., *Mineralized tissue cells are a principal source of FGF23*. Bone, 2007. **40**(6): p. 1565-73.
246. Shimada, T., et al., *FGF-23 is a potent regulator of vitamin D metabolism and phosphate homeostasis*. J Bone Miner Res, 2004. **19**(3): p. 429-35.
247. Larsson, T., et al., *Transgenic mice expressing fibroblast growth factor 23 under the control of the alpha1(I) collagen promoter exhibit growth retardation, osteomalacia, and disturbed phosphate homeostasis*. Endocrinology, 2004. **145**(7): p. 3087-94.
248. Shimada, T., et al., *Targeted ablation of Fgf23 demonstrates an essential physiological role of FGF23 in phosphate and vitamin D metabolism*. J Clin Invest, 2004. **113**(4): p. 561-8.
249. Sitara, D., et al., *Homozygous ablation of fibroblast growth factor-23 results in hyperphosphatemia and impaired skeletogenesis, and reverses hypophosphatemia in PheX-deficient mice*. Matrix Biol, 2004. **23**(7): p. 421-32.
250. Shimada, T., et al., *FGF-23 transgenic mice demonstrate hypophosphatemic rickets with reduced expression of sodium phosphate cotransporter type IIa*. Biochem Biophys Res Commun, 2004. **314**(2): p. 409-14.

251. Benet-Pages, A., et al., *An FGF23 missense mutation causes familial tumoral calcinosis with hyperphosphatemia*. Hum Mol Genet, 2005. **14**(3): p. 385-90.
252. Kuro-o, M., et al., *Mutation of the mouse klotho gene leads to a syndrome resembling ageing*. Nature, 1997. **390**(6655): p. 45-51.
253. van Loon, E.P., et al., *Shedding of klotho by ADAMs in the kidney*. Am J Physiol Renal Physiol, 2015. **309**(4): p. F359-68.
254. Urakawa, I., et al., *Klotho converts canonical FGF receptor into a specific receptor for FGF23*. Nature, 2006. **444**(7120): p. 770-4.
255. Chen, G., et al., *alpha-Klotho is a non-enzymatic molecular scaffold for FGF23 hormone signalling*. Nature, 2018. **553**(7689): p. 461-466.
256. Tsujikawa, H., et al., *Klotho, a gene related to a syndrome resembling human premature aging, functions in a negative regulatory circuit of vitamin D endocrine system*. Mol Endocrinol, 2003. **17**(12): p. 2393-403.
257. Yoshida, T., T. Fujimori, and Y. Nabeshima, *Mediation of unusually high concentrations of 1,25-dihydroxyvitamin D in homozygous klotho mutant mice by increased expression of renal 1alpha-hydroxylase gene*. Endocrinology, 2002. **143**(2): p. 683-9.
258. Gattineni, J., et al., *FGF23 decreases renal NaPi-2a and NaPi-2c expression and induces hypophosphatemia in vivo predominantly via FGF receptor 1*. Am J Physiol Renal Physiol, 2009. **297**(2): p. F282-91.
259. Liu, S., et al., *Fibroblast growth factor 23 is a counter-regulatory phosphaturic hormone for vitamin D*. J Am Soc Nephrol, 2006. **17**(5): p. 1305-15.
260. Perwad, F., et al., *Dietary and serum phosphorus regulate fibroblast growth factor 23 expression and 1,25-dihydroxyvitamin D metabolism in mice*. Endocrinology, 2005. **146**(12): p. 5358-64.
261. David, V., et al., *Calcium regulates FGF-23 expression in bone*. Endocrinology, 2013. **154**(12): p. 4469-82.
262. Liu, S., et al., *Phosphorylated acidic serine-aspartate-rich MEPE-associated motif peptide from matrix extracellular phosphoglycoprotein inhibits phosphate regulating gene with homologies to endopeptidases on the X-chromosome enzyme activity*. J Endocrinol, 2007. **192**(1): p. 261-7.
263. Martin, A., et al., *Degradation of MEPE, DMP1, and release of SIBLING ASARM-peptides (minhibins): ASARM-peptide(s) are directly responsible for defective mineralization in HYP*. Endocrinology, 2008. **149**(4): p. 1757-72.
264. David, V., et al., *ASARM peptides: PHEX-dependent and -independent regulation of serum phosphate*. Am J Physiol Renal Physiol, 2011. **300**(3): p. F783-91.
265. Wang, G.L., et al., *Hypoxia-inducible factor 1 is a basic-helix-loop-helix-PAS heterodimer regulated by cellular O₂ tension*. Proc Natl Acad Sci U S A, 1995. **92**(12): p. 5510-4.
266. Semenza, G.L., *Hydroxylation of HIF-1: oxygen sensing at the molecular level*. Physiology (Bethesda), 2004. **19**: p. 176-82.
267. Zhang, Q., et al., *The hypoxia-inducible factor-1alpha activates ectopic production of fibroblast growth factor 23 in tumor-induced osteomalacia*. Bone Res, 2016. **4**: p. 16011.
268. Farrow, E.G., et al., *Iron deficiency drives an autosomal dominant hypophosphatemic rickets (ADHR) phenotype in fibroblast growth factor-23 (Fgf23) knock-in mice*. Proc Natl Acad Sci U S A, 2011. **108**(46): p. E1146-55.

269. David, V., et al., *Inflammation and functional iron deficiency regulate fibroblast growth factor 23 production*. *Kidney Int*, 2016. **89**(1): p. 135-46.
270. Flamme, I., et al., *FGF23 expression in rodents is directly induced via erythropoietin after inhibition of hypoxia inducible factor proline hydroxylase*. *PLoS One*, 2017. **12**(10): p. e0186979.
271. Coe, L.M., et al., *FGF-23 is a negative regulator of prenatal and postnatal erythropoiesis*. *J Biol Chem*, 2014. **289**(14): p. 9795-810.
272. Toro, L., et al., *Erythropoietin induces bone marrow and plasma fibroblast growth factor 23 during acute kidney injury*. *Kidney Int*, 2018. **93**(5): p. 1131-1141.
273. Clinkenbeard, E.L., et al., *Erythropoietin stimulates murine and human fibroblast growth factor-23, revealing novel roles for bone and bone marrow*. *Haematologica*, 2017. **102**(11): p. e427-e430.
274. Daryadel, A., et al., *Erythropoietin stimulates fibroblast growth factor 23 (FGF23) in mice and men*. *Pflugers Arch*, 2018. **470**(10): p. 1569-1582.
275. Hanudel, M.R., et al., *Effects of erythropoietin on fibroblast growth factor 23 in mice and humans*. *Nephrol Dial Transplant*, 2018.
276. White, K.E., et al., *Autosomal-dominant hypophosphatemic rickets (ADHR) mutations stabilize FGF-23*. *Kidney Int*, 2001. **60**(6): p. 2079-86.
277. Yamamoto, H., et al., *Posttranslational processing of FGF23 in osteocytes during the osteoblast to osteocyte transition*. *Bone*, 2016. **84**: p. 120-30.
278. Ichikawa, S., et al., *Genetic rescue of glycosylation-deficient Fgf23 in the Galnt3 knockout mouse*. *Endocrinology*, 2014. **155**(10): p. 3891-8.
279. Bergwitz, C., et al., *Defective O-glycosylation due to a novel homozygous S129P mutation is associated with lack of fibroblast growth factor 23 secretion and tumoral calcinosis*. *J Clin Endocrinol Metab*, 2009. **94**(11): p. 4267-74.
280. Ferron, M., *Endocrine Functions of Bone*, in *Principles of Endocrinology and Hormone Action*, A. Belfiore and D. LeRoith, Editors. 2016, Springer International Publishing: Cham. p. 1-27.
281. Rafaelsen, S.H., et al., *Exome sequencing reveals FAM20c mutations associated with fibroblast growth factor 23-related hypophosphatemia, dental anomalies, and ectopic calcification*. *J Bone Miner Res*, 2013. **28**(6): p. 1378-85.
282. Wang, X., et al., *Inactivation of a novel FGF23 regulator, FAM20C, leads to hypophosphatemic rickets in mice*. *PLoS Genet*, 2012. **8**(5): p. e1002708.
283. Feng, J.Q., et al., *Loss of DMP1 causes rickets and osteomalacia and identifies a role for osteocytes in mineral metabolism*. *Nat Genet*, 2006. **38**(11): p. 1310-5.
284. *A gene (PEX) with homologies to endopeptidases is mutated in patients with X-linked hypophosphatemic rickets. The HYP Consortium*. *Nat Genet*, 1995. **11**(2): p. 130-6.
285. White, K.E., et al., *Mutations that cause osteoglophonic dysplasia define novel roles for FGFR1 in bone elongation*. *Am J Hum Genet*, 2005. **76**(2): p. 361-7.
286. Larsson, T., et al., *A novel recessive mutation in fibroblast growth factor-23 causes familial tumoral calcinosis*. *J Clin Endocrinol Metab*, 2005. **90**(4): p. 2424-7.
287. Ichikawa, S., et al., *A homozygous missense mutation in human KLOTHO causes severe tumoral calcinosis*. *J Clin Invest*, 2007. **117**(9): p. 2684-91.

288. Isakova, T., et al., *Fibroblast growth factor 23 is elevated before parathyroid hormone and phosphate in chronic kidney disease*. *Kidney Int*, 2011. **79**(12): p. 1370-8.
289. Rossaint, J., et al., *FGF23 signaling impairs neutrophil recruitment and host defense during CKD*. *J Clin Invest*, 2016. **126**(3): p. 962-74.
290. Singh, S., et al., *Fibroblast growth factor 23 directly targets hepatocytes to promote inflammation in chronic kidney disease*. *Kidney Int*, 2016. **90**(5): p. 985-996.
291. Grabner, A., et al., *Activation of Cardiac Fibroblast Growth Factor Receptor 4 Causes Left Ventricular Hypertrophy*. *Cell Metab*, 2015. **22**(6): p. 1020-32.
292. Gutierrez, O.M., et al., *Fibroblast growth factor 23 and left ventricular hypertrophy in chronic kidney disease*. *Circulation*, 2009. **119**(19): p. 2545-52.
293. Cohen, G., M. Haag-Weber, and W.H. Horl, *Immune dysfunction in uremia*. *Kidney Int Suppl*, 1997. **62**: p. S79-82.
294. Faul, C., et al., *FGF23 induces left ventricular hypertrophy*. *J Clin Invest*, 2011. **121**(11): p. 4393-408.
295. Munoz Mendoza, J., et al., *Fibroblast growth factor 23 and Inflammation in CKD*. *Clin J Am Soc Nephrol*, 2012. **7**(7): p. 1155-62.
296. Rossaint, J., M. Unruh, and A. Zarbock, *Fibroblast growth factor 23 actions in inflammation: a key factor in CKD outcomes*. *Nephrol Dial Transplant*, 2017. **32**(9): p. 1448-1453.
297. Semenov, A.G., et al., *Processing of pro-brain natriuretic peptide is suppressed by O-glycosylation in the region close to the cleavage site*. *Clin Chem*, 2009. **55**(3): p. 489-98.
298. Dhanvantari, S., N.G. Seidah, and P.L. Brubaker, *Role of prohormone convertases in the tissue-specific processing of proglucagon*. *Mol Endocrinol*, 1996. **10**(4): p. 342-55.
299. Benjannet, S., et al., *PC1 and PC2 are proprotein convertases capable of cleaving proopiomelanocortin at distinct pairs of basic residues*. *Proc Natl Acad Sci U S A*, 1991. **88**(9): p. 3564-8.
300. Essalmani, R., et al., *Furin is the primary in vivo convertase of angiotensin-like 3 and endothelial lipase in hepatocytes*. *J Biol Chem*, 2013. **288**(37): p. 26410-8.
301. Susan-Resiga, D., et al., *Furin is the major processing enzyme of the cardiac-specific growth factor bone morphogenetic protein 10*. *J Biol Chem*, 2011. **286**(26): p. 22785-94.
302. Al Rifai, O., et al., *Proprotein convertase furin regulates osteocalcin and bone endocrine function*. *J Clin Invest*, 2017. **127**(11): p. 4104-4117.
303. Creus, S., et al., *Human FSH isoforms: carbohydrate complexity as determinant of in-vitro bioactivity*. *Mol Cell Endocrinol*, 2001. **174**(1-2): p. 41-9.
304. Runkel, L., et al., *Structural and functional differences between glycosylated and non-glycosylated forms of human interferon-beta (IFN-beta)*. *Pharm Res*, 1998. **15**(4): p. 641-9.
305. Elliott, S., et al., *Enhancement of therapeutic protein in vivo activities through glycoengineering*. *Nat Biotechnol*, 2003. **21**(4): p. 414-21.
306. Cunningham, D.F. and B. O'Connor, *Proline specific peptidases*. *Biochim Biophys Acta*, 1997. **1343**(2): p. 160-86.
307. Hwang, Y.C., et al., *Association between the circulating total osteocalcin level and the development of cardiovascular disease in middle-aged men: a mean 8.7-year longitudinal follow-up study*. *J Atheroscler Thromb*, 2015. **22**(2): p. 136-43.

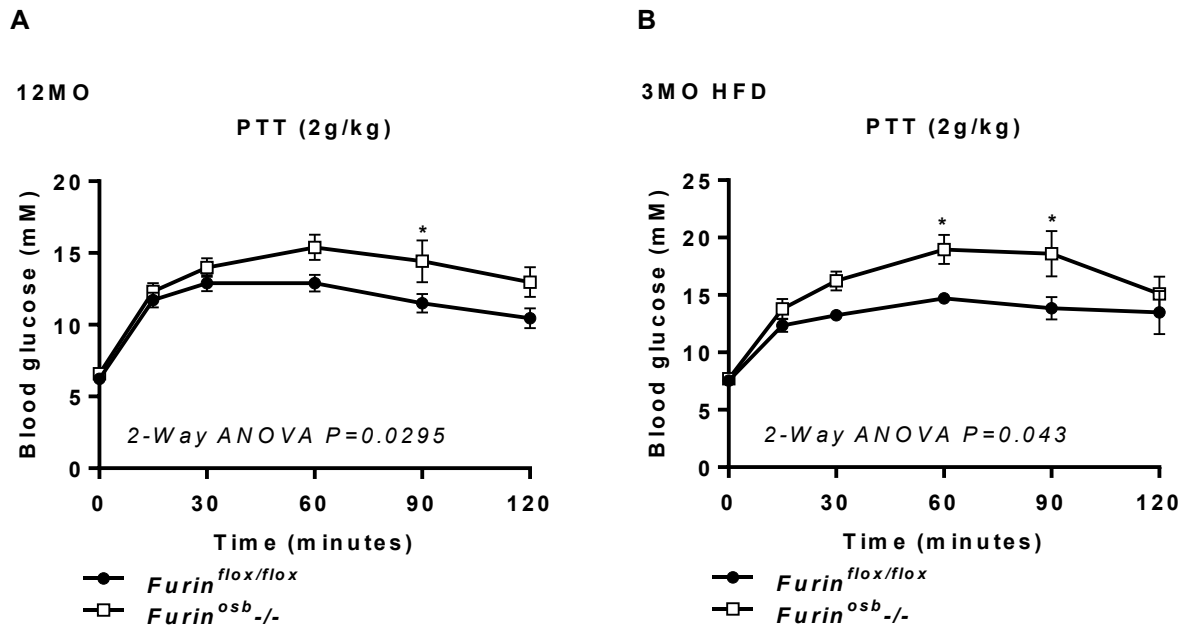
308. Hwang, Y.C., et al., *Circulating osteocalcin level is associated with improved glucose tolerance, insulin secretion and sensitivity independent of the plasma adiponectin level.* Osteoporos Int, 2012. **23**(4): p. 1337-42.
309. Kanazawa, I., et al., *Serum osteocalcin level is associated with glucose metabolism and atherosclerosis parameters in type 2 diabetes mellitus.* J Clin Endocrinol Metab, 2009. **94**(1): p. 45-9.
310. Consortium, C.A.D., et al., *Large-scale association analysis identifies new risk loci for coronary artery disease.* Nat Genet, 2013. **45**(1): p. 25-33.
311. Ueyama, C., et al., *Association of *FURIN* and *ZPR1* polymorphisms with metabolic syndrome.* Biomed Rep, 2015. **3**(5): p. 641-647.
312. Fernandez, C., et al., *Plasma levels of the proprotein convertase furin and incidence of diabetes and mortality.* J Intern Med, 2018. **284**(4): p. 377-387.
313. Wang, H.M., et al., *[Relationship between genetic variation of furin and insulin resistance in Chinese Kazakh population].* Zhonghua Xin Xue Guan Bing Za Zhi, 2012. **40**(10): p. 849-53.
314. Gundberg, C.M. and M.E. Clough, *The osteocalcin propeptide is not secreted in vivo or in vitro.* J Bone Miner Res, 1992. **7**(1): p. 73-80.
315. Hosoda, K., et al., *Secretion of osteocalcin and its propeptide from human osteoblastic cells: dissociation of the secretory patterns of osteocalcin and its propeptide.* J Bone Miner Res, 1993. **8**(5): p. 553-65.
316. Rehder, D.S., et al., *Gamma-carboxylation and fragmentation of osteocalcin in human serum defined by mass spectrometry.* Mol Cell Proteomics, 2015. **14**(6): p. 1546-55.
317. Ivaska, K.K., et al., *Release of intact and fragmented osteocalcin molecules from bone matrix during bone resorption in vitro.* J Biol Chem, 2004. **279**(18): p. 18361-9.
318. Taylor, A.K., et al., *Multiple osteocalcin fragments in human urine and serum as detected by a midmolecule osteocalcin radioimmunoassay.* J Clin Endocrinol Metab, 1990. **70**(2): p. 467-72.
319. Lacombe J, A.R.O., Loter L, Moran T, Turcotte A-F, Grenier-Larouche T, Tchernof A, Biertho L, Carpentier A, Prud'homme D, Rabasa-Lhoret R, Karsenty G, Gagnon C, Jiang W, and Ferron M, *Measurement of bioactive osteocalcin in humans using a novel immunoassay reveals association with glucose metabolism and β -cell function.* Am J Physiol Endocrinol Metab, 2020.
320. Gazdag, A.C., et al., *Calorie restriction increases insulin-stimulated glucose transport in skeletal muscle from *IRS-1* knockout mice.* Diabetes, 1999. **48**(10): p. 1930-6.
321. Browning, J.D., et al., *Alterations in hepatic glucose and energy metabolism as a result of calorie and carbohydrate restriction.* Hepatology, 2008. **48**(5): p. 1487-96.
322. Hagopian, K., J.J. Ramsey, and R. Weindruch, *Caloric restriction increases gluconeogenic and transaminase enzyme activities in mouse liver.* Exp Gerontol, 2003. **38**(3): p. 267-78.
323. Kim, S.P., et al., *Sclerostin influences body composition by regulating catabolic and anabolic metabolism in adipocytes.* Proc Natl Acad Sci U S A, 2017. **114**(52): p. E11238-E11247.
324. Seidah, N.G., et al., *Precursor convertases: an evolutionary ancient, cell-specific, combinatorial mechanism yielding diverse bioactive peptides and proteins.* Ann N Y Acad Sci, 1998. **839**: p. 9-24.

325. Shiryayev, S.A., et al., *High-resolution analysis and functional mapping of cleavage sites and substrate proteins of furin in the human proteome*. PLoS One, 2013. **8**(1): p. e54290.
326. van Bloemendaal, L., et al., *GLP-1 receptor activation modulates appetite- and reward-related brain areas in humans*. Diabetes, 2014. **63**(12): p. 4186-96.
327. Tschop, M., D.L. Smiley, and M.L. Heiman, *Ghrelin induces adiposity in rodents*. Nature, 2000. **407**(6806): p. 908-13.
328. Urabe, H., et al., *Haematopoietic cells produce BDNF and regulate appetite upon migration to the hypothalamus*. Nat Commun, 2013. **4**: p. 1526.
329. Nonomura, T., et al., *Brain-derived neurotrophic factor regulates energy expenditure through the central nervous system in obese diabetic mice*. Int J Exp Diabetes Res, 2001. **2**(3): p. 201-9.
330. Seidah, N.G., et al., *Cellular processing of the neurotrophin precursors of NT3 and BDNF by the mammalian proprotein convertases*. FEBS Lett, 1996. **379**(3): p. 247-50.
331. Yamashiro, T., et al., *Gene and protein expression of brain-derived neurotrophic factor and TrkB in bone and cartilage*. Bone, 2001. **28**(4): p. 404-9.
332. Wetsel, W.C., et al., *Disruption of the expression of the proprotein convertase PC7 reduces BDNF production and affects learning and memory in mice*. Proc Natl Acad Sci U S A, 2013. **110**(43): p. 17362-7.
333. Imel, E.A., S.L. Hui, and M.J. Econs, *FGF23 concentrations vary with disease status in autosomal dominant hypophosphatemic rickets*. J Bone Miner Res, 2007. **22**(4): p. 520-6.
334. Imel, E.A., et al., *Iron modifies plasma FGF23 differently in autosomal dominant hypophosphatemic rickets and healthy humans*. J Clin Endocrinol Metab, 2011. **96**(11): p. 3541-9.
335. Khosravi, A., et al., *Determination of the elimination half-life of fibroblast growth factor-23*. J Clin Endocrinol Metab, 2007. **92**(6): p. 2374-7.
336. Clinkenbeard, E.L., et al., *Conditional Deletion of Murine Fgf23: Interruption of the Normal Skeletal Responses to Phosphate Challenge and Rescue of Genetic Hypophosphatemia*. J Bone Miner Res, 2016. **31**(6): p. 1247-57.
337. Yuan, B., et al., *Aberrant Phex function in osteoblasts and osteocytes alone underlies murine X-linked hypophosphatemia*. J Clin Invest, 2008. **118**(2): p. 722-34.
338. Kapelari, K., et al., *Iron Supplementation Associated With Loss of Phenotype in Autosomal Dominant Hypophosphatemic Rickets*. J Clin Endocrinol Metab, 2015. **100**(9): p. 3388-92.
339. Imel, E.A., et al., *Oral Iron Replacement Normalizes Fibroblast Growth Factor 23 in Iron-Deficient Patients With Autosomal Dominant Hypophosphatemic Rickets*. J Bone Miner Res, 2019.
340. Staff, M.C. *Diabetes*. Available from: <https://www.mayoclinic.org/diseases-conditions/diabetes/symptoms-causes/syc-20371444>.
341. Deji, N., et al., *Structural and functional changes in the kidneys of high-fat diet-induced obese mice*. Am J Physiol Renal Physiol, 2009. **296**(1): p. F118-26.
342. Rios, R., et al., *Phosphorus restriction does not prevent the increase in fibroblast growth factor 23 elicited by high fat diet*. PLoS One, 2018. **13**(6): p. e0198481.
343. Bar, L., et al., *Insulin suppresses the production of fibroblast growth factor 23 (FGF23)*. Proc Natl Acad Sci U S A, 2018. **115**(22): p. 5804-5809.

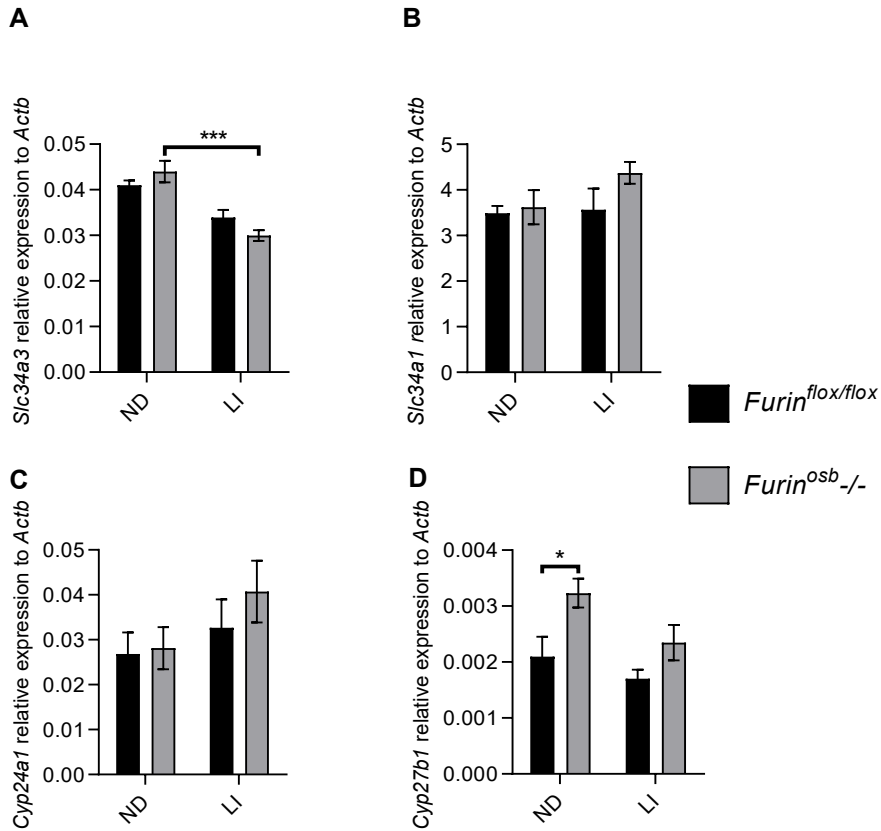
344. Hanks, L.J., et al., *Associations of fibroblast growth factor-23 with markers of inflammation, insulin resistance and obesity in adults*. PLoS One, 2015. **10**(3): p. e0122885.
345. Garland, J.S., et al., *Insulin resistance is associated with Fibroblast Growth Factor-23 in stage 3-5 chronic kidney disease patients*. J Diabetes Complications, 2014. **28**(1): p. 61-5.
346. Wojcik, M., et al., *FGF23 contributes to insulin sensitivity in obese adolescents - preliminary results*. Clin Endocrinol (Oxf), 2012. **77**(4): p. 537-40.
347. Zhang, X., et al., *FGF23(C-tail) improves diabetic nephropathy by attenuating renal fibrosis and inflammation*. BMC Biotechnol, 2018. **18**(1): p. 33.
348. Goetz, R., et al., *Isolated C-terminal tail of FGF23 alleviates hypophosphatemia by inhibiting FGF23-FGFR-Klotho complex formation*. Proc Natl Acad Sci U S A, 2010. **107**(1): p. 407-12.
349. Yuan, B., et al., *Hexa-D-arginine treatment increases 7B2*PC2 activity in hyp-mouse osteoblasts and rescues the HYP phenotype*. J Bone Miner Res, 2013. **28**(1): p. 56-72.
350. Benet-Pages, A., et al., *FGF23 is processed by proprotein convertases but not by PHEX*. Bone, 2004. **35**(2): p. 455-62.
351. Canalis, E., et al., *Notch signaling in osteocytes differentially regulates cancellous and cortical bone remodeling*. J Biol Chem, 2013. **288**(35): p. 25614-25.
352. Li, X., et al., *Targeted deletion of the sclerostin gene in mice results in increased bone formation and bone strength*. J Bone Miner Res, 2008. **23**(6): p. 860-9.
353. Youngstrom, D.W., et al., *Jagged1 expression by osteoblast-lineage cells regulates trabecular bone mass and periosteal expansion in mice*. Bone, 2016. **91**: p. 64-74.
354. Perry, M.J., et al., *Impaired growth plate function in bmp-6 null mice*. Bone, 2008. **42**(1): p. 216-25.
355. Shu, B., et al., *BMP2, but not BMP4, is crucial for chondrocyte proliferation and maturation during endochondral bone development*. J Cell Sci, 2011. **124**(Pt 20): p. 3428-40.
356. Wang, H.G., et al., *MEPE activated by furin promotes pulpal cell adhesion*. J Dent Res, 2011. **90**(4): p. 529-34.
357. Benjannet, S., et al., *7B2 is a specific intracellular binding protein of the prohormone convertase PC2*. J Neurochem, 1995. **64**(5): p. 2303-11.
358. Cao, J., et al., *Furin directly cleaves proMMP-2 in the trans-Golgi network resulting in a nonfunctioning proteinase*. J Biol Chem, 2005. **280**(12): p. 10974-80.
359. Nyman, J.S., et al., *Differential effects between the loss of MMP-2 and MMP-9 on structural and tissue-level properties of bone*. J Bone Miner Res, 2011. **26**(6): p. 1252-60.
360. Leighton, M. and K.E. Kadler, *Paired basic/Furin-like proprotein convertase cleavage of Pro-BMP-1 in the trans-Golgi network*. J Biol Chem, 2003. **278**(20): p. 18478-84.
361. Lu, C., et al., *Mepe is expressed during skeletal development and regeneration*. Histochem Cell Biol, 2004. **121**(6): p. 493-9.
362. Rusli, F., et al., *Intermittent calorie restriction largely counteracts the adverse health effects of a moderate-fat diet in aging C57BL/6J mice*. Mol Nutr Food Res, 2017. **61**(5).
363. Devlin, M.J., et al., *Caloric restriction leads to high marrow adiposity and low bone mass in growing mice*. J Bone Miner Res, 2010. **25**(9): p. 2078-88.
364. Botega, II, et al., *Bone callus formation is highly disrupted by dietary restriction in growing rats sustaining a femoral fracture¹*. Acta Cir Bras, 2019. **34**(1): p. e20190010000002.

365. Forlino, A., et al., *New perspectives on osteogenesis imperfecta*. Nat Rev Endocrinol, 2011. **7**(9): p. 540-57.
366. Van Dijk, F.S. and D.O. Sillence, *Osteogenesis imperfecta: clinical diagnosis, nomenclature and severity assessment*. Am J Med Genet A, 2014. **164A**(6): p. 1470-81.
367. Kozloff, K.M., et al., *Brittle IV mouse model for osteogenesis imperfecta IV demonstrates postpubertal adaptations to improve whole bone strength*. J Bone Miner Res, 2004. **19**(4): p. 614-22.
368. Uveges, T.E., et al., *Cellular mechanism of decreased bone in Brtl mouse model of OI: imbalance of decreased osteoblast function and increased osteoclasts and their precursors*. J Bone Miner Res, 2008. **23**(12): p. 1983-94.
369. Chen, F., et al., *First mouse model for combined osteogenesis imperfecta and Ehlers-Danlos syndrome*. J Bone Miner Res, 2014. **29**(6): p. 1412-23.
370. Kalajzic, I., et al., *Osteoblastic response to the defective matrix in the osteogenesis imperfecta murine (oim) mouse*. Endocrinology, 2002. **143**(5): p. 1594-601.
371. Roschger, A., et al., *Effect of sclerostin antibody treatment in a mouse model of severe osteogenesis imperfecta*. Bone, 2014. **66**: p. 182-8.
372. Cardinal, M., et al., *Sclerostin antibody reduces long bone fractures in the oim/oim model of osteogenesis imperfecta*. Bone, 2019. **124**: p. 137-147.
373. Doucet, A., et al., *Identification of proteolytic products and natural protein N-termini by Terminal Amine Isotopic Labeling of Substrates (TAILS)*. Methods Mol Biol, 2011. **753**: p. 273-87.
374. Prudova, A., et al., *TAILS N-Terminomics and Proteomics Show Protein Degradation Dominates over Proteolytic Processing by Cathepsins in Pancreatic Tumors*. Cell Rep, 2016. **16**(6): p. 1762-1773.

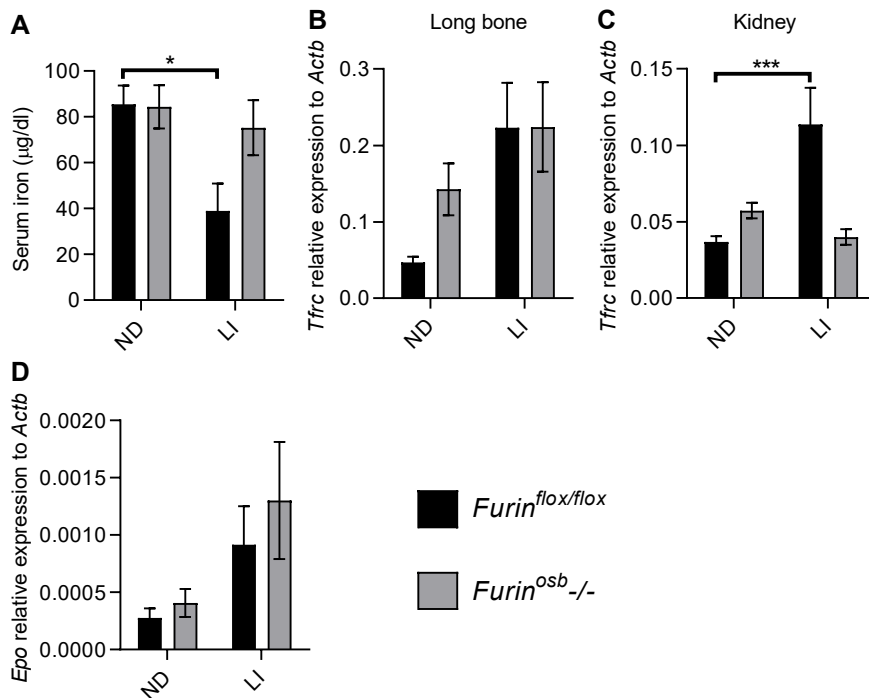
8.ANNEXES



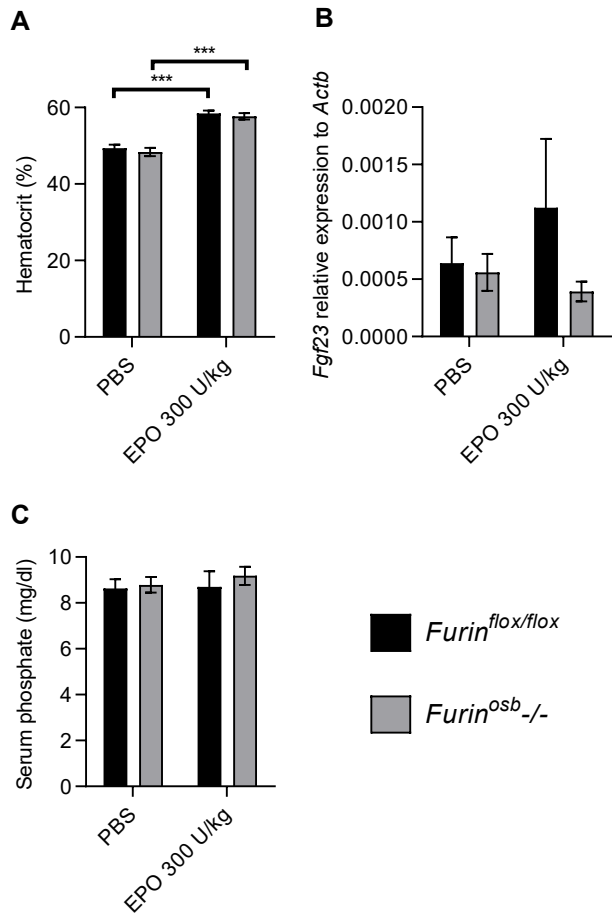
Annex Figure 8-1. Increase neoglucogenesis in *Furin^{osb-/-}* mice on normal and high fat high sucrose diet (HFHSD). A and B Pyruvate tolerance test on control and *Furin^{osb-/-}* mice. Normal chow diet at 12 months (MO) old (A) and high fat high sucrose diet (HFD) at 3 months (MO) old (B). Results represent the mean \pm SEM. * $P < 0.05$, by 2-way ANOVA for non repeated measurements with Bonferroni's multiple comparisons test.



Annex Figure 8-2. FGF23 target in control and *Furin^{osb-/-}* mice on normal or low iron diet. A-D) Sodium phosphate co-transporter and vitamin D producing enzyme expression in kidney. (A) *Slc34a3*, (B) *Slc34a1*, (C) *Cyp24a1* and (D) *Cyp27b1*. Results are normalized to beta actin *Actb*. Results represent the mean \pm SEM. * $P < 0.05$ and * $P < 0.001$, by 2-way ANOVA for non repeated measurements with Bonferroni's multiple comparisons test.**



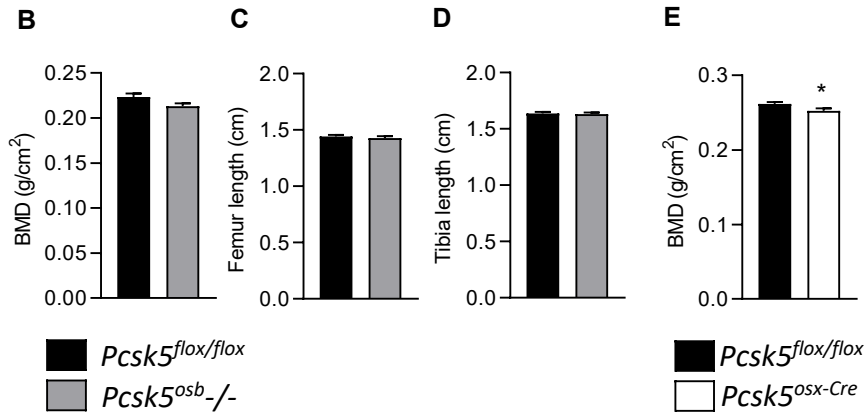
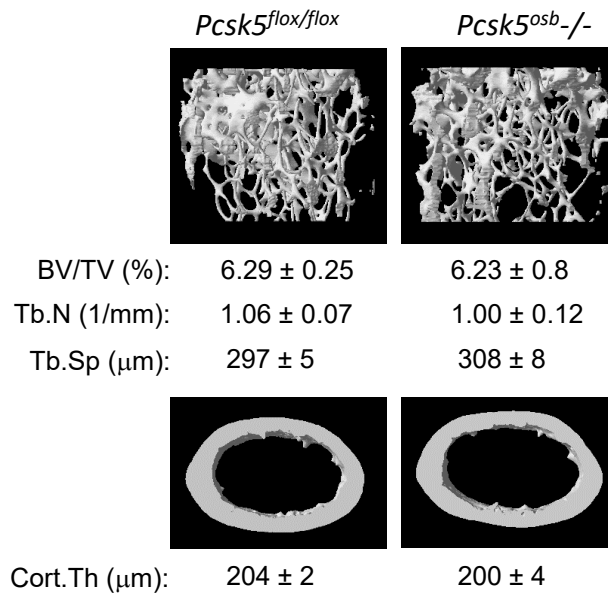
Annex Figure 8-3. *Furin^{osb-/-}* mice maintained normal serum iron. A-D) control and *Furin^{osb-/-}* mice were fed on normal or low iron diet. **A)** Serum iron levels. Transferrin receptor (*Tfrc*) expression in long bone **(B)** and kidney **(C)**. **D)** Erythropoietin (*Epo*) expression in kidney. Gene expression results are normalized to beta actin *Actb*. Results represent the mean \pm SEM. * $P < 0.05$ and *** $P < 0.001$, by 2-way ANOVA for non repeated measurements with Bonferroni's multiple comparisons test.



Annex Figure 8-4. *Furin^{osb-/-}* mice maintained normal serum phosphate following two weeks of Erythropoietin (EPO) injection. A-C) control and *Furin^{osb-/-}* mice were injected with rhEPO once each 2 days over 2 weeks. **A) Hematocrit. **(B)** *Fgf23* expression in long bone. **(C)** Serum phosphate levels. Gene expression results are normalized to beta actin *Actb*. Results represent the mean \pm SEM. *** $P < 0.001$, by 2-way ANOVA for non repeated measurements with Bonferroni's multiple comparisons test.**

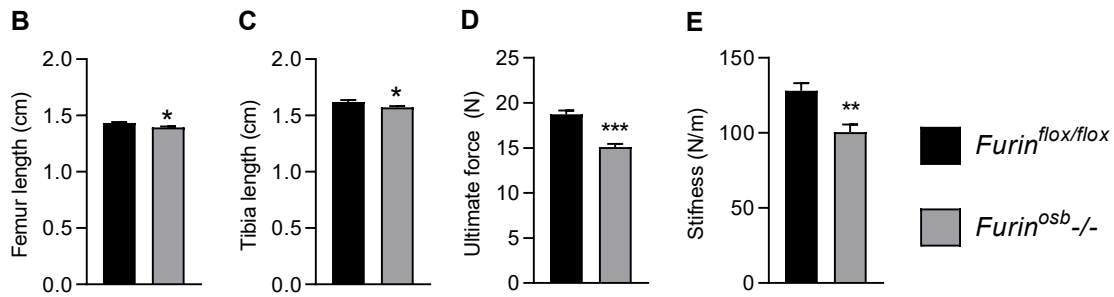
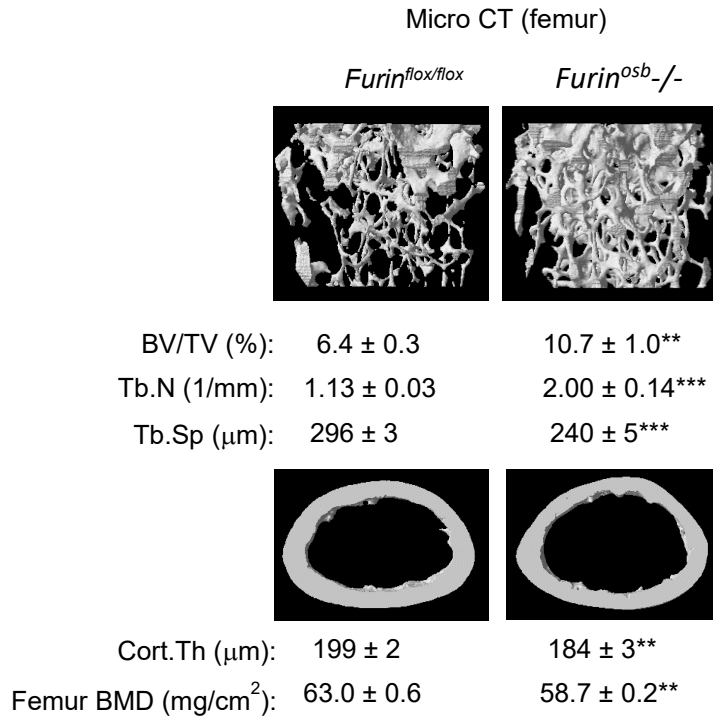
A

Micro CT (femur)

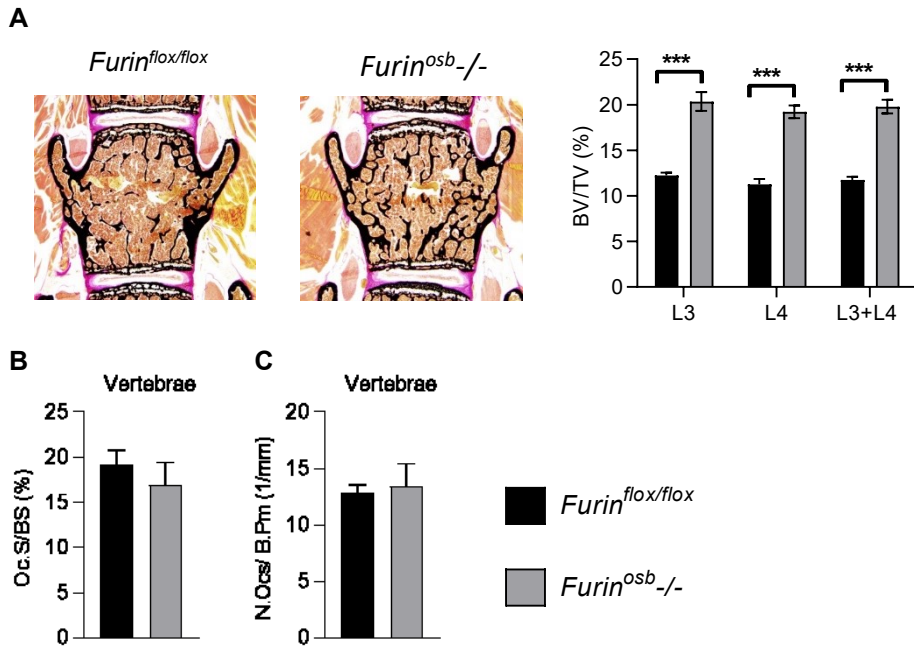


Annex Figure 8-5. Normal bone quality in *Pcsk5^{osb-/-}*. Bone parameters in control and *Pcsk5^{osb-/-}* mice on normal diet. **A)** Micro computed topography (micro-CT) on femur of control and *Furin^{osb-/-}* mice. Upper panel shows trabecular bone parameters at 1,5mm from the growth plate. Lower panel show cortical thickness at the long bone midshaft. **B)** Bone mineral density (BMD). **C)** Femur length. **D)** Tibia length. **E)** Bone mineral density (BMD) in control and *Pcsk5^{osx-Cre}* mice. Results represent the mean ± SEM. **P* < 0.05, ***P* < 0.01 and ****P* < 0.001, by unpaired student T-Test.

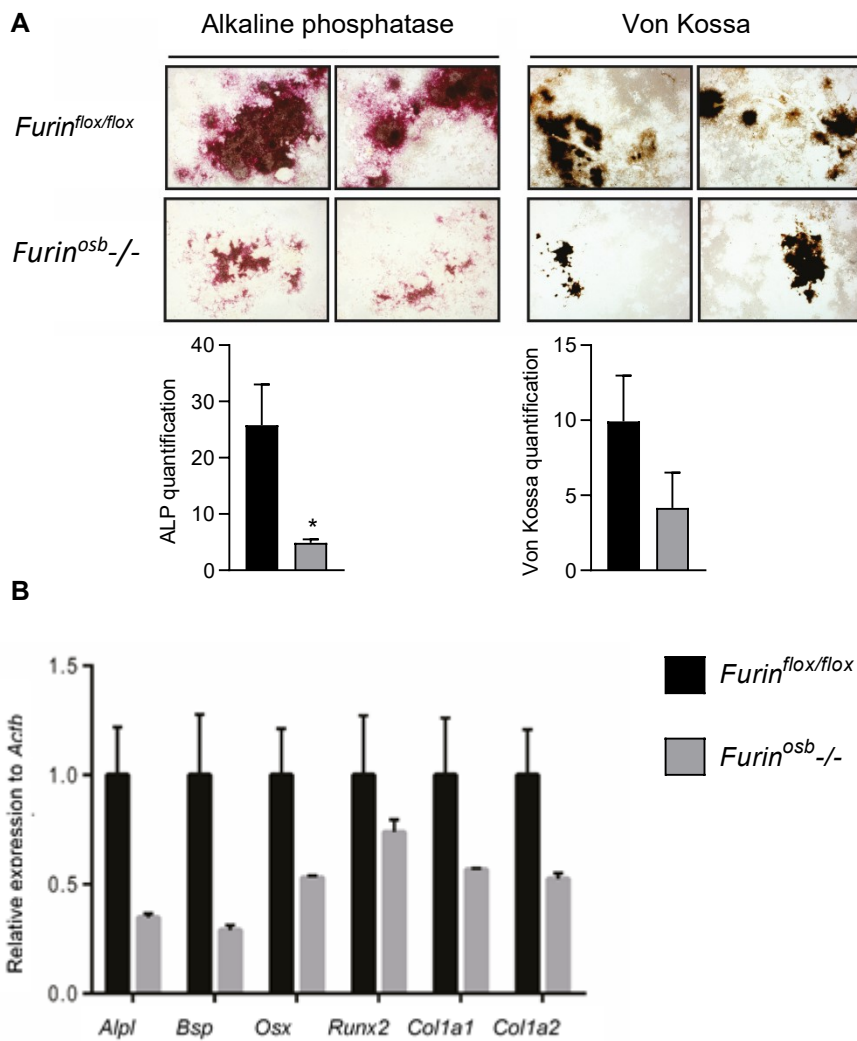
A



Annex Figure 8-6. Poor bone quality in *Furin^{osb-/-}*. Bone parameters in control and *Furin^{osb-/-}* mice on normal diet. **A)** Micro computed topography (micro-CT) on femur of control and *Furin^{osb-/-}* mice. Upper panel shows trabecular bone parameters at 1,5mm from the growth plate. Lower panel show cortical thickness at the long bone midshaft and the femur bone mineral density (BMD). **B)** Femur length. **C)** Tibia length. **D and E)** Three points bending test on femur of control and *Furin^{osb-/-}* mice. Ultimate force (**D**) and stiffness (**E**). Results represent the mean \pm SEM. * $P < 0.05$, ** $P < 0.01$ and *** $P < 0.001$, by unpaired student T-Test.



Annex Figure 8-7. Increase bone volume, osteoblasts and osteoclasts in the trabecular bone of *Furin^{osb-/-}* mice. Bone histomorphological analysis on the vertebra of control and *Furin^{osb-/-}* mice on normal diet (A-C). Von Kossa staining of the vertebra in the left panel and quantification of bone volume/ tissue volume (BV/TV) in the right panel (A). % of osteoclast surface over bone surface (B) and osteoclasts number normalized bone perimeter (C). Results represent the mean \pm SEM. * $P < 0.05$, by unpaired student T-Test.



Annex Figure 8-8. Decrease bone mineralization capacity of bone marrow osteoblasts derived from *Furin^{osb-/-}* mice.

Bone marrow derived osteoblasts from control and *Furin^{osb-/-}* mice was collected and differentiated over 21 days. **A)** Alkaline phosphatase staining (upper panel) and quantification (lower Panel). Von Kossa staining (upper panel) and quantification (lower Panel). **B)** Expression levels of differentiation markers in bone marrow osteoblasts derived from control and *Furin^{osb-/-}* mice. Results represent the mean \pm SEM. * $P < 0.05$, by unpaired student T-Test.

9. CURRICULUM VITAE

Omar Al Rifai

Email: Omar.alrifai@ircm.qc.ca; Omar.alrifai@umontreal.ca

Education

- **January 2015- 2020: PhD student in Molecular Biology, Molecular and Cellular medicine.** Institut de Recherches Cliniques de Montréal (IRCM), Université de Montréal, Faculté de Médecine. Supervisor: Dr. Mathieu Ferron.
- **August 2011- September 2014. Master's degree in biochemistry.** American university of Beirut graduated with distinction GPA=3.89. Supervisor: Dr. Julnar Usta.
- **September 2005- September 2008: BS in Biochemistry.** Lebanese University. Mention: good. Honor list in the first academic year 2005-2006.

Research Experience

January 2015-2020: PhD student at the Institut de Recherches Cliniques de Montréal (IRCM).

Research field: Bone endocrine functions, type 2 diabetes, bone physiology, bone rare disease, molecular biology, cell physiology, and translational research.

Important contributions:

- Identify the proprotein convertase (PC) furin as a pleiotropic regulators of osteoblasts endocrine function. It regulates glucose and energy metabolism through the processing of the bone derived hormone osteocalcin and through the regulation of appetite independently through an unknown mechanism. It also regulates FGF23 which is another bone derived hormone regulating phosphate excretion in the kidney proximal tubule.
- Characterize a novel osteocalcin post-translational modification, *O*-glycosylation, which is required for its half-life in vivo.
- Provide an approach to increase human osteocalcin half-life in circulation.
- Describe the role of furin in the regulation of bone mass accrual in vivo.

Supervisor: Dr. Mathieu Ferron

December 2008– 2014: Research Laboratory Manager and Master student at the American University of Beirut- Department of Biochemistry and Molecular Genetics.

Research field: Metabolic rare disease, Wilson Disease, hypercholesterolemia, liver cancer, biochemistry, analytical biochemistry, natural product.

Important contributions:

- Regulation of cholesterol production by Ubiquinone in hepatocytes.
- Genotype phenotype correlation in Wilson disease patients in Lebanese families.
- Toxicity of the natural extract linalool on the hepatic cells.

Supervisor: Dr. Julnar Usta

Managment Experience

December 2008– 2014: Research Laboratory Manager at the American University of Beirut- Department of Biochemistry and Molecular Genetics. Manage the stocks and laboratory orders, ensure the application of safety rules, train and help graduate students in their work, evaluate students for their practical work in the lab, proctoring during exams.

Funding history and awards

Funding

- FRQS doctoral scholarship; 21000/year; 2018.
- IRCM Challenge Scholarship; 10000\$/year; 2017.
- IRCM Challenge Scholarship; 10000\$/year; 2016.
- IRCM Challenge Scholarship; 10000\$/year; 2015.
- Bourse d'exemption des droits de scolarité-Université de Montréal; 17,000 \$/Y; 2015; declined.
- Bourse d'exemption des droits de scolarité- Ministry of Education in Lebanon; 17,000 \$/Y; 2015.
- Staff Educational scholarship- American University of Beirut; 11,907 US\$/Y; 2011.

Awards

- Thirteenth Annual Scientific Meeting Montreal Diabetes Research Center- best poster presentation award; 400 \$; 2019.
- Mechanistic and Therapeutic Advances in Rare Skeletal Diseases young investigator recognition award; 500 US\$; 2018.
- American Society of Bone and Mineral Research (ASBMR) young investigator travel award; 500 US\$; 2018.
- Montreal Diabetes Research Center travel award; 700 \$; 2018.
- Canadian Institute of Health Research- Institute of Aging travel award; 944 \$; 2018.
- University of Montreal travel award; 500 \$; 2018.
- Best poster presentation award – Molecular Biology Research day, Université de Montréal; 200 \$; 2017.

Publications

Published papers

1. Lacombe J, **Al Rifai O**, Loter L, Moran T, Turcotte AF, Grenier-Larouche T, Tchernof A, Biertho L, Carpentier AC, Prud'homme D, Rabasa-Lhoret R, Karsenty G, Gagnon C, Jiang W, Ferron M. Measurement of bioactive osteocalcin in humans using a novel immunoassay reveals association with glucose metabolism and β -cell function. *Am J Physiol Endocrinol Metab*, 2020, Jan.
2. **Al Rifai O**, Chow J, Lacombe J, Julien C, Faubert D, Susan-Resiga D, Essalmani R, Creemers JW, Seidah NG, Ferron M. Proprotein convertase furin regulates osteocalcin and bone endocrine function. *J Clin Invest*. 2017 Nov 1;127(11):4104-4117.
3. Boraschi-Diaz I, Tauer JT, **El-Rifai O**, Guillemette D, Lefebvre G, Rauch F, Ferron M, Komarova SV. Metabolic phenotype in the mouse model of osteogenesis imperfecta. *J Endocrinol*. 2017 Sep;234(3):279-289.
4. Al Wafai R, El-Rabih W, Katerji M, Safi R, El Sabban M, **El-Rifai O**, Usta J. Chemosensitivity of MCF-7 cells to eugenol: release of cytochrome-c and lactate dehydrogenase. *Sci Rep*. 2017 Mar 8;7:43730.

5. Usta J, Wehbeh A, Rida K, **El-Rifai O**, Estiphan TA, Majarian K, and Barada K. Phenotype-Genotype correlation in Wilson's disease in a huge Lebanese family: association of 2299 C-ins with hepatic and of A1003T/non 2299C-ins with neurologic phenotype. *PLoS One*. 2014, **9**(11):e109727.
6. Usta J, Hachem Y, **El-Rifai O**, Bou-Moughlabey Y, Echtay K, Griffiths D, Nakkash-Chmaisse H, Makki RF. Fragrance chemicals lylal and lilial decrease viability of HaCat cells by increasing free radical production and lowering intracellular ATP level: Protection by antioxidants. *Toxicol In Vitro*. 2013,**27**, 339-48.
7. Usta J, Abu Daya H, Halawi H, Al-Shareef I, **El-Rifai O**, Malli AH, Sharara AI, Habib RH and Barada K. Homozygosity for Non-H1069Q Missense Mutations in ATP7B Gene and Early Severe Liver Disease: Report of Two Families and a Meta-analysis. *JIMD Reports*, 2012, **4**, 129-137.

Papers in preparation

1. Jane Hendrickson-Rebizant, **Omar Al Rifai**, Juliana Marulanda, Geneviève Chiasson, Mathieu Ferron, and Monzur Murshed. Understanding the Chondrocyte-Specific Roles of γ -Glutamyl Carboxylase in Skeletal Development. *In preparation*.
2. **Omar Al Rifai**, Catherine Julien, Denis Faubert, Yoshiki Narimatsu, Henrik Clausen and Mathieu Ferron. O-glycosylation a Novel Post-Translational Modification of Osteocalcin Increases its Half-life In Vivo. *In preparation*.
3. **Omar Al Rifai**, Rachid Essalmani, John W.M. Creemers, Nabil G. Seidah and Mathieu Ferron: Genetic analysis of the contribution of the proprotein convertases furin and PC5 in the regulation of FGF23 in vivo. *In preparation*.

Published abstract at the American Society of Bone and Mineral Research meeting (ASBMR)

1. O-glycosylation a Novel Post-Translational Modification of Osteocalcin Increases its Half-life In Vivo. **Al Rifai O**, Julien C, Faubert D, Narimatsu Y, Clausen H, Ferron M. -23 September-2019, Orange County Convention Center, Orlando, Florida.
2. Measurement of Uncarboxylated Osteocalcin in Humans Using a Novel Immunoassay Reveals Association with Insulin Sensitivity and Diabetes. Lacombe J, **Al Rifai O**, Turcotte AF, Carpentier A, Rabasa-Lhoret R, Karsenty G, Gagnon C, Ferron M. 20-23 September-2019, Orange County Convention Center, Orlando, Florida.
3. Prevention of ectopic calcification by MGP: The role of its conserved residues. Parashar A, **Al Rifai O**, Marulanda J, Ferron M, Murshed M. 20-23 September-2019, Orange County Convention Center, Orlando, Florida.
4. Regulation of FGF23 and Bone Mass by the Proprotein Convertase Furin. **Al Rifai O**, Essalmani R, Creemers J, Seidah N and Ferron M. September 28 – October 1-2018, Palais des congrès de Montréal, Montréal.
5. Regulation of FGF23 and Bone Mass by the Proprotein Convertase Furin. **Al Rifai O**, Essalmani R, Creemers J, Seidah N and Ferron M. Mechanistic and Therapeutic Advances in Rare Skeletal Diseases meeting, September 26 – September 28- 2018, Palais des congrès de Montréal, Montréal.
6. Understanding the Role of Protein Gamma-Carboxylation in Craniofacial Development. Hendrickson-Rebizant J, Marulanda J, **Al Rifai O**, Chiasson G, Ferron M, Murshed M. American September 28 – October 1-2018, Palais des congrès de Montréal, Montréal.

Oral presentations

National and international meeting:

1. Proprotein convertase furin is a novel pleiotropic regulator of bone endocrine functions. Keystone Symposia Conference 2018- Novel Aspect of Bone Biology- June 13-17, Snowbird Resort, Snowbird, Utah, USA
2. Le clivage de la pro-ostéocalcine par la proprotéine convertase furin est essentiel pour la fonction endocrinienne des ostéoblastes. Réunion annuelle 2017 – SQLNM / CMDO / COLosSUS. 8 au 10 Février 2017, Hôtel Chéribourg, Magog-Orford.
3. Furin in osteoblasts is essential for pro-osteocalcin processing and for glucose homeostasis. Boston Ithaca Islet Club meeting, April 23, 2016, CRCHUM Montreal.

Local meeting

1. Osteocalcin half-life is regulated through its *O*-glycosylation in mice, but not in human. Al Rifai O, Julien C, Faubert D, Clausen H and Ferron M. Institut de Recherches Cliniques de Montréal Research retreat, 13-14 juin-2019 à l'Estrimont Suites & Spa, Orford.
2. *O*-glycosylation a Novel Species-Specific Post-Translational Modification of Osteocalcin Involved in the Regulation of Its Half-Life. Cardiovascular and Metabolic Axis Research Topics (CMART) April 24, 2019. Institut de Recherches Cliniques de Montréal.
3. Proprotein convertase furin regulates osteocalcin and bone endocrine function. Institut de Recherches Cliniques de Montréal Research retreat, June 7-8, 2018, Hôtel & Spa Mont Gabriel.
4. Proprotein convertase furin regulates osteocalcin and bone endocrine function. Institut de Recherches Cliniques de Montréal Research Day, May 26, 2017, IRCM.
5. Furin in osteoblasts is essential for pro-osteocalcin processing and bone endocrine regulation of energy metabolism. XXII^{ème} Journée scientifique des programmes de biologie moléculaire, May 20, 2016, Institute for Research in Immunology and Cancer (IRIC)- Montreal.
6. Role of pro-protein convertase in osteoblasts. Joint laboratory meeting 12-11-2015, Institut de Recherche Clinique de Montréal (IRCM).
7. Cholesterol and LDL receptors in ubiquinone treated primary hepatocytes and HepG2 cells. Master Thesis Defense. Sept 12-2014, Department of Biochemistry and Molecular Genetics, American University of Beirut.
8. Coenzyme Q: a possible regulator of cholesterol pathway. Feb 6-2012. Journal Club. Department of Biochemistry and Molecular Genetics, American University of Beirut.

Poster Presentations

National and international meeting:

1. La proprotéine convertase furin contrôle la fonction endocrine de l'os. **Al Rifai O**, Chow J, Lacombe J, Julien C, Faubert D, Susan-Resiga D, Essalmani R, Creemers J, Seidah N and Ferron M. Réunion annuelle 2017 – SQLNM / CMDO / COLosSUS. 7 au 9 Février 2018, Hôtel Chéribourg, Magog-Orford.

Local meeting: During my PhD, I presented my work at the Montreal clinical research institute retreat, the Montreal diabetes research center retreat and the Molecular biology research day of UdeM.

1. Stability of the bone-derived hormone osteocalcin is regulated through its *O*-glycosylation in mice, but not in human. **Al Rifai O**, Julien C, Faubert D, Clausen H and Ferron M. February 1, 2019, MDRC retreat at CRCHUM. **Best poster presentation award**
2. Proprotein convertase furin regulates osteocalcin and bone endocrine function. **Al Rifai Omar**, Chow J, Julien C, Lacombe J, Faubert D, Susan-Resiga D, Essalmani R, Creemers J, Seidah N and Ferron M. XXIII^{ème} Journée scientifique des programmes de biologie moléculaire, May 12, 2017, CRCHUM-Montreal. **Best poster presentation award.**

References

- Dr. Mathieu Ferron, Director of Molecular Physiology research unit.
Institut de Recherches Cliniques de Montréal (IRCM),
Phone: (514) 987-5754.
E-mail: mathieu.ferron@ircm.qc.ca
- Additional references are available upon request.